UNIVERSITÉ DE MONTRÉAL

CARACTÉRISATION DE LA MORPHOLOGIE DES PIÈCES OBTENUES EN MOULAGE PAR INJECTION ET EN INJECTION-SOUFFLAGE PAR LA TECHNIQUE DE SPECTROSCOPIE INFRAROUGE

HACHMI BEN DALY
DÉPARTEMENT DE GÉNIE MÉCANIQUE
ÉCOLE POLYTECHNIQUE DE MONTRÉAL

THÈSE PRÉSENTÉE EN VUE DE L'OBTENTION
DU DIPLÔME DE PHILOSOPHIAE DOCTOR (PH.D.)
(GÉNIE MÉCANIQUE)
MAI 1998

UNIVERSITÉ DE MONTRÉAL

ÉCOLE POLYTECHNIQUE DE MONTRÉAL

Cette thèse intitulée :

CARACTÉRISATION DE LA MORPHOLOGIE DES PIÈCES OBTENUES EN MOULAGE PAR INJECTION ET EN INJECTION-SOUFFLAGE PAR LA TECHNIQUE DE SPECTROSCOPIE INFRAROUGE

présentée par : **BEN DALY Hachmi**

en vue de l'obtention du diplôme de : Philosophiae Doctor

a été dûment acceptée par le jury d'examen constitué de :

M. Bohuslav Fisa, Ph.D., président

M. Sanschagrin Bernard, D.Sc.A., membre et directeur de recherche

M. Ky.T. Nguyen, Ph.D., membre et codirecteur de recherche

M^me^ Denault Johanne, Ph.D., membre

M. Ajji Abdallah, Ph.D., membre

À la mémoire de mon père Hassen,

à ma mère Hedé

et à Thouraya.

REMERCIEMENTS

Je tiens tout d'abord à exprimer ma reconnaissance à mon directeur de recherche, le professeur **Bernard Sanschagrin**, et à mon codirecteur de recherche, Docteur **Ky T. Nguyen**, pour leur soutien, leur patience, leur disponibilité et l'attention qu'ils m'ont prodigués tout au long de mes recherches. Je tiens en particulier à souligner aussi le soutien financier que m'a accordé le professeur B. Sanschagrin. Cela m'a permis de mener à terme mes études et de participer à plusieurs congrès.

Toute ma gratitude au Docteur **Kenneth C. Cole**, chercheur de l'Institut des Matériaux Industriels (IMI) de Boucherville pour le rôle d'expert qu'il a joué. Sa grande expérience dans le domaine de la caractérisation des matériaux plastiques par la technique de spectroscopie infrarouge nous a été d'un grand secours pour interpréter nos résultats. Aussi, je tiens à remercier tout le personnel de l'IMI, en particulier MM. **Éric Pellerin, Yves Simard, Michel Carmel** et **Christain Degrandpré**, pour leur disponibilité et leur aide. Tout au long de ce travail, j'ai trouvé à l'IMI des conditions exceptionnelles de travail tant sur le plan matériel qu'humain.

Je veux ensuite remercier mesdames et messieurs les membres de jury pour le soin qu'ils ont mis dans la correction de cette thèse et pour leurs commentaires positifs et judicieux qui m'ont permis d'améliorer son contenu.

Je dois finalement exprimer mon extrême et éternelle gratitude à ma famille : mes parents et mes frères, dont les encouragements et le soutien moral m'ont été indispensables, et à *Thouraya* qui n'a cessé de croire en moi. À tous, je dis merci.

RÉSUMÉ

L'orientation moléculaire et la cristallinité d'un polymère affectent considérablement les propriétés optiques et mécaniques des pièces plastiques. Plusieurs procédés de transformation des matériaux plastiques génèrent de l'orientation moléculaire et différents types de cristallinité dans les produits finis. Donc, il est d'une importance capitale d'étudier la morphologie de ces produits afin de mieux caractériser leurs comportements sous diverses sollicitations.

Dans cette étude, nous avons caractérisé la morphologie (orientation moléculaire et cristallinité) des pièces en polyéthylène téréphtalate, PET, obtenues par injection et injection-soufflage. Notre objectif était d'étudier la relation entre la cristallinité et l'orientation moléculaire dans ce type de pièces. Le PET a été utilisé car il a une faible cinétique (vitesse) de cristallisation et une température de transition vitreuse assez élevée ($T_g = 70°C$). En faisant varier les paramètres de mise en oeuvre, telle que la température du moule dans notre cas, on peut facilement affecter la cristallinité de ce polymère. Cela va nous permettre une meilleure caractérisation de l'effet de la cristallinité sur l'orientation moléculaire.

L'orientation moléculaire dans les pièces obtenues par injection et injection-soufflage a été caractérisée par la technique d'infrarouge en mode de réflexion. Contrairement à d'autres techniques de caractérisation de l'orientation moléculaire, cette

technique permet de calculer, à partir de deux spectres mesurés dans deux directions de polarisation mutuellement perpendiculaires, l'orientation de chaque groupement moléculaire constituant la chaîne séparément. De ce fait, nous pouvons obtenir une meilleure image de la disposition de la chaîne moléculaire dans l'échantillon orienté, et donc une meilleure caractérisation de son degré d'orientation par rapport à la direction de sollicitation. Aussi, la technique d'infrarouge permet, pour le cas du PET, de caractériser sa cristallinité en utilisant le "Structure factor spectrum", calculé à partir des deux spectres mesurés.

Pour caractériser l'orientation moléculaire et la cristallinité dans le coeur des pièces injectées, une nouvelle technique de préparation des surfaces à travers l'épaisseur de ces pièces a été développée. Cette technique consiste à usiner les pièces injectées par fraisage jusqu'au niveau où l'on veut mesurer l'orientation moléculaire et à polir la surface fraisée. Cette technique a été testée sur plusieurs polymères uniaxialement orientés et les résultats obtenus ont montré son efficacité.

Dans chacune des couches à travers l'épaisseur du PET injecté, nous avons mesuré deux spectres infrarouges. Le premier spectre a été mesuré parallèlement à la direction d'écoulement et le deuxième spectre perpendiculairement à cette direction. Ces spectres ont été utilisés pour calculer la fonction d'orientation des chaînes moléculaires ainsi que la cristallinité du PET (structure factor spectrum). Dans chaque couche, nous avons rapporté les remarques suivantes :

1) L'orientation moléculaire dans la couche peau des pièces injectées dépend, en plus des contraintes élongationnelles et de cisaillement générées lors du remplissage du moule, du temps de relaxation des chaînes moléculaires, de la rigidité de ces chaînes et de la vitesse de cristallisation du polymère utilisé. Plus le temps de relaxation et la vitesse de cristallisation sont importants, plus l'orientation moléculaire dans la couche peau est importante. L'augmentation de la rigidité de la chaîne moléculaire augmente aussi l'orientation à la surface des pièces injectées.

2) La température du moule affecte considérablement la distribution de la cristallinité du PET dans l'épaisseur des pièces injectées. À de faibles températures du moule (inférieures à 70°C), le maximum de cristallinité a été observé dans une couche intermédiaire, située à une distance égale à 0.4 mm de la surface externe de la pièce. La peau ainsi que le coeur de ces pièces sont pratiquement amorphes. Le maximum de cristallinité dans la couche intermédiaire est due au phénomène de cristallisation sous contrainte (shear-induced crystallization process), favorisé par la forte orientation des chaînes de polymère dans cette zone. En augmentant la température du moule (supérieure à 70°C), le maximum de cristallinité se déplace vers la couche peau (la surface de la pièce). Ce déplacement est dû à la diminution de l'épaisseur de cette couche par l'augmentation de la température du moule.

3) L'orientation moléculaire dans l'épaisseur des pièces injectées a la même distribution que la cristallinité de la matière (Shear-induced crystallization). Ce

résultat indique que la présence de la cristallinité lors du remplissage du moule (déformation de la matière) diminue la relaxation des chaînes moléculaires et conserve, en partie, le degré d'orientation généré durant cette phase.

La fonction d'orientation de Hermans utilisée précédemment pour caractériser l'orientation moléculaire dans les pièces en PET injectées ne peut être considérée que dans le cas des échantillons uniaxialement orientés. Pour le cas des échantillons biorientés, cette dernière équation devient totalement inefficace. Dans la deuxième partie de notre thèse, nous avons proposé une nouvelle approche pour caractériser l'orientation moléculaire dans des échantillons en PET, uniaxialement et biaxialement orientés. Cette approche consiste à comparer les spectres mesurés sur la surface d'un échantillon orienté à ceux mesurés sur la surface d'un échantillon non orienté. Dans chaque direction de polarisation, la différence entre ces spectres permet de caractériser le degré d'orientation des chaînes moléculaires dans l'échantillon orienté.

Cette approche a été testée sur des échantillons en PET uniaxialement et biaxialement orientés et les résultats obtenus ont montré son efficacité. De plus, cette approche a été utilisée pour mesurer l'orientation moléculaire à la surface des bouteilles en PET et HDPE obtenues par injection-soufflage. Les résultats de cette étude sont regroupés dans l'annexe A et seront bientôt soumis pour une nouvelle publication.

ABSTRACT

Many processing methods for producing polymeric articles can introduce molecular orientation and different kinds of crystallinity into the final products. Some of them, like injection molding, introduce uniaxial molecular orientation with a very fine sheared crystals at the external surfaces of the molding and a spherulitic shaped crystals in the center of the molding. Other processing methods, like extrusion blow molding, introduce some degree of biaxial orientation and a shear-induced crystallinity in all stretching directions. The presence of molecular orientation and crystallinity in the molded parts affects both their optical and mechanical propertires. Therefore, their exact determination is of great importance since it can provide a better characterization of the end properties of these products. In this work, we study the relationship between crystallinity and molecular orientation in injection molded and injection blow molded specimens of polyethylene terephthalate, PET. This material has been chosen because it has a very slow crystallization rate, which will permit us a better understanding of the effect of crystallinity on the final degree of molecular orientation.

Molecular orientation and crystallinity in the injection and injection blow-molded specimens of PET has been characterised using the infrared spectroscopy technique in reflexion mode. This technique has been found to be a powerful technique for the characterization of the morphology of amorphous and semi-crystalline polymers. It permits to calculate the orientation for each polymeric group separately, given then a better

understanding of the molecular configuration in the oriented specimens. When using this technique, the degree of orientation of each polymeric group can be calculated using the Hermans orientation function (f).

The molecular orientation and crystallinity in the injection-molded specimens of PET in the thickness direction has been characterized using a new technique recently proposed by the present author. This technique consists of milling the specimen to a depth where molecular has to be measured and to polish the milled surface. This technique has been tested on many polymeric materials showing different thermal (glass transition temperature) and mechanical properties and the obtained results have shown its efficiency. Using this technique, infrared spectra were measured at many layers across the thickness of the injected PET. These spectra were measured both parallel and perpendicular to the flow direction, then the Hermans orientation function (f) for different molecular groups has been calculated. Moreover, the measured spectra were used to calculate the structure factor spectrum in order to characterize the crystallinity of the PET at each layer. The obtained results can be summarized as follows :

1) Molecular orientation at the skin layer of the molding depends on many factors such as shear, normal and elongational stresses action during the filling of the polymer into the mold cavity, the relaxation time of polymer molecules, the polymer chain rigidity, and the crystallization rate or kinetics of the polymer used. Basically, a long relaxation time combined with a high crystallization rate will produce a higher

molecular orientation in the flow direction at the skin layer of the molding. An increase of the chain rigidity increases the degree of the orientation at this layer.

2) For slowly crystallizing polymers such as PET, the crystallinity in the thickness direction depends on the mold temperature. In fact, for low mold temperatures (lower than 70°C), the maximum crystallinity was observed at the subskin layer, (at about 0.4 mm from the external surface of the molding) due to the shear-induced crystallization process generated during the filling stage. The skin and the core layers of the molding were found to be essentially amorphous at these mold temperatures. By increasing the mold temperature to higher values (higher then 70°C), the maximum of crystallinity was found to shift from the subskin layer to the skin layer of the molding. This is due to the decrease of the thickness of this layer with the increase of the mold temperature.

3) For PET, molecular orientation in the thickness direction was found to have much the same distribution as the crystallinity of the polymer. It has been therefore concluded that the presence of the crystallinity during the filling stage (shear-induced crystallization) improves the degree of molecular orientation in the flow direction since it helps to preserve the orientation generated in that stage and reduces the relaxation process of the polymer molecules.

The Hermans orientation function used to characterize the orientation in the injected PET has been derived to measure molecular orientation in uniaxial oriented specimens. Biaxial degree of molecular orientation can not therefore be characterised using this function. In the second part of this study, we have proposed a new approach for the characterization of molecular orientation in uniaxially and biaxially stretched samples of PET. Basically, this approach consits of comparing spectra measured on the surface of an oriented specimen to those measured on the surface of a non-oriented specimen. In each polarization direction, the difference between these spectra can be used to characterize the degree of orientation in the oriented specimens.

Such an approach has been tested using uniaxially and biaxially stretched samples of PET and the obtained results have proved its efficiency. Moreover, this approach has been used to measure the molecular orientation at the surface of injection blow molded bottles of PET and HDPE. The obtained results are summarized in the annex A and will be submitted for a new publication.

TABLE DES MATIÈRES

LISTE DES TABLEAUX

LISTE DES FIGURES

LISTE DES SIGLES ET ABRÉVIATIONS

A_{ij} : intensité d'absorption d'un groupement moléculaire (i) dans une direction de polarisation (j)

A_o : intensité d'absorption pour un échantillon non orienté

A(H,h) : relaxation de déformation par unité de hauteur provoquée par une contrainte unitaire se trouvant à une distance y de la surface de l'échantillon lorsque la profondeur du trou est égale à h

a_o : constante

a_1 : constante

B : largeur du moule d'injection

C : constante (stress optical coefficient)

C_p : chaleur spécifique

D : rapport dichroic

D : tenseur de taux de déformation

E : module d'élasticité

f_H : fonction d'orientation de Hermans

f^B_{cM}, f^B_{cT} : fonctions d'orientation de White et Spruiell

G_1 : module du ressort du modèle de Maxwell

G_2 : module du ressort du modèle de Kelvin-Voigh

h : profondeur du trou

k : taux de déformation des particules du polymère

K_i : constante de calibration

n : indice de la loi de puissance

n_i : indice de réfraction dans la direction (i)

N_1 : première différence des contraintes normales

$N(\theta,\phi,\Psi)$: fonction de distribution de probabilité d'orientation

P_{lmn} : coefficient dans l'expression de $N(\theta,\phi,\Psi)$

r : rayon de courbure de l'échantillon

R : reflectance

R_j : rapport d'intensité des pics d'absorption à 1265 et 1725 cm^{-1}, mesurés à partir d'un échantillon en PET dans une direction de polarisation (j)

R_0 : rapport d'intensité des pics d'absorption à 1265 et 1725 cm^{-1} correspondant à un échantillon en PET non orienté

t : temps

t_1 : durée de trempe de la couche peau

t_2 : durée de trempe totale

T : température

T_o : température du polymère avant trempe

T_f : température du polymère après trempe

T_g : température de transition vitreuse du polymère

V : vitesse moyenne du front d'écoulement

V : vecteur vitesse

x : abcisse du centre de l'échantillon courbé

y : ordonnée du centre de l'échantillon courbé

z_{lmn} : fonction généralisée de Legendre

$2z_o$: épaisseur de l'échantillon

α : angle entre le moment de transition d'un groupement moléculaire et l'axe de la chaîne

γ : taux de cisaillement

λ : temps de relaxation moyen des chaînes moléculaires

θ : angle entre l'axe de la chaîne de polymère et la direction d'étirement

ϕ_o : spectre "structure factor"

$\phi_{//}$: fonction de polarisabilité mesurée parallèlement à la direction d'étirement

$\phi_{\perp}$: fonction de polarisabilité mesurée perpendiculairement à la direction d'étirement

σ_i : contrainte dans la direction (i)

σ : tenseur de contrainte de Cauchy

Δn : birefringence

Δ° : birefringence maximale

$\Delta\epsilon$: variation de la déformation

μ : coefficient de Poisson

μ_1 : viscosité du modèle de Maxwell

μ_2 : viscosité du modèle de Kelvin-Voigh

η : viscosité du polymère

$v(p,T)$: volume spécifique

ϵ_i : déformation dans la direction (i)

ρ : densité

ρ_i : courbure de l'échantillon dans la direction (i)

τ_{ij} : contrainte de cisaillement

χ : taux de cristallinité du polymère

CHAPITRE I

INTRODUCTION GÉNÉRALE

1.1 INTRODUCTION

De nos jours, les matériaux plastiques et composites sont de plus en plus utilisés pour remplacer les matériaux conventionnels dans plusieurs applications telles que l'électronique, l'aréospacial et l'aéronautique, l'automobile et les transports, etc. Ces matériaux présentent un bon rapport qualité prix. En effet, ils peuvent être transformés très facilement et en très grandes séries, ce qui diminue le prix de revient des produits finis. De plus, la majorité des procédés de transformation de ces matériaux permettent d'obtenir directement des produits finis qui ne nécessitent presqu'aucune opération d'usinage ou de finition. Toutefois, les caractéristiques mécaniques et optiques de ces matériaux après transformation dépendent beaucoup des paramètres de mise en oeuvre. Il est donc important de bien étudier la morphologie de ces matériaux pour mieux caractériser leur comportement sous diverses sollicitations.

Plusieurs techniques de transformation telles que le moulage par injection, l'extrusion et le soufflage peuvent considérablement affecter la morphologie (orientation moléculaire et cristallinité) des polymères thermoplastiques. Pour les polymères amorphes, le degré d'orientation à travers l'épaisseur des produits finis dépend essentiellement du taux

d'étirement (ou de cisaillement) de la matière durant la phase de transformation, du temps de relaxation des chaînes moléculaires et de la vitesse de refroidissement de la matière. Plus le temps de relaxation est grand et la vitesse de refroidissement de la matière est rapide, plus le degré d'orientation des chaînes moléculaires généré durant la phase de transformation est conservé. Dans les polymères semi-cristallins, la présence de la cristallinité avant et durant la phase de refroidissement peut aussi affecter le degré d'orientation final. Ce point n'a pas été largement discuté dans la littérature, vu que dans la majorité des travaux publiés, on utilise des polymères ayant une très grande vitesse de cristallisation. Le choix de ce type de polymère ne permet pas une caractérisation facile de la relation entre la cristallinité et l'orientation moléculaire durant et après le la phase de transformation.

L'orientation moléculaire dans les produits finis peut être caractérisée par diverses techniques. Parmi celles-ci, on distingue la spectroscopie infrarouge et la biréfringence optique. La spectroscopie infrarouge permet de caractériser l'orientation de chacun des groupements moléculaires de la chaîne. Par contre, la biréfringence est une mesure de l'orientation moléculaire totale dans l'échantillon considéré. Ces deux techniques peuvent être utilisées soit en mode de transmission (pour des échantillons de très faible épaisseur) ou en mode de réflexion. Dans ce dernier cas, l'échantillon doit avoir une excellente qualité de surface.

1.2 PRINCIPE DE MESURE DE L'ORIENTATION MOLÉCULAIRE PAR LA TECHNIQUE DE SPECTROSCOPIE INFRAROUGE EN MODE DE RÉFLEXION

Le principe de mesure de l'orientation moléculaire par la technique de spectroscopie infrarouge en mode de réflexion est présenté sur la Figure 1.1. Un rayon infrarouge polarisé, appelé rayon incident, est appliqué sur la surface de l'échantillon. Ce rayon est formé par un ensemble de photons qui possèdent différentes longueurs d'onde, donc différentes fréquences.

Lorsque ces photons arrivent sur la surface de l'échantillon, certains photons seront absorbés, le reste sera réfléchi. Chaque groupement moléculaire vibrant à une fréquence spécifique absorbera (par résonnance) les photons qui ont la même fréquence que lui. Si tous les groupements moléculaires de la chaîne vibrent à des fréquences différentes, on aura donc un spectre d'absorption. Dans ce spectre, l'absorption de chaque groupement moléculaire est donnée par :

$$I = C.(\vec{E}.\vec{M})^2 = (E \,.\, M\cos\theta)^2 \qquad (1.1)$$

où C est une constante, E est le vecteur champ électrique, M est le vecteur de transition du groupement moléculaire considéré (parallèle à la direction de vibration de ce groupement) et θ est l'angle entre E et M. D'après cette équation, si E et M sont parallèles, alors θ est nulle et l'absorption est maximale. Dans le cas contraire, si E et M sont perpendiculaires,

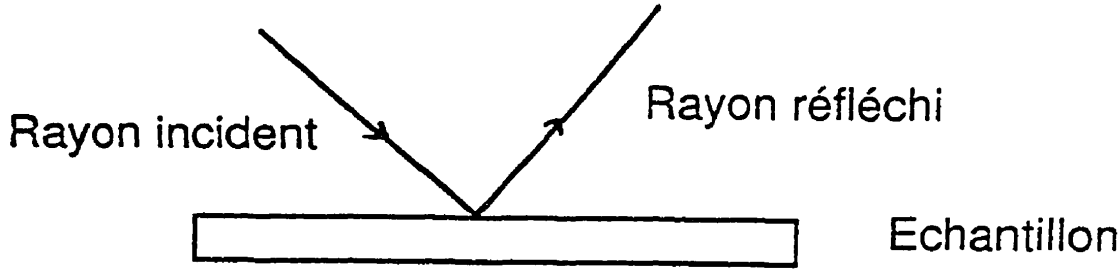

Figure 1.1 - Principe de mesure de l'orientation moléculaire par la technique spectroscopie infrarouge en mode de réflexion

alors θ est égale à 90° et l'absorption est nulle. La Figure 1.2 illustre l'effet de la direction de polarisation sur le degré d'absorption du groupement carbonyl C=O.

Dans un spectre infrarouge mesuré dans une direction de polarisation spécifique, la présence d'une absorption maximale pour un groupement moléculaire quelconque indique que ce dernier est orienté parallèlement à cette direction de polarisation. Connaissant la position (angle) de ce groupement moléculaire par rapport à l'axe de la chaîne, on peut donc très facilement prédire l'orientation de celle-ci par rapport à la direction de polarisation utilisée. Ainsi, à partir de deux spectres infrarouges mesurés dans deux directions de polarisation mutuellement perpendiculaires, on peut identifier la composition chimique du polymère considéré et le degré d'orientation de ses chaînes moléculaires.

1.3 PRINCIPE DE LA TECHNIQUE DE MICROTOMIE

Pour caractériser l'orientation moléculaire à travers l'épaisseur des produits finis, on fait souvent appel à la technique de microtomie, Figure 1.3. Cette technique permet d'obtenir, par découpage, des échantillons de très faibles épaisseurs. Ces échantillons seront ensuite analysés en utilisant l'une des deux techniques citées ci-haut pour déterminer la distribution de l'orientation moléculaire à travers l'épaisseur des produits finis.

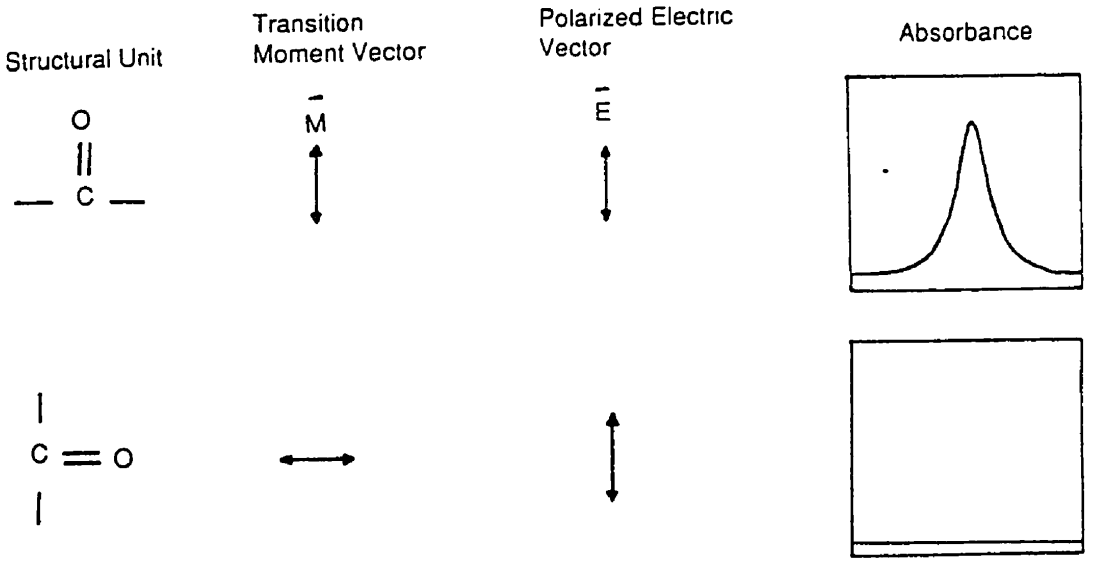

Figure 1.2 - Effet de la direction de la polarisation sur le degré d'absorption du groupement moléculaire C=O

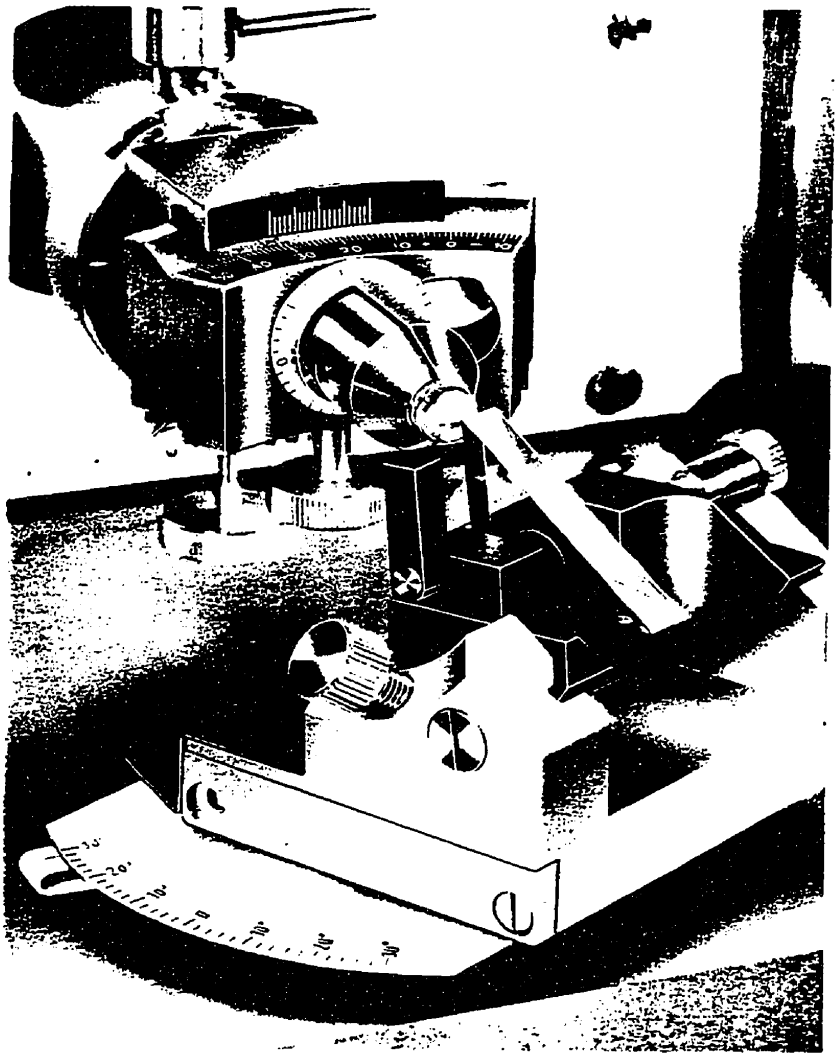

Figure 1.3 - Machine de microtomie

Les contraintes mécaniques et thermiques générées dans les échantillons découpés durant la microtomie peuvent facilement affecter le degré d'orientation des chaînes moléculaires dans ces échantillons. Dans le cas des produits fortement orientés, tels que ceux obtenus par étirage à hautes températures, l'effet de la microtomie sur l'orientation moléculaire peut être négligé. Par contre, dans le cas des produits ayant une orientation faible ou moyenne, tels que ceux obtenus par injection, l'effet de la microtomie ne peut plus être négligé vu que cette technique peut générer dans les échantillons découpés un niveau d'orientation égale à celui généré dans le produit fini durant son obtention. Cela pose donc un problème de taille pour la caractérisation de l'orientation moléculaire dans les pièces plastiques. Récemment, certains auteurs ont confirmé que les résultats obtenus par la technique de microtomie sont des résultats relatifs et ne peuvent pas être considérés comme absolus. Il faut donc trouver une autre technique de substitution pour une meilleure caractérisation de l'orientation moléculaire dans les pièces plastiques.

D'autres techniques de transformation des matériaux plastiques, telle que l'extrusion-soufflage, génèrent une orientation biaxiale dans les produits finis. Pour mesurer le degré d'orientation dans ces produits dans différentes directions, on utilise généralement la technique de biréfringence. La mesure de l'orientation biaxiale par la technique de spectroscopie infrarouge est plutôt une tâche très difficile. Pour ce faire, il faut mesurer trois spectres dans trois directions de polarisation mutuellement perpendiculaires. En pratique, on mesure souvent deux spectres sur la surface du produit fini dans deux directions de polarisation mutuellement perpendiculaires et un spectre à travers l'épaisseur. Dans une

direction de polarisation spécifique, la différence entre un spectre mesuré sur la surface et le spectre obtenu à travers l'épaisseur détermine le degré d'orientation des chaînes moléculaires dans cette direction de polarisation. Toutefois, les produits biorientés sont généralement des films biaxialement étirés ou soufflés, donc de très faible épaisseur. Cela ne permet pas une mesure facile des spectres à travers l'épaisseur, ce qui rend la caractérisation de l'orientation biaxiale par la technique de spectroscopie infrarouge très difficile, voir impossible dans certains cas. Si cette technique peut brillamment caractériser l'orientation uniaxiale, elle peut sûrement caractériser l'orientation biaxiale. Peu d'efforts ont été faits dans la littérature dans ce sens. Résoudre ce problème, c'est aussi permettre à la technique de spectroscopie infrarouge d'être plus compétitive dans le domaine de la caractérisation de la morphologie des pièces plastiques.

Le but de cette thèse est d'étudier la morphologie des pièces en polyéthylène téréphthalate (PET) obtenues par injection et injection-soufflage. En particulier, nous avons voulu étudier la relation entre la cristallinité et l'orientation moléculaire dans ce type de pièces. Cette thèse est divisée en quatre chapitres. Chacun de ces chapitres a fait l'objet d'une publication séparée. Les résumés de ces publications ainsi que les liens entre elles sont présentés dans ce qui suit.

1.4 SYNTHÈSE DES ARTICLES ET LIEN AVEC L'ENSEMBLE DES TRAVAUX

Dans cette synthèse, nous résumons les résultats obtenus dans ce travail de doctorat. Ce résumé sera bref et nos résultats seront discutés avec plus de détails dans les chapitres 2, 3, 4, 5 et dans l'annexe A.

Dans la première partie de cette thèse, chapitre 2, nous présentons une revue sur les résultats de la récente littérature expliquant les origines et la naissance des phénomènes d'orientation moléculaire, de cristallinité et des contraintes résiduelles dans les pièces obtenues par injection et injection-soufflage. Les différentes techniques utilisées pour mesurer ces phénomènes sont aussi présentées dans cette revue. Cette étude, nous a permis de mieux encadrer notre travail et interpréter nos résultats.

Tel que discuté précédemment, la caractérisation de l'orientation moléculaire dans l'épaisseur des pièces plastiques souffre de l'effet de la microtomie sur les caractéristiques des échantillons découpés. Dans la littérature, aucune technique de substitution n'a été proposée. Dans le chapitre 3 de cette thèse, on a proposé une nouvelle technique de caractérisation de l'orientation moléculaire dans l'épaisseur des pièces plastiques.

Cette technique consiste à usiner l'échantillon par fraisage jusqu'au niveau où l'on veut mesurer l'orientation moléculaire et à polir la surface fraisée. Les conditions de fraisage

et de polissage adoptées sont résumées dans le chapitre 3. L'orientation moléculaire au niveau de la surface polie a été caractérisée par la technique de spectroscopie infrarouge en mode de réflexion. Cette technique a été choisie car elle permet non seulement de mesurer le degré d'orientation des différents groupements moléculaires de la chaîne mais aussi de caractériser tout changement dans la configuration de ces chaînes après les opérations de fraisage et de polissage.

Cette technique de fraisage et de polissage a été testée sur plusieurs polymères ayant des propriétés thermiques (température de transition vitreuse) et mécaniques différentes. Ces polymères sont le polyéthylène téréphtalate (PET, Tg=70°C), le polyetherethercétone (PEEK, Tg=150°C), le polyéthylène à haute densité (HDPE, Tg=-120°C) et les polymères à cristaux liquides (LCP). Les PET, PEEK et HDPE ont été étirés à des taux d'étirement différents, à des températures supérieures à leur température de transition vitreuse pour obtenir des échantillons uniaxialement orientés. Par contre, le LCP a été injecté vu la difficulté d'orienter ces chaînes moléculaires dans une machine de traction. Des spectres infrarouges ont été initialement mesurés sur les surfaces de ces échantillons dans des directions de polarisation mutuellement perpendiculaires. Puis ces échantillons ont été fraisés et polis et des spectres infrarouges ont été mesurés sur les surfaces polies. Ces surfaces se trouvaient à une distance égale à 0.2 mm de la surface externe de chaque échantillon. Une comparaison entre les spectres mesurés avant et après le fraisage et le polissage, Figure 1.4, a montré que cette technique ne change pas le degré d'orientation dans les polymères ayant une température de transition vitreuse assez élevée, tels que le PET et le PEEK. En effet, pour ce type de

matériaux, les spectres obtenus avant et après fraisage et polissage se ressemblaient beaucoup, indiquant la présence du même degré d'orientation dans les surfaces mesurées. De plus, et contrairement aux mesures réalisées sur les surfaces de ces polymères, les mesures réalisées après fraisage et polissage ont montré une meilleure qualité des spectres dans différentes directions de polarisation (ligne de base, intensité, etc.), ce qui permet une meilleure caractérisation du degré d'orientation des chaînes moléculaires dans ces polymères. Dans le cas des polymères à faible température de transition vitreuse, tel que le HDPE, la technique de fraisage et de polissage change le degré d'orientation dans les échantillons utilisés. Ce changement est dû à la relaxation des chaînes polymériques durant le polissage. Ce phénomène de relaxation peut être évité en améliorant les conditions de refroidissement de l'échantillon durant cette phase de préparation (en utilisant de l'azote liquide à la place de l'eau). Pour le cas des polymères à cristaux liquides (LCP) injectés, les résultats obtenus coïncident avec ceux publiés dans la récente littérature et montrent que le degré d'orientation des chaînes moléculaires dans les couches intermédiaires du LCP est plus faible que celle générée dans la couche peau. Ces résultats , ainsi que ceux obtenus précédemment pour le PET et le PEEK indiquent que la technique de fraisage et de polissage peut remplacer avantageusement la technique de microtomie (trop chère) et qu'elle peut être utilisée pour mieux caractériser l'orientation moléculaire dans le coeur des pièces plastiques ayant une température de transition vitreuse et une rigidité des chaînes élevées.

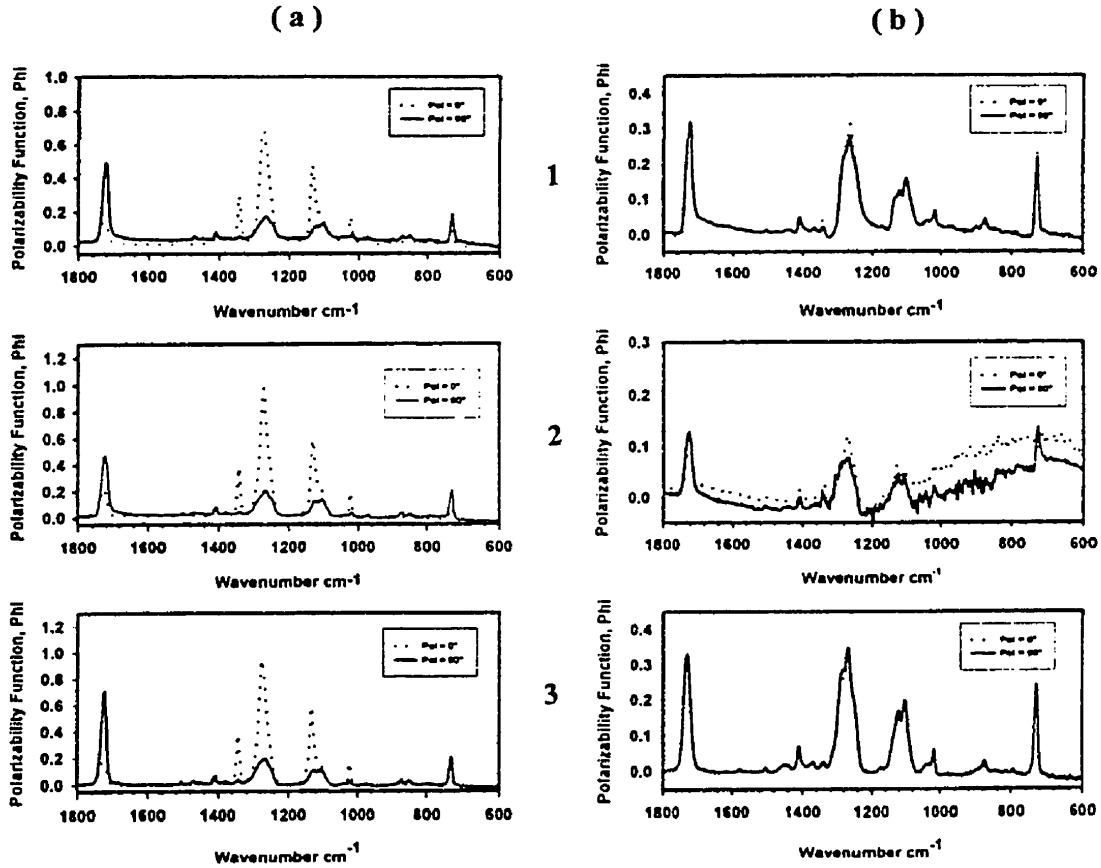

Figure 1.4 - Spectres infrarouges mesurés sur la surface d'un échantillion en PET orienté (a) et non orienté (b) avant (1), pendant (2) et à la fin (3) du fraisage et polissage

En effet, cette technique de fraisage et polissage a été utilisée pour étudier la morphologie (orientation moléculaire et cristallinité) dans chaque couche à travers l'épaisseur des pièces en PET injectées. Les résultats de ce travail sont résumés dans le chapitre 4. Ce matériau a été utilisé car il a une faible vitesse de cristallisation. En faisant varier les paramètres de moulage, la température du moule dans notre cas, on peut facilement affecter sa cristallinité. Cela va nous permettre d'étudier la relation entre la cristallinité et l'orientation moléculaire dans ce type de matériau. De plus, dans cette étude, nous avons utilisé d'autres polymères ayant des caractéristiques rhéologiques et de cristallisation très différentes. Ces polymères sont le HDPE, PS et les LCP. Ces polymères ont été injectés et l'orientation moléculaire à la surface des pièces obtenues, ainsi que dans les pièces en PET, a été mesurée en utilisant la technique de spectroscopie infrarouge en mode de réflection. À partir de deux spectres mesurés parallèlement et perpendiculairement à la direction d'écoulement de la matière dans le moule, le degré d'orientation des chaînes moléculaires peut être calculé en utilisant la fonction d'orientation de Hermans (f) suivante (équation 4.2) :

$$f = \frac{D - 1}{D + 2} \frac{2}{3\cos^2\alpha - 1}$$

où $D = A_{//} / A_{\perp}$ est le rapport dichroic d'un groupement moléculaire spécifique et $A_{//}$ et $A_{\perp}$ représentent respectivement l'absorption de ce groupement moléculaire dans des spectres mesurés parallèlement et perpendiculairement à la direction d'écoulement; α étant l'angle entre la direction du moment de transition du groupement moléculaire considéré et l'axe de la chaîne. Le degré de cristallinité du PET dans chaque couche à travers l'épaisseur des

pièces injectées est proportionnel à l'aire sous le pic d'absorption à 1340 cm^{-1} dans le spectre appelé "Structure factor spectrum ϕ_o" définie comme suit (équation 4.4) :

$$\phi_o = \frac{1}{3}\phi_{//} + \frac{2}{3}\phi_{\perp}$$

où $\phi_{//}$ et $\phi_{\perp}$ sont respectivement les spectres mesurés avec une polarisation parallèle et perpendiculaire à la direction d'écoulement. Les résultats de cette étude peuvent être résumés comme suit (Figures 1.5 et 1.6) :

1) L'orientation moléculaire dans la couche peau des pièces injectées dépend, en plus des contraintes élongationnelles et de cisaillement générées lors du remplissage du moule, du temps de relaxation des chaînes moléculaires, de la rigidité de la chaîne moléculaire et de la vitesse de cristallisation du polymère utilisé. Il a été noté que plus le temps de relaxation est important et la vitesse de cristallisation du polymère est rapide, plus l'orientation moléculaire dans la couche peau est importante. De plus, il a été remarqué qu'une augmentation de la rigidité des chaînes moléculaires augmente le degré d'orientation dans cette couche. Ce résultat a été noté en comparant le degré d'orientation à la surface des LCP à celui obtenu pour le reste des matériaux utilisés. En effet, il est bien connu que les polymères à cristaux liquides ont une rigidité des chaînes moléculaires beaucoup plus importante que celle des polymères conventionnels. À la température de fusion de ce type de polymère, les chaînes

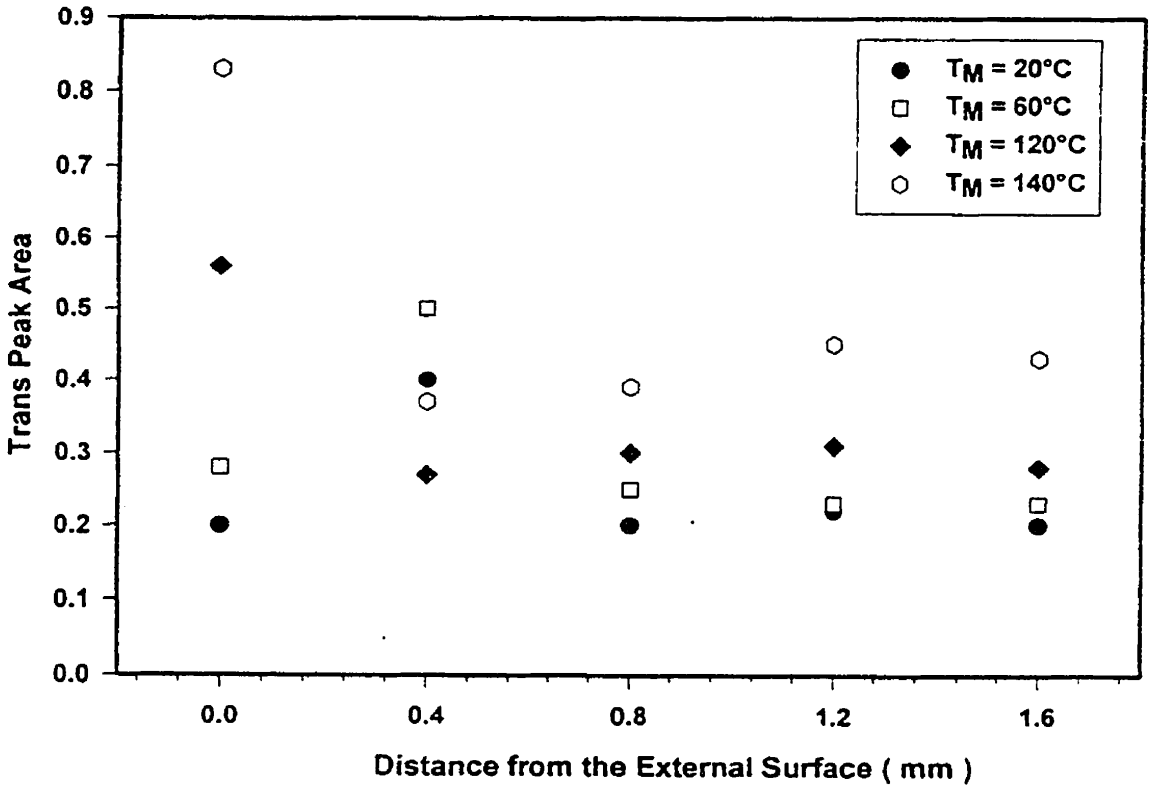

Figure 1.5 - Distribution de la cristallinité à travers l'épaisseur du PET injecté (près du seuil) pour différentes températures du moule d'injection

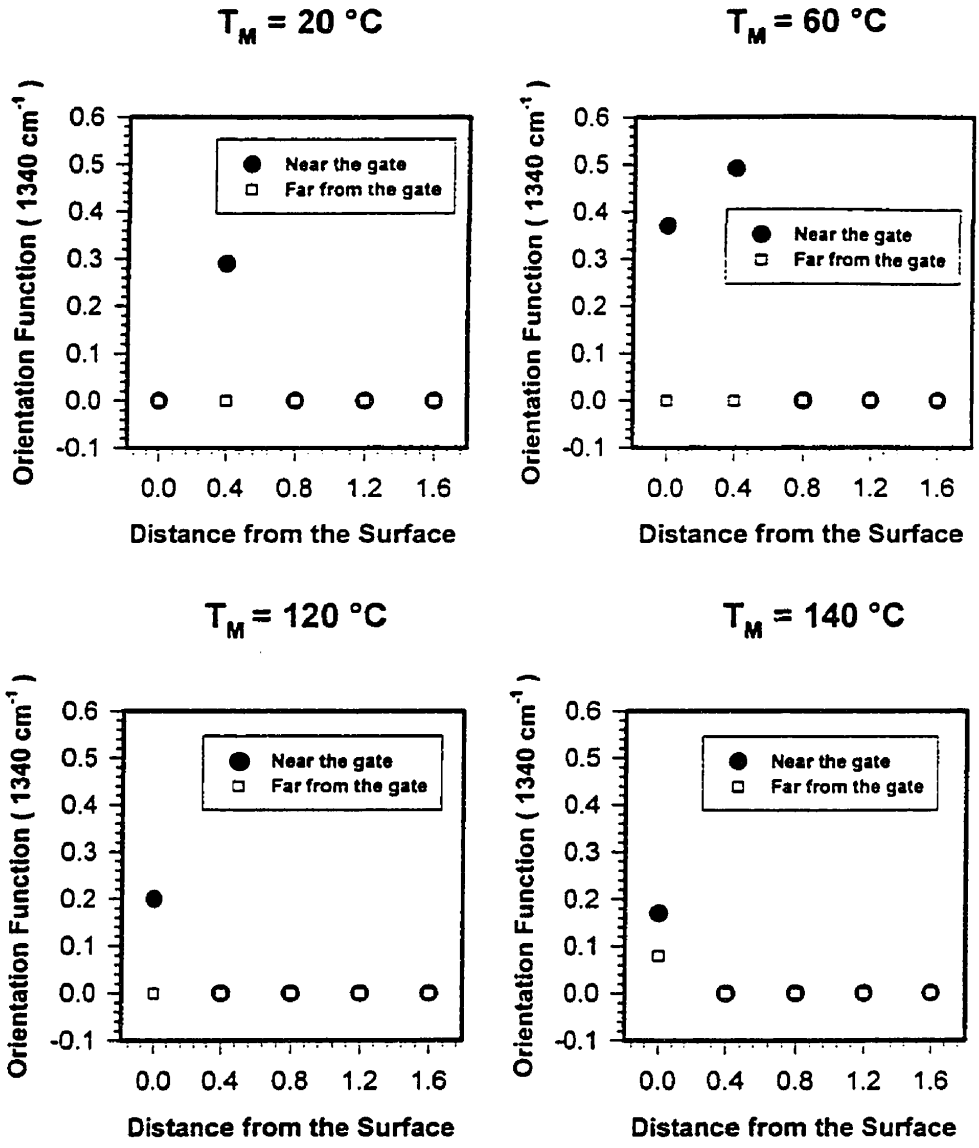

Figure 1.6 - Distribution de l'orientation moléculaire à travers l'épaisseur du PET injecté pour différentes températures du moule d'injection

polymériques se regroupent ensemble pour former des cristaux à l'état liquide, d'ou leur nom polymères à cristaux liquides. Durant la phase de remplissage, et à cause de l'effet élongationnel au niveau du front d'écoulement, ces cristaux vont s'orienter dans la direction d'écoulement de la matière, obligeant par conséquent les chaînes qui les forment à s'orienter dans cette direction. Vu que ces chaînes appartiennent déjà à un réseau cristallin, même avant leur orientation dans le moule, cela va donc empêcher leur relaxation lors d'un éventuel refroidissement.

2) Pour le cas du PET, la distribution de la cristallinité dans l'épaisseur dépend considérablement de la température du moule utilisée. Pour des faibles températures du moule, inférieures à la température de transition vitreuse du PET (T_g = 70°C), on a noté un minimum de cristallinité dans la couche peau et dans le coeur des pièces injectées et un maximum de cristallinité dans les couches intermédiaires (situées à une distance égale à 0.4 mm de la surface externe de l'échantillon). Ce maximum de cristallinité dans ces couches est due au phénomène de cristallisation sous tension ou (shear-induced crystallization), favorisé par la forte orientation des chaînes moléculaires dans cette zone. En effet, plus les chaînes polymériques sont orientées, plus elles deviennent parallèles les unes aux autres, et cela va leur permettre de se cristalliser très rapidement même à de très hautes températures. Ce phénomène de cristallisation sous contrainte (shear-induced crystallization) a fait l'objet de

plusieurs recherches dans la littérature récente et il a été montré qu'il peut se manifester durant le cisaillement de la matière à de hautes températures et que plus le temps de cisaillement augmente, plus la cristallinité du polymère augmente.

De plus, pour le cas du PET, nous avons noté qu'en augmentant la température du moule à des valeurs supérieures à la température de transition vitreuse du PET, le maximum de cristallinité (shear-induced crystallization process) se déplace de la couche intermédiaire à la couche peau. Ce déplacement est dû à la diminution de l'épaisseur de cette couche en augmentant la température du moule.

3) L'orientation moléculaire à travers l'épaisseur du PET injecté a la même distribution que la cristallinité de la matière (shear-induced crystallization). Ce résultat montre que la présence de la cristallinité lors du remplissage du moule (shear-induced crystallization) diminue la relaxation des chaînes moléculaires et conserve, en partie, le degré d'orientation généré durant cette phase.

Les distributions de la cristallinité à travers l'épaisseur du PET injecté discutées ci-haut concordent avec celles récemment publiées dans la littérature. Cela montre, encore une autre fois, que la technique de fraisage et polissage proposée dans le chapitre 3 peut être

considérée comme une technique fiable pour la caractérisation de la morphologie des pièces plastiques ayant une température de transition vitreuse assez élevée.

La fonction d'orientation de Hermans utilisée précédemment, chapitre 4, a été développée pour caractériser l'orientation moléculaire dans des échantillons uniaxialement orientés, tels que ceux obtenus par étirage ou moulage par injection. Pour déterminer le degré d'orientation des chaînes dans ces échantillons, nous aurons besoin de deux spectres mesurés dans deux directions de polarisation mutuellement perpendiculaires. Pour chaque pic d'absorption, le rapport $A_{//}$ / $A_{\perp}$ doit être calculé pour déterminer la fonction d'orientation (f). Pour le cas des échantillons biaxialement orientés, tels que ceux obtenus par injection-soufflage par exemple, l'équation d'orientation de Hermans (f) n'est plus valable. En effet, dans le cas d'une orientation équibiaxiale, $A_{//}$ et $A_{\perp}$ sont égales et (f) est nulle, indiquant qu'on est en présence d'un échantillon non-orienté. Il faudra donc proposer une autre équation d'orientation plus générale. Dans la dernière partie de notre thèse, chapitre 5, une nouvelle approche a été proposée pour déterminer le degré d'orientation des chaînes moléculaires dans des échantillons en PET uniaxialement et biaxialement orientés.

Cette approche consiste à comparer les spectres mesurés sur un échantillon orienté à ceux mesurés sur un échantillon non orienté. Dans une direction spécifique de polarisation, la différence entre ces spectres permet de caractériser le degré d'orientation des chaînes moléculaires dans l'échantillon orienté.

Contrairement à la fonction d'orientation de Hermans, dans cette étude, nous avons défini un autre rapport dichroic. Ce rapport, noté R, est égal au rapport des hauteurs des pics d'absorption à 1265 et 1725 cm^{-1}. Ces pics correspondent respectivement aux vibrations de certains groupements moléculaires orientés parallèlement et perpendiculairement à l'axe de la chaîne. Ces pics ont été choisis car le rapport de leur hauteur est très sensible à l'orientation.

Pour un échantillon orienté, dans une direction spécifique de polarisation (i), l'intensité d'absorption (A_i) d'un groupement moléculaire quelconque est donnée par (équation 5.4) :

$$A_i = A_o [\, 1 + f_i (3\cos^2\alpha - 1) \,]$$

où A_o est le degré d'absorption de ce groupement dans un échantillon non-orienté et f_i est la fonction d'orientation de l'échantillon orienté. Pour des échantillons biaxialement orientés, A_o peut être calculé en utilisant l'équation suivante (équation 5.6) :

$$A_o = \frac{1}{3} (A_M + A_T + A_N)$$

où M, N, et T représentent trois directions de polarisation mutuellement perpendiculaires, telles que les directions de longueur, largeur et épaisseur de l'échantillon. Si A_o est calculée, alors il devient possible de déterminer les fonctions d'orientation dans les échantillons biaxialement orientés. Toutefois, la mesure du degré d'absorption dans la direction de

l'épaisseur de l'échantillon, i.e direction N, est toujours complexe à réaliser. Une façon de contourner ce problème est d'utiliser le rapport R des hauteurs de deux pics dans le même spectre d'absorption. Si on note A_{1i} et A_{2i} les degrés d'absorption de ces deux pics dans une direction de polarisation spécifique (i), le rapport R est donné par (équation 5.8) :

$$R_i = \frac{A_{1i}}{A_{2i}} = \frac{A_{10}}{A_{20}} \frac{1 + f_i \ (3\cos^2\alpha_1 - 1)}{1 + f_i \ (3\cos^2\alpha_2 - 1)}$$

ce qui donne (équation 5.9) :

$$f_i = \frac{R_i - R_o}{R_o \ (3\cos^2\alpha_1 - 1) - R_i \ (3\cos^2\alpha_2 - 1)}$$

avec $R_o = A_{10} / A_{20}$ est le rapport dichroic obtenu à partir d'un échantillon nonorienté. Pour les pics d'absorption à 1265 et 1725 cm^{-1}, nous avons dérivé (voir le chapitre 5) l'équation d'orientation suivante (équation 5.10) :

$$f_i = \frac{R_i - 1.12}{0.657 + 0.528 \ R_i}$$

où R_i est le rapport des hauteurs de pics à 1265 et 1725 cm^{-1}.

Cette équation a été testée sur des échantillons de PET uniaxialement et biaxialement orientés et les résultats obtenus ont montré son efficacité. Il a été noté que dans le cas d'un échantillon uniaxialement orienté, l'équation de Hermans et notre approche donnent exactement les mêmes résultats. Dans le cas d'un échantillon biaxialement orienté, les résultats obtenus par notre approche coïncident avec ceux obtenus par la technique de biréfringence, largement utilisée pour caractériser l'orientation moléculaire dans des échantillons uniaxialement et biaxialement orientés.

Cette équation, ainsi qu'une autre équation semblable à celle-ci développée pour caractériser l'orientation uniaxiale et biaxiale dans des échantillons en HDPE, ont été utilisées pour mesurer l'orientation moléculaire à la surface des bouteilles en PET et HDPE obtenues par injection-soufflage. Les résultats de cette étude sont regroupés dans l'annexe A, et seront bientôt soumis pour une nouvelle publication.

CHAPITRE II

REVUE DE LA LITTÉRATURE

Dans cette étude, nous présentons et discutons les résultats de la littérature sur les origines et la distribution de l'orientation moléculaire, de la cristallinité et des contraintes résiduelles dans les pièces obtenues par injection et injection-soufflage. Ce travail nous permettra, dans une phase ultérieure, de bien encadrer notre recherche et mieux discuter nos résultats.

2.1 MOULAGE PAR INJECTION

Le moulage par injection est l'un des procédés de transformation des matériaux plastiques les plus utilisés après l'extrusion. Les caractéristiques de ce procédé ainsi que les caractéristiques des pièces injectées (orientation moléculaire, cristallinité et contraintes résiduelles) sont discutées en détail dans l'article inclus dans ce chapitre. Cet article est intitulé "The build-up and Measurement of Molecular Orientation, Crystalline Morphology and residual stresses in Injection-molded Parts: A Review".

2.2 MOULAGE PAR SOUFFLAGE

Le moulage par soufflage est un autre procédé largement utilisé de nos jours pour l'obtention des pièces creuses de petites et grandes dimensions. Dépendant du mode d'obtention de ces pièces, on distingue trois types de moulage par soufflage [1] : soit le procédé d'extrusion-soufflage (extrusion-blow molding), le procédé d'injection-soufflage (injection-blow molding) et le procédé d'étirage-soufflage (stretch-blow molding), Figure 2.1.

Le procédé d'injection soufflage est généralement utilisé pour obtenir des pièces (bouteilles) de petites dimensions (de volume inférieur ou égal à 350 ml). Dans ce procédé, il s'agit d'associer deux techniques : (i) la technique d'injection, reconnue pour sa précision dimensionnelle, sa rapidité, son contrôle des paramètres rhéologiques et sa répétitivité du cycle et (ii) la technique de soufflage qui est un moyen économique, rapide et fiable pour obtenir des corps creux. Le cycle d'injection-soufflage est le suivant :

1) l'injection d'un tube (préforme), dont les caractéristiques de géométrie et de température déterminent la qualité de la pièce à obtenir;
2) le tube est ensuite transféré dans une unité de soufflage;
3) le moule de soufflage est fermé et la préforme est étirée à la longueur du moule. Durant l'étirement, une faible pression est appliquée afin de décoller avec précaution la matière qui adhère encore au poinçon;

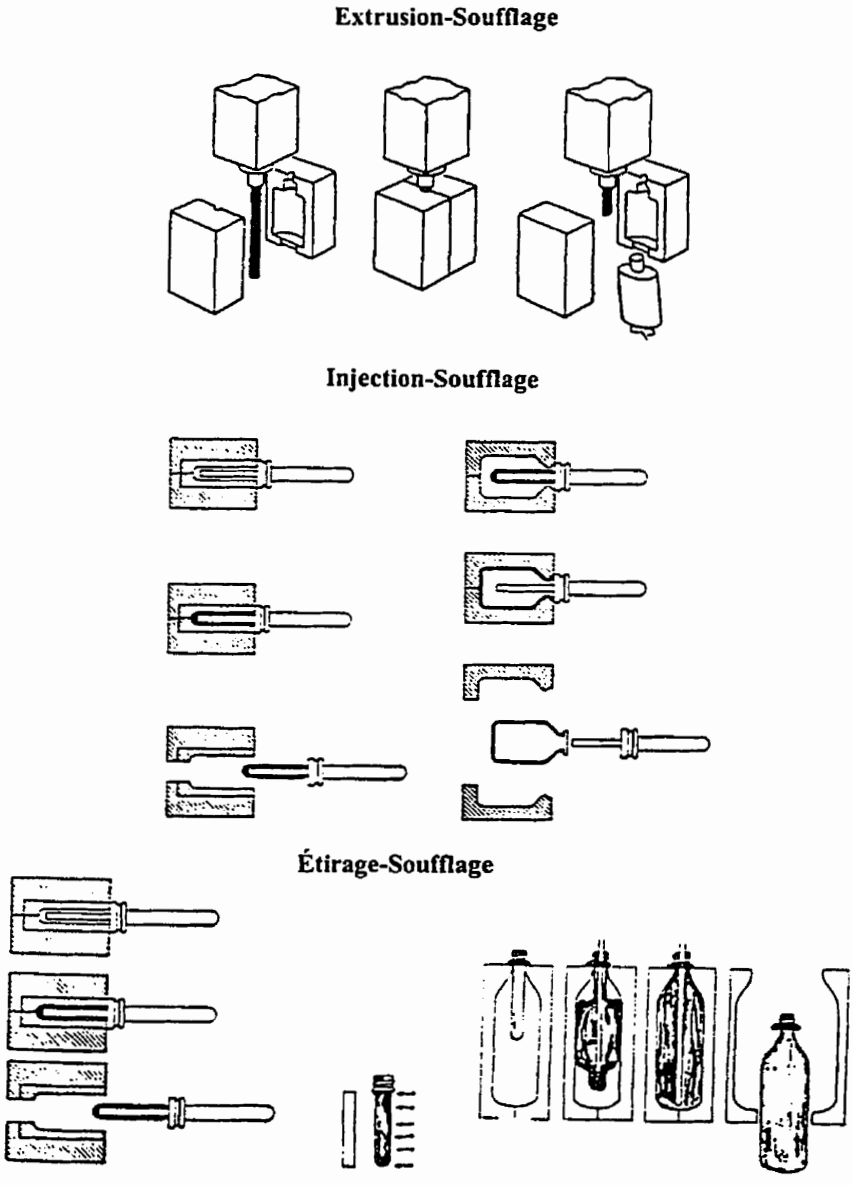

Figure 2.1- Différents types de moulage par soufflage [1]

4) le soufflage de la préforme à haute pression pour obtenir le développement complet de la matière contre les parois du moule de soufflage;
5) l'éjection de la pièce obtenue

et les caractéristiques du polymère qui peuvent affecter les propriétés des produits finis sont :

1) le dégré de déformation du polymère durant le soufflage;
2) la vitesse de cristallisation du polymère avant la phase de soufflage;
3) les vitesses de cristallisation du polymère durant les phases de soufflage et de refroidissement de la pièce dans le moule.

Plusieurs polymères peuvent être transformés avec succès par injection-soufflage (PE, PP, PS, PET, PVC, etc). Ces matériaux ouvrent ainsi à cette technique des débouchés nouveaux dans le domaine de la pharmacie, de la cosmétologie, de la parfumerie, etc., grâce aux qualités des articles réalisés par cette technique.

Durant la phase de soufflage, les chaînes de polymère dans les préformes (tubes) injectées peuvent s'orienter dans toutes les directions. Pour améliorer le degré d'orientation de ces chaînes, il faut que la température du polymère (préforme) soit supérieure ou égale à sa température de transition vitreuse. Plus la température du polymère augmente, plus le degré d'orientation lors du soufflage est important. Cependant, à de hautes températures du polymère, les chaînes moléculaires déjà orientées peuvent être facilement relaxées. Il y a

deux façons d'éviter ce phénomène de relaxation des chaînes moléculaires durant le refroidissement de la matière: (i) en augmentant la vitesse de refroidissement du polymère dans le moule ou (ii) en augmentant sa vitesse de cristallisation. La présence de la cristallinité durant la phase de soufflage peut diminuer le phénomène de relaxation des chaînes moléculaires et par conséquent conserver, en partie, l'orientation générée durant cette phase. Généralement, les pièces soufflées sont biaxialement orientées et le degré d'orientation dans chaque direction dépend des dimensions du moule de soufflage utilisé et des dimensions de la préforme..

Le comportement à l'étirage des polymères usuels utilisés pour la fabrication des corps creux biorientés est principalement déterminé par la morphologie initiale des préformes et son évolution lors de l'étirage. En pratique, trois types de comportements fondamentaux ont été observés [2]:

Première catégorie : Il s'agit des polymères amorphes. Ces polymères présentent une bonne transparence à l'état non orienté, mais bénéficient d'une amélioration limitée de leurs propriétés lors de l'étirage. La préforme injectée doit avoir un rapport L/D relativement faible pour éviter le problème de distorsion avant soufflage. Ces matériaux disposent d'une grande plage d'étirabilité. La biorientation s'effectuera à 10-30°C au-dessus de la température de transition vitreuse du polymère utilisé.

Deuxième catégorie : Il s'agit des polymères semi-cristallins ayant une vitesse de cristallisation très rapide, ne pouvant pas être obtenus à l'état amorphe par trempe, i.e PE, PP, etc. La structure cristalline de ces polymères est constituée par des sphérulites disposées de façon aléatoire et induisant, de ce fait, une opalescence marquée selon l'épaisseur du produit, et la taille des sphérulites.

La forme sphérulitique des zones cristallines a pour conséquence, au cours du biétirage, une forte tendance à la striction qui se traduit par une hétérogénéité très marquée d'étirage, rendant l'obtention des produits finis d'épaisseur uniforme particulièrement difficile. La biorientation de ce type de polymère a pour objectif d'améliorer les propriétés optiques des produits et leur résistance aux chocs, sans modification notable de leur rigidité. Elle s'effectue entre 5 et 30°C en dessous du point de fusion du polymère.

Troisième catégorie : Il s'agit des polymères semi-cristallins, pour lesquels, la préforme peut être moulée tout en conservant le polymère à l'état amorphe (PET). Pour ce type de polymère, lors de l'étirage, il se produit une cristallisation sous contrainte (shear-induced crystallization) qui, de ce fait, ne présente pas les caractéristiques de la forme sphérulitique ordinaire. Cette cristallisation régularise spontanément l'étirage du matériau et augmente considérablement le niveau d'orientation induit par la partie amorphe. De ce fait, se trouvent simultanément assurées les qualités de transparence, de brillance, de résistance aux chocs et de rigidité des produits finis. La biorientation, comme dans le cas des polymères amorphes, s'effectue de 10 à 30°C au-dessus de la température de transition vitreuse du polymère.

Cependant, elle nécessite un abaissement de température important lors du refroidissement de la matière.

Généralement, lors de la phase de soufflage, ce sont les points les plus chauds de la préforme qui commencent à s'étirer les premiers. Pour les polymères ayant une vitesse de cristallisation importante tels que le polyéthylène PE et le polypropylène PP, les points les plus froids et possédant une forte cristallinité ne seront pas facilement déformés, permettant ainsi au phénomène de soufflage de générer de grandes déformations dans les points les plus chauds de la préforme (formation des bulles). Cela favorisera soit l'éclatement des produits soufflés ou l'obtention de produits d'épaisseurs non uniformes. Pour le cas des polymères ayant une faible vitesse de cristallisation tel que le polyéthylène téréphtalate (PET), l'étirement des points chauds engendrera une cristallinité sous contrainte dans ces points (shear-induced crystallization), donc une augmentation de la rigidité de ces points. Plus le degré d'étirement augmente, plus le module de ces points augmente. Au moment où le module de ces points sera supérieur à celui des points adjacents, ce sont ces derniers points qui vont subir le phénomène de soufflage. À la fin de la phase de soufflage, les produits obtenus à partir de ce type de polymère auront donc des épaisseurs beaucoup plus uniformes que ceux obtenus en utilisant les polymères à haute vitesse de cristallisation.

Le degré d'orientation dans les produits soufflés dépend considérablement de la forme du moule de soufflage utilisé, des dimensions des préformes injectées et des paramètres de mise en oeuvre. La forme du moule dicte le taux d'étirement de la matière

dans chaque direction. Dans la pratique, on définit deux taux d'étirement H et A [3]. H étant le taux d'étirement dans la direction circonférentielle et A étant le taux d'étirement dans la direction axiale. Ils sont définis comme suit :

$$H = \frac{D_1}{D_2} \tag{2.1}$$

$$A = \frac{L_1}{L_2} \tag{2.2}$$

où D_1, L_1, D_2 et L_2 représentent respectivement le diamètre des produits finis, la longueur de ces produits, le diamètre de la préforme injectée et sa longueur. Ces deux taux de déformation peuvent être utilisés pour calculer un autre taux, appelé taux de déformation total BUR (blowup ratio) égale à :

$$BUR = H \cdot A = \frac{D_1}{D_2} \cdot \frac{L_1}{L_2} \tag{2.3}$$

Le BUR est largement utilisé dans la littérature. Pour générer une orientation biaxiale dans des bouteilles en PET, certains auteurs ont trouvé que le taux d'étirement dans la direction circonférentielle H doit être compris entre 4 et 7 et que le BUR doit être supérieure ou égale à 10 [3].

Pour mieux assimiler et analyser le phénomène d'orientation généré durant l'étirage et le soufflage des préformes, plusieurs auteurs ont utilisé des films de polymère et les ont orientés biaxialement. Ces films ont été orientés mécaniquement en utilisant deux modes d'étirement : soit le mode séquentiel ou le mode simultané d'étirement. Récemment, Chandran et Jabarin [4] ont présenté une comparaison entre la morphologie des films de PET obtenue en mode séquentiel d'étirement et celle obtenue après un mode simultané d'étirement. Les résultats de cette comparaison sont les suivants:

1) Lors de l'orientation uniaxiale du PET, le phénomène de cristallisation sous contrainte (shear-induced crystallization) se produit à des taux d'étirement supérieures ou égales à 2.5.
2) Pour les échantillons en PET équibiaxialement orientés, le mode simultané d'étirement génère le même degré d'orientation des chaînes dans les deux directions d'étirement. Dans le cas du mode séquentiel d'étirement, les chaînes polymériques s'orientent dans la deuxième direction d'étirement et leur degré d'orientation augmente avec le taux de déformation total BUR.
3) Pour des échantillons ayant subi des taux d'étirement différents dans les deux directions, le mode séquentiel d'étirement oriente d'abord les chaînes dans la première direction d'étirement. Plus le taux d'étirement augmente, plus le degré d'orientation dans cette direction augmente. Lorsque le taux d'étirement dépasse 2.5, on observe le phénomène de cristallisation sous contrainte (shear-induced crystallization). Durant la deuxième phase d'étirement, les chaînes

commencent à s'orienter dans la deuxième direction. A des valeurs importantes de BUR, les chaînes seront complètement orientées dans la deuxième direction d'étirement. Ce changement d'orientation de la première à la deuxième direction se fait à un BUR supérieure ou égale à 7.

Durant les différentes phases d'obtention des bouteilles (étirement de la préforme dans la direction axiale et soufflage), le polymère, dépendemment de la forme du moule de soufflage, peut subir l'un ou l'autre de ces deux modes d'étirement. Chaque mode d'étirement dictera la distribution finale de l'orientation moléculaire dans les produits moulés. De plus, l'existence d'un gradient de température le long des préformes ainsi qu'à travers l'épaisseur peut aussi affecter l'orientation moléculaire finale dans ces produits. Ainsi, pour bien caractériser la morphologie des produits soufflés, il est donc impératif de bien caractériser les conditions initiales de soufflage telles que la nature de la matière utilisée, la température de la matière avant soufflage, le taux d'étirement dans chaque direction, le mode d'étirement, etc.

Plusieurs auteurs ont étudié la morphologie (orientation moléculaire, cristallinité et contraintes résiduelles) des produits soufflés. Il a été trouvé que cette morphologie change à travers l'épaisseur [5], vue que les différentes couches de la préforme subissent, lors du soufflage, des sollicitations thermiques et mécaniques très différentes. Par exemple, Kamal et *al.* [6] ont trouvé, pour le cas des bouteilles en polyéthylène, que la cristallinité est maximale à la surface interne de la bouteille et minimale à la surface externe, Figure 2.2. Ce

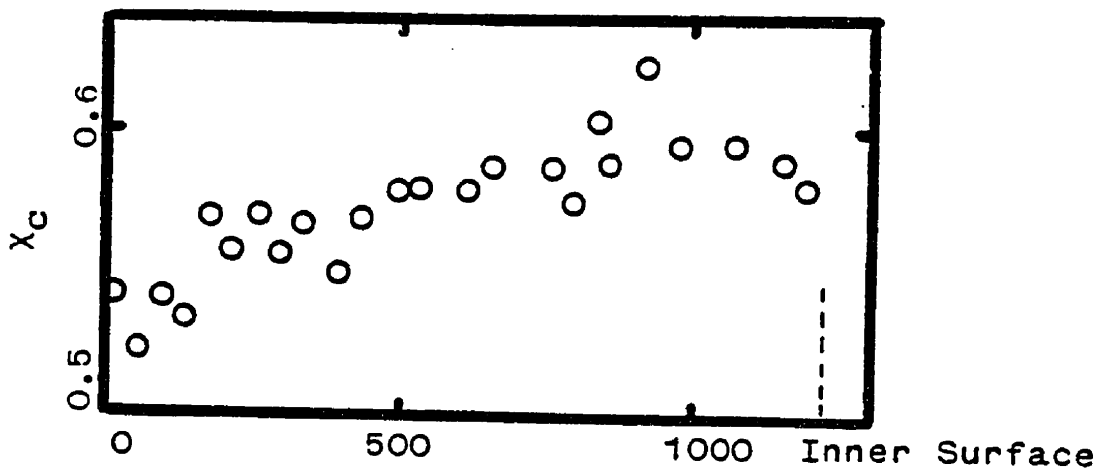

Figure 2.2 - Distribution de la cristallinité à travers l'épaisseur du PE soufflé [6]

minimum de cristallinité à la surface externe est due au phénomène de trempe que subit le polymère lorsqu'il touche aux parois du moule de soufflage. Cependant, à la surface interne, le polymère a suffisamment de temps pour se cristalliser et cela explique la forte cristallinité dans cette zone. L'orientation moléculaire change aussi à travers l'épaisseur des pièces soufflées. Elle est maximale à la surface externe et minimale à la surface interne [7], Figure 2.3. Le faible degré d'orientation moléculaire au niveau de la surface interne est due au phénomène de relaxation des chaînes lors de la phase de refroidissement.

Pour le cas du PET [5], il a été trouvé que la surface interne des bouteilles soufflées est plus orientée que la surface externe, indiquant par conséquent l'existence d'un gradient d'orientation à travers l'épaisseur de ces bouteilles . Cela est probablement due à l'existence d'un gradient de température dans cette direction.

Les contraintes résiduelles changent aussi à travers l'épaisseur des pièces soufflées. Ces contraintes sont principalement dues au phénomène de trempe que subit le polymère lorsqu'il touche aux parois du moule froid. Peu d'études ont été publiés pour étudier la distribution des contraintes résiduelles dans les produits soufflés. Selon Jeong et al [8], ces contraintes sont négatives au niveau des surfaces externes et positives sur les surfaces internes, Figure 2.4. Cette distribution des contraintes résiduelles peut être affectée par le changement des paramètres de mise en oeuvre. Par exemple, il a été trouvé que la diminution de la température du moule de soufflage change le niveau des contraintes dans les surfaces internes des bouteilles soufflées. En effet, cette dernière passe d'une contrainte de tension,

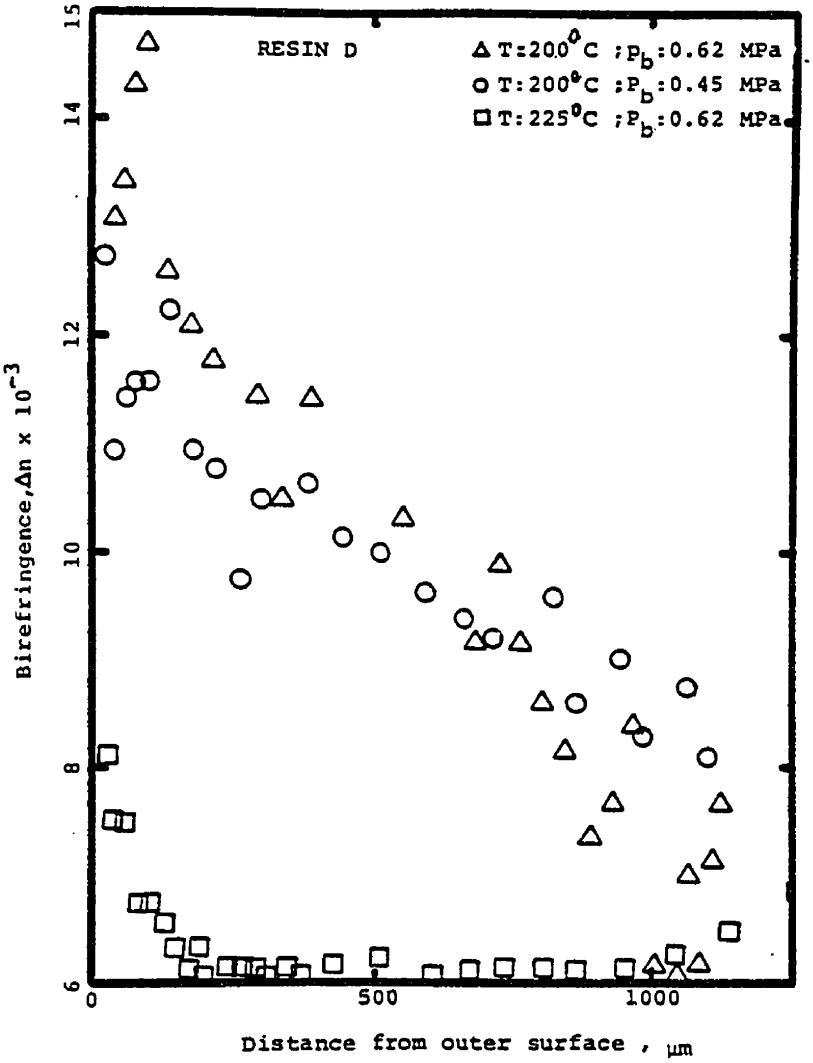

Figure 2.3 - Distribution de l'orientation moléculaire à travers l'épaisseur du PE soufflé [7]

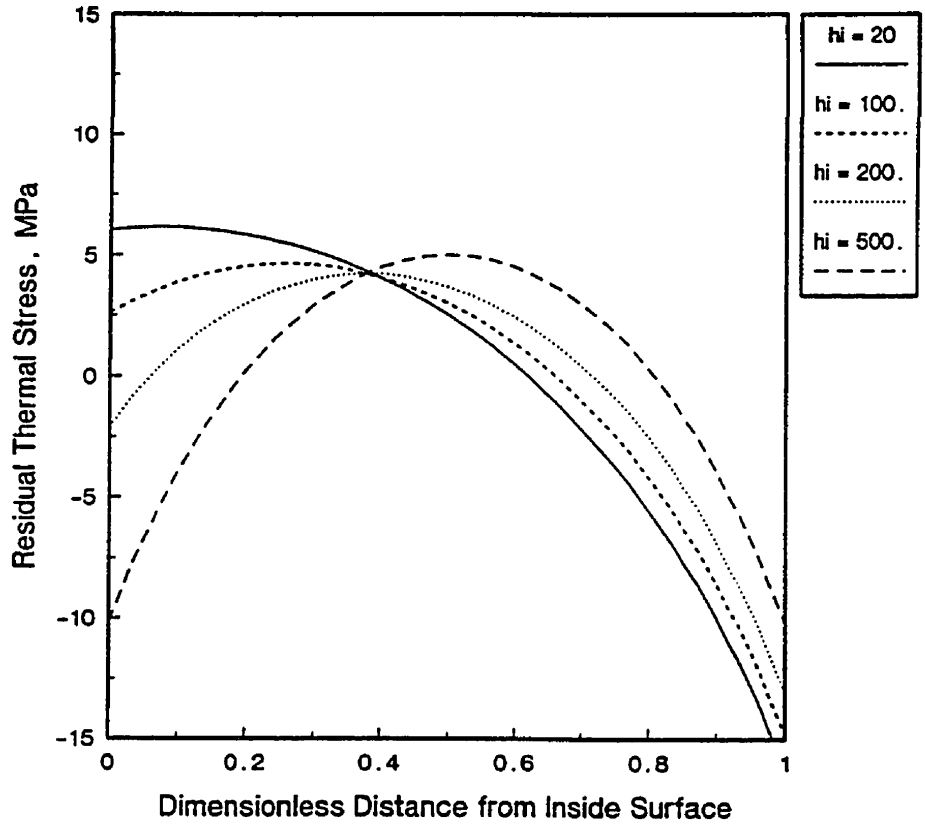

Figure 2.4 - Distribution des contraintes résiduelles à travers l'épaisseur des produits soufflés [8]

à des hautes températures du moule, à des contraintes de compression lorsque la température du moule devient très faible.

Les techniques utilisées pour mesurer l'orientation moléculaire et la cristallinité dans les produits soufflés sont les mêmes que celles utilisées pour caractériser la morphologie des pièces injectées. Une revue détaillée de ces techniques est présentée dans l'article inclus dans ce chapitre.

2.3 RÉFÉRENCES

1. ROSATO, D.V. et ROSATO, D.V. (1989). Blow Molding Handbook, Hanser Publishers.
2. BOST, J. (1982). Matières plastiques, II, technologie plasturgie, Technique et documentation Lavoisier.
3. LEE, N. (1990). Plastic Blow Molding Handbook, Chapman and Hall
4. CHANDRAN, P. et JABARIN, S. (1993). Biaxial Orientation of Poly (ethylene Terephthalate). Part III: Comparative Structure and Property Changes Resulting From Simultaneous and Sequential Orientation. Advances in Polymer Technology, 12, 153-165
5. CAKMAK, M., SPRUIELL, J.E. et WHITE, J.L. (1984). A Basic Study of Orientation in Poly (ethylene Terephthalate) Stretch-Blow Molded Bottles. Polymer Engineering and Science, 24, 1390-1395

6. KAMAL, M.R. et KALYON, D. (1983). Heat Transfert and Microstructure in Extrusion Blowmolding. Polymer Engineering and Science, 23, 503-509

7. KAMAL, M.R, KALYON, D. et TAN, V. (1982). Anisotropy and Dimensions of Blow-Molded Polyethylene Bottles, Polymer Engineering and Science, 22, 287-291.

8. YU, J.S et KALYON, D.M. (1991). Microstructure Development in Blow Molded Amorphous Engineering Plastics. Plastics, Rubber and Composites Processing and Applications, 15, 95-101.

2.4 THE BUILD-UP AND MEASUREMENTS OF MOLECULAR ORIENTATION, CRYSTALLINE MORPHOLOGY AND RESIDUAL STRESSES IN INJECTION MOLDED PARTS: A REVIEW

H. BEN DALY[1], K.T. NGUYEN[2*] and B. SANSCHAGRIN[1]

[1]Center of Applied Polymer Research (CRASP), École Polytechnique

C.P. 6079, Succ. Centre-Ville, Montréal, Québec, Canada H3C 3A7

[2]Industrial Materials Institute, National Research Council Canada,

75 De Mortagne Blvd., Boucherville, Québec, Canada, J4B 6Y4.

This chapter has been submitted for publication in Journal of Injection Molding Technology.

2.4.1 Abstract

Recently proposed mechanisms for the build-up of molecular orientation, crystalline morphology and residual stresses in injection-molded products are summarized. New advances in the characterization and prediction of these features during different stages of the process are described. The interaction between crystallinity and orientation is elucidated from recent results. Traditional techniques for measuring molecular orientation including birefringence, Wide Angle X-ray Scattering (WAXS) and Fourier Transform Infrared Spectroscopy (FTIR) have been reviewed. The microtoming method, used in conjunction with the birefringence and FTIR, was found to change the degree of orientation in the samples. An alternative technique is proposed. Commonly used techniques for determining the residual stresses in polymeric materials have been surveyed such as the solvent crazing, the hole drilling and the layer removal techniques. For the layer removal technique, the emphasis is on new methods for measuring the specimen's curvature after the removal of layers and the determination of residual stresses in axisymmetric specimens, such as tubes or rings. Several proposed methods for reducing the orientation and residual stresses in injection molded parts have been examined and proved to be very effective.

2.4.2 Introduction

Injection molding is one of the most common processes for manufacturing products of complex shape. It is a flexible technique characterized by high production rates, low cost and tight geometrical tolerances.

The injection molding process consisted of five major steps. In the first step, the raw material is fed into the heated barrel where it is melted and mixed to form a homogeneous melt with a constant temperature. The melt is then injected into the mold to fill the cavity. Once the mold is filled, a holding pressure will be exerted to force additional material into the cavity to compensate for the subsequent shrinkage of the product. As soon as the gate freezes, no more packing is needed and the material cools down further, thus lowering the pressure inside the cavity. After adequate solidification is achieved, the mold opens and the part is ejected. Figure 1 shows a general representation of the molding cycle. During the process, the polymer experiences a very complex thermomechanical history. This history is affected by molding conditions such as melt temperature, mold temperature, injection rate, cavity dimensions and material properties, and introduces in the injected parts molecular orientation [1], shrinkage [2,3] and residual stresses [4,5] resulting in warpage [6] and highly anisotropic mechanical properties [7,8].

The effect of the filling process on the molecular orientation has been widely discussed in the literature. Basically, it has been suggested that the molecular orientation at

the skin layer of the injection-molded products is due to the fountain-like flow at the melt front which orients the polymer molecules in the flow direction parallel to the mold surface. In the center of the molding, however, it has been found that the shear flow dominates in orienting the polymer molecules in the flow direction. Therefore, during the filling stage, both shear and extensional stresses [9,10] are present in the polymer melt. The intensity of these stresses will be considerably affected by the molding conditions such as flow rate and the temperature of the melt. The variation of the intensity of the shear and elongational stresses will influence the degree of molecular orientation in the injected part. Generally, a higher flow rate results in a higher molecular orientation while a higher melt temperature reduces the molecular orientation due to the molecular relaxation after the cessation of the flow.

Many authors [11,12] have used different techniques to measure the molecular orientation in the thickness direction of injection molded products. Their results indicated that the distribution of the orientation over the thickness of the molding shows two maxima near the external surfaces and a low orientation level in the core. According to Kamal and Tan [12], the first minimum between these two maxima is associated with the instantaneous freezing of the melt when it touches the mold wall and the following maximum is associated with the thickness of the frozen layer at the end of the filling process. The low degree of orientation observed in the center of the part is due to both the low level of shear stress and the relaxation in this zone.

Residual stresses are mechanical stresses that are present in the part in the absence of external load. These stresses are the results of changes from the equilibrium position of atoms and the distortion of valence angles in the molecular chains as well as from changes in the distances between segments in the molecules [13]. In the case of injection molding, it has been suggested that the build-up of residual stresses is a two-step process involving flow-induced stresses at the beginning followed by thermally-induced stresses. Flow-induced stresses arise from the presence of the shear and normal stresses during the filling and packing of the polymer in the mold cavity. During subsequent cooling, part of these stresses will be frozen in the final product due to incomplete relaxation. Thermally-induced stresses occur during the cooling phase. They are usually caused by differential cooling rates in various layers of the part's thickness. The rapid cooling and solidification of the surface layer is constrained from shrinkage and, at the same time, restrains the still warm interior from contracting upon further cooling. The result is tensile stresses in the interior and compressive stresses in the exterior layers. The total residual stress generated in the parts is the sum of the flow-induced stress and the thermally-induced stress. If the cooling process of the molded part is symmetric, so will be the final residual stress distribution. In the opposite case, a non-symmetrical residual stress profile will be obtained causing a change in the shape of the part.

The aim of this review is to describe the current state of knowledge regarding some features of injection-molded polymers such as molecular orientation, crystalline morphology and residual stresses. The present summary consists of two parts. The first part describes the basic mechanisms recently proposed in the literature for the build-up of both the molecular

orientation and the crystalline morphology in the thickness direction of injection-molded products. Different techniques for the characterization of these two features are presented in this part. The distributions of both the molecular orientation and the crystallinity in the thickness as well as in the flow direction and their interactions, in the case of semi-crystalline polymers, will be briefly discussed. The second part of this review deals with the origins of residual stresses in the injection-molded products. Different mechanisms for the build-up of thermal and flow stresses will be presented and discussed in some details. In this part, some experimental techniques used to measure these stresses will also be discussed.

2.4.3 **The morphology of injected parts**

It has long been known that the properties of injection-molded parts depend not only on the chemical constitution of the material but also on the processing conditions such as injection rate, mold temperature, gate location, melt temperature, etc., which affect the morphological characteristics such as the molecular orientation, crystalline structure, degree of crystallinity and residual stresses.

2.4.3.1 Mechanisms for the build-up of molecular orientation and crystalline structure

Molecular orientation is the alignment of molecular chains in one direction. The build up of the molecular orientation takes place during the filling and cooling of the polymer in the mold cavity. Figure 2.6 elucidates the origin of the molecular orientation during the

filling process. Consider first a rectangular fluid particle in the core of the mold, moving toward the front zone. According to Tadmor [10], as this fluid particle approaches the front, it will decelerate in the flow direction and acquire a velocity component in the gapwise y direction. As a result of this elongational flow, this particle will be stretched in the gapwise direction and change its shape. If a and b are the initial dimensions of the fluid particle these will become $a.e^{kt}$ and $b.e^{-kt}$ after a flowing time of t where k is the rate of elongation given by:

$$k = \frac{n}{2(n+1)B} V \tag{2.4}$$

where n is the power law index, V the mean velocity of the flow and B one half of the cavity gap. Moreover, since the advancing front has almost a semicircular form [14,15], the orthogonally stretched fluid particles at the melt front will flow along the free surface in a curved path until they reach the cold mold wall. There, they will immediately solidify and their orientation will be in the flow direction parallel to the mold wall.

Well behind the frontal region and far from the skin layer, molecular chains are oriented due to the shear flow present at this area. Such a shear-induced orientation is a result of the parabolic melt velocity profile in the gapwise direction [16] which orients the polymer chains in the flow direction during the filling stage. Upon the cessation of the flow, the shear-induced molecular orientation will begin to relax. The final degree of orientation in the center of the molding will depend on both the relaxation time of the polymer chains and the time needed for the polymer to reach its glass transition temperature. If the relaxation time is

smaller than the cooling time of the polymer, the polymer chains in the core will be completely unoriented at the end of the cycle.

More recently, many authors have associated the build-up of molecular orientation in amorphous polymers with the presence of frozen-in normal and shear stresses in the parts [17,18]. The origin as well as the distribution of these stresses during different stages of the injection molding process will be discussed in detail in the following sections. It has been stipulated, however, that the presence of these stresses orients the polymer chains and their final distributions, after complete solidification, have been used to predict the frozen-in molecular orientation profile across the part' thickness using the following stress-optical rule:

$$\Delta n = C(N_1^2 + 4\tau_{xz}^2)^{1/2} \tag{2.5}$$

where Δn is the birefringence which is used to characterize the molecular orientation (as will be discussed below), C a stress optical coefficient, N_1 the first normal stress difference, τ_{xz} the shear stress, and x and z are coordinates in the flow and thickness directions, respectively.

For semi-crystalline polymers, the study of the molecular orientation within injection-molded parts becomes much more complicated due to the presence of crystalline entities during the filling and cooling stages. The presence of these entities can change both the level and the distribution of the molecular orientation across the part' thickness since they can

retain to a certain extent the orientation generated during the filling stage and reduce the relaxation process of polymer chains during subsequent cooling.

The ability of a polymer to crystallize depends to a large extent on its molecular structure and its backbone flexibility. Polymers having a flexible backbone with a regular structure undergo quite rapid crystallization since flexible chains can readily adjust their sequences into a growing crystalline structure [19,20]. This class of polymers is called fast crystallizing polymers. In the opposite case, polymers having a semi-rigid backbone are called slowly crystallizing polymers and their crystallization behavior depends on both processing conditions and the level of stress introduced in the polymer during processing [21].

When injection-molded, these two classes of polymer give different morphological characteristics across the thickness. Trotignon and Verdu [22] proposed a simplified four-step mechanism to describe the crystallization process in the thickness direction of injection-molded specimens. Such a mechanism was proposed for fast crystallizing polymers and was based on the evolution of the temperature and pressure inside the mold cavity. During the filling process, the melt temperature is above the crystallization range, except near the mold surfaces. Therefore, in this zone, a more highly oriented layer with a low degree of crystallinity is obtained. Near the end of the filling phase, the melt velocity is reduced and the pressure inside the cavity remains low. Thus the orientation generated during the filling process begins to relax in the sub-skin layer until the temperature of crystallization is

reached. It is to be noted that at this layer, the rate of crystallization is higher because it is favored by the chain orientation. During the packing stage, the pressure inside the cavity increases, moving therefore the crystallization front toward the core and leaving behind layers of low degree of crystallinity. When the gate is frozen, the pressure inside the mold cavity decreases and the morphology of a slow crystallization process will develop.

Several authors have investigated the microstructure of injection-molded fast crystallizing polymers. An excellent review on this topic was done by Katti and Schultz [23]. Here, results obtained for the most common polymers such as polyethylene [24] and polypropylene [25,26] are reported. The morphology of injection-molded polyethylene in the thickness direction was found to be characterized by four distinct regions depending on the shape and the size of crystalline entities [24]. The skin layer has a non-spherulitic structure and when observed in the longitudinal cross-section, it exhibits tiny slots of vertical bright lines arranged in rows and running parallel to the surface of the molding. Such a structure was interpreted as stacks of lamellae with chain axes oriented in the flow direction and growing in the depth direction. In the second region, fine asymmetric spherulites of almost uniform size were obtained. These are spherulites formed under large thermal gradients, the size of which are limited by the fast nucleation rate. The third region contains asymmetric oblate spherulites with axis of symmetry in the depth direction; i.e. in the direction of the thermal gradient. These spherulites have a higher growth potential. The last region contains randomly nucleated spherulites which grow in all directions until they are stopped by impingement. Such a distribution of crystallinity was found to change along the flow

direction. It has also been suggested that the crystalline entities in the skin layer and in the second region are formed during the filling stage, while the others tend to be formed during the subsequent stages of the molding cycle.

Kantz et *al.* [25,26] studied the morphology of injection-molded polypropylene using samples microtomed parallel and perpendicular to the flow direction. Their results confirmed the layered structure in the thickness direction and revealed the presence of three distinct crystalline zones, namely, a highly oriented non-spherulitic skin, a shear-nucleated spherulitic intermediate layer and a typically spherulitic core. The spherulites in the intermediate layer are row nucleated and their size increases with increasing distance from the skin-shear zone boundary. In the core, the spherulites are randomly nucleated and have the largest size. However, Trotignon and Verdu [22] noted the presence of a fourth layer, situated just above the core, in which no crystalline structure is present. Trotignon and Verdu also measured the degree of crystallinity in the thickness direction of the part. Their results confirmed the presence of four distinct crystalline zones with high and low crystalline ratio. The locations of these four distinct zones correlated well with those obtained by optical microscopy studies. More recently Wenig and Herzog [27] investigated the morphological characteristics in the skin layer of injection-molded polypropylene. They found that it consisted of a shish-kebab crystalline structure due to the high shear stresses generated in this layer during the filling process.

In the case of slowly crystallizing polymers, the morphology of the injected part across the thickness is completely different from the one discussed above for fast crystallizing polymers. The semi-rigid backbone of these polymers gives rise to a strong tendency to crystallize under the effect of stress. Since the distribution of the stress field across the thickness during the injection process is non-uniform [16], the crystallinity of the polymer changes from one layer to another depending on the intensity of stresses at each layer.

Figure 2.7 shows the crystallinity distribution in the gapwise direction for injected poly(aryl ether ketone) for different mold temperatures [28]. At low mold temperature (20°C), three different crystalline layers are obtained across the thickness: the amorphous skin layer, the crystalline intermediate layer, and the amorphous core. The relative thickness of these layers was found to be affected by the injection rate. As the mold temperature increases (150°C), the crystallinity also increases as a result of the lower cooling rate. When the mold temperature becomes very high (200°C), the thermal crystallization rate increases and the structure of the part becomes much more uniform and highly crystalline.

The development of the multilayer amorphous-crystalline-amorphous structure in the thickness direction is a result of the complex interaction between the thermal and stress histories experienced by the polymer during the injection process. Hsiung and Cakmak [28] used the time-temperature-transformation (TTT) continuous cooling diagrams, commonly used in metallurgy, to explain the origin of this multilayer structure, Figure 2.8. In these

diagrams, both cooling curves (temperature vs. time) and the induction time envelopes (locations at which crystallization begins under different stress levels) are shown. The induction time is defined as the time elapsed from the start of stressing of the molten polymer to the onset of crystallization. It varies considerably with temperature and the stress level applied on the polymer melt. Chien and Weiss [21] studied the effect of shearing on the induction time. They reported that an increase in the shearing rate reduced the induction time significantly. It was also found that the shearing is the predominant factor in the initiation of nucleation at higher temperatures, and therefore encourages the crystallization process since it lowers the energy barrier for nucleation. In a recent work, Ferrara and Goncharko [29], using Differential Thermal Rheometry (DTR), confirmed these results and noted that an increase in the applied stress during processing raises not only the onset crystallization temperature but also the crystallinity of the polymer. Hence, the induction time becomes shorter and crystallization occurs at higher temperatures when the polymer is under high stresses, Figure 2.8.

At the skin layer of the molding, the material undergoes a high cooling rate and high shear stresses, Figure 2.8a. Although the induction time is very short, the cooling curve does not intercept the induction time envelope. As a result, the polymer vitrifies and remains amorphous. Not far from the surface, the cooling rate is lower due to the added insulation effect of the skin layer. In this layer, as the induction time envelope recedes to longer times, the two curves cross each other and crystallization will take place therein. In the core where the polymer experiences lower stresses and a lower cooling rate, the cooling curve and the

induction time envelope does not intersect and the polymer in this area stays essentially amorphous, Figure 2.8c.

More recently, Hsiung et al. [30] used a Lagrangian approach to predict the development of the structure gradient across as well as along the flow direction of injection-molded slowly crystallizing polymers. The crystallinity distribution is computed from the temperature and stress histories of individual fluid particles, called markers, by following their flow paths during the injection process. Depending on the time (**E**arly, **M**id, or **L**ate) and the location (**S**urface or **C**ore) at which these fluid particles enter the mold cavity, they may be roughly classified into five categories designated as **ES** for early and surface, **EC** for early and core, **MS** for middle and surface, **MC** for middle and core, and finally **LC** for late and core. It was shown that the essentially amorphous skin consists mainly of particles in the **EC** category (due to the short residence time despite the high stress level from the fountain flow); the particles in the **ES** category form the amorphous skin near the gate (due to quenching effect) and the high crystallinity subskin layer (due to shear induced crystallization); the **MC** particles constitute the amorphous the amorphous region at the end of the cavity, while the amorphous core is made up by **LC** particles; finally the **MS** particles appear in the relatively low crystallinity zone between the amorphous core and the shear-induced crystallized subskin. Figure 2.9 shows the locations of these five regions.

Such a crystallinity distribution across the thickness direction has a large effect on the final degree of molecular orientation at different layers of the molding. The distribution

of molecular orientation across the thickness of both amorphous and crystalline polymers will be discussed in details in section II.3.

2.4.3.2 Measurement of the molecular orientation and the crystalline structure

The characterization of molecular orientation by means of optical methods has been described in details by Ward and coworkers, Roe and Krigbaum, Wilkes and Zbinden [31-37]. To completely describe the molecular orientation, it is necessary to determine the detailed probability distribution function for the orientation of a coordinate axis system fixed in the molecular frame with respect to one fixed in the sample. For samples produced by industrial processes, the sample axis system is usually defined in terms of machine (M), transverse (T), and normal (N) or thickness directions. The molecular axis system (a, b, c) is usually chosen so that one axis (generally c) coincides with the chain axis of the polymer molecule. The orientation of the molecule is defined by the Euler angles θ, ϕ, ψ where θ and ϕ are the polar and azimuthal angles which determine the direction of the c-axis and ψ represents the rotation of the molecule about the c-axis which takes the a-axis out of the M-c plane, Figure 2.10. The orientation distribution can then be described by a function $N(\theta,\phi,\psi)$ where $N(\theta,\phi,\psi)\sin\theta d\theta d\phi d\psi$ is the fraction of molecules whose axies lie in the generalized solid angle $\sin\theta d\theta d\phi d\psi$. This function can be expanded in a series of generalized spherical harmonic functions [35]:

$$N(\theta,\phi,\psi) = \sum_{l=0}^{\infty} \sum_{m=-l}^{l} \sum_{n=-l}^{l} P_{lmn}\, Z_{lmn}(\cos\theta)\, e^{-im\phi}\, e^{-in\psi} \tag{2.6}$$

where Z_{lmn} are a generalized Legendre function, which reduces to the associated Legendre polynomials P_{lm} when $n = 0$. The coefficients P_{lmn} are averages of functions $Z_{lmn}(\theta,\phi,\psi)$ taken over the aggregates of molecules and are determined by:

$$P_{lmn} = \frac{1}{4\pi^2} \int_0^{2\pi} \int_0^{2\pi} \int_{-1}^{1} Z_{lmn}(\cos\theta)\, N(\theta,\phi,\psi)\, e^{im\phi}\, e^{in\psi}\, d(\cos\theta)\, d\phi\, d\psi \tag{2.7}$$

Specific values of P_{lmn} can be related to the more commonly defined orientation function [36, 31]. In particular, for uniaxial orientation, it can be shown that:

$$P_{000} = P_0 = 1 \tag{2.8a}$$

$$P_{200} = P_2 = \frac{3(\cos^2 \theta_{cM}) - 1}{2} \tag{2.8b}$$

$$P_{400} = P_4 = \frac{1}{8}\left(3 - 30\,(\cos^2 \theta_{cM}) + 35(\cos^4 \theta_{cM})\right) \tag{2.8c}$$

where θ is the angle between the chain axis and the machine direction, and the angle brackets indicate an average over all chain orientations. P_{200} is identical to the Hermans orientation function [38-39]. Expressions of P_{lmn} in terms of higher moments of $\cos\theta$ for other types of orientation can be found in [32].

In many cases, including amorphous polymers, the polymer structural units may be considered as having rotational symmetry around the chain axis and the distinction between the a and b axes can be neglected. Under these circumstances, it is sufficient to define the orientation of the chain axis c, which can be described in terms of three Hermans-type orientation functions:

$$f_{cM} = \frac{1}{2}\left(3(\cos^2 \theta_{cM}) - 1\right) \tag{2.9a}$$

$$f_{cT} = \frac{1}{2}\left(3(\cos^2 \theta_{cT}) - 1\right) \tag{2.9b}$$

$$f_{cN} = \frac{1}{2}\left(3(\cos^2 \theta_{cN}) - 1\right) \tag{2.9c}$$

where the three θ variables represent the angles made by the chain axis c with respect to the M, T, and N directions. The three angles are not independent. The sum of the three squared cosines is equal to unity, and the sum of the three orientation functions is equal to zero:

$$f_{cM} + f_{cT} + f_{cN} = 0 \tag{2.10}$$

Thus any two f values are sufficient to define the orientation, and the third can be determined by difference. The value of f ranges from –0.5, if the chain axes are perfectly perpendicular to the reference axis, to +1 if they are perfectly parallel. This representation of the orientation amounts to approximating the exact distribution function by an ellipsoid [37], but

for moderate levels of orientation this is sufficient and in fact, many techniques including birefringence and infrared spectroscopy cannot provide a more detailed representation.

A number of techniques have been employed to measure the molecular orientation in plastic products such as heat shrinkage [11], birefringence [12], X-ray diffraction [40], spectroscopy (infrared [41], Raman [42], nuclear magnetic resonance [43]), differential scanning calorimetry [44], etc., each of which provides a different level of detailed representation. Some of the more popular techniques are described next. The general purpose is to understand the quantities being measured in each method and how they are related to the different orientation functions defined above.

2.4.3.2.1 *Birefringence*

Birefringence is one of the most widely employed techniques for the measurement of orientation because of its simplicity. The refractive index of a system is related to its molecular polarizability. A linearly polarized light vibrating parallel to the chain axis of the molecule will induce a greater polarization of bond electrons and thus experience a higher refractive index light polarized parallel to the other two directions. The birefringence Δn is a measure of the optical anisotropy and is defined as the difference in refractive index along two perpendicular axes as measured with polarized light. As such, there exists three values of birefringence but only two are independent. If the polymer molecules are randomly

oriented, the system is isotropic (cubic symmetry) and the three refractive indices are equal ($n_1 = n_2 = n_3$) while in a biaxially oriented system, they are all different ($n_1 \neq n_2 \neq n_3$).

Hermans and Platzek [38] originally suggested a relation between the measured birefringence Δn_{12} in fibers and the orientation factor f_H which is equivalent to the coefficient P_{200} defined previously. The subscripts 1and 2 denote the axial and radial direction of the fiber, respectively. For amorphous polymers:

$$f_H = \frac{1}{2}\left(3\ (\cos^2 - \theta) - 1\right) = \frac{\Delta n_{12}}{\Delta^0} \qquad (2.11)$$

where θ is now the angle between the fiber axis and the polymer chain axis and Δ^0 is the maximum or intrinsic birefringence. For partially crystalline filament, the mean Hermans orientation factor is given by:

$$f_H = \chi f_c + (1 - \chi) f_H^{am} \qquad (2.12)$$

where χ is the volume fraction crystallinity, f_c is the orientation factor of the crystalline polymer chain axis and f_H^{am} is the Hermans orientation factor of the amorphous region.

For biaxially oriented systems, White and Spruiell [45] have proposed somewhat different but related orientation factors and their relationship to the measured birefringence:

$$f_{cM}^{B} = \frac{2}{3}\left(f_{cM} - f_{cN}\right) = \frac{2}{3}\left(2f_{cM} + f_{cT}\right) = \frac{\Delta n_{MN}}{\Delta^0} \tag{2.13a}$$

$$f_{cT}^{B} = \frac{2}{3}\left(f_{cT} - f_{cN}\right) = \frac{2}{3}\left(2f_{cT} + f_{cM}\right) = \frac{\Delta n_{TN}}{\Delta^0} \tag{2.13b}$$

where $\Delta n_{MN} = n_M - n_N$ and $\Delta n_{TN} = n_T - n_N$.

A number of methods can be used to measure the birefringence such as refractometry [46], monochromatic polarized light retardation [47-48] and multi-wavelength polarized light retardation [49-51]. The refractometry technique requires the use of a contact liquid which is not appropriate in many cases. The monochromatic light techniques can be used to measure both uniaxial and biaxial orientation but are suitable only for low degree of orientation. The multi-wavelength method has the advantage of being able to measure absolute orientation; however, it is limited to uniaxial orientation and thin materials. Recently a new multiwavelength technique has been developed by Ajji et al. [52]. The novelty of this technique is the use of two beams (instead of one) at two different angles which allows measurements of the biaxial birefringence of highly oriented and thick samples.

2.4.3.2.2 *X-ray diffraction*

X-ray diffraction is one of the oldest and most widely used methods to probe the crystal orientation in semicrystalline polymers [33-36,53]. When an X-ray beam is directed on a sample, it is partly absorbed, partly scattered and the rest is transmitted unmodified. The scattering occurs as a result of interaction with electrons on crystal lattices and is governed by Bragg's law:

$$\frac{\lambda}{d_{hkl}} = 2\sin\left(\frac{\theta}{2}\right) \tag{2.14}$$

where λ is the wavelength of the x ray, d_{hkl} is the interplanar spacing and θ is the radial scattering angle which is twice the Bragg angle θ_B, also known as the internal scattering angle. The x rays scattered from different electrons interfere with each other and produce a diffraction pattern which varies with the scattering angle. X-ray diffraction techniques are usually classified into wide-angle x-ray scattering (WAXS) and small-angle x-ray scattering (SAXS) depending on whether the desired information is contained in the intensities at large or small scattering angles. For a given wavelength, it is obvious that a larger interplanar spacing leads to scattering at smaller angles and vice versa. Thus, WAXS is more suitable to obtain structural information on small scale (1nm or less) while SAXS is useful for larger scale structure (1-1000 nm).

The orientation characteristics of semicrystalline polymers can be determined from the diffraction pattern and the diffracted beam intensity. In an unoriented sample, the

diffraction pattern shows a series of concentric rings, each of which corresponds to an (hkl) Bragg reflection. When the sample is oriented, the circles break up into arcs. The Hermans orientation function f_{hkl} can be related to the measured intensity distribution through the average of $\cos^2\phi$ defined by:

$$(\cos^2\phi) = \frac{\int_0^{\pi/2} I_{hkl}(\phi)\cos^2\phi \sin\phi \, d\phi}{\int_0^{\pi/2} I_{hkl}(\phi)\sin\phi \, d\phi} \tag{2.15}$$

where $I_{hkl}(\phi)$ is the intensity diffracted from a (hkl) plane and ϕ is the angle between the normal vector to this plane and a unique direction in the sample, e.g. machine direction. If the plane normal coincides with the crystallographic axes a, b and c and the crystals have orthorhombic symmetry:

$$f_a + f_b + f_c = 0 \tag{2.16}$$

which means one of the orientation factor can be obtained without direct experimental measurement. Generally speaking, when f_{hkl} values for any two planes, which are not parallel, are known, f_{hkl} for any other (hkl) plane can be calculated. This problem was treated in detail by Wilchinsky [54] and Sack [55]. More complete description of the crystal orientation can be determined by higher order coefficients P_{lmn} in equation (4). This was obtained by

measuring a set of diffracted intensities $I(\chi,\eta)$ at a fixed Bragg angle where χ and η two angles which specify the relative orientation of the sample with respect to the incident and diffracted x ray beams [33]. Even though the amorphous orientation can be quantified by WAXS [56,57], this technique has limited application.

2.4.3.2.3 *Infrared spectroscopy*

Infrared (IR) spectroscopy is another valuable technique for characterizing orientation [37], and has the advantage of being able to provide specific information on the different components (amorphous, crystalline, copolymers, blends) and molecular conformations present in the polymer. Dichroic IR spectroscopy measures the absorption intensity of different molecular vibrational modes with an IR beam whose electric field vector is polarized in a specific direction with respect to the sample. Each vibrational mode possesses a transition moment that can usually be considered to make a fixed angle α with respect to the chain axis. For the case of rotational symmetry about the chain axis, when a sample is analyzed with radiation polarized in any particular direction J, it can be shown that the absorption intensity of a particular band is given by:

$$A_j = A_0 \left\{1 + \frac{1}{2}\left(3(\cos^2 \theta_{cJ})-1\right)\right\} (3\cos^2 \alpha - 1) = A_0 \left\{1 + f_{cJ} (3\cos^2 \alpha - 1)\right\} \quad (2.17)$$

where A_0 represents the absorption intensity that would be observed for an equivalent unoriented sample, θ_{cJ} is the angle between the chain axis and the direction of polarization

J, and f_{cJ} is the orientation function with respect to that direction. Thus if measurements are made in the three directions M, T, and N, the following quantities are obtained:

$$A_M = A_0\{1 + f_{cM}\,(3\cos^2\alpha - 1)\} \tag{2.18a}$$

$$A_T = A_0\{1 + f_{cT}\,(3\cos^2\alpha - 1)\} \tag{2.18b}$$

$$A_N = A_0\{1 + f_{cN}\,(3\cos^2\alpha - 1)\} \tag{2.18c}$$

and A_0 can be calculated from:

$$A_0 = \frac{1}{3}\,(A_M + A_T + A_N) \tag{2.19}$$

For the case of uniaxial orientation, where $f_{cT} = f_{cN} = -\frac{1}{2} f_{cM}$ one needs to make measurements only in the M and T directions, then calculate the dichroic ratio D to eliminate the unknown quantity A_0:

$$D = \frac{A_M}{A_T} = \frac{1 + f_{cM}\,(3\cos^2\alpha - 1)}{1 + f_{cT}\,(3\cos^2\alpha - 1)} \tag{2.20}$$

Equation (17) can be inverted to give the well known relation which is equivalent to the Hermans orientation function:

$$f_{cM} = \frac{D - 1}{D + 2} \frac{2}{3\cos^2 \alpha - 1} \tag{2.21}$$

For general biaxial orientation, the M, T, and N directions are all different. In principle, it is possible to calculate f_{cM} and f_{cT} by means of equations (15a) and (15b), but this requires the knowledge of A_0. Usually this quantity is unknown, because it depends on the properties of the particular specimen being analyzed (for example, the thickness in the case of a transmission spectrum, or the surface quality in the case of a reflection spectrum). Thus for biaxially oriented samples, the usual approach is to measure the absorption intensities A_M, A_T, and A_N in all three directions, calculate A_0 from equation (16), then determine f_{cM}, f_{cT}, and f_{cN} according to equation (15). However, the measurement of the spectrum in the normal direction is more difficult than that for the other two. For thin films in transmission it can be obtained by making measurements on tilted films, and for attenuated total reflection (a.t.r.) it can be obtained by making measurements with different positions of the sample with respect to the plane of incidence. However, in both cases the analysis is considerably more tedious than that required for uniaxial samples. An alternative approach is to overcome the dependence of A_0 on specimen properties by using the ratio of two different bands in the same spectrum. This approach has been applied by Mirabella [58-60] to a.t.r. spectra of oriented polypropylene.

In recent papers, Cole and his coworkers [41,61-62] as well as other groups [63-66] have demonstrated the possibilities of using front-surface infrared reflection for

characterizing the surface orientation of thick uniaxially drawn samples. Furthermore, the present authors have shown that for polymers with glass transition temperatures above room temperature, careful milling and polishing of the specimen results in spectra of high quality without affecting the polymer structure [67]. One way to apply this technique to biaxially oriented samples (i.e. to determine A_N) is to section the sample and make measurements in the N direction with an infrared microscope. Because of the special equipment and considerable work required for this, an alternative approach, based on the peak ratio approach used by Mirabella, has been developed and applied to front-surface reflection spectra of poly(ethylene terephthalate), or PET. The orientation function with respect ot any direction J can be determined by making a measurement with the polarization in that direction:

$$f_{cJ} = \frac{R_J - R_0}{R_0\,(3\cos^2\alpha_1 - 1) - R_J\,(3\cos^2\alpha_2 - 1)} \tag{2.22}$$

where R_J is given by:

$$R_J = \frac{A_{1J}}{A_{2J}} = \frac{A_{10}}{A_{20}}\,\frac{1+f_{cJ}\,(3\cos^2\alpha_1 - 1)}{1+f_{cJ}\,(3\cos^2\alpha_2 - 1)} = R_0\,\frac{1+f_{cJ}\,(3\cos^2\alpha - 1)}{1+f_{cJ}\,(3\cos^2\alpha_2 - 1)} \tag{2.23}$$

The subscripts 1 and 2 designate the two different bands and $R_0 = A_{10}/A_{20}$ is the band ratio corresponding to an unoriented sample. Thus for biaxially oriented samples, measurements in the M and T directions allow determination of f_{cM} and f_{cT}, from which f_{cN} can be calculated

from equation (7). The validity and limitations of this approach are discussed in details in [68].

2.4.3.2.4 *Raman spectroscopy*

Raman spectroscopy is another method which provides information on molecular vibration [31,36,42,69,70,71]. In contrast with IR spectroscopy whereby the molecules are excited to higher energy vibration states by absorption of incident radiation, Raman spectroscopy is characterized by the scattering effect and thus a type of emission spectroscopy. When an intense beam of frequency ν_0 is incident on the sample, most of the power is undeviated while a small fraction is absorbed by the molecule and raises it to a higher energy state. Upon returning to the lower energy state, radiation is emitted at frequencies ν_0-$\delta\nu$ ("Stokes" lines) and ν_0+$\delta\nu$ ("anti-Stokes" lines). The intensity of the scattered radiation can be related to the second, P_2, and fourth, P_4, moments in the orientation distribution function [71].

In IR, the intensity of the spectra depends on the change in dipole moment of the molecules while in RS it is determined by the change in polarizability resulting from the vibration. As such, vibrations which are very intense in IR spectrum show only weak bands in Raman spectrum and vice versa. Thus IR and Raman spectroscopy can be considered as complimentary techniques. However, Raman spectroscopy has not gained as wide acceptance as IR due to both experimental and theoretical difficulties. The determination of orientation

from Raman spectroscopy is much more involved. Furthermore, since only a small amount of incident radiation is scattered, the intensity of Raman signal is extremely low. With the development of high power lasers, this technique is gaining in popularity.

2.4.3.2.5 *Sample preparation techniques*

In the birefringence and FTIR in transmission mode, a transparent sample is needed for measurement. The microtoming method is usually employed to cut thin slices, or sections, from the molded part. The thickness of these sections may vary between few microns to 0.1 micron when using an ultramicrotoming machine. Sections cut in different directions with respect to the flow direction will permit to measure the three-directional birefringence distribution in the molded part. This will in turn permit to quantify the degree of molecular orientation in different directions. The microtoming technique was initially developed for biological materials, but today it is widely used in preparing thin sections from polymeric materials. During the cutting process, considerable forces may be transmitted from the knife to the section. This will significantly change the dimension and therefore the morphological characteristics of these sections. The degree of change depends on many factors such as the local increase in temperature between the knife and the specimen, the knife's characteristics and the cutting conditions (the thickness of the section, the cutting velocity, etc.). Recently, Reid and Beesley [72] summarized the sectioning problems and showed that the variation of the section's thickness, the scratches and chatters formed at the surface and the change in dimensions are the major problems arisen during the cutting

process. Lundberg et al. [73] conducted an extensive study on the effect of cutting conditions on the section's characteristics. They noted that during the cutting process, the section becomes shorter. Such a decrease in the length of the section increases with both decreasing cutting velocity and the section's thickness and with increasing preorientation in the specimen. Moreover, it was shown that the sectioning by microtoming affects the measured orientation in both amorphous and semi-crystalline polymers. In the case of amorphous polymers (e.g., PC), the measured orientation decreases with increasing reduction in length. If the section is cut perpendicular to the preorientation direction, this leads to the lowest decrease in length and therefore to the best measure of the preorientation. In the case of semi-crystalline polymers (e.g., PP), the effect of the sectioning was found to be much more complex. For these polymers, the thickness of the section can change the crystallinity of the polymer in some cases. For unoriented specimen, the crystallinity was found to be independent of the section's thickness, but it is largely reduced by increasing the thickness of the section in the case of preoriented specimen. Different suggestions were proposed to explain the origin of these problems and it was concluded that results obtained by using the microtoming technique should not be considered as absolute but as relative measurements, depending on the cutting conditions [74].

To overcome these problems, Hemsley and Robinson [75] proposed a method which is both simple in sample preparation and rapid for measurement of the three-dimensional birefringence distribution in transparent parts. In this method, wedges are cut from the part and mounted on an optically isotropic glass block with a thin layer of a specific liquid in

between as shown in Figure 2.11. This liquid should have a refractive index intermediate between the glass and the polymer to reduce considerably the refraction and scattering effects at the interface. When the whole assembly is examined in a particular direction, e.g. direction 3, with the wedge in 45° position between crossed polarizers and exposed to a green light, a series of dark fringes is obtained due to the thickness variation in the plane of observation (Figure 2.12). The birefringence between two points A and B, which are on two consecutive dark fringes, is given by:

$$n_1 - n_3 = \frac{\lambda}{L \tan\theta} \tag{2.24}$$

where λ is the wavelength of the light, L the distance between A and B, θ the angle of the wedge, n_1 and n_3 are the refractive index in the thickness and observation direction, respectively. A series of lines such as AB across a single photograph can therefore be used to determine the variation of the birefringence through the thickness of the molding. Similar procedure can be applied to determine the birefringence distribution in other directions.

In recent works [67], a relatively easy technique for the characterization of molecular orientation at the surface and at different depths across the specimen's thickness was proposed using infrared spectroscopy in the reflection mode. This technique consists of milling and repeated polishing of the specimen at the depth where molecular orientation is to be measured. The milling process has to be conducted under a temperature lower than the glass transition temperature of the polymer, using both a single point cutter and a high cutting

speed in order to minimize the energy dissipated during the fracture and deformation of the polymer [76]. The milled surface is then polished using a rotating polishing machine. The step-by-step polishing process is summarized in reference [67]. It is to be noted however that after each step of the polishing process, the quality of the polished surface has to be checked by an optical microscope and is considered acceptable only if scratches generated during the previous polishing step are completely eliminated. Such a technique has been tested for several polymers having different thermal and mechanical characteristics. It was found that for polymers having high glass transition temperatures, such as PEEK and PET, the overall milling and polishing process did not significantly disturb or generate molecular orientation in the specimen. This was not the case for polymers with low glass transition temperatures such as PE. For this polymer, it is suggested that liquid nitrogen be used as a cooling medium to avoid the disturbance and relaxation of molecular orientation during the polishing process. Moreover, it was found that spectra obtained after the whole milling and polishing process have a higher overall intensities and a quite flat "baseline", which permit a better comparison of spectra measured in different polarization directions and therefore, a better characterization of molecular orientation.

2.4.3.3 Molecular orientation in injection molded amorphous and semi-crystalline polymers

Menges and Wubken [11], using the heat shrinkage technique to measure the degree of orientation in injection molded polystyrene, noted that the molecular orientation in the flow direction is maximum at the external surfaces of the molding. It decreases gradually,

reaches a second maximum at a short distance from the surface and then decreases steadily toward the center of the molding. In the direction transverse to the flow, it was found that the molecular orientation is also maximum at the external surface and close to zero at the center; however, no secondary maximum was observed in the sub-skin layers. It has been suggested that the presence of the secondary maximum in the flow direction is due to the high shear rate at the solidified layer/polymer melt interface which orients polymer chains in the flow direction. Similar results have been obtained using birefringence measurements [12]. A typical distribution of Δn in the thickness direction is shown in Figure 2.13. In this Figure, x, y and z denote the flow, transverse and thickness directions respectively. Again, the molecular orientation is characterized by a maxima at the skin and sub-skin layers and a minimum in the center of the molding. This is due to the effect of the cooling rate on the molecular relaxation. In fact, while the polymer chains at the external surfaces of the molding, highly oriented by the advancing front and shear flow, will immediately solidify when they touch the cold mold wall, those in the center of the molding will relax to a certain extent due to the presence of a slow cooling rate in this area. According to Kamal and Tan [12], the thickness of the frozen layer when the polymer hits the mold wall and at the end of the filling process is given by segments AB and AC respectively, Figure 2.13.

Molecular orientation along the flow path was reported by Harland et al. [77]. It was found that the orientation is the highest in the gate area. It decreases very rapidly and, at a short distance from the gate, starts growing again to reach a second maximum at almost the midpoint of the flow path. Far from the gate, the molecular orientation decreases

dramatically. Harland et al. explained the observed pattern of molecular orientation in terms of die swell, radial, elongational and shear flow. While flowing in the runner, molecular chains are oriented in one direction, resulting in internal tension normal to the flow direction. These normal stresses cause the expansion of the melt when it emerges from the gate to fill the mold cavity. This mechanism, known as die swell, causes a loss of molecular orientation in the flow direction and explains its rapid fall at short distance from the gate. Beyond this area, the shear flow is restored and tends to orient molecular chains. However, the maximum of orientation is reached at almost the midpoint of the flow path, Figure 2.14. This delay is due to the presence of a radial flow emanating from the gate which causes a stretching of the advancing melt orthogonal to the flow direction. Far from the gate, the contribution of the shear flow to orient polymer chains will diminish due to a lower pressure gradient in this area resulting in a decreasing molecular orientation. It should be noted that this is only true for this case where a constant gate pressure is maintained. For a constant flow rate at the gate, the molecular orientation is expected to reach a plateau far from the gate.

The distribution of the molecular orientation along the flow path could also be explained using the distribution of the velocity of the flow front in this direction. Figure 2.15 shows the successive flow fronts during the filling of a rectangular cavity. As the melt emerges from the gate, the flow front velocity decreases as the flow front area is enlarged in the radial direction. The flow front continues to decelerate until it reaches the side wall of the mold. From there, the front area decreases and the front velocity accelerates until it arrives at a distance roughly equal to the width of the mold cavity where its velocity becomes

almost constant. In terms of velocity gradient, it is easy to conclude that this quantity is negative near the gate, positive in intermediate zones and equal to zero far from the gate. If it is assumed that the molecular orientation is dependent on the velocity gradient of the flow front in the flow direction, it follows that the orientation decreases near and far from the gate and increases in the intermediate zones, Figure 2.14.

Moy and Kamal [40] studied the distribution of both the molecular orientation and the orientation behavior of polyethylene crystallographic axis in the thickness direction of the injection molded parts. Their results showed that the total molecular orientation, measured by birefringence, is maximum at the external surfaces of the molding and decreases gradually towards the center. Moreover, it was found that near the surface, the major contribution to the total orientation comes from the amorphous phase, while in the core, it is the crystalline phase. At intermediate zones between the surface and the core, both the amorphous and crystalline phases contribute about equally to the total orientation. Using X-ray measurements, these authors also observed that the degree of crystalline orientation, as represented by the crystallographic a-axis, increases with the distance from the surface but remains always oriented parallel to the flow direction. The crystallographic b-axis, which represents the growth direction of the polyethylene crystallites, was found to be always oriented perpendicular to the flow direction. This will rotate the crystallographic c-axis, representing the molecular chain axis, and orient it in the flow direction near the surface of the molding, and in a direction perpendicular to the flow as the distance from the surface increases.

Most of the above works were performed using fast crystallizing polymers. For slowly crystallizing materials, stress-induced crystallization plays a dominant role [30] and the interaction between the degree of crystallinity and molecular orientation becomes important. Recently, the present authors have conducted extensive investigations on the effect of the crystallinity on the molecular orientation at different layers of the injection molded PET using infrared spectroscopy and the milling and polishing technique described above [78]. For PET, infrared technique allows simultaneous measurement of crystallinity and orientation. The distribution of crystallinity was similar to that observed by Hsiung et al. for another slowly crystallizing polymer. Furthermore, for mold temperatures lower than the glass transition temperature of the PET, the maximum of molecular orientation is obtained in the subskin layer where the shear-induced crystallization takes place; for mold temperatures higher than the glass transition temperature of the PET, the maximum of orientation is observed at the skin layer of the molding due to the decrease in the thickness of the skin layer which shifts the shear-induced crystallization zone toward the surface. It was thus stipulated that the shear-induced crystallization can retain, to a certain extent, the molecular orientation generated during the filling and markedly reduce the relaxation of the polymer chains during the cooling stage.

This anisotropy of the morphology in the thickness direction of injection-molded products will affect their mechanical behavior. Moreover, it has been found that the presence of a such morphological gradient in the thickness direction can generate internal stresses in

the final products. The origins as well as different experimental techniques for measuring these stresses will be discussed in the following sections.

2.4.4 **Residual stresses in injection molded parts and their measurements**

2.4.4.1 The origin of residual stresses

Residual stresses are mechanical stresses present in the part in the absence of external loads. The knowledge of the level of residual stresses is essential in predicting the final dimensions and shape of products. In polymers, the term residual stress is used to describe the state of polymer chains after processing. A molded part contains frozen-in stresses or strains if its polymer chains are in nonequilibrium configuration. According to Menges et al. [13], the departure from the equilibrium configuration is the result of changes in equilibrium positions of atoms, distortion of valence angles and variations in the distance between segments in the molecules.

McKelvey [79] associated the presence of residual strains in injection-molded parts with the viscoelastic behaviour of the polymer melt during the filling and cooling stages. He used a simplified mechanical model to simulate the build-up of residual strains in plastic products, Figure 2.16. This model consists of a Maxwell and a Voigt element connected in series. If a sudden load is applied, the total deformation of this model is the sum of the instantaneous elastic deformation, the irrecoverable viscous flow and the retarded elastic deformation. These deformations have been associated respectively with the bending and stretching of primary valence bonds, the slippage of polymer chains or chain segments past one another and the transformation of a given equilibrium molecular configuration into a

biased configuration in which an elongated and oriented structure is formed. It has also been suggested that the instantaneous elastic deformation and the irrecoverable viscous flow can be respectively represented by the shear modulus G_1 and the viscosity μ_1 of the model shown in Figure 2.16. The retarded elastic deformation, however, depends on the ratio μ_2 / G_2, called the retardation time.

Consider now the removal of the external load under isothermal conditions. If the temperature is sufficiently high, the previously generated deformations will be completely recovered so that the model returns to its equilibrium position. If the temperature decreases as the model deforms, the recovery process will be slower due to the increase in the viscosity. In the case where the removal of the external load is carried out at a temperature below a specific value, part of the deformations will be frozen-in in the model. These deformations correspond, on the molecular level, to the freezing of polymer chains in a position of partial orientation.

During the injection molding process, it has been shown that two kinds of residual stresses could be generated. Basically, one distinguishes between *flow-induced residual stresses* which develop during the filling and packing of the polymer into the mold cavity, and *thermally-induced residual stresses* arisen during the rapid cooling stage. In the following sections, the build-up and general features of these two kinds of residual stresses will be described.

2.4.4.1.1 *Flow-induced residual stresses*

In an earlier work [80], Vinogradov presented a qualitative study on the generation of residual stresses during the filling and packing stages. It was suggested that during the filling stage, molecular chains are stretched and oriented in the flow direction with a maximum orientation located in the outer layers of the molding, resulting in high elastic deformations in the molded part. As these deformations relax during the subsequent cooling phase, the linear dimensions of the different layers across the part's thickness will change. These changes are directly related to the degree of orientation of the polymer chains at these layers. Polymer chains in the outer layers, which are more oriented, undergo the most important relaxation process. However, such a relaxation is hindered by the less oriented inner layers. Consequently, in a completely solidified part, residual stresses arisen from the filling stage are **tensile in the surface layers**, in the direction of orientation, and **compressive in the core**. During the packing stage, the polymer melt undergoes a different stress field. The distribution of these stresses depend on the thickness and length of the molded part, the cooling rate and the degree of compression of the melt in the mold. In zones where the polymer melt is not sufficiently compressed, the thickness of the outer layers plays an important role on the stress distribution. In fact, if during the cooling stage the pressure in the core falls to zero at the instant when the thickness of the outer layer is small, then upon further cooling, the inner layers of the material reduce their volume and compress the outer layers while themselves remain stretched. This yields a **compressive skin/tensile core** distribution as shown in Figure 2.17a accompanied by a sink mark. In the case where the

pressure inside the molded part reaches zero at the time when the outer layers is much greater than that of the inner layers, then the final residual stresses assume a more complex **tensile skin/compressive subskin/tensile core** distribution, Figure 2.17b. In zones where the melt is over-compressed, the pressure in the core of the molding remains excessive even after a complete cooling. Consequently, the residual stress distribution will be **tensile skin/compressive core** as in Figure 2.17c, which is completely opposite to that obtained in Figure 2.17a. Since the pressure is not uniform along the flow path during the injection cycle, all three types of residual stress distribution discussed above can be present. In fact, near the gate, the polymer is usually over-compressed and a residual stress distribution such as the one described in Figure 13c is expected. In the middle of the part, the melt pressure decreases and the residual stress distribution in this region will resemble the one presented in Figure 2.17b. Near the end of the cavity, the melt pressure is lowest and the residual stress distribution therein may have the shape indicated in Figure 2.17a.

Other authors have attempted to predict quantitatively the *flow-induced residual stresses* in molded parts from the shear, normal and extensional stresses developed during the non-isothermal flow of the polymer in the mold cavity [9,10,16]. Generally speaking, shear stresses are generated from the high strain rates occured well behind the flow front and extensional stresses resulted mainly from the fountain flow near the flow front, while normal stresses are due to the viscoelastic nature of the polymeric melts. The development of unequal normal stress components during the injection process arises from the fact that the microstructure of the melt polymer becomes highly anisotropic during flow. If chain

molecules at rest occupy initially a spherical volume, they will deform during processing towards an ellipsoidal shape, the major axes of which are tilted towards the flow direction [81], Figure 2.18. Hence, an isotropic restoring forces will be generated in the deformed microstructure which are much more important in the flow direction than in any other directions. Even though the magnitude of these stresses is relatively small, their presence gives rise to a large molecular orientation and anisotropic shrinkage behavior of the polymer.

Since the viscosity of polymer melts is very high, the inertia and the body forces are usually negligible. The non-isothermal flow of viscoelastic fluids is then governed by [82]:

The conservation of mass $$\overset{\circ}{\rho} + \rho\nabla \cdot \underline{v} = 0 \tag{2.25}$$

The conservation of momentum $$\nabla \cdot \underline{\underline{\sigma}} = 0 \tag{2.26}$$

The conservation of energy $$\rho\overset{\circ}{\epsilon} = \nabla \cdot k\nabla T + \underline{\underline{\sigma}} : \underline{\underline{D}} + \rho r \tag{2.27}$$

where $\circ$ denotes the total derivative, ρ the density, $\underline{v}$ the velocity vector, $\underline{\underline{\sigma}}$ the Cauchy stress tensor, ϵ the specific internal energy, $\underline{\underline{D}}$ the rate of strain tensor, k the thermal conductivity, T the temperature and r the internal heat source.

The Cauchy stress tensor is commonly decomposed into a hydrostatic part, p, and a deviatoric part, $\underline{\underline{\sigma}}^d$:

$$\underline{\underline{\sigma}} = -p\underline{\underline{I}} + \underline{\underline{\sigma}}^{d} \tag{2.28}$$

where $\underline{\underline{I}}$ is the identity tensor and $\underline{\underline{\sigma}}^{d}$ depends on the strain rate tensor. The internal heat source is disregarded at the moment for the sake of simplicity. If elastic effects on the specific internal energy are negligible, it can be shown that:

$$\overset{\circ}{\epsilon} = C_p \overset{\circ}{T} - \frac{p}{\rho} tr(\underline{\underline{D}}) + \frac{T}{\rho^2} \overset{\circ}{p} \frac{\partial \rho}{\partial T} \tag{2.29}$$

where C_p is the specific heat at constant pressure and tr(●) denotes the trace of the tensor. To close the above set of equations, constitutive relations are required for the density and the Cauchy stress together with appropriate boundary conditions.

Isayev and Hieber [16] assumed the polymer behaved as an incompressible material with a Leonov constitutive model for the Cauchy stress, the flow is quasi-steady, fully developed between two parallel plates. As such, the packing phase and the fountain flow were not taken into account. Even with such simplified model, the authors were able to provide a detailed description of the non-isothermal stress generation and relaxation during the filling. Their results indicated that at the mold wall, Figure 2.19, the melt velocity and the shear rate markedly decrease with increasing time, probably because of the formation of the rigid layer in this area. In order to maintain a constant flow rate, the melt velocity in the core of the molding has to increase, therefore moving the maximum shear rate gradually

toward the center of the molding. The shear stress was found to be linear in the depth direction and its magnitude increases with the injection time. They also noted that the first and the second normal stress differences are almost linear initially, but transform to a parabolic profile at longer time, with minima at the mold wall and in the core. During the filling stage, normal stresses in the vicinity of the mold wall will get frozen and their maximum will continually increase in magnitude and move gradually inwards from the wall.

Baaijens and Douven [83] considered both the filling and the post-filling stage. To account for the compressibility of the material during the packing stage, the dependence of density on pressure and temperature is represented by a co-called Tait equation which has been a successful model for amorphous polymers:

$$\nu\ (p,T) = \left[\ a_0 + a_1(T - T_g)\right]\left[\ 1 - 0.0894\ \ln(1 + \frac{p}{b})\right] \qquad (2.30)$$

where ν is the specific volume, a_0 and a_1 are constants, T_g the pressure dependent glass transition temperature and b a temperature dependent coefficient. A compressible Leonov model was also derived for the Cauchy stress. Two different approaches were investigated. In the *direct* approach, the viscoelastic behavior of the material was fully accounted for in deriving a pressure equation using the thin cavity approximation for a general 3-D geometry. In the *indirect* approach, the pressure problem was derived employing a generalized Newtonian model, while the resulting flow kinematics was used as input into the viscoelastic constitutive equation for residual stress calculation. The results are comparable for the two

approaches but the indirect approach reduces computational time considerably. Their results showed that, during the compression stage, normal stresses in the core decrease considerably and are essentially negligible at the end of this stage. Both the low flow rate and high core temperature are responsible for the relaxation of the normal stress at this stage. Close to the mold wall, the normal stress is frozen-in and only relax partially due to the very high cooling rate in this zone. Moreover, during the post-filling stage, a small quantity of hot material will continue to enter the mold cavity and such a process will raise the normal stress in the hot core near the gate.

The so-called fountain flow near the flow front, as described earlier in Figure 2.6, has a large effect on the molecular orientation and residual stresses as it imparts high extensional stresses on fluid particles. A detailed study on this subject was presented by Mavridis et al. [84]. A fully two-dimensional problem in the flow and thickness direction was considered. A multi-mode Leonov constitutive equations was assumed and the resulting equations were solved by the finite element technique. They noted that, just behind the flow front, the first normal stress difference is negative in the core and attains a large, positive value at the external surfaces. Such a normal stress distribution through the specimen's thickness during the filling stage clearly indicate the compression process of fluid particles at the center line of the molding and their extreme stretching (extension) as they move outwards towards the mold wall. The authors also showed that, by incorporating the fountain flow effect, a maximum birefringence was predicted at the surface and a minimum in the subskin layer.

Kabanemi et al. [85] also considered the 1-dimensional filling of a thin rectangular cavity and followed the indirect approach suggested by Baaijens and Douven [83]. They obtained the flow kinematics for an incompressible generalized Newtonian fluid under non-isothermal conditions. The flow stresses were then computed using the known kinematics by integrating the Cauchy-Green tensor along the path lines using the Wagner single integral constitutive equation. The stresses during the cooling stage was based on a thermoviscoelastic model with structural relaxation. Their results showed that near the gate, the maximum shear stress is at the mold wall, while far from the gate, the maximum shear stress is observed in the subskin layer. This maximum moves towards the center of the molding and its magnitude decreases with increasing distance from the gate. They also found that at the end of the filling stage, the normal stress is maximum near the mold wall (in the subskin layer), decreases gradually toward the center. At the mold wall however, these stresses vanish due to the cooling effect in this area. After completion of the cooling stage, the shear stresses undergo almost complete relaxation while the maximum normal stress observed near the wall at the end of the filling stage remains but its magnitude diminishes considerably.

During the cooling process, all the above mentioned stresses can be relaxed. However, because of the increase of the melt relaxation time as the melt temperature decreases, part of these stresses will get frozen in final products.

2.4.4.1.2 *Thermally-induced residual stresses*

During the rapid cooling of the melt in the mold cavity, a high temperature gradient exists between the part's surface and the core giving rise to differential shrinkage, and hence residual stresses. The magnitude of these stresses was found to be one order higher than that of flow-induced stresses [86].

The theory of thermal stresses for linear elastic material had a long history and was well documented by Boley and Weiner [87]. The thermo-viscoelastic theory of residual stresses was initially developed for inorganic glasses [88-91] and applied to polymers under free quenching by Struik [92]. He assumed that the cooling occured in two steps. In the first step, the outside layer of the sheet undergoes an instantaneous step change in temperature from the melt temperature (T_o) to the quench temperature (T_f), while the core remains at T_o at time t_1. In the second step, the core of the sheet cools down to T_f instantaneously at time t_2. During the first cooling step, the outside layer of the sheet contracts and becomes rigid. This contraction is limited to a certain extent by the core of the molding, resulting in compressive stresses in the skin layer of the part. During the second cooling step, the core of the sheet will cool down, contract and become rigid. The contraction of the core is now limited by the presence of the rigid shell giving rise to the tensile stress in the core. Therefore, at the end of this step, a **compressive skin/tensile core** distribution is obtained. This mechanism for the generation of thermal stresses assumes that elastic properties of the sheet change twice in the thickness direction during the quenching process. Other authors

have extended this analysis assuming a continous change of elastic properties during the cooling process and noted that the thermally-induced residual stress distribution for free quenching generaly exhibits a gapwise parabolic profile which is compressive in the outer layers and tensile in the core of the molding [7].

Thermal stresses in injection-molded parts were found to be very different from those in free quenching where material points on the surface are free to move. In injection molding, the materials on the surface are constrained by the high cavity pressure, mold/part adhesion as well as the mold geometry. Such a contact will change the stress build-up mechanism during the cooling stage. When the polymer hits the cold wall and adheres to it, the external layer of the molding will not be completly contracted due to the difference in the thermal expansion coefficient of the polymer melt and the mold surface causing tensile stresses in this layer. The same mechanism takes place in the core so that only tensile stresses is present across the thickness. These stresses will remain in the molding until the latter is released from the mold surface. The moment of release is therefore a critical factor in the determination of residual stress distribution in the injection-molded products. If the specimen is released from the mold wall just after the solidification of the skin layer, then the residual stress distribution in the thickness direction will be very similar to that in free quenching. On the other hand, if the specimen is released only after complete solidification of the whole part, the state of stress in the specimen is entirely tensile with a maximum in the core. A more complicated stress distribution is usually obtained since the part normally detaches from the wall while it is only partially solidified as shown in Figure 2.20 [93].

In recent years, progresses have been made in dealing with theoretical predictions of thermally-induced residual stresses under free and constrained cooling during injection molding of polymers. Most analyses assumed a linear thermo-viscoelastic behavior. The conservation of momentum and energy are similar to those given in the previous section with the Cauchy stress determined by [82,86,94-97]:

$$p = \int_0^t \left[\frac{\alpha}{\kappa} T - \frac{1}{\kappa} tr(\underline{\underline{D}}) \right] ds \tag{2.31}$$

$$\underline{\underline{\sigma}}^d = 2 \int_0^t G\,(\xi(t), \xi(s))\, \underline{\underline{D}}(s)\, ds \tag{2.32}$$

$$\xi(t) = \int_0^t \frac{1}{a_T}\, ds \tag{2.33}$$

where α is coefficient of thermal expansion, κ the coeffiecient of compressibility, G(t,s) the shear relaxation modulus, ξ the reduced time and a_T is the shift factor of the time-temperature superposition principle. The boundary conditions for free quenching is given by:

$$\underline{\underline{\sigma}} \cdot \underline{n} = 0 \tag{2.34}$$

while for constrained quenching:

$$\underline{u} = 0 \tag{2.35}$$

where $\underline{n}$ is the unit vector normal to the surface, and $\underline{u}$ is the dispacement on the surface.

Baaijens and coworkers [82,86,94] assumed a multi-mode Leonov model which reduced to a multi-mode Maxwell model after linearization. Santhanam [95] approximated the shear relaxation modulus using the Prony series which yielded also a Maxwell model with a constant shear modulus at long time. Generally speaking, the thermally-induced residual stress showed a distribution with tensile skin, compressive subskin and a tensile core. This distribution was explained qualitatively as following [94]. At the begening of the cooling process, the material near the mold walls contracts. Such a process is hindered by adhesion at the walls and as a consequence, tensile stresses is introduced in the outer layers. The core of the molding remains however unstressed. When a holding pressure, P_h, is excerted on the melt, the thermal residual stress distribution across the injected part changes, becomes compressive and equal to the holding pressure P_h in the core. In the outer layers, however, the level of stress will decrease by an amout $\Delta\sigma\_ = \nu P_h / (1-\nu)$ due to the elastic behavior of these layers as mentioned above. During the holding stage, the temperature behind the rigid shell continously decreases and a small layer of material will solidify. This process will continue until the pressure inside the mold cavity vanish. At this moment, stresses in the solidified layers will increase by $\Delta\sigma$. At the end of the cooling process, the injected part will be released from the mold walls. The mechanism for the stress build-up in the hot core will now be analogous to the one proposed by Struik (92), Figure 17, which will generate tensile stresses in the core of the molding. The theory is generally in agreement with the predictions.

Bushko and Stokes [96,97} included also the effect of material being added during the packing phase, the pressure- and cooling rate dependent shift functions. They noted that the packing pressure has a large effect on the shrinkage but only a minor effect on the residual stresses.

For semi-crystalline polymers, the thermal stress distribution in the thickness direction becomes much more complicated to quantify. The significant change of the crystallinity of the specimen in the thickness direction causes the presence of crystallization stresses. For example, in the case of fast crystallizing polymers, it was shown that the highest degree of crystalinity is obtained in the inner layers of the molding. The outer layers are mainly amorphous. Consequently, the volume change by shrinkage in the inner layers will be much more important then that at outer layers of the molding and such a process will cause the build-up of crystallization stresses. These stresses will therefore have the same distribution as thermal stresses caused by a free quenching, i.e. tensile in the core and compressive at the outer layers.

2.4.4.1.3 *Reduction of residual stresses*

Residual stresses in injection-molded products are the sum of the flow, thermal and crystallization stresses. Their exact magnitude and directions depend strongly on the processing conditions, the polymers and the mold design. The residual stresses can have a large influence on the quality of the product such as optical properties, dimensional stability,

etc. In simple parts, e.g., discs and plates, which have been cooled symmetrically from both sides, the residual stress distribution is symmetric over the thickness, preventing therefore any warpage of the final product. However, they could be added to any external loading and cause a premature and unexpected failure of the product. In more complex parts, the final residual stress profile [98] is usually non-symmetric giving rise to warpage. If the warpage is severe after demolding, the productivity is affected. If the warpage occurs over long time, the service life is reduced resulting in very unsatisfied customers.

The reduction of residual stresses is therefore of particular interest. Since the large part of residual stresses arose from the large temperature gradient between the mold and the polymer, mold temperature control is specially important. In recent years, several ingenious methods have been devised for that purpose.

Liou and Suh [99] employed the idea of Low Thermal Inertia Molding (LTIM) by applying a passive insulation layer on the surface of the cavity. When designed properly, the freezing of the polymer is prevented during the filling stage, allowing the flow-induced stresses to relax prior to solidification. The experiments showed that the birefringence in the molded part was reduced by 35%.

Kim and Roth [100] used high performance thermoelectric devices in the LTIM cavity. The mold temperature could be elevated in excess of 350°C making it possible to mold engineering resins such as PC and liquid crystal polymers. Residual stresses were

indirectly evaluated using the critical fracture energy and a 15% reduction was obtained with this method.

Jansen and coworkers [101-104] constructed a fast response heating elements and studied its influence on the birefringence distribution in injection molded parts. The heating elements achieved an increase of 80°C within 0.3 seconds and thus has a small effect on the total cycle time. Yet, the with a heating pulse of 2 seconds, the birefringence is seen to reduce by a factor of 3 while for surface residual stresses, the reduction is by a factor of about 2.

2.4.4.2 The measurement of residual stress

Since residual stresses affect the mechanical behavior and the final shape of the molded part, their accurate measurement has been an important topic. In plastic products, the residual stress measurement has followed practices developed previously for metals. However, since the morphological and the mechanical properties of these two classes of materials are completely different, special attentions have to be paid in the interpretation of results obtained with plastics.

Basically, the two conventional methods, i.e. destructive and non-destructive methods, have been used for the characterization of residual stresses in plastics. The principle of the destructive method is to measure the relaxed strains at one of the specimen's surface,

after the removing of a specific amount of material from the other surface. These strains will be then used to compute residual stresses in the removed material. The residual stress distribution across the part's thickness could be therefore characterized by such a method by changing the thickness of the removed material. In contrast, the non-destructive methods have been mainly devoted to measure stresses at the surface of the molding. In the following section, typical examples of each of these two methods will be presented. The chosen examples include the solvent crazing, the hole drilling and the layer removal methods.

2.4.4.2.1 *Solvent crazing method*

When a stressed article is exposed to some solvents, it will craze and the process is known as solvent crazing. Therefore, the presence of residual stresses in a molded part can be detected qualitatively by immersing this part in an appropriate stress-cracking solution for a short time and observing the crazing due to the surface stresses. The size of these cracks depends on both the magnitude and the type of stresses at the external surface of the molding.

Two main hypotheses for the action of the solvent agent on the crack initiation were proposed [105]. The first hypothesis suggests that by wetting the molding surface with organic solvent, the surface energy of the molded part decreases and this process will be accompanied by craze formation. Other authors [106] speculated however that the plasticizing mechanism is the major factor responsible for the craze initiation. It has been suggested that the presence of the organic solvent on the surface of the molding reduces the

viscosity in the glassy state, and this will in turn initiate more easily crazing process. Both of these two interpretations seem to be realistic. However, results obtained by Kambour et al. [107-109] supported the plasticizing mechanism and showed that the crazing properties might be explained by T_g alone and do not depend on the presence of solvent solution on the external surface of the molding.

The solvent crazing method has not been widely used to measure residual stresses. One of its major limitation is its inability to measure the residual stress distribution across the part's thickness. However, because of its simplicity, such a method has been used to give a first and rapid approximation of stresses in the surface layer of the molding. Vinogradov [80] presented a comprehensive study on the use of the solvent crazing method for the characterization of residual stresses in plastic products. According to this author, residual stresses are usually concentrated in structure defects. In polymers, and due to movement of polymer chains arised from the thermal fluctuations, residual stresses can break the chemical bonds of these chains and can even cause the failure of the final product. Such a phenomena is accentuated if the polymer product is exposed to an active medium. The presence of these solutions weakens the inter and intramolecular bonds, increases both the number of the structure defects and their rate of growth. If t represents the time needed to detect the first crack at the polymer surface, after immersing the sample in the appropriate active medium, the residual stress σ therein can be evaluated using the following relation:

$$Log(t) = Log\theta + \lambda\, Log\sigma \qquad (2.36)$$

where θ and λ are experimental constants and depend on the polymer/active medium system used. To determine these constants, annealed samples with a specific level of residual stress, introduced by mechanical means, have to be prepared and immersed in the active medium. For each level of residual stress, one can evaluate the time needed to detect the first crack at the surface of the specimen. The constants θ and λ are then obtained from the plot of $\log\sigma$ vs. $\log t$. In the case of opaque samples, special equipments have to be added to the active medium to visualize the cracks at the moment of their appearance.

More recently, Cornelis and Kander [110] studied the crazing process in semi-crystalline polymers. These authors used different polypropylene specimens, each of them having been crystallized under different thermal conditions and subsequently exposed to some solvent solutions. It was observed that the crazing process mainly depends on the specimen's crystallinity. Specimens with the lowest degree of crystallinity, obtained by quenching, was found not to craze at all; however, those which were sufficiently crystallized showed a noticeable amount of crazes. Moreover, it was also found that in crazed specimens, the crazing process takes place mainly in the amorphous interspherulitic region and crazes do not cross the spherulitic structure. According to the authors, samples with higher degree of crystallinity are more susceptible to crazing. This is due to the fact that large spherulitic structures act as stress concentrations as well as change the uniformity of the elastic modulus across and along the specimen. In this case, the crazing path will be between spherulites, following the path of the lowest elastic modulus, i.e. amorphous regions.

2.4.4.2.2 *Hole drilling method*

The hole drilling method, first introduced by Methar [111], consists of drilling a hole in a stressed specimen and measuring the strains at the external surface in the surrounding of the hole using a special strain-gage rosette. As the material is removed from the hole, the stresses in its vicinity are perturbed, resulting in a local change in surface strain which can be used to reconstruct the original stress in the removed material. The hole drilling method is considered semi-destructive if holes of very small diameters are used.

A number of methods have been proposed to evaluate the residual stress distribution across the specimen's thickness from the relaxed strain data. Recently, Schajer [112], in his comprehensive review on the hole drilling method, presented four of them. They are the incremental strain, the average stress, the power series and the integral methods. The incremental strain and the integral methods, being the first and the most recent procedures for residual stress reconstruction, will be reviewed in some details.

In the incremental strain method, the incremental surface strain, arisen from a small increment in the hole depth, is assumed to be proportional to the stresses existed within that depth increment [113]. If $(\Delta\epsilon_1)$ and $(\Delta\epsilon_2)$ are the two incremental changes in the surface strain in two mutually perpendicular directions respectively, the residual stresses within the removed material are determined by:

$$\sigma_1 = \frac{E}{K_1^2 - \nu^2 K_2^2} \left(K_1(\Delta\epsilon_1) + \nu K_2(\Delta\epsilon_2) \right) \quad (2.37)$$

$$\sigma_2 = \frac{E}{K_1^2 - \nu^2 K_2^2} \left(K_1(\Delta\epsilon_2) + \nu K_2(\Delta\epsilon_1) \right) \quad (2.38)$$

where E is the modulus, ν the Poisson ratio and K_1 and K_2 are calibration constants. These constants are different for each hole depth and can be determined experimentally by incremental drilling into the specimen and measuring the strains under known, externally applied stresses.

Even though the incremental strain method is easy to use, it presents two major limitations. First, the calibration process is too long and the calibration constants K_1 and K_2 depend on many factors such as the hole diameter, the gage type and the kind of material used. Secondly, the incremental strain method neglects the effect of the hole geometry change on the strain relaxation process at the surface of the specimen [112] . Such an effect was verified by Niku-Lari et al. [114] and an increase in strains at the surface of stress-relieved specimens was found with increasing hole depth.

In the integral method, the measured strain relaxation $\epsilon(h)$, resulted from a hole of depth h, is the integral of the infinitesimal strain relaxation components from the stresses at all depths from 0 to h and is given by [115]:

$$\epsilon\ (h) = \frac{1 + \nu}{E} \int_0^h A(y,h)\ \sigma(y)\ dy \qquad (2.39)$$

where A(y,h) is the strain relaxation per unit depth caused by a unit stress at depth y when the hole depth is h, ν is the Poisson ratio, E the modulus and $\sigma(y)$ the stress at depth y.

The strain relaxation response $\epsilon(h)$ is readily measurable from strain gauges with gradually increasing hole depths. If the strain relaxation function A(y,h) is known, the above integral equation can be solved to yield the stress distribution $\sigma(y)$. Schajer [115] obtained the function A(y,h) numerically by the finite element method and results were tabulated for a specific range of hole depths and sizes. The reconstructed stresses were solved in terms of transformed stress variables to decouple the stress-strain equations and simplify the mathematical structure. It was also shown that the incremental strain and the average stress methods are special cases of the integral method.

Results obtained using the integral method indicated that stresses can be measured with reasonable accuracy to a depth of about one-half the mean radius of the strain-gage rosette below the specimen's surface. Beyond this depth, the resulting matrix equation is ill-conditioned and the results become erratic. Another difficulty with this method is related to the ill-posedness of integral equations, that is a small error in the data can lead to large fluctuation in the recovered solution. The results are thus extremely sensitive to the accuracy and noises in the experimental measurements.

One disadvantage in the hole drilling technique is the geometrical configurations which may not be receptive to the installation of the rosette. Another disadvantage is the time consuming task of installation and the alignment of the hole and the strain-gage rosette centers. Any misalignment can produce large errors in measured strains and therefore leads to an inaccurate evaluation of residual stresses. Other techniques have been proposed to overcome these disadvantages. Theoretically, an extension of the integral method to off-center hole was thus reported recently by Vangi [116]. To avoid the use of strain gauges, photoelastic-coating [117] and Moiré interferometry [118] have been employed to measure strains or displacements on the surface of the specimen. Another interesting technique is the holographic hole drilling method [119-122]. In this technique, a hologram is obtained by exposing a recording plate to a reference laser beam and one reflected from the area of interest. A small, shallow square-bottomed blind hole is drilled into the object, causing the material around the hole to deform both in-plane and out-of plane. This surface displacement alters the path length of the reflected beam, producing a pattern of optical interference fringes which can be analyzed quickly to determine the state of stresses prior to the introduction of the hole. This method can provide more rapid measurements compared to the use of rosettes; however, it requires higher equipment costs as well as special test fixture to minimize the relative motion between the test object and the hologram recording plate. The stress profile at greater depth can also be obtained by drilling a larger hole directly over a preceding smaller one [122].

2.4.4.2.3 *Layer removal technique*

The layer removal technique is one of the most popular methods for the determination of residual stresses in molded parts. In this technique, rectangular specimen is cut from the part at positions where the stresses are to be measured. Thin, uniform layers are then removed from one surface of the specimen, thus perturbing the residual stress equilibrium. To regain equilibrium, the specimen is deformed into the shape of a circular arc. After each layer removal, the radius of curvature of the remaining specimen is measured and a plot of curvatures against the thickness of the removed material is generated. The relation between the unknown residual stress σ at depth z_1 and the measured curvature ρ was first derived by Treuting and Read [123]:

$$\sigma_x(z_1) = -\frac{E}{6(1-\nu^2)}\left\{\begin{array}{l}(z_o+z_1)^2\left[\dfrac{d\rho_x(z_1)}{dz_1}+\nu\dfrac{d\rho_y(z_1)}{dz_1}\right] \\ +4(z_0+z_1)[\rho_x(z_1)+\nu\rho_y(z_1)]-2\displaystyle\int_{z_1}^{z_2}[\rho_x(z_1)+\nu\rho_y(z_1)]dz\end{array}\right\} \qquad (2.40)$$

where σ_x is the longitudinal stress, z_0 the half thickness of the specimen, E the elastic modulus, ν the Poisson ratio and ρ_x and ρ_y are the longitudinal and transverse curvatures, respectively. A similar expression for the transverse stress $\sigma_y(z_1)$ can be obtained by interchanging subscripts x and y in equation (37). Values of $d\rho/dz$ and $\int\rho dz$ used in equation (37) are determined from the plot of $\rho(z_1)$.

Strictly speaking, equation (37) is only applicable to linear elastic materials with constant properties throughout the specimen. Furthermore, it was assumed that the stresses vary only in the thickness direction, are symmetric across the central plane. Most important is the assumption that no additional stresses are introduced into the specimen during the layer removal process. Usually, most or all of these assumptions are not satisfied for injection molded thermoplastics [124,125]. It has been shown that the elastic modulus changes in the thickness direction. Due to the viscoelastic nature of polymers, stress relaxation and creep may occur during the sample preparation and measurement. Since the material undergoes a very complex thermomechanical history during the injection molding cycle, the stresses are rarely uniform in the planar direction or symmetric across the thickness. Therefore extreme precautions have to be taken in appying this technique.

White et al. [126-128] has presented an analysis taking into account the variation of modulus over the thickness of the specimen. After a detailed study the authors concluded that for the majority of cases, the unmodified equation is still adequate provided that the appropriate modulus is used at each thickness position [128].

To minimize the stress relaxation and creep during sample preparation, the sample should be kept at very low temperature, ideally near the glass transition temperature. In addition, the use of a sharp cutter at high speed during the removal of layers can prevent undesired deformations and local heating. It was shown that under these conditions, additional stresses are negligible [101,129].

The precision of the layer removal method depends to a large extent on the accurate measurement of the curvature. The usual procedure is to measure the positions of three points along the same line on the surface of the specimen and fit a circle of radius r through them. Let (x_i,y_i), where i is between 1 and 3, be the coordinates of the three points, then the coordinates of the center and the radius r are determined by:

$$x = \frac{(x_2^2 - x_1^2) + (y_2^2 - y_1^2) - 2y\,(y_2 - y_1)}{2(x_2 - x_1)} \tag{2.41}$$

$$y = -\frac{(x_2-x_1)[(x_3^2-x_1^2) + (y_3^2-y_1^2)] + (x_3-x_1)[(x_2^2-x_1^2) + (y_2^2-y_1^2)]}{2[(y_2-y_1)(x_3-x_1) - (y_3-y_1)(x_2-x_1)]} \tag{2.42}$$

$$r^2 = (x - x_2)^2 + (y - y_2)^2 \tag{2.43}$$

Various methods have been proposed to measure the coordinates of the three points including dial gauge, coordinate machine and optical methods [130].

In the dial gauge method, the sample is placed convex upwards on two knife edges and a probe with a micrometer drive is used to measure the deflection h, Figure 2.22. In this special case, equations (38-40) are simplified to:

$$(\frac{L}{2})^2 = r^2 - (r - h)^2 \tag{2.44}$$

where L is the distance between the two knife edges. Different mechanical devices, such as a vertical probe, steel balls and magnets, or peg and pegboard, attached to a coordinate machine have also been employed to measure the positions of surface points, Figure 2.23. Essentially, the coordinate machine provides the longitudinal positions x_i while the vertival position of the probe gives the transverse positions y_i of the measured points. Mechanical methods have a common disadvantage that the surface coordinates of the specimen can be affected by the weight of the sample and the contact between the probe and the specimen. This problem can be avoided by using a non-contact optical technique. In the technique developed by White et al. [126,127], two mirors are attached to the surface of the curved specimen a known distance apart. The position of the reflection of a laser beam, which pivots about a point approximately 1m from the specimen, is recorded on a screen. A relationship between the radius of curvature of the specimen (r) and the position of the reflected laser beam on the screen was derived by Sandilands [131]. The accuracy of this method depends greatly on the contact between the mirors and the specimen's surface, and special attentions are required during the mounting of these mirors. A further step was taken by Akay and Ozden [130] using a laser beam scanner. In this method, the specimen is placed freely onto the table of a coordinate machine, concave surface down, and a highly accurate laser beam measurement gauge scans the surface of that specimen. The y_i coordinate of each point on the external surface of the specimen is recorded using the monitor of the scanner. This

method was found to be the most accurate and practical for measuring the specimen's curvature.

The technique developed by Treuting and Read [123] is only applicable to rectangular samples. For axisymmetric samples such as rings and tubes, the residual stresses consist of a radial component, σ_r, and a hoop component, σ_θ which must satisfy the following equilibrium equation and boundary conditions:

$$\frac{d\sigma_r}{dr} + \frac{\sigma_r - \sigma_\theta}{r} = 0 \tag{2.45}$$

$$\text{at } r = a \text{ and } b \tag{2.46}$$

The radial stress can then be shown to relate to the hoop stress by:

$$\sigma_r(r) = -\frac{1}{r}\int_r^b \sigma_\theta \, dr \tag{2.47}$$

where a and b are, respectively, the inner and outer radius of the tube.

Several procedures have been proposed for the determination of the residual hoop stress distribution such as the ring removal, the tube slitting, the radial cut, and the ring-sector layer removal. The stresses are computed either from the gap displacement due to slitting, from the relaxed strain data measured by single element strain gages bonded on the

surface of the specimen or from the displacement response measured by the Moire interferometry [132-134].

In the ring removal technique [131], an outer (or inner) layer is removed and the radial displacement is measured at the inner (or outer) surface. Let $\Delta u(r)$ be the change in radial displacement due to the removal of a thin ring at position r, then :

$$\sigma_\theta = -\frac{E}{2}\left[\frac{\Delta u}{a}\left[1+\left(\frac{a}{r}\right)^2\right]+\frac{d\Delta u}{d\,(r/a)}\left(\frac{r}{a^2}\right)\left[1-\left(\frac{a}{r}\right)^2\right]\right] \tag{2.48}$$

It turned out that the strain measurement using strain gauges is difficult and the radial displacement is quite small. This leads to the slitting technique in which the tube is slitted axially, after the removal of an outer (or inner) layer, resulting in a gap δ which depends on the remained thickness h of the tube after the layer removal. For a thin-walled tube with outer layer removal, Williams et al. [132] derived the following relation:

$$\sigma_\theta = \frac{E}{12\pi a^2}\left[4h\delta + h^2\frac{d\delta}{dh} + 2\int\delta dh\right] + \sigma_0 \tag{2.49}$$

where σ_0 is a constant which may be obtained from the zero hoop load condition:

$$\int_0^{h_0}\sigma_\theta\, dh = 0, \qquad h_0 = b - a \tag{2.50}$$

Similar expressions were obtained for inner layer removal and for thick-walled tube.

In the radial cut technique, a diamond band saw is used to make cuts of different depths along a radius of the tube. At each depth, responses from six strain gages installed in the hoop direction are recorded during the cutting process as shown in Figure 1 of reference [133]. In the ring sector outer layers removal method, a ring sector of 45° is cut from the ring. The outer layers of the sector are removed while strains are measured from the inner surface. The average of these responses is used together with the orthotropic elasticity solution in order to obtain the residual hoop and radial stress distributions across the specimen's thickness. Different expressions were derived for the radial cut, the ring outer layer removal and the ring sector outer layers removal technique [133,134]. Experimental data obtained from different techniques were compared. The results showed the same trend for both radial and hoop stresses. The values for hoop stresses were in close agreement for different techniques except near the outer wall. However, the variations in radial stress are much higher. The differences may come from the non-uniform layer being removed due to the deformation of the tube.

2.4.5 **Conclusion**

In this work, recent advances in the understanding of the build-up of molecular orientation, crystalline structure and residual stresses in injection-molded parts have been reviewed.

Different methods for the measurement of the molecular orientation were presented, specially the details on sample preparation techniques. New, theoretical models were discussed which showed marked improvements in predicting the general distribution of orientation throughout the molded part. The interaction between the crystallinity and orientation was elucidated whereby the crystallization helps retain the degree of orientation.

The mechanisms for the generation of residual stresses were described. It was shown that each mechanism yields its own characteristic distribution which is dependent not only on the material properties and processing conditions but also on the mold geometry. The interaction of these mechanisms gives rise to a complex distribution in the final product. However, with new advances in numerical simulations, a consistent picture starts to emerge. Several methods for reducing orientation and residual stresses have been proposed and proved to be very effective.

On the other hand, the measurement of residual stresses remains a difficult task. In this review, the classical techniques for measuring residual stresses as applied to polymers

were discussed including the solvent crazing, the hole drilling and the layer removal techniques. The emphasis here is not on the theoretical development of the techniques themselves but rather on the practical details for sample preparation and accurate measurement of deformations and/or curvature after the drilling or removing of layers. In the case of the layer removal technique, the determination of residual stresses in axisymetric specimens such as tube or rings were also examined.

2.4.6 **References**

1. A. I. Isayev, *Polym. Eng. Sci.*, **23,** 271 (1983).
2. M. F. Bain, S. L. Janicki, A. S. Ulmer, and L. S. Thomas, *SPE ANTEC Tech. Paper*, 977 (1992).
3. P. Delbarre, J. Pabiot, J. F. Daurelle, V. Lamblin, and F. Rietsch, *SPE ANTEC Tech. Paper*, 301 (1991).
4. C. S. Hindle, J. R. White, D. Dawson, W. J. Greenwood, and K. Thomas, *SPE ANTEC Tech Paper*, 783 (1981).
5. A. Siegmann, S. Kenig, and A. Buchman, *Polym. Eng. Sci.*, **27,** 1069 (1987).
6. R. Y. Chang and B. D. Tsaur, *Polym. Eng. Sci.*, **35,** 1222 (1995).
7. A. Siegmann, A. Buchman, and S. Kenig, *Polym. Eng. Sci.*, **21,** 997 (1981).
8. L. Hoare and D. Hull, *Polym. Eng. Sci.*, **17,** 204 (1977).
9. W. Dietz and J. L. White, *Rheol. Acta*, **17,** 676 (1978).
10. Z. Tadmor, *J. App. Polym. Sci.*, **18,** 1753 (1974).

11. G. Menges and G. Wübken, *SPE ANTEC Tech. Paper*, 519 (1973).

12. M. R. Kamal and V. Tan, *Polym. Eng. Sci.*, **19,** 558 (1979).

13. G. Menges, A. Dierkes, L. Schmidt, and E. Winkel, *SPE ANTEC Tech Paper*, 300 (1980).

14. J. L. White and H. B. Dee, *Polym. Eng. Sci.*, **14,** 212 (1974).

15. L. R. Schmidt, *Polym. Eng. Sci.*, **14,** 797 (1974).

16. A. I. Isayev and C. A. Hieber, *Rheol. Acta*, **19,** 168 (1980).

17. A. A. M. Flaman, *Polym. Eng. Sci.*, **33,** 193 (1993).

18. A. A. M. Flaman, *Polym. Eng. Sci.*, **33,** 202 (1993).

19. L. Mandelkern, *Crystallization of Polymers*, McGraw Hill: New York (1964).

20. B. Wunderlich, *Macromolecular Physics*, Academic: New York (1973); Vols. 1 and 2.

21. M. C. Chien and R. A. Weiss, *Polym. Eng. Sci.*, **28,** 6 (1988).

22. J. P. Trotignon and J. Verdu, *J. Appl. Polym. Sci.*, **34,** 1 (1987).

23. S. S. Katti and J. M. Schultz, *Polym. Eng. Sci.*, **22,** 1001 (1982).

24. V. Tan and M. R. Kamal, *J. Appl. Polym. Sci.*, **22,** 2341 (1978).

25. M. R. Kantz, *Int. J. Polym. Mater.*, **3,** 245 (1974).

26. M. R. Kantz, H. D. Newman, JR., and F. H. Stigale, *J. Appl. Polym. Sci.*, **16,** 1249 (1972).

27. W. Wenig and F. Herzog, *J. Appl. Polym. Sci.*, **50,** 2163 (1993).

28. C. M. Hsiung and M. Cakmak, *J. Appl. Polym. Sci.*, **47,** 125 (1993).

29. J. A. Ferrara and M. Goncharko, *SPE ANTEC Tech Paper*, 2440 (1996).

30. C. M. Hsiung, M. Cakmak and Y. Ulcer, *Polymer*, **37,** 4555 (1996).

31. I. M. Ward, *Adv. Polym. Sci.*, **66**, 81 (1985).

32. D. A. Jarvis, I. J. Hutchinson, D. I. Bower and I. M. Ward, *Polymer*, **21**, 41 (1980).

33. R. J. Roe and W. R. Krigbaum, *J. Chem. Phys.*, **40**, 2608 (1964).

34. R. J. Roe, *J. Appl. Phys.*, **36**, 2024 (1965).

35. R. J. Roe, *Encyclopedia of Polymer Science and Engineering*, H. F. Mark et al (Eds.), **17**, John Wiley & Sons, New York (1989)

36. G. L. Wilkes, *Encyclopedia of Polymer Science and Engineering*, H. F. Mark et al (Eds.), **14**, John Wiley & Sons, New York (1988).

37. R. Zbinden, *Infrared Spectroscopy of High Polymers*, Academic Press (1964).

38. P. H. Hermans and P. Platzek, *Kolloid Z*, **88,** 68 (1939).

39. P. H. Hermans, J. J. Hermans, D. Vermaas, and A. Weidinger, *J. Polym. Sci.*, **3,** 1 (1948).

40. F. H. Moy and M. R. Kamal, *Polym. Eng. Sci.*, **20**, 957 (1980).

41. K. C. Cole, J. Guèvremont, A. Ajji, and M. M. Dumoulin, *Appl. Spectrosc.*, **48,** 1513 (1994).

42. M. Pigeon, R. E. Prud'homme, and M. Pézolet, *Macromol.*, **24,** 5687 (1991).

43. S. Röber and H. G. Zachmann, *Polymer*, **33,** 2061 (1992).

44. M. G. Rogers, *J. Mater. Sci.*, **26,** 4285 (1991).

45. J. L. White and J. E. Spruiell, *Polym. Eng. Sci.*, **21**, 859 (1981).

46. R. J. Samuels, *Polym. Eng. Sci.*, **23**, 257 (1983).

47. R. D. L. Marsh, J. C. Duncan and S. Brister, *J. Therm. Analys.*, **45**, 891 (1995).

48. H. U. Hoppler, A. Dinkel and I. Tomka, *Polymer*, **36**, 3809 (1995).

49. V. Abetz and G. G. Fuller, *Rheol. Acta*, **29**, 11 (1990).

50. K. Hongladarom and W. R. Burghardt, *Macromol.*, **26**, 785 (1993).

51. F. Beekmans and A. P. de Boer, *Macromol.*, **29**, 8726 (1996).

52. A. Ajji, J. Guèvremont, R. G. Matthews and M. M. Dumoulin, *SPE ANTEC Tech. Paper*, (1998) (submitted for publication).

53. J. L. White and M. Cakmak, *Encyclopedia of Polymer Science and Engineering*, H. F. Mark et al (Eds.), **10**, John Wiley & Sons, New York (1987).

54. Z. W. Wilchinsky, *J. Appl. Phys.*, **30,** 792 (1959).

55. R. A. Sack, *J. Polym. Sci.*, **54,** 543 (1961).

56. M. Pick, R. Lovell and A. H. Windle, *Polymer*, **21**, 1071 (1980).

57. G. R. Mitchell and A. H. Windle, *Polymer*, **24**, 285 (1983).

58. F. M. Mirabella, Jr., *J. Polym. Sci.: Polym. Phys. Ed.*, **22**, 1283 (1984).

59. F. M. Mirabella, Jr., *J. Polym. Sci.: Polym. Phys. Ed.*, **22**, 1293 (1984).

60. F. M. Mirabella, Jr., *Appl. Spectrosc.*, **42**, 1258 (1988).

61. J. Guèvremont, A. Ajji, K. C. Cole and M. M. Dumoulin, *Polymer*, **36**, 3385 (1995).

62. A. Ajji, J. Guèvremont, K. C. Cole and M. M. Dumoulin, *Polymer*, **37**, 3707 (1996).

63. A. Kaito and K. Nakayama, *Macromol.*, **25**, 4882 (1992).

64. S. Bensaad, B. Jasse and C. Noel, *Polymer*, **34**, 1602 (1993).

65. J. A. J. Jansen, F. N. Paridaans and I. E. J. Heynderickx, *Polymer*, **35**, 2970 (1994).

66. N. J. Everall, J. M. Chalmers, A. Local and S. Allen, *Vibrational Spectrosc.*, **10**, 253 (1996).

67. H. Ben Daly, K. C. Cole, B. Sanschagrin and K. T. Nguyen, *Polym. Eng. Sci.* (submitted for publication).

68. K. C. Cole, H. Ben Daly, B. Sanschagrin and K. T. Nguyen, *Polymer* (submitted for publication).

69. G. Kampf, *Characterization of Plastics by Physical Methods: Experimental Techniques and Practical Application*, Hanser Publishers (1986).

70. N. E. Schlotter, *Encyclopedia of Polymer Science and Engineering*, H. F. Mark et al (Eds.), **14**, John Wiley & Sons, New York (1988).

71. D. I. Bower, *J. Polym. Sci. : Polym. Phys. Ed.*, **10**, 2135 (1972).

72. N. Reid and J. E. Beesley, *Sectioning and Cryosectioning for Electron Microscopy*, Elsevier, (1991).

73. L. Lundberg, Y. Sjönell, B. Stenberg, B. Terselius, and J. F. Jansson, *Polymer Testing*, **13**, 441 (1994).

74. Y. Sjönell, B. terselius, and J. F. Jansson, *Polym. Eng. Sci.*, **35**, 950 (1995).

75. D. A. Hemsley and A. M. Robinson, *Polymer Testing*, **11**, 373 (1992).

76. B. Haworth, C. S. Hindle, G. J. Sandilands, and J. R. White, *Plast. Rubber. Proc. Appli.*, **2**, 59 (1982).

77. W. H. Harland, P. Kantas and T. Habipis, *Plastics and Rubber: Processing*, **20**, 65 (1980).

78. H. Ben Daly, K.T. Nguyen, K.C. Cole, and B. Sanschagrin, *Polym. Eng. Sci.* (submitted for publication).

79. J. M. McKelvey, *Polymer Processing*, John Wiley & Sons, New York (1962).

80. V. M. Vinogradov, *Inter. Polym. Sci. Tech.*, **2,** T/91 (1975).

81. H. A. Barnes, J. F. Hutton, and K. Walters, *An Introduction to Rheology*, Elsevier (1989).

82. F. P. T. Baaijens, *Rheol. Acta*, **30,** 284 (1991).

83. F. P. T. Baaijens and L. F. A. Douven, *Appli. Sci. Resear.*, **48,** 141 (1991).

84. H. Mavridis, A. N. Hrymak, and J. Vlachopoulos, *J. Rheol.*, **32,** 639 (1988).

85. K. K. Kabanemi, A. Aït-Kadi, and P. A. Tanguy, *Rheol. Acta*, **34,** 97 (1995).

86. L. F. A. Douven, *Towards the Computation of Properties in Injection Moulded Products: Flow- and Thermally Induced Stresses in Amorphous Thermoplastics*, PhD Thesis, Eindhoven Technical University (1991).

87. B. A. Boley and J. H. Weiner, *Theory of Thermal Stresses*, Wiley, New York (1960).

88. B. D. Aggarwala and E. Saibel, *Phys. Chem. Glasses*, **2,** 137 (1961).

89. E. H. Lee, T. G. Rogers and T. C. Woo, *J. Am. Cer. Soc.*, **48,** 143 (1965).

90. O. S. Narayanaswamy and R. Gardon, *J. Am. Cer. Soc.*, **52,** 554 (1969).

91. R. Gardon and O. S. Narayanaswamy, *J. Am. Cer. Soc.*, **53,** 380 (1970).

92. L. C. E. Struik, *Polym. Eng. Sci.*, **18,** 799 (1978).

93. R. Wimberger-Friedl and R. D. H. M. Hendriks, *Polymer*, **30,** 1143 (1989).

94. W. F. Zoetelief, L. F. A. Douven, and A. J. I. Housz, *Polym. Eng. Sci.*, **36,** 1886 (1996).

95. N. Santhanam, *Analysis of Residual Stresses and Post-Molding Deformation in Injection Molded Components*, PhD Thesis, Cornell University (1992).

96. W. C. Bushko and V. K. Stokes, *Polym. Eng. Sci.*, **35**, 351 (1995).

97. W. C. Bushko and V. K. Stokes, *Polym. Eng. Sci.*, **35**, 365 (1995).

98. M. Thompson and J. R. White, *Polym. Eng. Sci.*, **24**, 227 (1984).

99. M. G. Liou and N. P. Suh, *Polym. Eng. Sci.*, **29**, 441 (1989).

100. B. H. Kim and O. Roth, *Polym. Plast. Techn. Eng.*, **27**, 467 (1988).

101. K.M.B. Jansen, *Calculation and Control of Heat Transfer in Injection Moulding*, Ph.D. Thesis, Delft University (1993).

102. K.M.B. Jansen and A.A.M. Flaman, *Polym. Eng. Sci.* **34**, 894 (1994).

103. K.M.B. Jansen and A.A.M. Flaman, *Polym. Eng. Sci.* **34**, 898 (1994).

104. K.M.B. Jansen, *Int. J. Heat Mass Transf.*, **38**, 309 (1995).

105. R. P. Kambour, *J. Polymer. Sci.: Macromolecular Reviews*, **7**, 1 (1973).

106. B. Maxwell and L. F. Rahm, *Ind. Eng. Chem.*, **41**, 1988 (1949).

107. G. A. Bernier and R. P. Kambour, *Macromolecules*, **1**, 393 (1968).

108. R. P. Kambour, E. E. Romagosa, and C. L. Gruner, *Macromolecules*, **5**, 335 (1972).

109. R. P. Kambour, C. L. Gruner, and E. E. Romagosa, *J. Polym. Sci. Phys.*, **11**, 1879 (1973).

110. H. Cornélis and R. G. Kander, *Polym. Eng. Sci.*, **36**, 869 (1996).

111. J. Methar, *Trans. ASME*, **56**, 249 (1934).

112. G. S. Schajer, *J. Eng. Mater. Tech.*, **110**, 338 (1988).

113. R. A. Kelsey, *Proceedings SESA*, **14,** 181 (1956).

114. A. Niku-Lari, J. Lu and J. F. Flavenot, *Experimental Mechanics*, **25,** 175 (1985).

115. G. S. Schajer, *J. Eng. Mater. Tech.*, **110,** 344 (1988).

116. D. Vangi, *J. Eng. Mater.Tech.*, **119**, 79 (1997).

117. C. P. Hu, *Proc. 4th Pan Pacific Conf. on Nondestructive Testing, Sec.M2, Sidney, Australia,* (1983).

118. A. McDonach, J. McKelvie, P. MacKenzie, and C. A. Walker, *Exp. Tech.*, **7,** 20 (1983).

119. D. V. Nelson and J. T. McCrickerd, *Experimental Mechanics*, **26,** 371 (1986).

120. A. Makino and D.V. Nelson, *Exp. Mech.*, **34**, 66 (1994).

121. D.V. Nelson, A. Makino, E. Fuchs and D.R. Williams, *Exp. Mech.*, **34**, 79 (1994).

122. A. Makino and D.V. Nelson, *J. Eng. Mater.Tech.*, **119**, 95 (1997).

123. R. G. Treuting and W. T. Read, JR, *J. Appli Phys*, **22,** 130 (1951).

124. B. O'Donnell and J. R. White, *J. appli. Polym. Sci.*, **47,** 189 (1993).

125. A.I. Isayev and D.L. Crouthamel, *Polym. Plast. Techn. Eng.*, **22**, 177 (1984).

126. B. Haworth, C.S, Hindle, G.J. Sandilands and J.R. White, *Plast. Rubb. Proc. Appl.*, **2,** 59 (1982).

127. J.R. White, *J. Mater. Sci.*, **20**, 2377 (1985).

128. M.W.A. Paterson and J.R. White, *J. Mater. Sci.*, **24**, 3521 (1989).

129. G.G.J. Schennink, *Thermal Stresses in Amorphous Polymers*, PhD Thesis, Twente University (1990).

130. M. Akay and S. Ozden, *Polymer Testing*, **13,** 323 (1994).

131. G. J. Sandilands, *Ph.D Thesis, University of Newcastle upon Tyne*, (1983).

132. J.G. Williams, J.M. Hodgkinson and A. Gray, *Polym. Eng. Sci.*, **21**, 822 (1981).

133. M. G. Abdallah, *Proc. 4th International Conf. on residual stresses, Baltimore, Maryland*, 81 (1994).

134. M. G. Abdallah, *Proc. 7th international Cong. on Experimental Mechanics, Las Vegas, Nevada*, 1063 (1992).

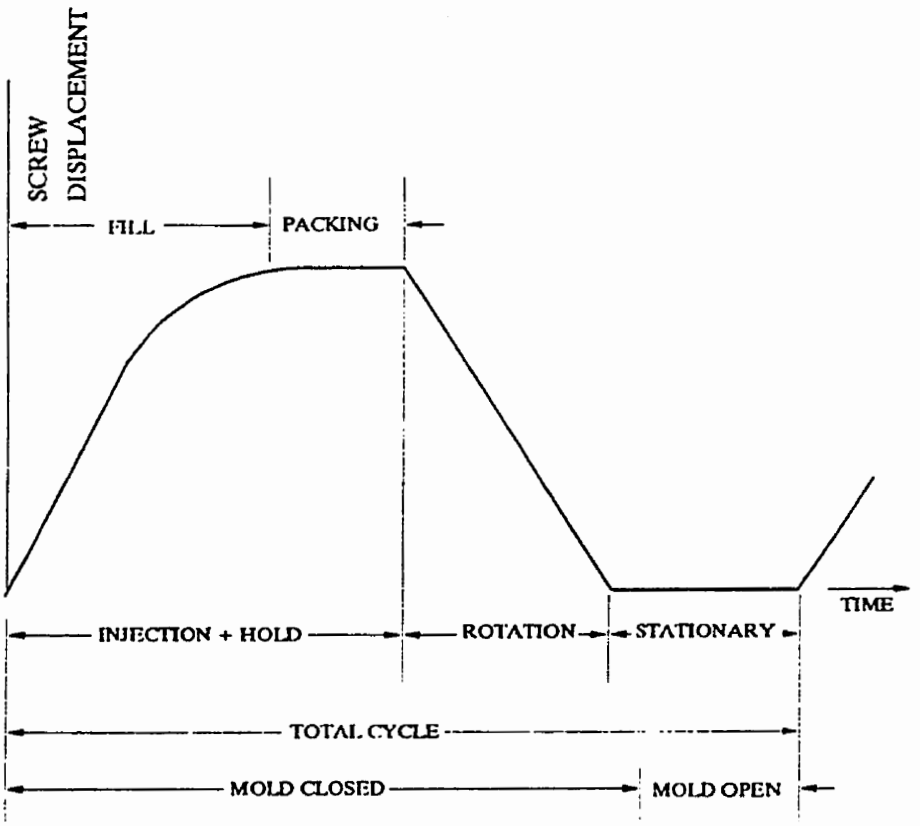

Figure 2.5 - Injection molding cycle

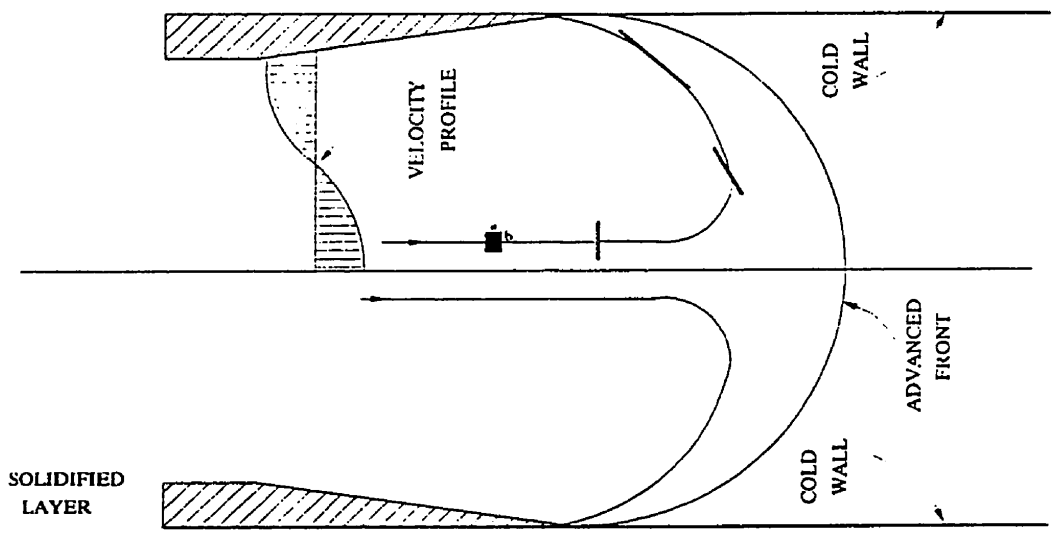

Figure 2.6 - Schematic representation of the flow pattern in the advancing front between two parallel plates [10]

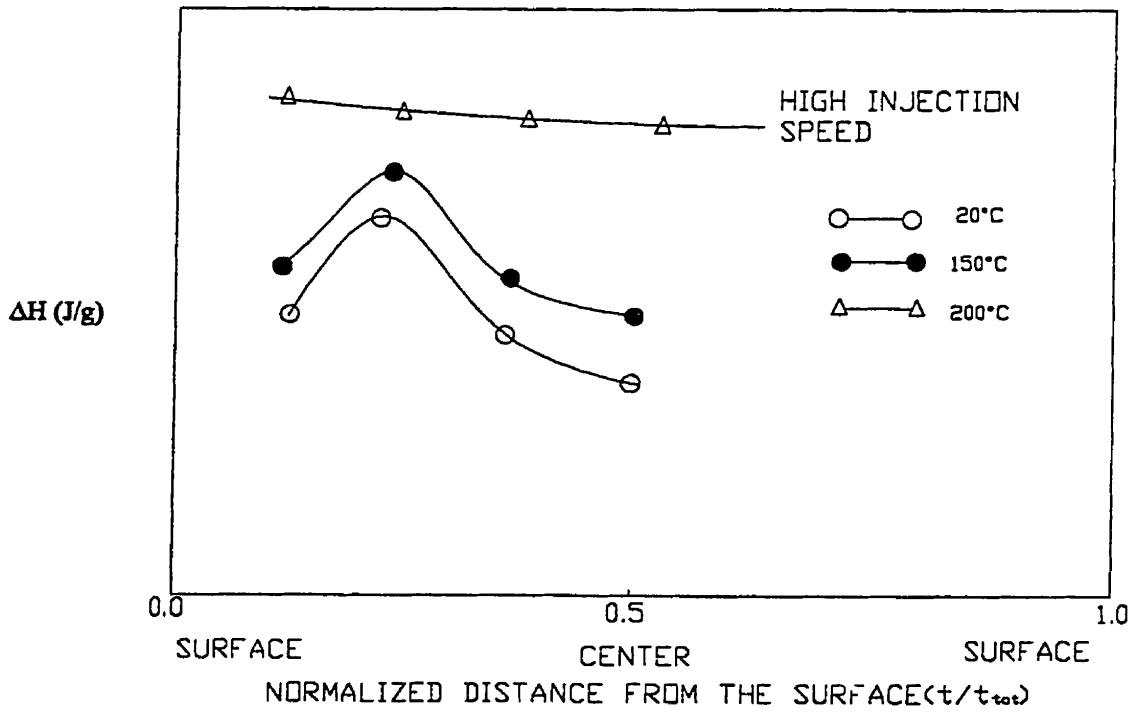

Figure 2.7 - Crystallinity variation from skin to core (center) near the gate [28]

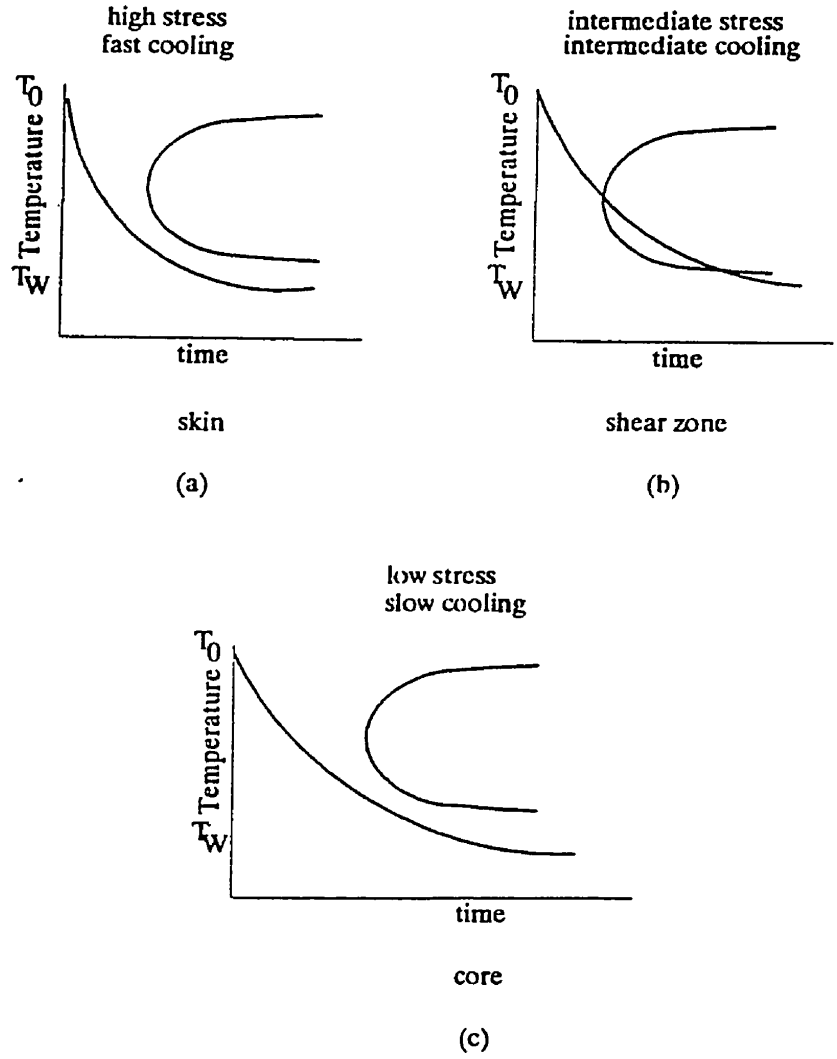

Figure 2.8 - TTT diagrams showing the behavior at (a) skin, (b) intermediate layer, and (c) at the core in samples molded at low mold temperatures [28]

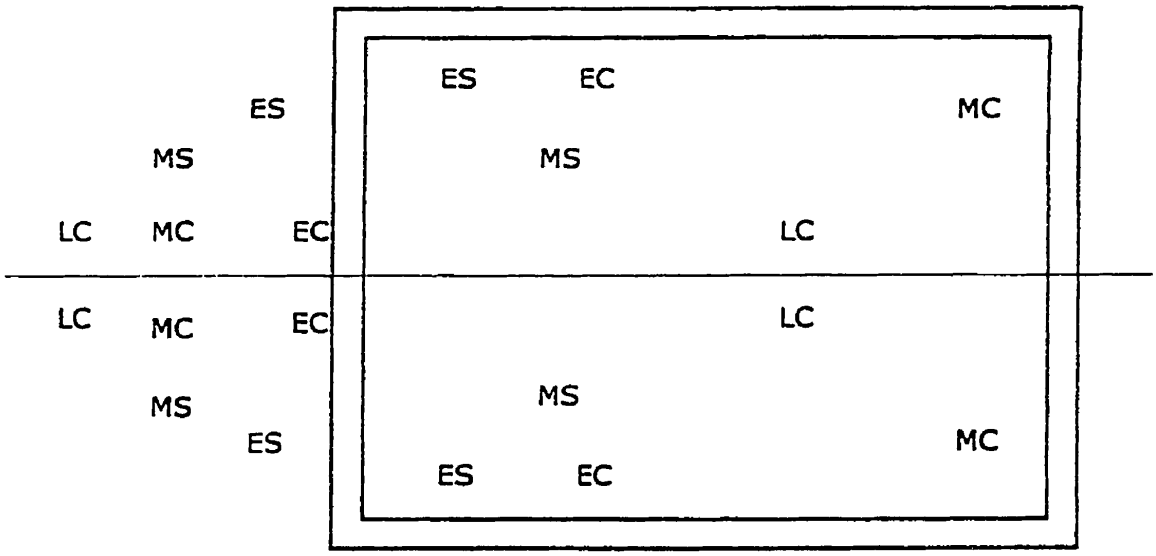

Figure 2.9 - Grouping of markers according to their original locations [30]

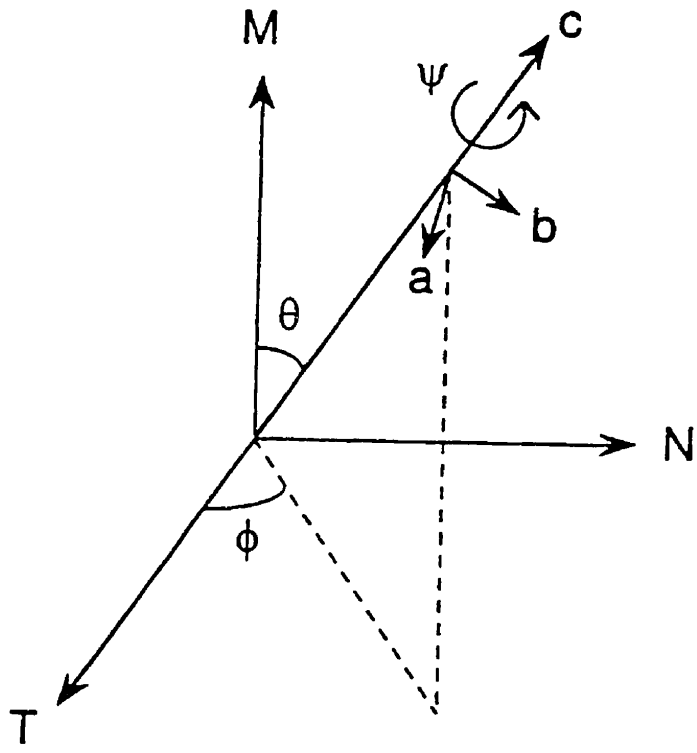

Figure 2.10 - Definition of orientation in terms of the Euler angles

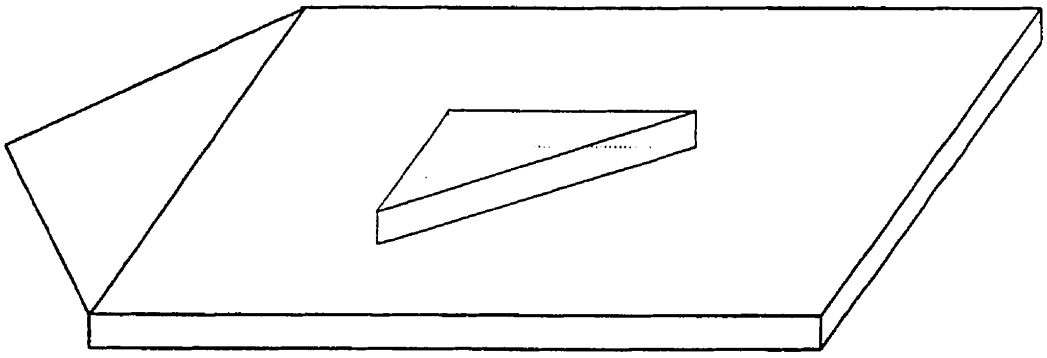

Figure 2.11 - The orientation of the wedges cut for out-of-the-plane measurements [75]

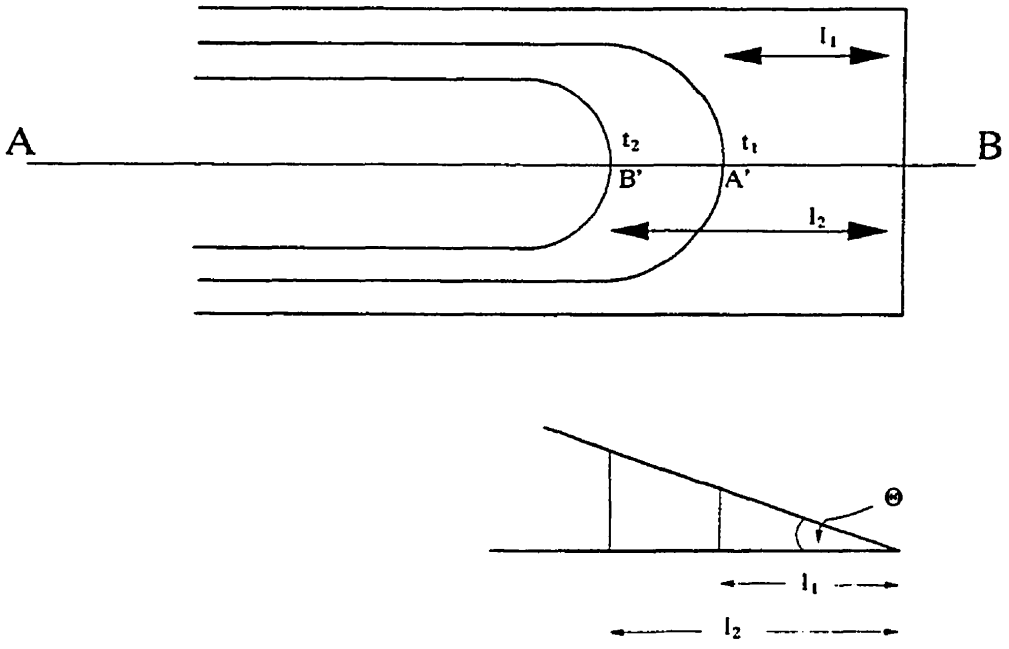

Figure 2.12 - A diagramatic representation of the wedge image showing the parameters used in calculating the birefringence along the ligne AB [75]

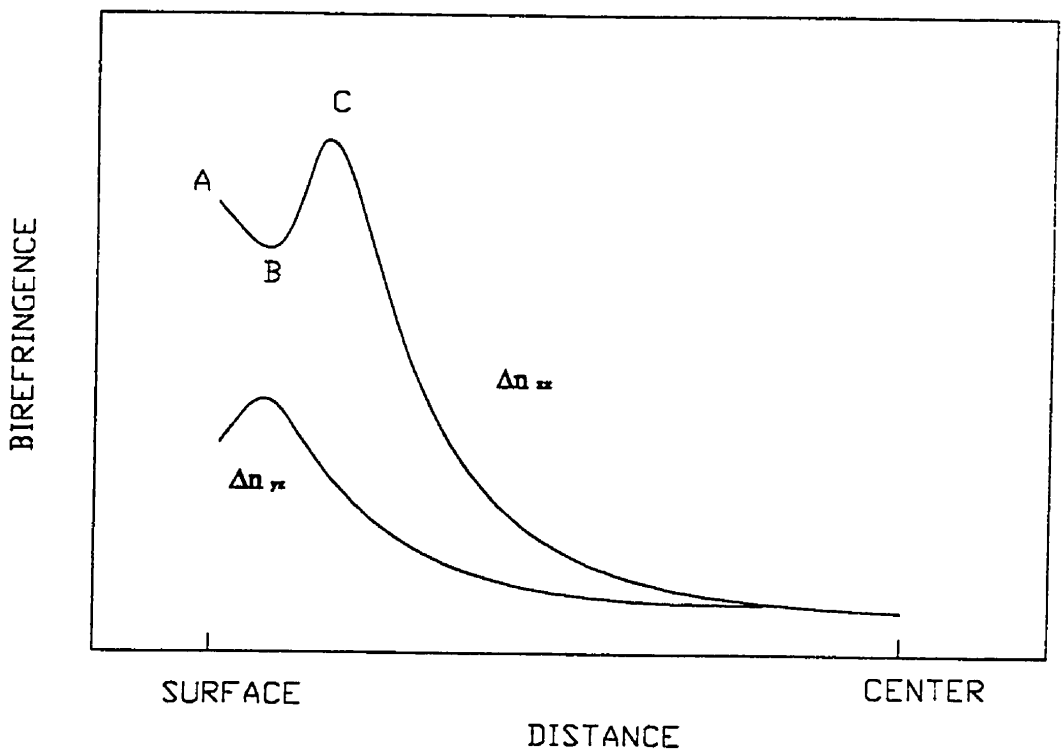

Figure 2.13 - Distribution of birefringence with depth [12]

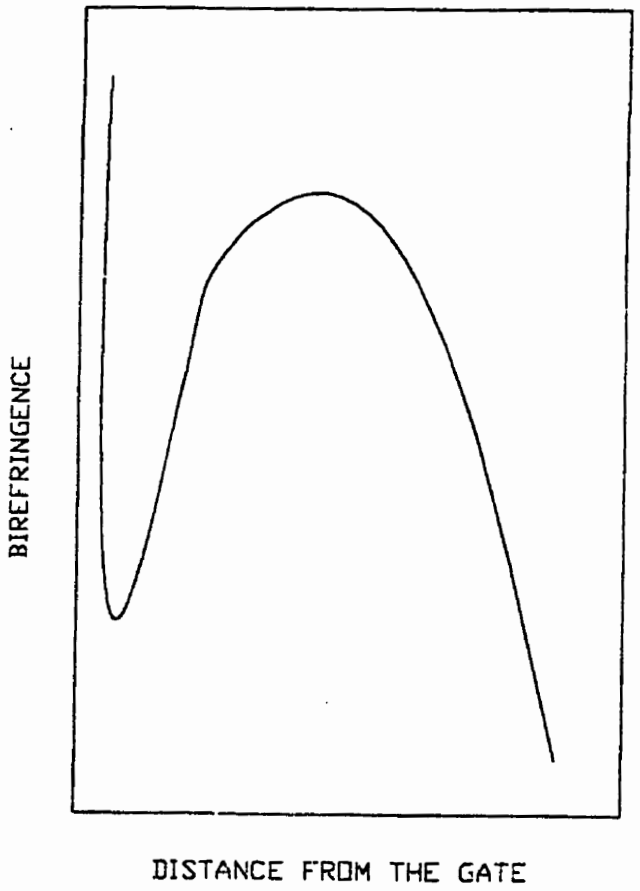

Figure 2.14 - Orientation along flow path from edge gate [77]

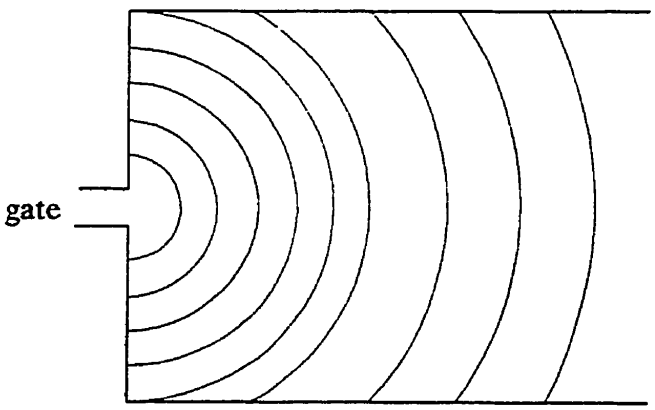

Figure 2.15- Flow in cavity, small gate

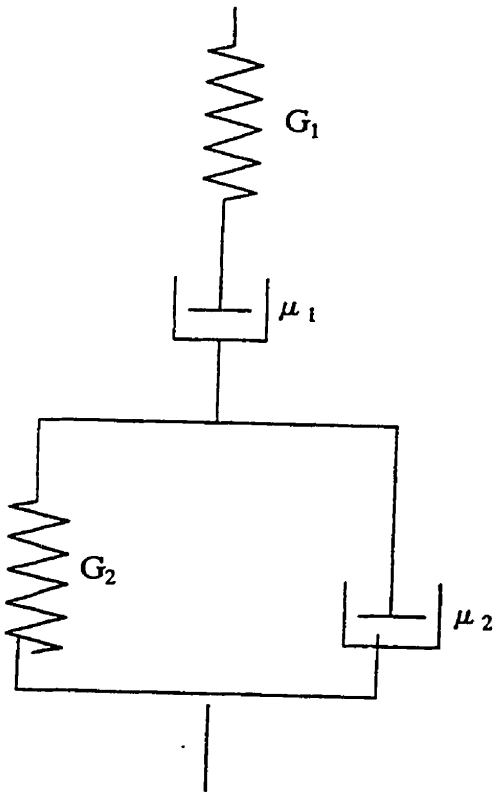

Figure 2.16 - Four-element mechanical model that simulates the shear behavior of amorphous linear polymers [79]

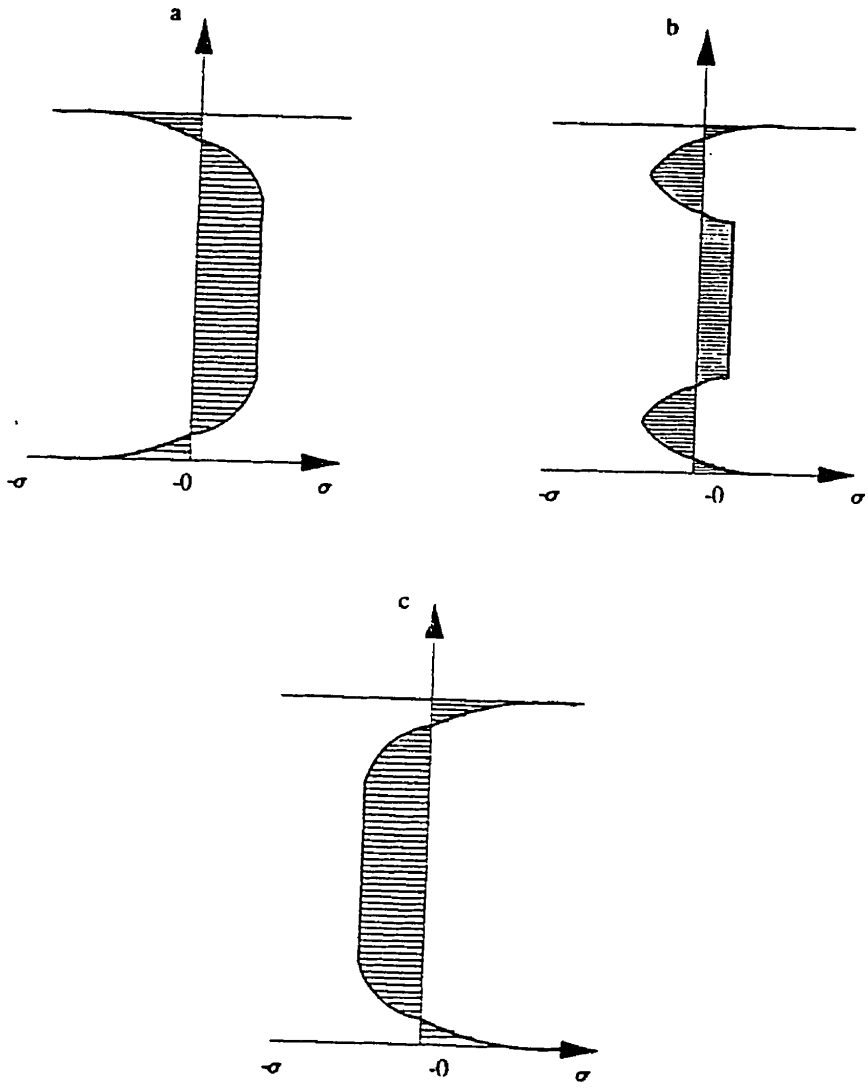

Figure 2.17 - Distribution of residual stresses over the wall thickness of an article injection-molded with under-compression of the melt (a, b) and with over-compression (c) [80]

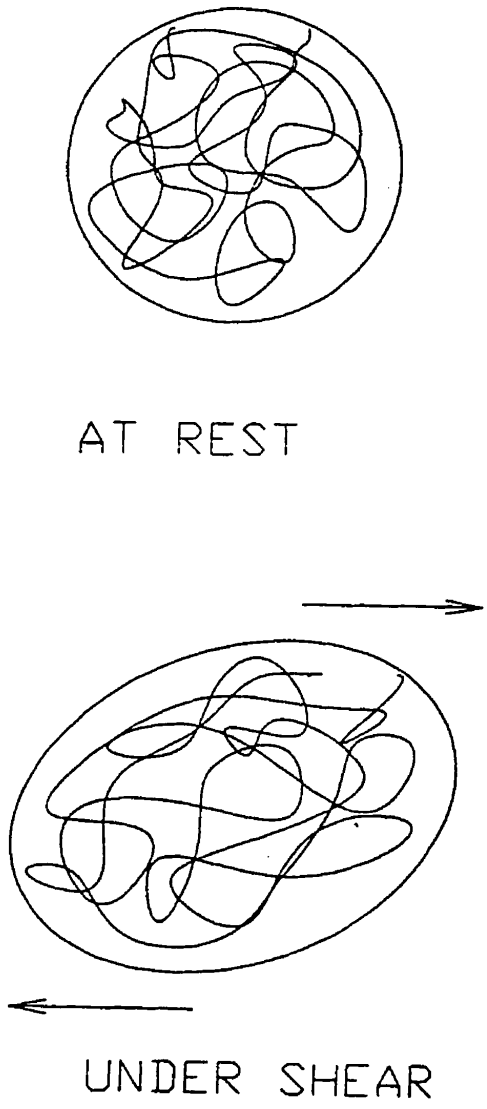

Figure 2.18 - The molecular envelope before and during shear deformation [81]

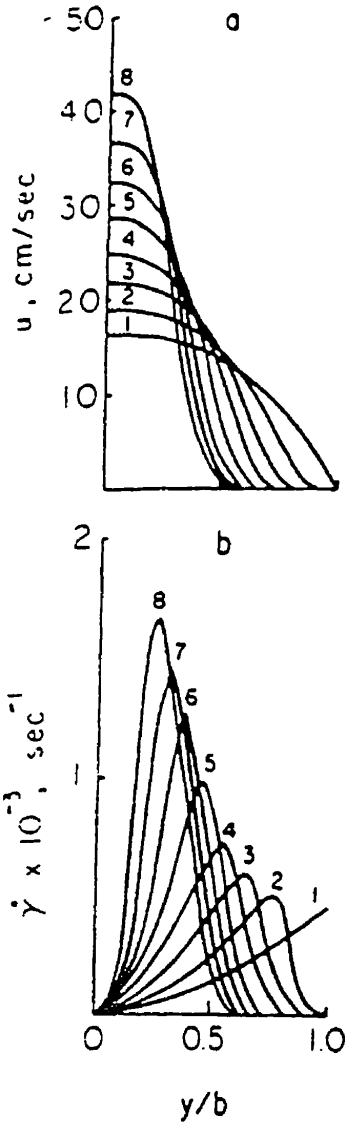

Figure 2.19- Gapwise distribution of linear velocity (a) and shear rate (b) at different filling times [16]

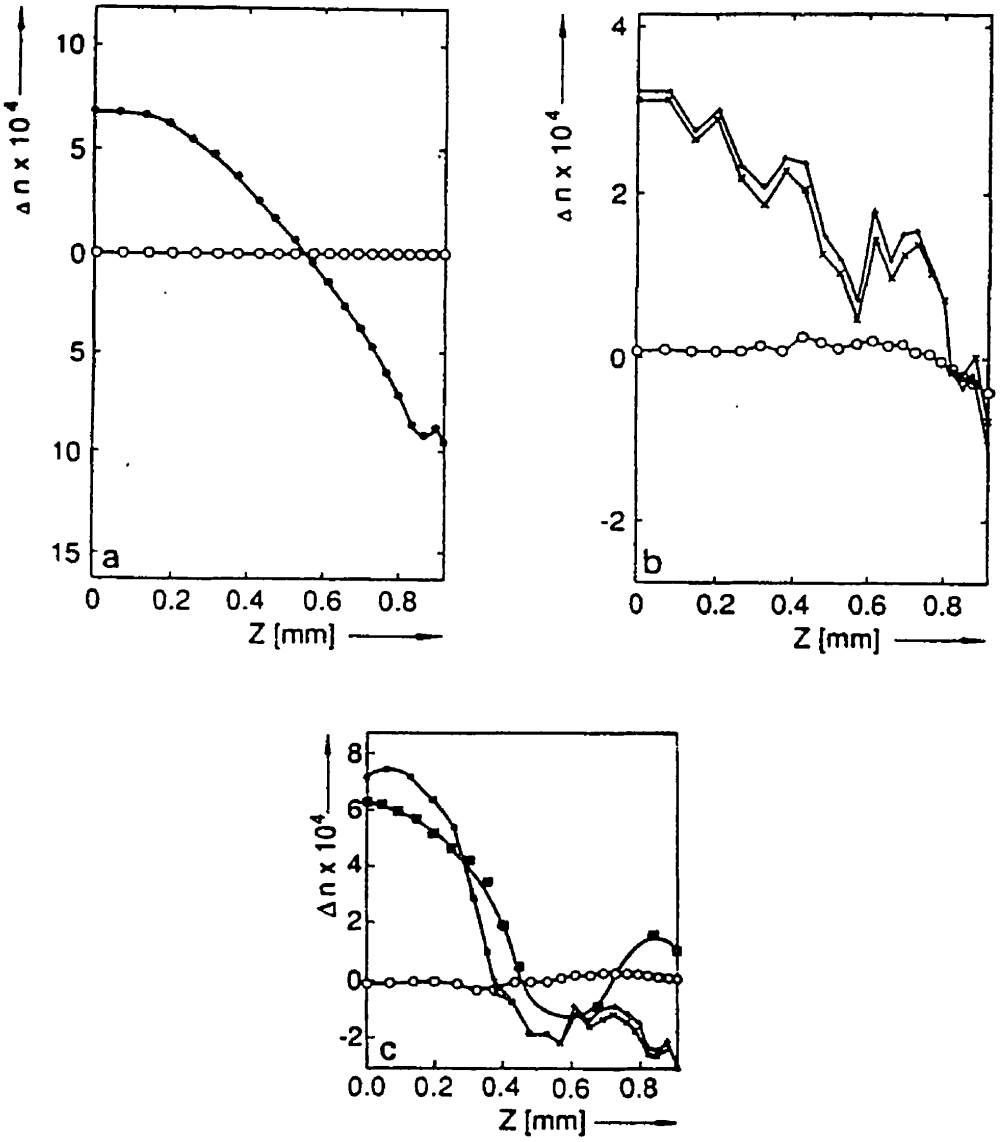

Figure 2.20 - (a) Birefringence distribution vs half of the thickness in constrained quench disc, release time = 0,9 s, (b) as (a) but release time = 3,0 s, (c) as (a) but release time = 2,65 s, (o) $\Delta n_{r\phi}$, (+) Δn_{rz}, (x) $\Delta n_{\phi z}$ [93]

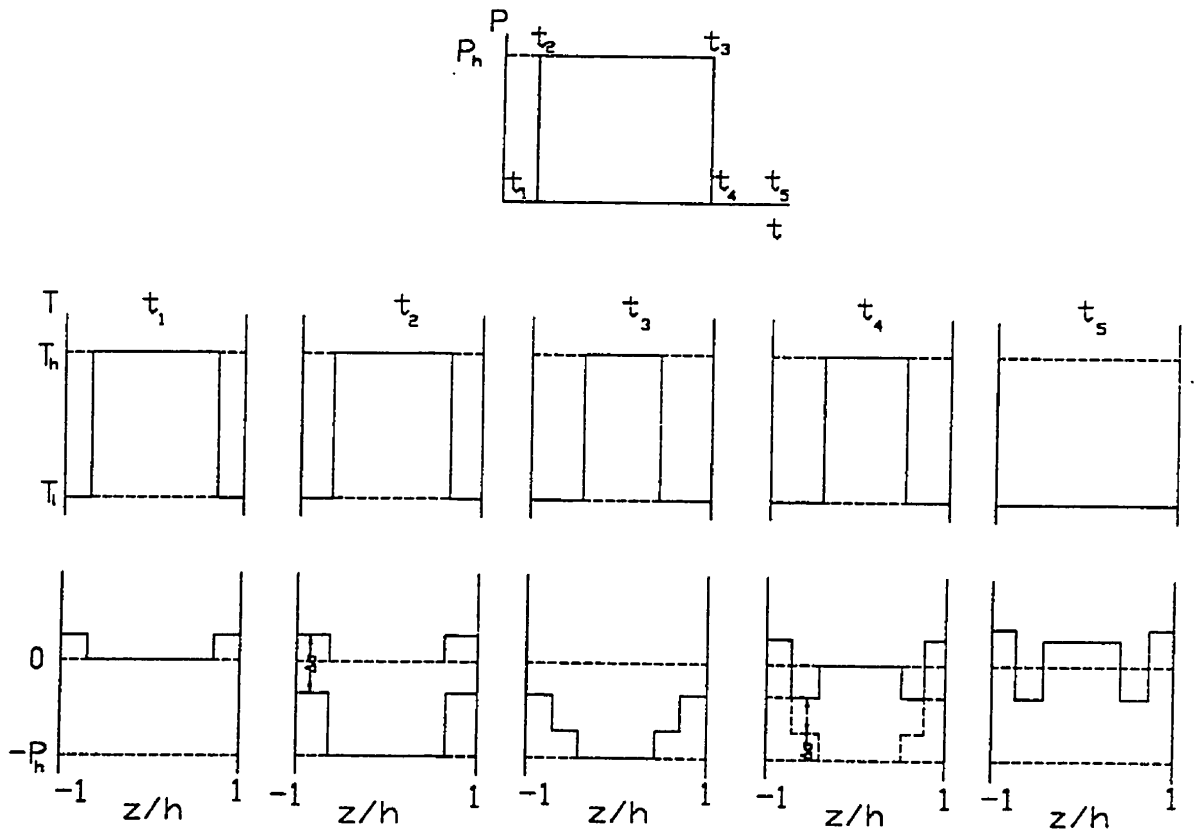

Figure 2.21 - Residual thermal stress development in injection molded products [94]

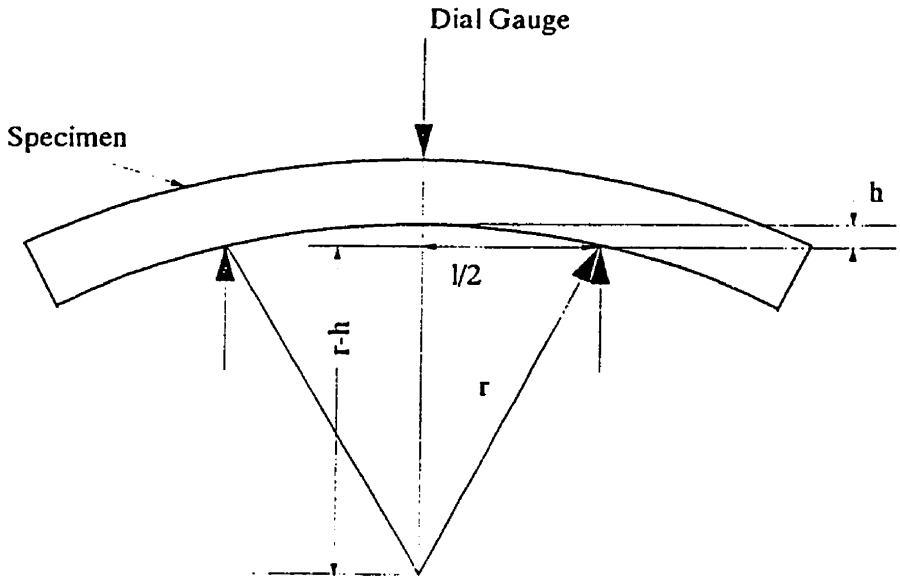

Figure 2.22 - Measurement of curvature with a dial gauge [130]

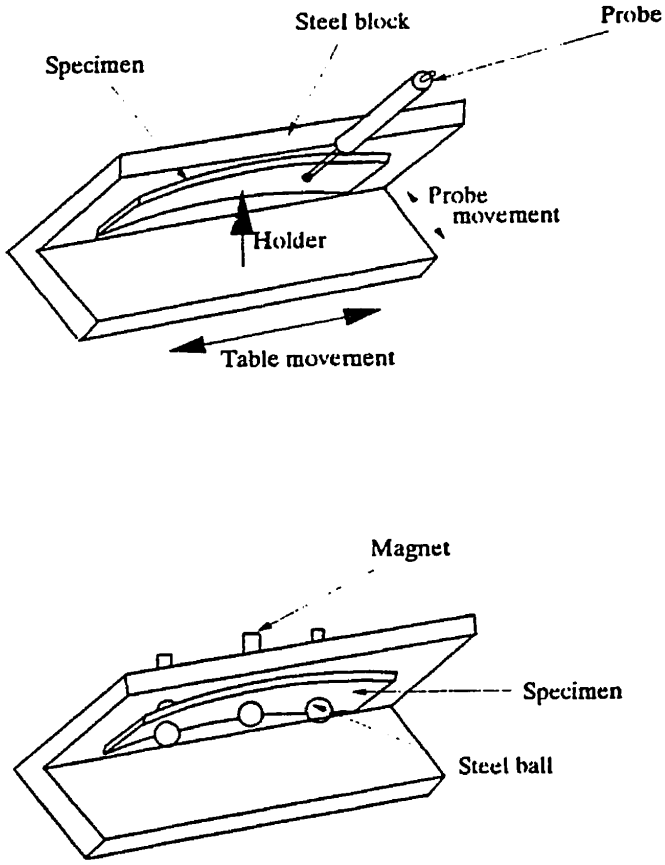

Figure 2.23 - Illustrations of the curvature measurement with a (a) vertical probe, (b) stell balls and magnets, (c) by the peg method, and (d) by the scan method [130]

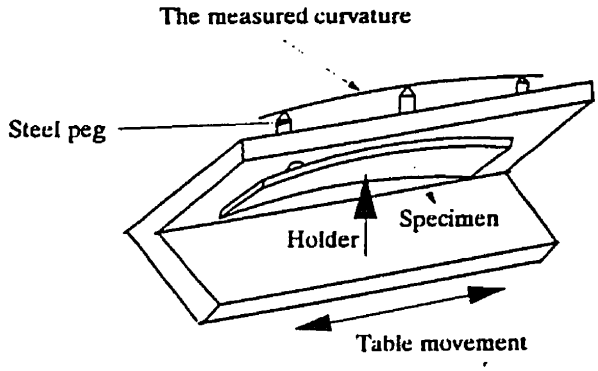

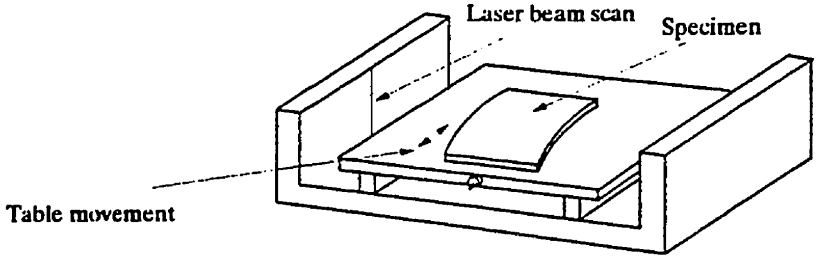

Figure 2.23 - Illustrations of the curvature measurement with a (a) vertical probe, (b) stell balls and magnets, (c) by the peg method, and (d) by the scan method [130] (suite)

CHAPITRE III

An Experimental Technique for the Characterization of Molecular Orientation through the Thickness of Plastic Products

H. BEN DALY[1], K.C. COLE[2*], B. SANSCHAGRIN[1], and K.T. NGUYEN[2]

[1] *Center for Applied Research on Polymers*

École Polytechnique

C.P. 6079, succursale Centre-ville, Montréal, Québec, Canada H3C 3A7

[2] *Industrial Materials Institute*

National Research Council Canada

75, boul. De Mortagne, Boucherville, Québec, Canada J4B 6Y4

This chapter has been submitted for publication in Polymer Engineering and Science.

3.1 RÉSUMÉ

Plusieurs techniques peuvent être utilisées pour mesurer l'orientation moléculaire à la surface des pièces plastiques. Pour caractériser l'orientation dans le coeur de ces pièces, on fait toujours appel à la technique de microtomie. Cette technique consiste à découper des petits échantillons le long de l'épaisseur de ces pièces pour une éventuelle analyse optique. Durant l'opération de découpage, les efforts appliqués sur ces échantillons ainsi que la température générée entre le couteau et l'échantillon peuvent affecter l'orientation moléculaire dans ces échantillons. Dans ce chapitre, nous proposons une nouvelle technique pour caractériser l'orientation moléculaire dans l'épaisseur des pièces plastiques.

Cette technique consiste à usiner la pièce par fraisage jusqu'au niveau où l'on veut mesurer l'orientation moléculaire et à polir la surface fraisée. Les conditions de fraisage et de polissage sont résumées dans l'article inclus dans ce chapitre. L'orientation moléculaire avant et après fraisage et polissage a été caractérisée par spectroscopie infrarouge en mode de réflexion.

La technique de fraisage et de polissage a été testée sur plusieurs polymères, uniaxialement orientés, ayant des propriétés thermique (température de transition vitreuse) et mécanique très différentes. Ces polymères sont le polyéthylène téréphtalate (PET, T_g = 70°C), le polyetheretherketone (PEEK, T_g = 150°C), le polyéthylène à haute densité (HDPE, T_g = -120°C) et les polymères à cristaux liquide (LCP). Le PET, PEEK et HDPE ont été

étirés à des hautes températures pour obtenir des échantillons uniaxialement orientés. Par contre, le LCP a été injecté vue la difficulté d'orienter ces chaînes moléculaires dans la machine de traction. Des spectres infrarouges ont été initialement mesurés sur la surface de ces polymères dans des directions de polarisation mutuellement perpendiculaires. Puis ces polymères ont été fraisés et polis et des spectres infrarouges ont été mesurés au niveau des surfaces polies. Une comparaison entre les spectres mesurés avant et après fraisage et polissage a montré que cette technique ne change pas le degré d'orientation dans les polymères ayant une température de transition vitreuse assez élevée, tels que le PET et le PEEK. En effet, pour ces polymères, les spectres mesurés avant et après fraisage et polissage se ressemblent beaucoup, indiquant la présence du même degré d'orientation dans les surfaces mesurées. De plus, cette technique a permis d'obtenir une excellente qualité des spectres (ligne de base, intensité, ..., etc.), ce qui permet une meilleure caractérisation du degré d'orientation moléculaire. Pour le cas des polymères à faible température de transition vitreuse, tel que le HDPE, la technique modifie légèrement le degré d'orientation. Ce changement est du à la relaxation des chaînes moléculaires lors du polissage. Ce phénomène peut être minimisé en améliorant les conditions de refroidissement durant cette phase (en utilisant de l'azote liquide à la place de l'eau). Pour le cas du LCP injecté, les résultats obtenus dans une couche située à 0.2 mm de la surface externe coïncident avec ceux publiés dans la littérature, indiquant que la technique de fraisage et de polissage peut remplacer la technique de microtomie et être utilisée pour mieux caractériser l'orientation moléculaire dans le coeur de certains plastiques.

3.2 ABSTRACT

An experimental technique has been developed for the characterization of the molecular orientation through the thickness of plastic products. The technique consists of milling the specimen to the depth where the molecular orientation is to be measured, polishing the exposed surface, and characterizing the polished surface by external reflection infrared spectroscopy. The technique was first tested on both unoriented and oriented poly(ethylene terephthalate). It was found that the intermediate steps of the process change the apparent surface orientation, but carrying the process to completion (to a finish of 0.05 μm) removes the altered material and leaves a surface whose orientation corresponds to that of the original sample. The technique was also tested on polyetheretherketone (PEEK), high density polyethylene (HDPE), and liquid crystal polymer (LCP). For polymers with a high transition temperature, like PEEK and LCP, the conclusions are the same as for PET. However, for polymers like HDPE, with a low glass transition temperature, the milling and polishing process used to prepare the samples can alter the orientation to a greater extent. This effect can be reduced by cooling the sample with liquid nitrogen during preparation.

3.3 INTRODUCTION

Molecular orientation in plastic products can be greatly affected by manufacturing methods. In injection molding, for example, it has been found that polymer molecules at the surface of the molding can be oriented in the flow direction parallel to the mold wall, while in the center the molecules may be completely unoriented [1,2]. Such a variation in the molecular orientation in the thickness direction will generate a difference in both the optical and mechanical properties of different layers through the thickness direction of the injected part, and consequently will affect the quality and performance of the final product [3]. Therefore, the exact determination of the variation of orientation of the polymer molecules with respect to the specimen's thickness is of great importance, since it can provide a better characterization of plastic products.

For many years, the molecular orientation across plastic products has been characterized by means of both microtoming and optical techniques such as birefringence and infrared spectroscopy [1,2]. Microtoming involves cutting from the molded specimen thin slices, or sections, with a thickness low enough to allow visible or infrared radiation to pass through. The technique is not without problems, however, because the morphological characteristics of the cut sections are affected by the cutting conditions and the quality of the knife. These problems have recently been discussed in detail [4]. It was pointed out that the local increase in temperature where the knife contacts the specimen and the compression of the section during the cutting are the major factors affecting the dimensions and the

morphology of the sections. Recent work involving infrared measurements [5,6] has also indicated that the microtoming process induces a small but significant change (around 0.05) in the orientation function.

It is the aim of this study to present an alternative method for the characterization of molecular orientation across the thickness of plastic products. It involves the removal of successive layers of polymer from the sample by means of milling and polishing, followed by measurement of the infrared spectrum by means of external specular reflection. The advantages of the latter technique for studying orientation in polymer samples have been demonstrated recently by one of the authors and coworkers [7,8] as well as by other groups [9-12].

3.4 EXPERIMENTAL

The material used in the initial experiments to develop the method was DuPont Selar PT 7086 extrusion grade poly(ethylene terephthalate), without nucleating agent. This material has a glass transition temperature of 70 °C and a crystalline melting temperature of 245 °C. A sample of undrawn PET with low crystallinity and orientation was obtained by compression molding of dried granules at 280 °C, followed by rapid cooling in a water bath. A sample of oriented PET with a draw ratio (denoted as λ) equal to 5.2 was obtained by drawing semicrystalline material in a roll-drawing process [13]. Both the drawn and undrawn specimens were considered to possess a constant molecular orientation through the thickness.

The method was then tested on other materials having different thermal and mechanical properties. These include polymers with high and low glass transition temperatures, as well as a polymer that shows morphological changes under both high temperatures and high shear rates, which may occur during the polishing process. The materials were: extrusion-grade polyetheretherketone (PEEK), Victrex 450G from ICI; extrusion-grade high density polyethylene (HDPE), extruded profile obtained from Fabco Plastics Inc.; and 20% glass-fiber-filled liquid crystal polymer (LCP), Vectra B420. The PEEK and HDPE were first extruded to obtain flat profiles (approximately 1 cm thick and 10 cm wide), then stretched by roll-drawing at high temperatures [13]. The PEEK was drawn at 250°C to $\lambda = 3.1$, and the HDPE was drawn at 110°C to $\lambda = 9.6$. The LCP composite was injection-molded on a 70-ton injection-molding machine. The injection parameters were as follows: mold temperature = 50°C; melt temperature = 300°C; injection rate = 5.08 cm/s; holding pressure = 4.14 MPa; holding time = 10 s; and cooling time = 10 s.

The molecular orientation at the surface of the samples was characterized at different stages of the milling and polishing process by means of front-surface external specular reflection infrared spectroscopy [7]. The milling process was conducted with water cooling (to maintain the temperature as low as possible) using both a single point cutter and a high cutting speed, in order to minimize the energy dissipated during the fracture and the deformation of the polymer [14]. Before the polishing process, samples cut from the milled specimens were placed in a rubber mold, milled surface down, and an epoxy resin was poured into the mold and cured (at room temperature) to provide support for the samples.

The next step was to mount the samples in a rotating polishing machine and to polish the milled surface. The step-by-step polishing process is summarized in Table 3.1. The different polishing systems were purchased from Buehler Company, USA. After each step of the polishing process, the quality of the polished surface was checked using an optical microscope and considered acceptable if the scratches generated during a previous polishing step were completely eliminated.

At each stage of the milling-polishing process, infrared reflectance spectra were measured on a Nicolet 170SX FT-IR spectrometer equipped with a Model 134 specular reflectance accessory and zinc selenide wire grid polarizer from Spectra-Tech Inc. Each spectrum was the result of an accumulation of 128 scans at a resolution of 4 cm^{-1}. The angle of incidence was 11° and a front-surface gold mirror was used as reference. For oriented specimens, spectra were measured with polarization both parallel and perpendicular to the draw direction. For unoriented specimens, spectra were measured with polarization in two arbitrary but mutually perpendicular directions. The measured reflectance spectra were subjected to Kramers-Kronig transformation in order to obtain the refractive index (n) and absorption index (k) spectra. This was done by means of the commercial software Spectra-Calc™ from Galactic Industries Corporation, with the use of their Maclaurin's series algorithm to perform integration. The software was slightly modified in-house to allow calculation of the imaginary molecular polarizability function ϕ from the n and k spectra. The molecular polarizability correlates more closely with the molecular properties, especially

for the more intense absorption bands [15]. From the ϕ spectra, dichroic ratios and orientation functions were calculated according to the usual procedures [7].

3.5 RESULTS AND DISCUSSION

3.5.1 Poly(ethylene terephthalate) (PET)

The reflectance spectra obtained for the undrawn highly amorphous PET sample at the different stages of the milling and polishing process are shown in Figure 3.1. They are all shown at the same reflectance scale in order to illustrate the effect of surface quality on the overall reflectance. The molecular polarizability spectra obtained from the reflectance spectra are shown in Figure 3.2. In this case, the y-axis scale is adjusted for each case in order to better show the details of the spectra.

Figures 3.1a and 3.2a show the spectra obtained from the surface of the undrawn specimen before any milling or polishing. Contrary to what might be expected, the two polarization directions do not give exactly the same result, although they are very similar. The small difference indicates the presence of slight molecular orientation at the surface of the specimen. The main difference is noted for the CH_2 wagging peak of the trans glycol conformers at 1340 cm^{-1}, which has a dichroic ratio D equal to 1.9. This peak is highly sensitive to orientation. The slight orientation is believed to be due to the excessive

compression of the polymer melt in the mold during the molding process, which can orient polymer chains at the surface of the specimen in one arbitrary direction.

Figures 3.1b and 3.2b show the spectra obtained after the milling process. The surface exposed by the milling was 0.1 mm below the original surface of the specimen. It can be seen that the overall intensity of these spectra is considerably lower than that of the preceding ones. This is due to increased surface roughness. As a result, much of the incident radiation is diffusely reflected and therefore not detected by the specular reflection accessory; this gives rise to a low apparent reflectance and poor signal-to-noise ratio. In fact, the weaker peaks are barely visible.

In order to overcome this problem, the quality of the milled surface was improved by progressive polishing. The first step of the polishing process was sanding with 320 grit paper to reduce both the number and the size of defects generated during the milling. The spectra obtained are shown in Figures 3.1c and 3.2c. Because the surface is still fairly rough, they are no better than those of the milled surface. The only improvement, if any, is a somewhat straighter baseline.

After further sanding, to 800 grit, the spectra shown in Figures 3.1d and 3.2d are obtained. Because of the reduced roughness, the reflectance spectra become much more intense and well defined, and all the main characteristic peaks of PET are observed. However the peaks in the ϕ spectra are slightly deformed, indicating that the Kramers-Kronig

transformation does not cleanly separate the n and k contributions. Furthermore, comparison of the parallel and perpendicular spectra shows the presence of dichroism, particularly evident for the 1340 cm^{-1} peak. This suggests that the sanding has induced some orientation at the surface of the specimen.

The next stage of the specimen preparation was polishing with 3 μm diamond paste. The resulting spectra are shown in Figures 3.1e and 3.2e. On comparison with the preceding spectra, it can be seen that the overall reflectance level has improved slightly, and, more important, the dichroism has practically disappeared. The oriented material produced by the 800 grit sanding appears to have been removed.

The final stage of the process was polishing with 0.05 μm diamond paste. The spectra, shown in Figures 3.1f and 3.2f, are of excellent quality and are virtually identical in shape. There is no indication of any orientation, as expected for a hot-pressed undrawn sample. The slight orientation observed at the original surface is not seen at lower depths.

Figures 3.3 and 3.4 show a similar set of spectra obtained for the highly oriented PET sample. In this case, as expected, the spectra recorded for the initial surface show strong dichroism. The carbonyl band at 1729 cm^{-1} and the benzene ring out-of-plane C-H band at 730 cm^{-1} show perpendicular dichroism because their transition moments are more-or-less perpendicular to the polymer chain axis. Parallel dichroism, on the other hand, is observed

for the CH_2 wagging peak at 1340 cm^{-1}, the in-plane benzene ring C-H peak at 1018 cm^{-1}, and the strong ester peaks around 1330-1240 and 1160-1080 cm^{-1}.

For the oriented sample, the milling process seems to have little effect on the measured reflectance spectra (Figures 3.3b, 3.4b). This result is rather surprising, since it was found that in the case of the unoriented sample the milling process drastically reduced the overall intensity of the spectra (Figures 3.1b, 3.2b). One possible explanation is a difference in the quality of the milling tool used. Jansen has shown [11] that for liquid crystal polymer ultra-milling has a negligible effect on the orientation, but it is critical that the knife be of excellent quality [16]. A second possible explanation is a different response of the unoriented and the oriented PET to the milling. The oriented sample was semicrystalline to begin with, and the combination of orientation and higher crystallinity will produce higher mechanical properties. It is of interest to note that the strong complex bands around 1330-1240 and 1160-1080 cm^{-1} show a slightly different shape after milling (Figure 3.3b) compared to before (Figure 3.3a). The shape of these bands is sensitive to the PET crystallinity, so this may indicate that the milling has changed the structure somewhat. It can be concluded that while the milling process may work well in certain circumstances, it cannot be considered as a foolproof technique for the characterization of molecular orientation through the thickness of plastic products. It appears that the characteristics of the milled surface can depend on the sharpness of the cutting tool, the milling direction, and the material's properties.

As was the case for the undrawn sample, the spectra recorded after 320 grit sanding were very poor (Figures 3.3c, 3.4c). After sanding to 800 grit (Figures 3.3d, 3.4d), the overall intensity increases significantly but the ϕ spectra show somewhat deformed peaks and much lower dichroism than the initial surface. The surface layer at this stage has lost much of its orientation. The next stage (3 μm diamond polishing) removes most of this disturbed material and restores much of the dichroism (Figures 3.3e, 3.4e), but the peaks in the ϕ spectra are still somewhat deformed. It is the final polishing step (0.05 μm diamond) that gives the highest reflectance level and the greatest difference between parallel and perpendicular polarizations (Figures 3.3f, 3.4f). Furthermore, and this is the most important observation, the spectra obtained after the final polishing step are virtually identical to those obtained from the original surface (Figures 3.3a, 3.4a), except that they are more intense overall. We conclude therefore that the complete milling and polishing process results in a surface whose properties correspond to those of the original sample. This is true even though the intermediate stages may produce surfaces that are rough and contain material that has been altered by the treatment. The final polishing step removes the altered material and leaves a surface that is smooth enough to eliminate any effects of polarization scrambling.

There may be some question as to whether the drawn sample indeed possessed the same degree of orientation at the surface as at the depth exposed by our procedure. This is difficult to verify, but we believe it to be the case. It is known that for drawn samples orientation gradients are much smaller than those observed in injection molded samples [2]. If a gradient did exist in our sample, in order for the two sets of spectra (Figures 3.3a and

3.3f) to match so well our procedure would have to alter the orientation of the newly exposed surface by an amount just sufficient to exactly compensate for the gradient difference. This is highly unlikely.

In an attempt to quantify the effects just discussed, dichroic ratios were calculated from the ϕ spectra for various peaks in the PET spectrum. Unfortunately, the overall intensity of a front-surface reflection spectrum is affected by a number of factors, such as surface roughness and sample positioning in the accessory. Even when the surface is highly polished, and parallel and perpendicular spectra are measured consecutively without moving the sample, variations are observed. Thus for the polished unoriented PET sample (Figure 3.1f), where the two spectra should be identical, there is a slight difference in overall intensity, even though the shape of the spectra is the same. This variation in intensity must be taken into account in calculating dichroic ratios. Fortunately, in the case of PET it is possible to normalize the spectra with respect to a reference peak at 1410 cm^{-1}, which is known to be insensitive to both orientation and crystallinity [17]. After the spectra are multiplied by the factors required to bring the area of this peak to a fixed chosen value, dichroic ratios can be calculated for other peaks by taking the ratio of the peak areas in the parallel and perpendicular spectra.

Apparent dichroic ratios were thus calculated for different peaks in the ϕ spectra of Figures 3.2 and 3.4, by taking ratios of integrated peak areas and applying a correction based on the 1410 cm^{-1} reference peak. The results obtained for the undrawn and drawn

samples of PET are summarized in Tables 3.2 and 3.3 respectively. In the case of the amorphous undrawn PET (Table 3.2), the dichroic ratios for all the characteristic peaks after the final step of the polishing process are close to 1, indicating that there is no molecular orientation in this specimen. As mentioned previously, the initial surface of this sample shows evidence of slight orientation. At intermediate steps of the process, however, such as after milling and 800 grit sanding, the calculated apparent orientation is not negligible and the measured dichroic ratios differ significantly from 1. This may be attributed to the imperfect quality of the surface and the possible presence of deformed polymer on it. However, after the final step this material is removed and these effects disappear. Thus the overall process of the milling and polishing operations does not disturb or generate molecular orientation in PET. In the case of the semicrystalline oriented PET (Table 3.3), it was also found that the measured dichroic ratio depends on the quality of the polished surface. The final dichroic ratios are virtually identical to the ones recorded at the surface of the specimen, given the experimental errors involved. However, as for the case of the undrawn sample, the apparent dichroic ratios at intermediate stages of the process, especially after the sanding steps, are substantially different from the true values.

3.5.2 Polyetheretherketone (PEEK)

Polyetheretherketone was included in the study because of its high glass transition temperature, $T_g \simeq 150°C$. Spectra recorded at the surface of the oriented PEEK sample in directions parallel and perpendicular to the draw direction are shown in Figure 3.5a. Almost

all the absorption bands show significant dichroism, suggesting the presence of high molecular orientation at the surface of this specimen. It can be seen that the two spectra of Figure 3.5a do not have the same "baseline" reflectance values in regions where there are no absorption peaks (for example, at 2000 cm^{-1}). Some of the reasons for this variation in overall reflectance intensity were discussed above in connection with PET, where the problem can be overcome by using the 1410 cm^{-1} peak as an internal reference. Unfortunately no such peak has been identified for PEEK, so it was necessary to use a different procedure to correct the spectra. The theoretical value of the reflectance R at normal incidence when there is no absorption is given by $R = [(n-1)/(n+1)]^2$, where n is the refractive index. For unoriented PEEK, n = 1.68 so the calculated baseline reflectance is 0.064 or 6.4%. Hence the reflectance spectra were scaled to give R = 6.4% at 2000 cm^{-1}, before performing the Kramers-Kronig transformation to give the ϕ spectra required to calculate the dichroic ratios. In actual fact, oriented PEEK will have different refractive indices in the draw and transverse directions (i.e. birefringence) and so will be expected to give somewhat different values of R for the parallel and perpendicular polarizations. Hence the approach just described must be considered an approximation and the values of the dichroic ratios obtained will be slightly different from the true values. However, for the present work this is not a serious problem because the error is systematic and the object is not to determine absolute values of the orientation but rather to compare on a relative basis the values obtained at different stages.

In the present investigation, the specific bands considered occur at 1648, 1599, 1492, and 1190 cm^{-1}. The band at 1648 cm^{-1} is associated with the stretching of the carbonyl group and has a transition moment angle α equal to 90° [18]. The bands at 1599 and 1492 cm^{-1} are associated with phenyl ring vibrations and the one at 1190 cm^{-1} is characteristic of the diphenyl ether group. From a correlation of their dichroic behavior with that of the carbonyl band, the transition moment angles for the peaks at 1599, 1492, and 1190 cm^{-1} have been estimated to be 37°, 28°, and 31° respectively [19]. Based on these values, the orientation function f for each of these bands has been computed and the results obtained are summarized in Table 3.4. The orientation is found to be rather high, with an average value of f around 0.55.

Figure 3.6 shows spectra recorded from the surface of the PEEK sample after the final step of the same milling and polishing procedure used for the PET samples. This surface was 0.1 mm below the original surface of the specimen. The spectra have exactly the same appearance as those obtained for the original surface, but their overall intensity is considerably higher because of the better quality of the polished surface. Moreover, Table 3.4 shows that the orientation functions computed for the bands considered above are almost identical to those obtained for the original surface, suggesting that the milling and polishing process has not significantly changed the molecular orientation in the drawn PEEK. These results, together with those already obtained for PET, show that the milling and polishing process is a reliable technique for the characterization of molecular orientation in polymers with high glass transition temperatures.

3.5.3 High Density Polyethylene (HDPE)

High density polyethylene was chosen because of its low glass transition temperature of -120°C. Spectra recorded before and after the milling and polishing process are shown in Figures 3.7 and 3.8 respectively. In comparison with PET and PEEK, the vibrational bands of HDPE are fewer and weaker because of the very different chemical structure. In Figure 3.7, only the C–H stretching bands at 2918 and 2857 cm^{-1} are well defined, and the spectra are complicated by a small degree of reflection from the back surface of the sample. The spectra of Figure 3.8 are of much better quality. Mounting the sample in epoxy resin eliminates the back surface reflection, and polishing leads to higher overall reflectance and a straighter baseline. Before they were used to calculate the polarizability spectra, the reflectance spectra were corrected in a manner similar to that used for PEEK, except that they were normalized to R = 4% (n = 1.5) at 4000 cm^{-1}. All the major peaks in polyethylene show perpendicular dichroism. From a look at dichroism of the 2918-2850 peaks in Figures 3.7b and 3.8b, it is clear that the polished surface exhibits a lower apparent degree of molecular orientation. Dichroic ratios and orientation functions were calculated for the vibrations at 2918-2850 cm^{-1}, 1473-1460 cm^{-1}, and 730-720 cm^{-1} based on the reported transition moment angles of 70°, 79°, and 90° respectively [20]. The results, summarized in Table 3.5, confirm the lower orientation for the polished surface. The effect is most pronounced for the 2918-2850 cm^{-1} band, which is also the most intense and therefore subject to less experimental error. A probable reason for the lower apparent orientation is that the milling and polishing were done with water as a cooling medium, at a temperature higher

than the glass transition of the polymer, so the polymer orientation may have been altered by the process. To check this, a second specimen was prepared using liquid nitrogen at a temperature of –196°C as a cooling medium. The spectra obtained from this surface are shown in Figure 3.9. The dichroism and the calculated orientation functions (Table 3.5) are higher than for the water-cooled specimen, suggesting that the low values obtained for the water-cooled specimen are indeed at least partly due to changes induced by the polishing process. However, the values obtained with liquid nitrogen polishing are still lower than those for the original surface. Hence while the use of liquid nitrogen during the different polishing steps appears to reduce the extent of relaxation of the polymer chains in HDPE, it does not prevent it completely. Perhaps further optimization of the polishing conditions to ensure more thorough cooling of the HDPE would improve the results.

An interesting trend in Table 3.5 is worth noting. The higher the frequency of the band used, the greater is the variation of the apparent dichroism as a function of the surface preparation. This may be a wavelength-related effect. At 2900 cm^{-1} the wavelength is 3.4 μm, whereas at 725 cm^{-1} it is 13.8 μm. Since the depth of the sample that is probed is proportional to the wavelength, the shorter-wavelength bands "see" less deep into the sample and would be expected to be more affected by a thin surface layer of disturbed material.

3.5.4 Liquid Crystal Polymer (LCP)

The milling and polishing technique was also applied to a new class of polymer that is finding increasing use, namely thermotropic liquid crystalline polymers (LCP). These materials are recognized for their high strength, high modulus, and high chemical resistance. One of them was chosen for study because they can easily change their morphological characteristics under both high temperatures and high shear rates [21], for example during the polishing process. Unlike the roll-drawn samples of PET, PEEK, and HDPE previously discussed, the LCP sample used in this study was injection-molded and contained glass reinforcement.

It has been reported in the literature that the microstructure of injection-molded LCP specimens in the thickness direction shows the presence of the so-called skin-core structure [22]. The skin layer is highly oriented due to the advancing melt front, which orients polymer chains parallel to the mold wall in the flow direction. Between the skin and the core layers exists a sub-skin layer that is less oriented because of the shear flow therein. In the core of the molding, however, the molecular chains were found to be poorly oriented because of the presence of plug flow in this area.

Figure 3.10 shows spectra recorded at the surface of the LCP molding, measured with polarization direction parallel and perpendicular to the flow direction. From this figure it can be clearly seen that several bands show significant dichroism, suggesting that polymer

chains at the surface of the molding are highly oriented. To compute the orientation function *f*, the following bands were considered: 1735, 1631, 1509, and 1470 cm^{-1}. The band at 1735 cm^{-1} is associated with the carbonyl stretching vibration, whose transition moment should be more-or-less perpendicular to the molecular chain axis. The other major bands are known to be parallel bands associated with skeletal vibrations of the benzene and naphthalene rings in the polymer [23]. As was done for the other polymers, the reflectance spectra were normalized to a common reference value (5% at 2200 cm^{-1}) and transformed into molecular polarizability spectra that were then used to calculate dichroic ratios. Approximate orientation functions were calculated by assuming transition moment angles of 0° for the parallel bands and 90° for the carbonyl band. The results, given in Table 3.6, confirm that the polymer chains are oriented in the flow direction, as pointed out by many authors. As already mentioned, this is due to the effect of the advancing melt front which orients the polymer chains in the flow direction.

Spectra recorded at the sub-skin layer of this specimen, after the polishing process, are shown in Figure 3.11. It is clear that the difference between parallel and perpendicular polarizations is less pronounced than in Figure 3.10. The calculated dichroic ratios and orientation functions for the bands of interest are given in Table 3.6 and they clearly show a lower degree of molecular orientation in the sub-skin layer of the molding. In this case the difference is real and not a result of the polishing process. Similar results have been obtained by Jansen et al. [11], and Barres et al. [24]. Such a decrease of the molecular orientation at

the sub-skin layer has been attributed to the shear flow in this area, which according to Ide and Ophir [22,25] produces significantly less molecular orientation.

On comparing Figures 3.10 and 3.11, it can be seen that the sub-skin layer gives a very different spectrum from the surface layer at wavenumbers less than 1100 cm^{-1}. This is because the polishing exposes the reinforcing glass fibers, which possess strong IR absorption bands in this region. It is interesting to consider the possibility that reflection infrared spectroscopy might be used to obtain information on the orientation of the fibers themselves within the matrix, a phenomenon that is usually studied by polishing and visible-light microscopy. However, such an analysis might be difficult because of the complex optical effects arising from interaction between the infrared radiation and the two-phase system.

3.6 CONCLUSION

The aim of this study was to develop a relatively easy technique for the accurate characterization of molecular orientation across the thickness of plastic products. This technique consists of milling the specimen to the depth where molecular orientation is to be measured, polishing the surface produced by the milling process, and characterizing the polished surface by external reflection infrared spectroscopy. In the case of PET, it has been found that at intermediate steps of the milling and polishing process, the apparent molecular orientation can change depending on the quality of the resulting surface. However, when the

polishing is taken to the final finish of 0.05 μm, the material disturbed by the previous polishing steps is removed, the quality of the reflectance spectra is greatly improved, and if any disturbed material is still present, its thickness is negligible in comparison with the infrared sampling depth. As a result, the reflectance spectra give an accurate measure of the true orientation and the milling and polishing procedure used can be considered a reliable technique for the characterization of molecular orientation in the thickness direction of plastic products.

A similar result was obtained for another polymer with a high glass transition temperature, namely PEEK. However the technique was found to be less reliable for polymers with a low glass transition temperature, such as HDPE. In this case, it appears that the heat generated by the polishing process affects the sample to a greater extent than in PET or PEEK, so the measured molecular orientation was found to be significantly affected by the milling and polishing process. Cooling with liquid nitrogen instead of water during the polishing operations was found to reduce the extent of the problem but did not eliminate it completely.

The technique was also applied to injection-molded glass-reinforced LCP. In this case, it showed that there is a lower level of orientation at the sub-skin layer of the molding compared to the surface. This is in agreement with results recently reported in the literature for injection-molded LCP materials and further confirms the utility of our technique for the characterization of molecular orientation in the thickness direction of plastic products.

ACKNOWLEDGEMENTS

The authors wish to thank Dr. A. Ajji and Messrs. E. Pellerin and Y. Simard for supplying the specimens used in this study and for their kind cooperation and assistance.

3.7 REFERENCES

1. M. R. Kamal and V. Tan, *Polym. Eng. & Sci.*, **19**, 558 (1979).
2. M. Houska and M. Brummell, *Polym. Eng. & Sci.*, **27**, 917 (1987).
3. L. Hoare and D. Hull, *Polym. Eng. & Sci.*, **17**, 204 (1977).
4. N. Reid and J. E. Beesley, *Sectioning and Cryosectioning for Electron Microscopy*, Elsevier, 1991.
5. L. Lundberg, Y. Sjönell, B. Stenberg, B. Terselius, and J.-F. Jansson, *Polymer Testing*, **13**, 441 (1994).
6. N. J. Clayden, J. G. Eaves, and L. Croot, *Polymer*, **38**, 159 (1997).
7. K. C. Cole, J. Guèvremont, A. Ajji, and M. M. Dumoulin, *Appl. Spectrosc.*, **48**, 1513 (1994).
8. J. Guèvremont, A. Ajji, K. C. Cole, and M. M. Dumoulin, *Polymer*, **36**, 3385 (1995).
9. A. Kaito and K. Nakayama, *Macromolecules*, **25**, 4882 (1992).
10. S. Bensaad, B. Jasse, and C. Noël, *Polymer*, **34**, 1602 (1993).

11. J. A. J. Jansen, F. N. Paridaans, and I. E. J. Heynderickx, *Polymer*, **35**, 2970 (1994).

12. N. J. Everall, J. M. Chalmers, A. Local, and S. Allen, *Vibrational Spectrosc.*, **10**, 253 (1996).

13. A. Ajji, M. M. Dumoulin, and K. C. Cole, *Proc. ANTEC '95*, 1900 (1995).

14. B. Haworth, C. S. Hindle, G. J. Sandilands, and J. R. White, *Plast. Rubber Proc. Appl.*, **2**, 59 (1982).

15. J. E. Bertie, S. L. Zhang, and C. D. Keefe, *J. Mol. Struct.*, **324**, 157 (1994).

16. J. A. J. Jansen, personal communication.

17. D. J. Walls, *Appl. Spectrosc.*, **45**, 1193 (1991).

18. A. M. Voice, D. I. Bower, and I. M. Ward, *Polymer*, **34**, 1164 (1993).

19. K. C. Cole, A. Ajji, and C. Bimbeau, *Proc. Composites '96 and Oriented Polymers Symp.* (National Research Council Canada, Boucherville, QC), Oct. 9-11, 1996, pp. 119-132.

20. R. Zbinden, *Infrared Spectroscopy of High Polymers*, Academic Press, 1964.

21. K. Geiger, pp. 19-41 in *Processing and Properties of Liquid Crystalline Polymers and LCP-Based Blends*, D. Acierno and F. P. La Mantia (Eds.), ChemTec Publishing, Toronto, 1993.

22. Y. Ide and Z. Ophir, *Polym. Eng. & Sci.*, **23**, 261 (1983).

23. I. Ouchi, M. Hosoi, and S. Shimotsuma, *J. Appl. Polym. Sci.*, **21**, 3445 (1977).

24. O. Barres, C. Friedrich, B. Jasse, and C. Noël, *Makromol. Chem., Macromol. Symp.*, **52**, 161 (1991).

25. Z. Ophir and Y. Ide, *Polym. Eng. & Sci.*, **23**, 792 (1983).

Table 3.1 - Details on different steps of the polishing process.

Step	Lap Surface	Abrasive and Size	Cooling Medium	Load (N) (6 specimens)	Speed (rpm)	Time (s)
1	CARBIMET	320 grit SiC	Water	100	150	15
2	CARBIMET	400, 600 grit SiC	Water	100	150	20
	MICROCUT	800 grit SiC	Water	100	150	20
3	TEXMET	3μ Diamond (poly)	—	120	150	180
4	MASTERTEX	MASTERPREP	—	120	150	240

Table 3.2 - Evolution of the apparent dichroic ratio for the unoriented PET sample after each step of the milling and polishing process. Where the transition moment angle is known, calculated orientation functions are shown in parentheses.

Peak → (cm^{-1})	**1340**	**1020**	**727**	**1725**	**1263**	**1100**
Surface	1.90 (0.29)	1.02 (0.00	1.09 (–0.04)	0.92	1.12	1.06
Milling	1.02 (0.01)	0.89 (–0.05)	—	0.53	1.05	0.97
Step 1	0.90 (–0.04)	—	1.60 (–0.33)	1.26	1.10	0.91
Step 2	4.46 (0.66)	2.21 (0.34)	0.79 (0.15)	0.79	1.43	1.21
Step 3	0.92 (–0.03)	0.89 (–0.05)	1.14 (–0.09)	1.07	0.97	1.01
Step 4	0.93 (–0.03)	0.98 (–0.01)	1.07 (–0.04)	0.97	0.99	1.01

Table 3.3 - Evolution of the apparent dichroic ratio for the oriented PET sample after each step of the milling and polishing process. Where the transition moment angle is known, calculated orientation functions are shown in parentheses.

Peak → (cm^{-1})	**1340**	**1020**	**727**	**1725**	**1263**	**1100**
Surface	9.46 (0.90)	3.59 (0.55)	0.30 (0.60)	0.22	2.08	1.83
Milling	8.67 (0.89)	4.18 (0.61)	0.24 (0.68)	0.28	1.98	1.75
Step 1	0.47 (–0.26)	0.89 (–0.03)	2.87 (–0.76)	1.31	0.71	0.89
Step 2	1.80 (0.26)	1.40 (0.13)	0.59 (0.32)	0.94	0.71	1.20
Step 3	5.40 (0.73)	2.44 (0.38)	0.35 (0.54)	0.35	1.30	1.45
Step 4	8.14 (0.86)	4.30 (0.63)	0.34 (0.56)	0.22	2.03	1.90

Table 3.4 - Dichroic ratios and orientation functions (in parentheses) obtained for the oriented PEEK sample.

Peak (cm^{-1}) →	1648	1599	1492	1190
Original surface	0.27 (0.64)	1.98 (0.52)	3.22 (0.62)	2.26 (0.48)
Sub-skin layer	0.29 (0.60)	1.92 (0.50)	2.78 (0.55)	2.09 (0.43)

Table 3.5 - Dichroic ratios and orientation functions (in parentheses) obtained for the oriented HDPE sample.

Peak (cm^{-1}) →	2918 – 2850	1473 – 1460	730 – 719
Original surface	0.22 (1.00)	0.20 (0.80)	0.10 (0.84)
Sub-skin layer (water cooling)	0.54 (0.52)	0.33 (0.63)	0.14 (0.80)
Sub-skin layer (liquid nitrogen cooling)	0.38 (0.77)	0.30 (0.67)	0.12 (0.82)

Table 3.6 - Dichroic ratios and orientation functions (in parentheses) obtained for the injection-molded LCP sample.

Peak (cm^{-1}) →	1735	1631	1509	1470
Original surface	0.54 (0.35)	4.42 (0.53)	2.81 (0.37)	3.33 (0.43)
Sub-skin layer	0.79 (0.15)	1.40 (0.11)	1.31 (0.09)	1.48 (0.13)

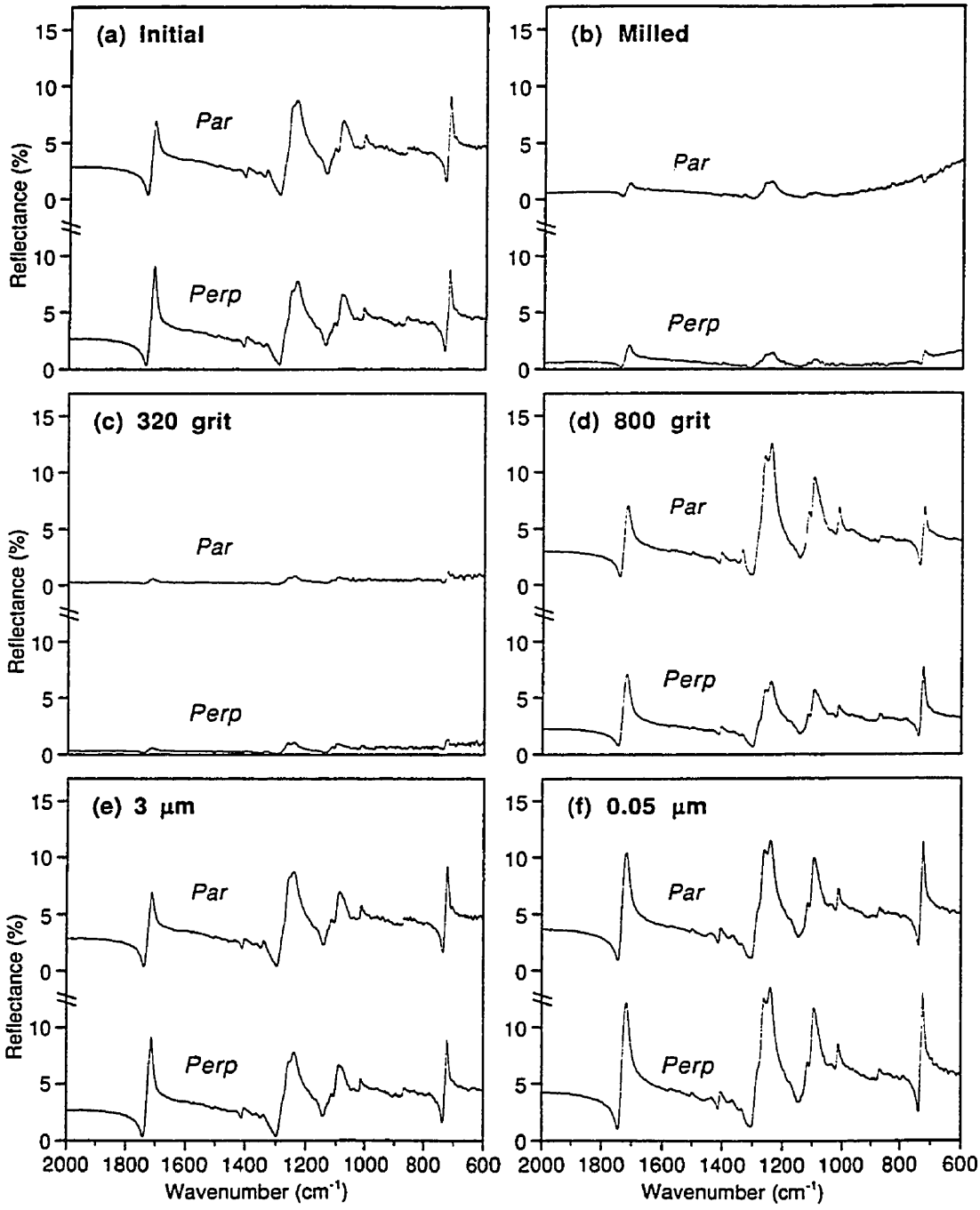

Figure 3.1. External reflection spectra measured at the surface of the unoriented PET sample at different stages of the milling and polishing process.

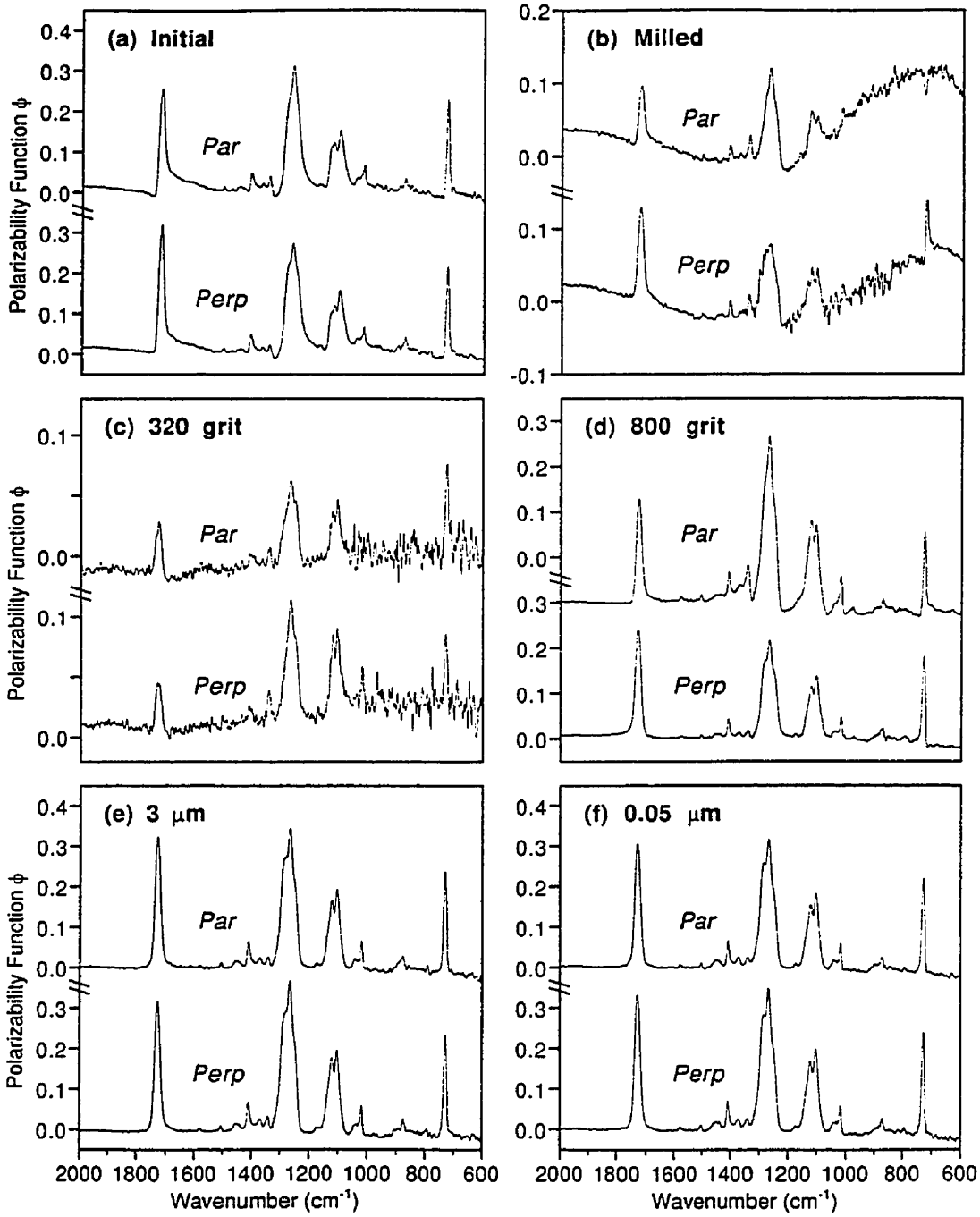

Figure 3.2. The spectra of Figure 3.1 after conversion into the imaginary molecular polarizability function by means of the Kramers-Kronig transformation.

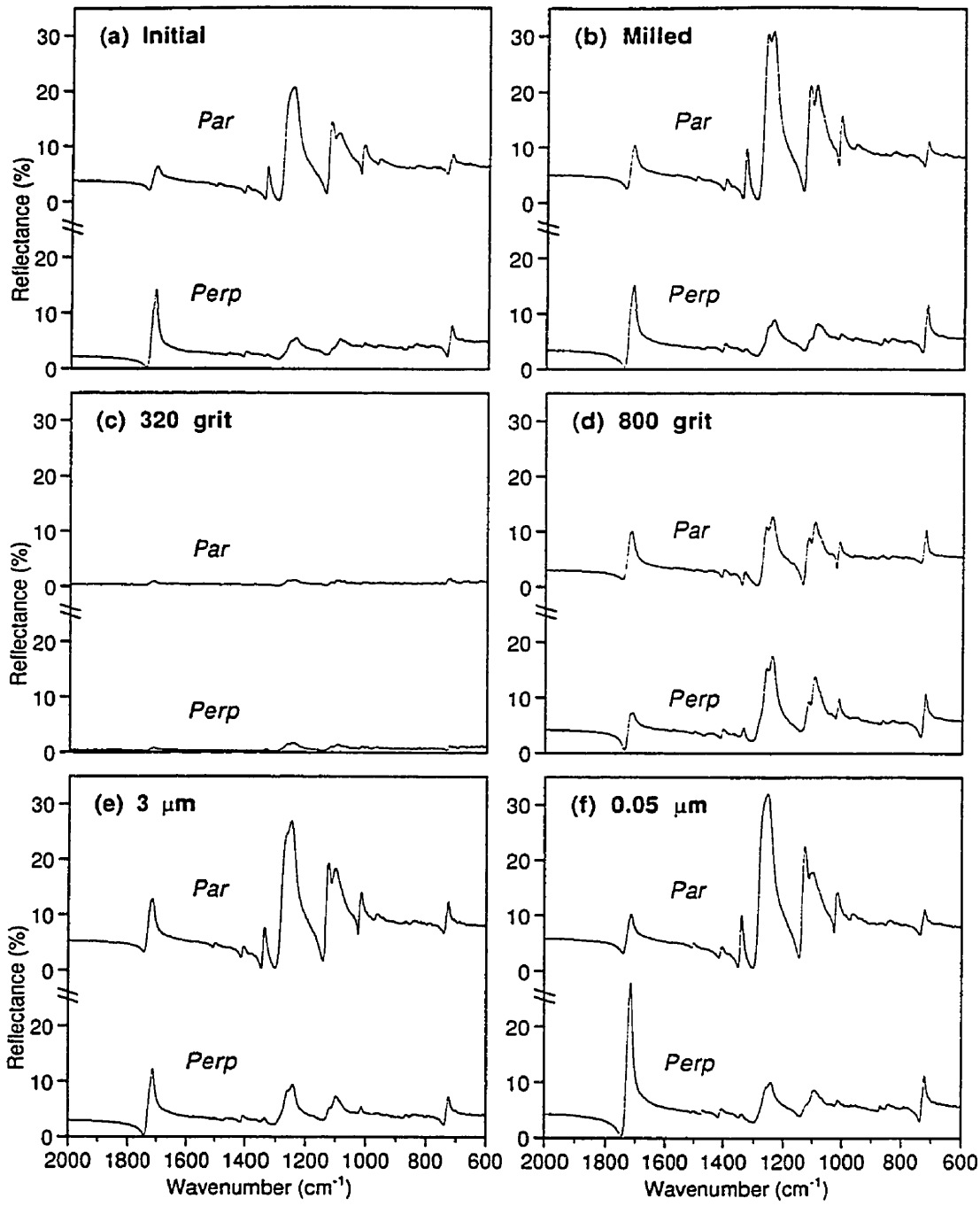

Figure 3.3. External reflection spectra measured at the surface of the oriented PET sample at different stages of the milling and polishing process.

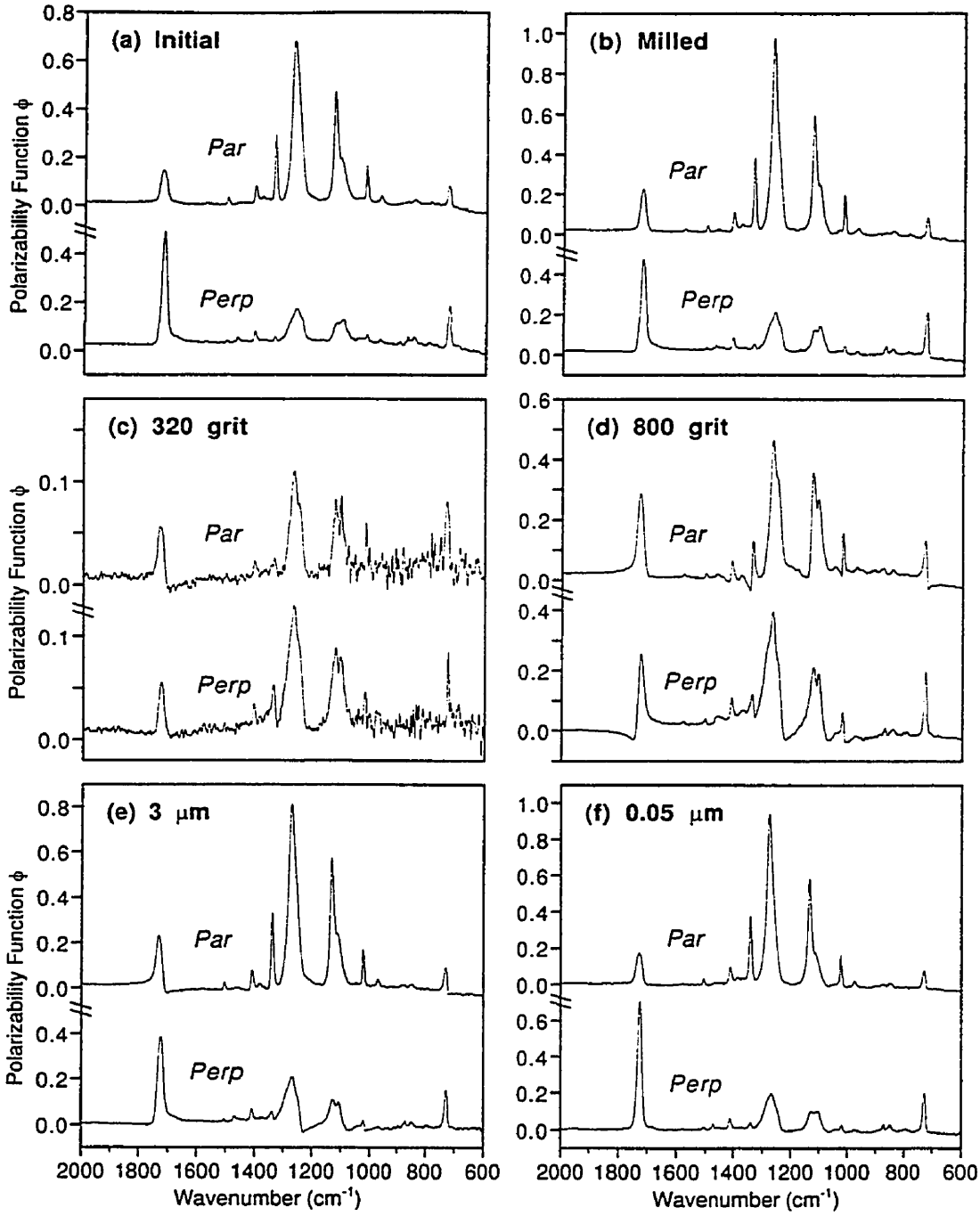

Figure 3.4. The spectra of Figure 3.3 after conversion into the imaginary molecular polarizability function by means of the Kramers-Kronig transformation.

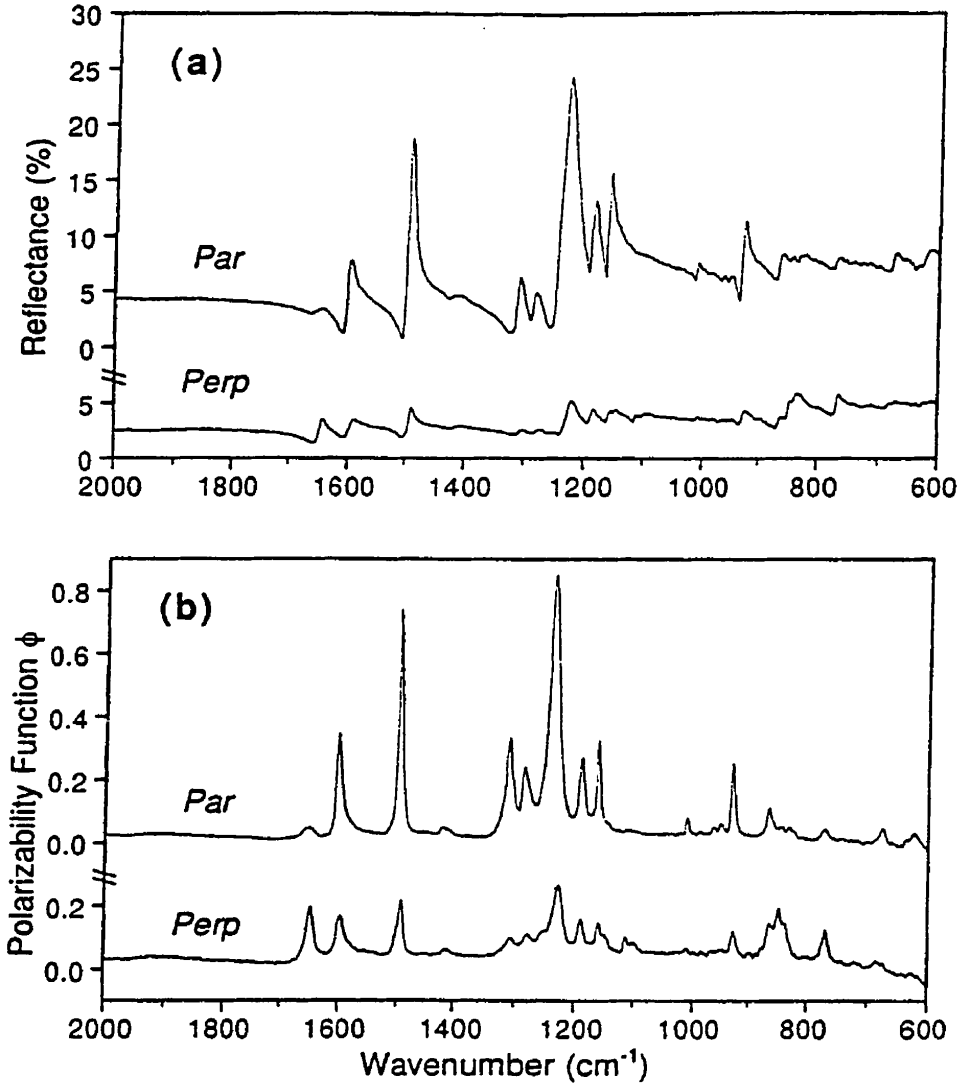

Figure 3.5 - Reflectance spectra (a) and corresponding polarizability spectra (b) measured at the original surface of the oriented PEEK sample

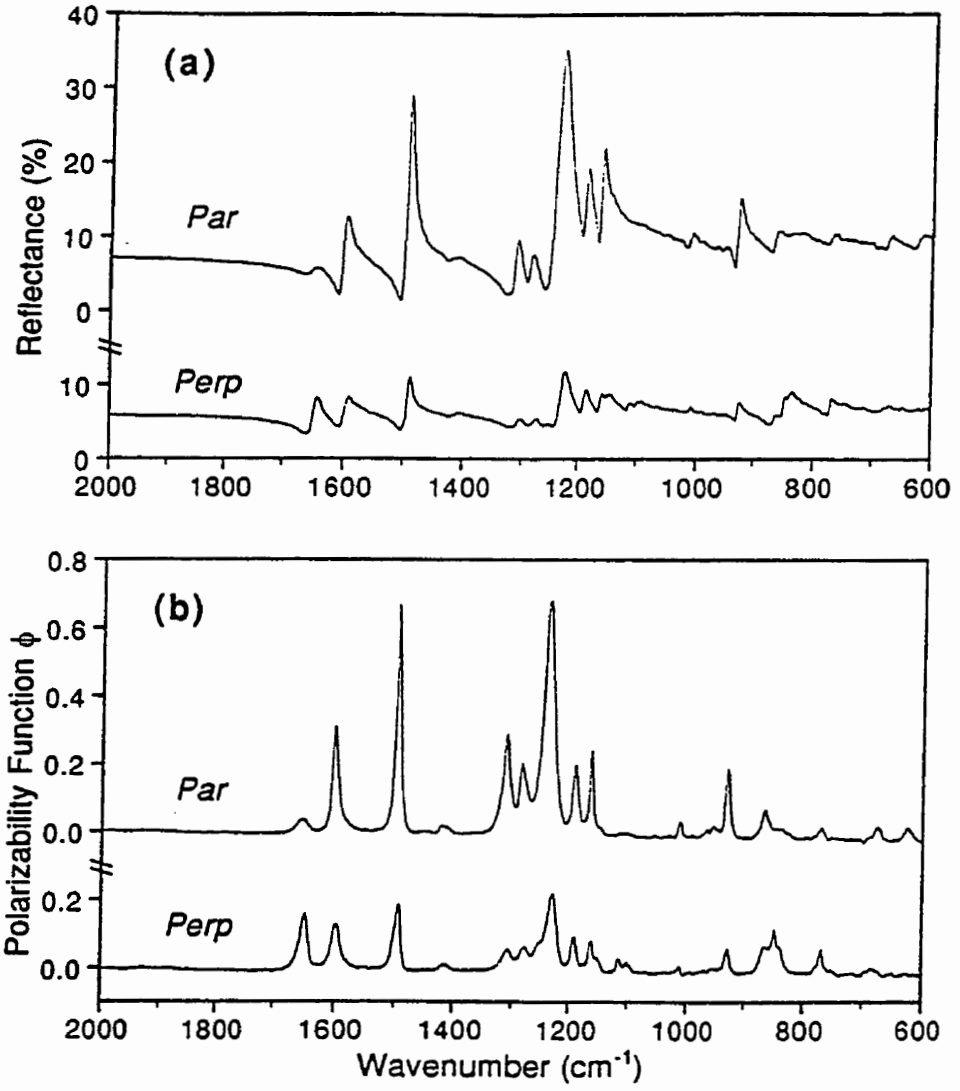

Figure 3.6 - Reflectance spectra (a) and corresponding polarizability spectra (b) measured at the surface of the oriented PEEK sample after the complete milling and polishing process

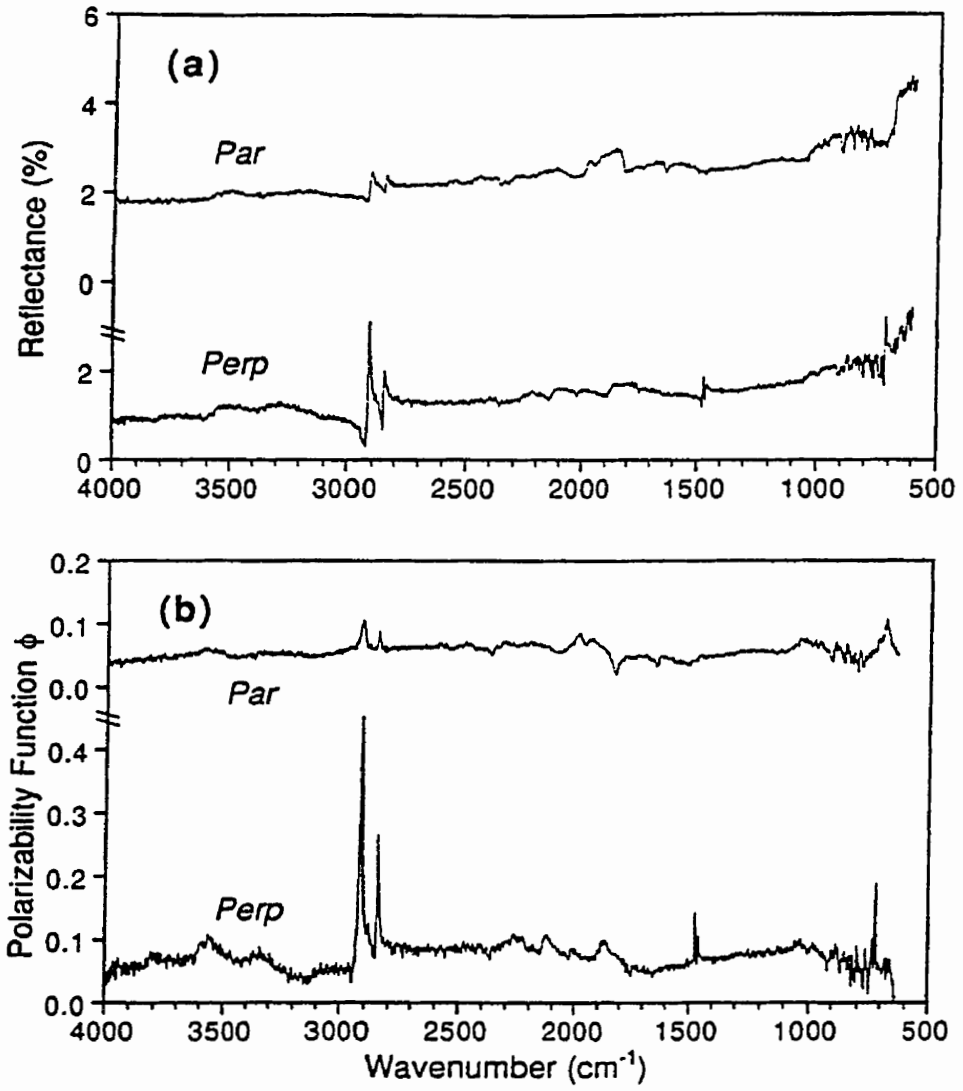

Figure 3.7 - Reflectance spectra (a) and corresponding polarizability spectra (b) measured at the original surface of the oriented HDPE sample

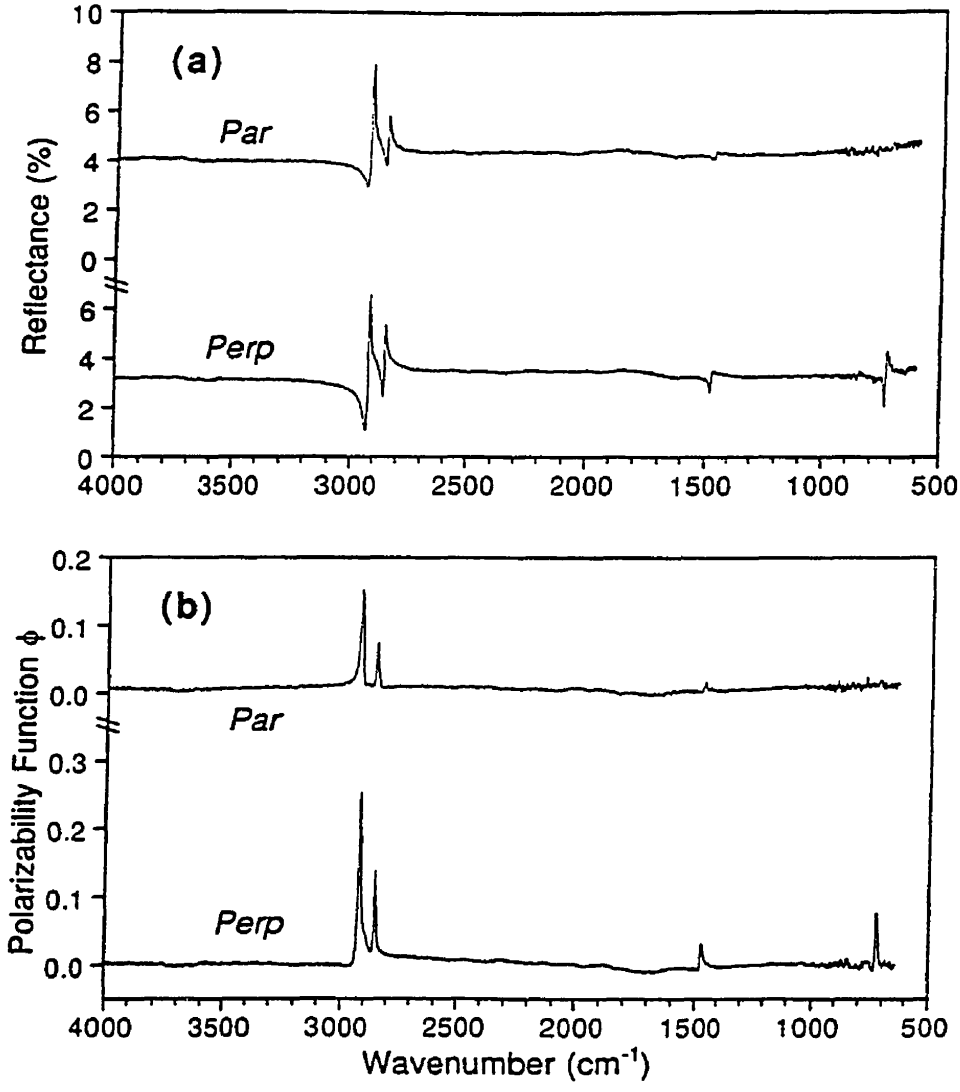

Figure 3.8 - Reflectance spectra (a) and corresponding polarizability spectra (b) measured at the surface of the oriented HDPE sample after milling and polishing with water as cooling medium

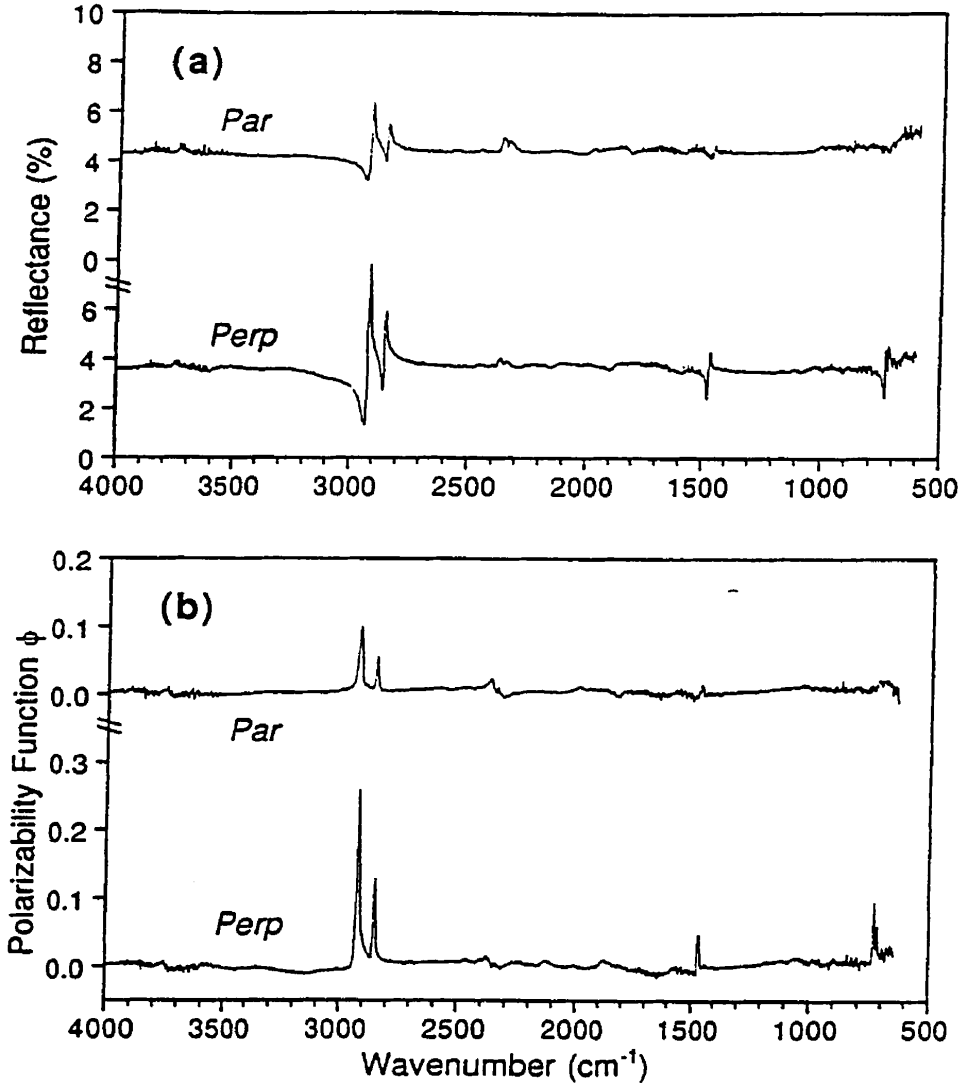

Figure 3.9 - Reflectance spectra (a) and corresponding polarizability spectra (b) measured at the surface of the oriented HDPE sample after milling and polishing with the aid of liquid nitrogen as cooling medium

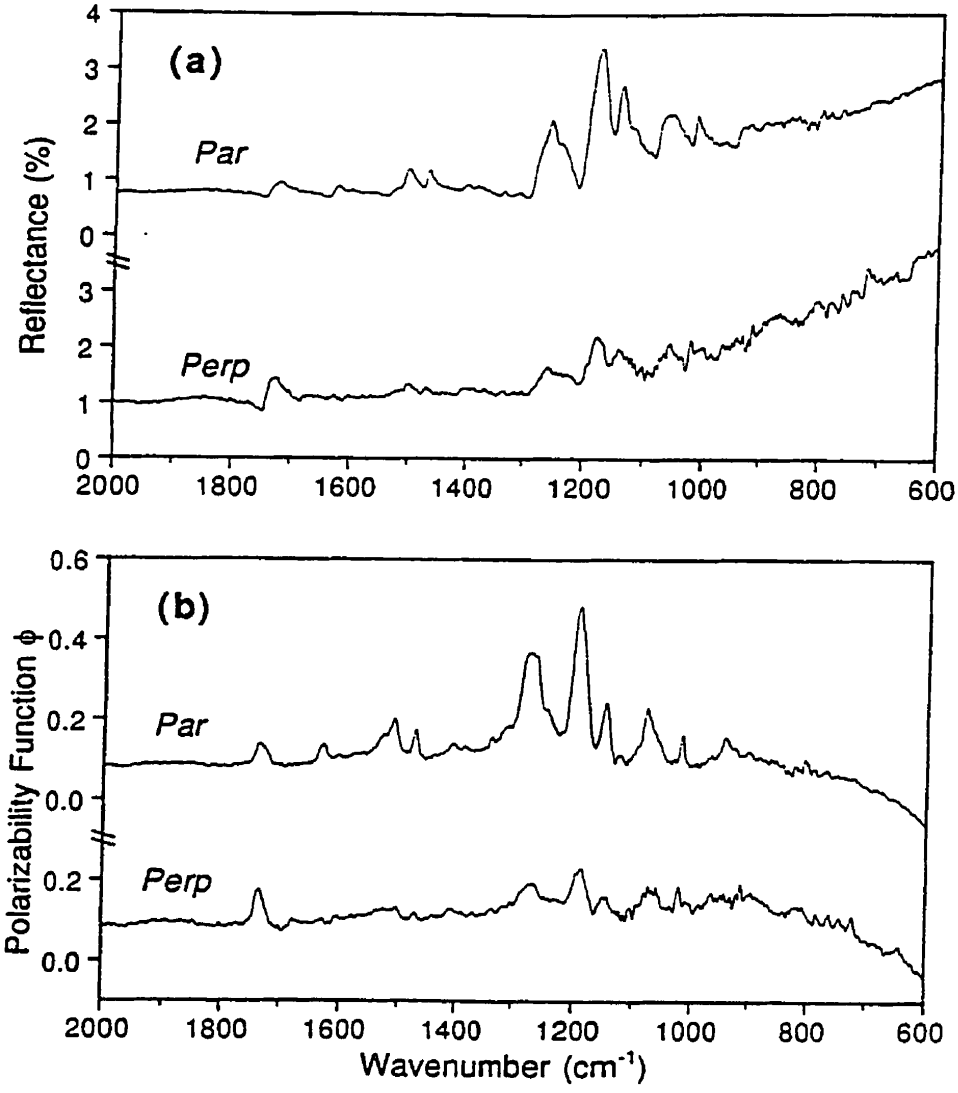

Figure 3.10 - Reflectance spectra (a) and corresponding polarizability spectra (b) measured at the original surface of the injection-molded glass-filled LCP sample

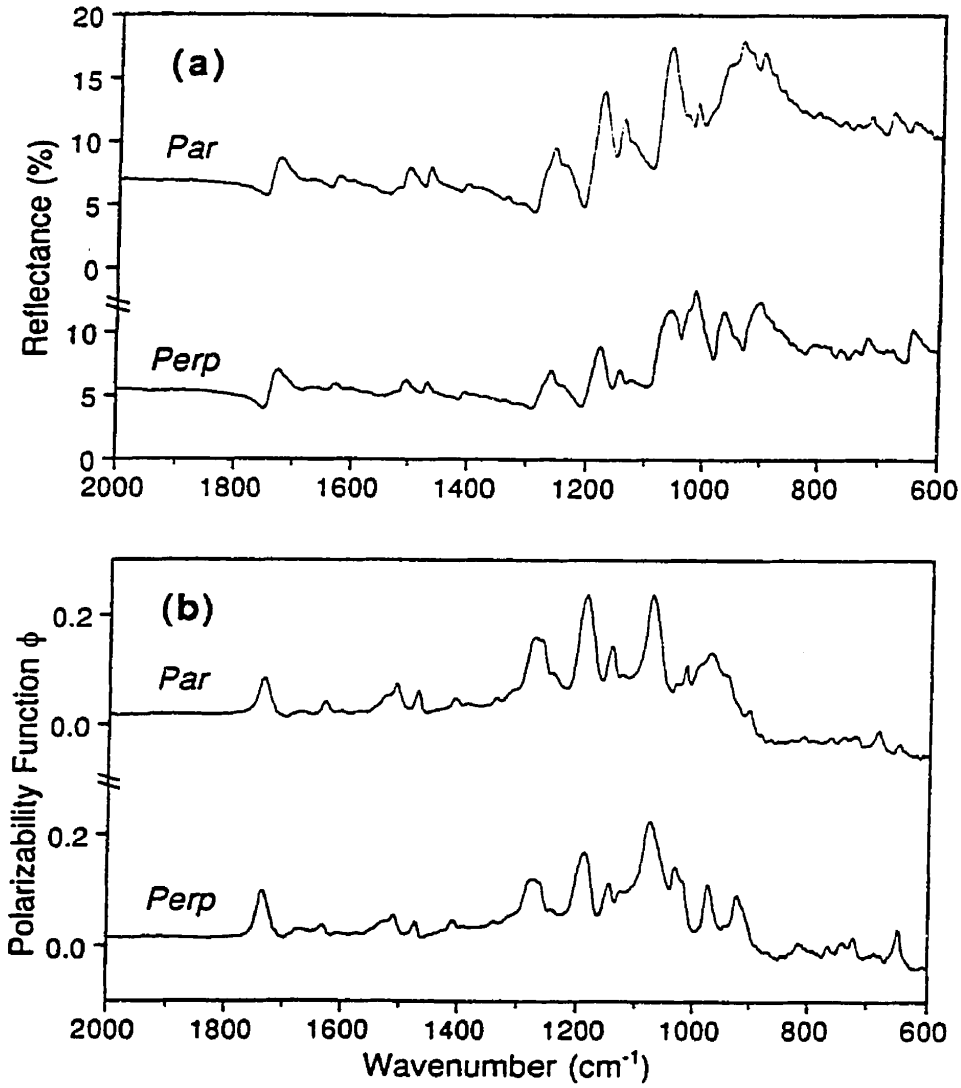

Figure 3.11 - Reflectance spectra (a) and corresponding polarizability spectra (b) measured at the surface of the injection-molded glass-filled LCP sample after milling and polishing

CHAPITRE IV

Effect of Polymer Properties on the Structure of Injection-Molded Parts

H. BEN DALY[1], B. SANSCHAGRIN[1], K.T. NGUYEN[2*], and K.C. COLE[2]

[1] *Center for Applied Research on Polymers (CRASP)*

École Polytechnique

C.P. 6079, succursale Centre-ville, Montréal, Québec, Canada H3C 3A7

[2] *Industrial Materials Institute*

National Research Council Canada

75, boul. De Mortagne, Boucherville, Québec, Canada J4B 6Y4

This chapter has been submitted for publication in Polymer Engineering and Science.

4.1 RÉSUMÉ

La technique de fraisage et de polissage proposée dans le chapitre 3 a été utilisée pour caractériser la morphologie (orientation moléculaire et cristallinité) des pièces en PET injectées. Ce matériau a été utilisé car il a une faible vitesse de cristallisation. En faisant varier les paramètres de moulage, température du moule dans notre cas, on peut facilement affecter sa cristallinité. Cela va nous permettre d'étudier la relation entre cristallinité et orientation moléculaire dans les pièces injectées. De plus, dans cette étude, nous avons utilisé d'autres polymères ayant des caractéristiques rhéologiques et de cristallisation très différentes. Ces polymères sont le HDPE, le PS et le LCP. Ces polymères ont été injectés et l'orientation moléculaire à la surface des pièces obtenues, ainsi qu'à travers l'épaisseur des pièces en PET, a été mesurée en utilisant la technique d'infrarouge en mode de réflexion. À partir des spectres mesurés, le degré d'orientation des chaînes moléculaires est calculé en utilisant la fonction d'orientation de Hermans (f) suivante (equation 4.2):

$$f = \frac{D - 1}{D + 2} \frac{2}{3\cos^2\alpha - 1}$$

où $D = A_{//} / A_{\perp}$ est le rapport dichroic d'un groupement moléculaire spécifique et $A_{//}$ et $A_{\perp}$ représentent respectivement l'absorption de ce groupement dans des spectres mesurés parallèlement et perpendiculairement à la direction d'écoulement. α étant l'angle entre la direction du moment de transition du groupement moléculaire considéré et l'axe de la chaîne.

Le degré de cristallinité du PET dans chaque couche à travers l'épaisseur des pièces injectées est proportionnel à l'aire sous le pic d'absorption à 1340 cm^{-1} dans le spectre appelé "Structure factor Spectrum ϕ_o" définie comme suit (equation 4.4):

$$\phi_o = \frac{1}{3}\phi_{//} + \frac{2}{3}\phi_{\perp}$$

où $\phi_{//}$ et $\phi_{\perp}$ sont respectivement les spectres mesurés avec une polarisation parallèle et perpendiculaire à la direction d'écoulement.

Les résultats de cette étude peuvent être résumés comme suit :

1) L'orientation moléculaire dans la couche peau des pièces injectées dépend non seulement de l'écoulement élongationnel au niveau de front d'écoulement, mais aussi du temps de relaxation des chaînes moléculaires, de la rigidité des chaînes moléculaires et de la vitesse de cristallisation du polymère utilisé.

2) Pour le PET, la distribution de la cristallinité dans l'épaisseur des pièces injectées dépend de la température du moule. Pour de faibles températures du moule, inférieures à la température du transition vitreuse du PET, le maximum de cristallinité est noté dans une couche située à 0.4 mm de la surface de la pièce. Ce maximum de cristallinité est due au phénomène de cristallisation sous contrainte (shear-induced crystallization), favorisée par la forte orientation moléculaire dans cette zone. En augmentant la température du moule à des

températures supérieures à la température du transition vitreuse du PET, le maximum de cristallinité se déplace vers la couche peau. Ce déplacement est due à la diminution de l'épaisseur de la couche peau en augmentant la température du moule.

3) Pour le PET, la distribution de l'orientation moléculaire dans l'épaisseur ressemble beaucoup à celle de la cristallinité (shear-induced crystallization). Ce résultat indique que la présence de la cristallinité lors du remplissage du moule diminue la relaxation des chaînes moléculaires et conserve, en partie, le degré d'orientation généré durant cette phase.

4.2 ABSTRACT

In this study, the distributions of both molecular orientation and crystallinity along the flow direction as well as across the thickness direction of injection-molded specimens of poly(ethylene terephthalate) (PET) molded at different mold temperatures were investigated. The degree of molecular orientation at the surface of the specimens was compared to that of other injected materials (polystyrene, high density polyethylene, liquid crystal polymer) showing different thermal, rheological and crystallization characteristics. It was found that the molecular orientation at the skin layer of the molding increases with the polymer relaxation time, the rigidity of the polymer molecules, and the crystallization rate

of the polymer. Moreover, in the case of PET, it was found that the crystallinity at the skin layer and in the core of the molding depends on the mold temperature. For low mold temperatures, near the gate, the maximum of crystallinity was observed at the subskin layer because of the "shear-induced crystallization" generated during the filling stage. On increasing the mold temperature, the maximum of crystallinity was found to shift to the skin layer as a result of the decrease of the thickness of this layer. For low mold temperatures, the variation of the molecular orientation in the thickness direction was found to be much the same as for the crystallinity of the polymer. This result indicates that the shear-induced crystallization process improves the degree of molecular orientation in the flow direction since it inhibits the relaxation process of the polymer molecules.

4.3 INTRODUCTION

Injection molding, characterized by high production rates and dimensional precision, is one of the most widely employed methods for the fabrication of plastic products. During this process, the polymer undergoes a very complex thermo-mechanical history which introduces molecular orientation, residual stresses, and strains into the final products. This results in highly anisotropic mechanical behavior, warpage and shrinkage. For semi-crystalline polymers, this is further complicated by crystallization.

Molecular orientation is the alignment of polymer molecules in a specific direction. The buildup of the molecular orientation in injection moldings takes place during the filling and the cooling of the polymer in the mold cavity [1]. Menges and Wübken [2] studied the molecular orientation distribution across the thickness of polystyrene (PS) moldings by means of post-shrinkage measurements of samples microtomed parallel to the specimen's surface. They found that in the flow direction, the molecular orientation is highest at the skin and the subskin layers and close to zero at the center of the molding. In a direction transverse to the flow, molecular orientation was also found to be highest at the skin layer and to almost vanish in the center of the molding, but no secondary maximum was observed in the subskin layer. The high molecular orientation at the skin layer in the flow direction was attributed to the elongational flow at the advancing front, which stretches and orients polymer chains in the flow direction during the filling process [1]. As these chains reach the cold mold wall, they will immediately freeze, thus preserving their orientation in the flow direction. Well behind the flow front, it is the shear flow that will orient polymer chains in the subskin layer in the flow direction. Such an increase in the degree of molecular orientation is responsible for the high degree of the post-shrinkage in this layer. In the core of the molding, however, the molecular orientation shows its lowest value because of both the low level of shear stresses and the high melt temperature that are present in this zone. Kamal and Tan [3], using birefringence measurements, confirmed these results for PS and noted in the flow direction the presence of two birefringence maxima near the external surfaces of the molding and a low value in the center. The first minimum of the birefringence between these two maxima was associated with the instantaneous freezing of the melt when it touches the mold wall and

the second maximum was attributed to the thickness of the frozen layer at the end of the filling process.

More recently, Wimberger-Friedl [4] conducted an extensive study on the effect of processing conditions on the molecular orientation in injection-molded polycarbonate specimens. In this study, the molecular orientation was characterized by means of both the microtoming and the birefringence techniques. The microtomed samples were cut parallel and perpendicular to the flow direction, then exposed to a polarizing microscope to measure the birefringences Δn_{xz} and Δn_{yz} where x, y and z are the flow, the transverse and the thickness directions respectively. It was found that the birefringence at the external surface of the molding is always equibiaxial, i.e. equal in the flow and transverse directions, except in cases where no packing pressure was applied. In these cases, the birefringence was slightly lower in the transverse direction. In the center of the molding, the birefringence was found to have almost the same distribution as found previously [2]. Accordingly, it was suggested that the maximum of birefringence at the skin layer of the molding can be explained not only by the elongational flow at the advancing flow front as discussed above, but also by a significant contribution from transition-pressure-induced deviatoric stresses in the vitrifying layer during the compression and packing stages, which leads to the frozen-in birefringence at the surface of the molding. However, not all authors agree on the effect of the flow front on the molecular orientation. According to Ballman and Toor [5], the birefringence at the surface of the molding is relatively small due to the low molecular orientation generated

therein during the filling process. These authors suggested that since the velocity of the polymer melt is zero at the mold wall, there must be a radial flow at the flow front away from the center towards the mold wall in order to fill the mold cavity. This results in part of the unoriented front being deposited against the wall and freezing before it can be subjected to large shear forces. As this material is unoriented before it touches the mold wall and freezes immediately upon contact, there will be very little orientation at the skin layer of the molding. Somewhat closer toward the center, the plastic is heavily oriented because of the fast flow during the filling. This outside layer (situated just below the thin skin layer) will cool down very quickly and retain its high orientation. More toward the center, the plastic also flows fast but is cooled more slowly. As a result, some of the orientation will be lost because of fast relaxation at high temperature. The center of the molding remains hot long enough to eliminate much of the orientation generated during the filling process.

Semicrystalline polymers, depending on their chemical composition, can be classified into two main groups: fast-crystallizing polymers such as polyethylene (PE) and polypropylene (PP), and slow-crystallizing polymers such as polyetheretherketone (PEEK) and polyethylene terephthalate (PET). Basically, fast-crystallizing polymers have flexible backbones with regular structure. This allows them to undergo quite rapid crystallization because the flexible molecular chains can readily adjust their sequences into a growing crystalline structure [6, 7]. In contrast, slowly crystallizing polymers have more rigid

backbones. Their crystallization behavior depends on both the cooling rate and the level of stress introduced in the polymer during processing [8-11].

Several authors have investigated the microstructure of injection-molded fast crystallizing polymers. An excellent review on this topic was published by Katti and Schultz [12]. In the case of injected polyethylene [13], for example, it was found that the crystalline morphology in the thickness direction is characterized by four distinct layers, differentiated on the basis of the shape and the size of the crystalline entities at each layer. The skin layer has a nonspherulitic structure and when viewed in longitudinal cross-section exhibits tiny slots of vertical bright lines arranged in rows and running parallel to the surface of the molding. Such a crystalline structure was interpreted as stacks of lamellae with chain axes nucleated in the flow direction and growing in the depth direction. In the second layer, fine asymmetric spherulites of almost uniform size were obtained. These are spherulites formed under large thermal gradients, the size of which is limited by the fast nucleation rate. The third layer contains asymmetric oblate spherulites with axis of symmetry in the depth direction. The last layer contains randomly nucleated spherulites which grow in all directions until they are stopped by impingement. Such a crystallinity distribution in the thickness direction was found to change along the flow direction. Moreover, it was suggested that the crystallites in the skin layer and in the second layer are formed during the filling process, while the others, at layers three and four, tend to be formed during the subsequent stages of the molding cycle. Similar results were obtained by Ito et al. [14].

For slow-crystallizing polymers, it was found that the crystalline structure in the thickness direction of the injected part is completely different from that discussed above. It consists of three different layers, namely the amorphous skin layer, the crystalline intermediate layer and the amorphous core layer [8-11]. The intermediate crystalline layer is a result of the stress-induced crystallization produced by the high level of shear rate and stress at this layer. The amorphous morphology obtained in the skin and the core layers is due to the high cooling rate in the skin, close to the mold wall, and to the low level of shear stresses in the center of the molding.

The development of crystallinity during the filling process can greatly affect the final molecular orientation of injected semi-crystalline products. In the literature, many studies concerning the distribution of the molecular orientation in the thickness direction of injection-molded parts of fast crystallizing polymers such as PE [15] and PP [16-17] have been published. However, few studies have been devoted to investigating the molecular orientation in slow-crystallizing polymers. In the present study, the distribution of both molecular orientation and crystallinity across the thickness of molded samples of PET is discussed. The degree of molecular orientation at the surface of the specimens was compared to that of other materials showing different rheological, thermal and crystallization characteristics.

4.4 EXPERIMENTAL

Four injection-grade polymers were used: polyethylene terephthalate (PET, Eastman Kodak 9921); high density polyethylene (HDPE, Exxon 6706); polystyrene (PS, Arco Chemical 232); and liquid crystal polymer (LCP, ICI Vectra B420). These polymers were chosen because of their different rheological, thermal and crystallization behavior. The molding conditions for each of these polymers are summarized in Table 4.1. Figure 4.1 shows schematically the dimensions of the injection-molded specimens and the locations where the molecular orientation was measured.

Molecular orientation was measured by means of external specular reflectance infrared spectroscopy. This technique has been shown to be a useful tool to investigate the molecular orientation in plastic products [18]. Reflectance spectra were measured on a Nicolet 170SX FT-IR spectrometer equipped with a Model 134 specular reflectance accessory and zinc selenide wire grid polarizer from Spectra-Tech Inc. Each spectrum was the result of an accumulation of 128 scans at a resolution of 4 cm^{-1}. The angle of incidence was 11° and a front-surface gold mirror was used as a reference. For the specimens used in this study, spectra were measured with polarization in the flow and transverse directions. The refractive index and absorption index spectra, denoted by n and k respectively, were obtained by performing Kramers-Kronig transformation of the reflectance spectra with the aid of Spectra-Calc™ software from Galactic Industries Corporation. The software was slightly

modified to allow the calculation of the imaginary molecular polarizability function ϕ from the n and k spectra [19]. Generally speaking, the ϕ spectrum resembles the k spectrum, but some differences in shape are observed for the more intense absorption bands. The polarizability function correlates more closely with the molecular properties [20].

For a given vibrational mode, in the case of uniaxial orientation, the degree of orientation can be related to the dichroic ratio D, defined as the ratio of the absorption intensities of a particular band when measured with parallel ($\phi_{\parallel}$) and perpendicular ($\phi_{\perp}$) polarization of the radiation with respect to the direction of orientation (flow direction):

$$D = \frac{\phi_{//}}{\phi_{\perp}} \qquad (4.1)$$

and the orientation function f for this particular vibrational band is given by:

$$f = \frac{D - 1}{D + 2} \frac{2}{3\cos^2\alpha - 1} \qquad (4.2)$$

where α is the angle between the transition moment of the particular molecular vibration and the polymer chain axis.

Measurements of molecular orientation at different depths in the thickness direction were performed with the use of the milling and polishing technique described elsewhere [21]. It has been found that this technique does not significantly disturb or generate molecular orientation in plastic products having a relatively high glass transition temperature. Moreover, it was noted that the milling and polishing technique increases the overall quality of the spectra by reducing diffusion losses and back-surface reflection, thus permitting a better characterization of the molecular orientation. However, since the spectra measured in different polarization directions were found to have somewhat different overall intensities, in part as a result of difficulties in positioning the specimen in exactly the same plane as the reference, they needed to be normalized. In the case of PET, it has been demonstrated [22] that the benzene ring band at 1410 cm^{-1} is insensitive to both orientation and crystallinity and therefore suitable for this purpose. Thus, all PET polarizability function spectra were normalized so that the area under this peak was equal to 1. In the case of the other polymers no such peak was available, so a different approach was used. The measured reflectance spectra were scaled so that the baseline reflectance corresponded to the theoretical value calculated from the refractive index of the polymer.

The crystallization kinetics of the PET and HDPE were characterized by differential scanning calorimetry performed on a Perkin-Elmer DSC-7 instrument. The tests were done on samples of about 10 mg. These samples were heated at 20°C/min from room temperature to a temperature above their melt temperatures (280°C for the PET and 240°C for the

HDPE). After a given residence time at that temperature, the samples were cooled down at various cooling rates ranging from 1 to 160°C/min. All experiments were performed under nitrogen atmosphere. During the cooling process, the exothermal peak of crystallization was recorded. By integrating the area under this peak, the variation of the relative crystallinity of the polymer as a function of time can be obtained. For the same cooling rate, the crystallization kinetics of the PET and HDPE were compared by comparing different features of their crystallization curves.

Rheological measurements of all polymers at shear rates between 10^{-2} and 10^{2} s^{-1} were carried out using a Rheometrics mechanical spectrometer, RMS Model 605. For higher shear rates, steady-state capillary flow experiments were performed using a Rosand capillary rheometer, RCR Model RH-7. For the RMS dynamic tests, disk-shaped specimens with a thickness of 2 mm and a diameter of 25 mm were used. These specimens were compression molded using a Carver laboratory press equipped with water cooled platens. The total molding time was 15 min, including cooling at a rate of 20°C/min.

Tensile dynamic mechanical moduli of samples cut from the surface of the injection-molded specimens were measured using a Rheometrics Model Mark 2 dynamic mechanical thermal analyser (DMTA). Specimens with a thickness of 0.2 mm were cut both parallel and perpendicular to the flow direction using a high speed milling machine. The tensile dynamic

tests were conducted at room temperature at a frequency of 1 Hz. The reported storage moduli were the average values from three specimens.

4.5 RESULTS AND DISCUSSION

4.5.1 Molecular Orientation at the Surface of the Injected Part

4.5.1.1 Effect of gate geometry

The molecular polarizability function spectra measured at the surface of the injection-molded PET in three polarization directions (0°, 30°, and 90°) with respect to the flow direction are shown in Figure 4.2. These spectra were measured both near and far from the mold entrance for a mold temperature of 20°C. The spectra obtained in different polarization directions are all the same, and resemble that of amorphous unoriented PET [18], indicating that molecular orientation is negligible at the surface of this specimen. Such a lack of molecular orientation in the flow direction is probably due to the effect of the gate size and geometry on the final distribution of molecular orientation in the injected part. In fact, in this study, a large gate was used (Figure 4.1), which can stretch and orient polymer molecules mainly in the transverse (y) direction before they enter the cavity. During the filling stage,

as these molecules reach the flow front, they will flow along the free surface in a curved path until they reach the cold mold wall. Such an elongational flow will force the polymer molecules to orient in the flow direction [1]. Therefore, the final degree of molecular orientation at the external surface of the molding will depend on the competition between the elongational flow imposed during the filling process, and the transverse flow generated at the gate.

To test this hypothesis, samples were molded using different gate sizes and geometries and the molecular orientation at the surface of these specimens was measured. Figure 4.3 shows results obtained for a pinpoint gate near the mold entrance. This gate size was chosen to avoid the transverse flow at the gate before the beginning of the cavity filling and to permit the polymer molecules at the external surface of the molding to be essentially oriented in the flow direction. On comparing the polarizability spectra shown in Figure 4.3 to those in Figure 4.2, it is observed that the change of the gate size and geometry did not alter the molecular orientation at the skin of the injected PET, since the spectra in these two figures are exactly the same. It is therefore concluded that any molecular orientation imposed at the gate before the filling process has no effect on the final degree of orientation at the skin layer of the molding in this case.

Many other factors apart from shear, normal and elongational stresses acting during the filling process can affect the final degree of molecular orientation in injection-molded

products. These are the relaxation time of polymer molecules, the polymer chain rigidity, and the crystallization rate of the polymer used. In the case of semicrystalline polymers, it has been suggested [23] that the final degree of molecular orientation depends on the competition between the stress relaxation and the crystallization processes. If stresses acting during the filling stage are completely relaxed before the beginning of the crystallization process, then polymer molecules in the injected part will relax and the crystalline structure within these parts will be essentially spherulitic. In the case of amorphous polymers, the final degree of molecular orientation is a function of the relaxation time. The shorter the relaxation time, the lower will be the molecular orientation in the injection-molded part.

In the present study, polymeric materials showing different thermal, rheological, and crystallization behaviors were used. These are: polystyrene (PS), high density polyethylene (HDPE) and liquid crystal polymer (LCP). These materials were injection-molded, Table 4.1, and the molecular orientation at the external surface of the resulting specimens was measured. The degree of orientation at the surface of these specimens will be compared to that measured at the surface of the injected PET in order to characterize the effect of the crystallization rate and the relaxation time on the final degree of molecular orientation at the skin layer of the injected part.

4.5.1.2 Effect of the crystallization behavior

Figure 4.4 shows the crystallization behavior of PET and HDPE as characterized under quiescent conditions by means of DSC measurements. The results show that the high density polyethylene (HDPE) has a higher crystallization rate. In fact, it can crystallize under all cooling rates used in this study and can achieve its crystallization process much faster than PET. For example, at the same cooling rate of 5 °C/min, it was found that the HDPE has a crystallization time of 95 s, compared to 600 s for PET. Such a difference in the crystallization behavior between these two polymers can have a great effect on their final degree of molecular orientation when they are injection-molded. Basically, molecular chains in polymers having a higher crystallization rate should be much more oriented in the flow direction since the formation of the crystalline entities at earlier steps of the filling and cooling processes [14] can help retain to a certain extent the orientation generated during the filling of the mold cavity and therefore reduce the relaxation process of the polymer molecules. Moreover, the presence of shear flow during the filling stage enhances the crystallization process of semi-crystalline polymers. Recent studies have shown that the crystallization rate of HDPE and PET increases with increasing shear rate [24-27]. Such an increase in the crystallization rate will in turn continue to markedly reduce the relaxation process of polymer molecules in injection-molded parts and will therefore improve the degree of molecular orientation in the flow direction.

4.5.1.3 Effect of the relaxation time

The crystallization process is not the only factor affecting the final degree of molecular orientation in injection-molded products. The relaxation time is another important parameter that can affect the degree of orientation in both amorphous and semicrystalline polymers. A long relaxation time combined with a high crystallization rate will produce a higher molecular orientation. In this study, the relaxation time of the three materials used (HDPE, PET, PS) was evaluated at different temperatures from rheological data (not shown). For each polymer and temperature, these data were fitted using the Carreau-Yasuda model given by:

$$\eta = a_t \eta_0 \left[1 + (a_t \lambda \dot{\gamma})^a\right]^{\frac{n-1}{a}} \qquad (4.3)$$

where η_0, a, and n are the model parameters, a_t is the temperature shift factor, $\dot{\gamma}$ is the shear rate, and λ is the average relaxation time of the polymer molecules at the chosen temperature. Figure 4.5 shows the variation of the relaxation time for the three polymers as a function of temperature. As expected, the relaxation time decreases as the temperature of the polymer increases. Moreover, it appears that PET has the lowest relaxation time, which allows its molecules to return to their equilibrum random coil configurations much faster than other polymers. In the injection-molded part, the amorphous regions in the PET should therefore

have the lowest degree of molecular orientation compared to that obtained in the injected HDPE and PS.

Figures 4.6a and 4.6b show the polarizability spectra measured at the surface of the injected HDPE and PS for a mold temperature of 20°C. These spectra were measured parallel (0°) and perpendicular (90°) to the flow direction. Only the most intense absorption bands are clearly seen by IR external specular reflection spectroscopy. For both polymers, the two polarization directions give different spectra, suggesting the presence of significant molecular orientation at the surface of these specimens. In the case of HDPE (Figure 4.6a) the vibrational bands at 2918 and 2850 cm^{-1} show perpendicular dichroism; however, in the case of polystyrene, parallel dichroism is observed for the peak at 700 cm^{-1} (Figure 4.6b). If we consider that the transition moments of these absorption bands are respectively perpendicular and parallel to the chain axis [28, 29], then it is concluded that polymer molecules at the surface of the injected HDPE and PS are oriented in the flow direction and not randomly oriented as in the case of PET (Figure 4.2). For PET, the skin layer was found to be essentially amorphous, as will be discussed later. Therefore, the high molecular orientation obtained at the surface of the injected HDPE is due to its very fast crystallization rate (Figure 4.4) and to the formation during the filling process of crystalline entities [14] that are believed to act as pseudo-crosslinks [30], helping to retain in part the orientation generated during that process. In the case of PS, it is the very long relaxation time (Figure 4.5) that will prevent the polymer molecules from undergoing complete relaxation after the

cessation of the flow. These molecules will therefore be oriented essentially in the flow direction.

The molecular orientation results in changes in mechanical properties of the final part, as shown by DMTA measurements conducted at room temperature. Specimens from the skin layer of the injection-molded PET, HDPE, and PS were cut parallel and perpendicular to the flow direction by means of the high speed milling technique. The minimum thickness of these samples was about 0.2 mm because of geometrical limitations and difficulties associated with the sample preparation. Figure 4.7 shows typical DMTA traces at the skin layers of the three materials used. It can be seen that the elastic modulus of the PET measured parallel and perpendicular to the flow direction are exactly the same, indicating that there is no molecular orientation at the surface of this specimen. In the case of HDPE and PS, the elastic modulus is higher in the direction parallel to the flow than in the direction perpendicular to the flow. As mentioned above, this difference is due to the presence of significant molecular orientation at the surface of the injected HDPE and PS. Moreover, it can be noted that in the case of HDPE, the difference between the parallel and perpendicular elastic moduli is more pronounced, compared to PS, which correlates with the stronger dichroism observed at the surface of this specimen (Figure 4.6a).

Both the crystallinity and the extent of relaxation of the polymer molecules at the skin layer of injection-molded PET can be affected by increasing the mold temperature. In the

present study, specimens of PET were molded at different mold temperatures of 60, 120, and 140°C. Spectra were measured at the surface of these specimens in directions parallel ($\phi_{\parallel}$) and perpendicular ($\phi_{\perp}$) to the flow direction, and the molecular orientation function was calculated for the *trans* conformers of the ethylene glycol group from the CH_2 wagging band at 1340 cm^{-1} by means of Eq. 4.2 with $\alpha = 21°$. Moreover, from these spectra, and on the assumption of uniaxial molecular orientation in the flow direction, a "structure factor" spectrum ϕ_0 was calculated from the following equation [18]:

$$\phi_0 = \frac{1}{3}\phi_{//} + \frac{2}{3}\phi_{\perp} \qquad (4.4)$$

This spectrum represents the result exclusive of contributions arising from orientation of the polymer, i.e. the spectrum of an isotropic sample. In this spectrum, the area under the absorption band at 1340 cm^{-1} corresponding to *trans* glycol groups can be related to the amount of crystallinity at the surface of the specimen under investigation. The higher the area under this peak, the higher will be the crystallinity of the polymer. Figure 4.8 shows how this peak increases with mold temperature at the skin layer of the injected PET, while Figure 4.9 shows the effect of the mold temperature on both the number of *trans* glycol groups (as expressed in terms of the peak area) and their orientation. At 20°C, the number of *trans* groups is low and there is no orientation. On going to 60°C (still below the PET T_g of 70°C), the number of *trans* groups increases and they are highly oriented in the flow direction. This is the result of shear-induced crystallization. When the mold temperature is increased to 120°C or 140°C, well above the glass transition temperature, the polymer molecules at the

skin layer of the molding begin to relax while the degree of crystallinity at this layer increases significantly. Such a decrease of the molecular orientation is due to the shorter relaxation time of the polymer molecules at these high mold temperatures. On the other hand the high degree of crystallinity at this layer is the result of the slower thermal crystallization mechanism, which does not contribute to the orientation, in contrast with the fast kinetics of the shear-induced crystallization. These results confirm our previous speculation and indicate that the final degree of molecular orientation in semicrystalline polymers is a competition between the crystallization and the relaxation processes.

4.5.1.4 Effect of the chain rigidity

Another factor which can affect the final degree of molecular orientation in injection-molded parts is the rigidity of polymer chains. Liquid crystalline polymers (LCPs) are materials characterized by their rigid rod-like molecules or extended chains.

Nematic crystals are ordered in one direction; the long axes of the molecules are parallel and the local direction of alignment is called "director". By heating thermotropic LCPs to the melting stage, polymeric crystals may form either smectic or nematic structures, but may give a complete nematic structure once the temperature is futher increased. If the temperature becomes relatively high, a completely isotropic melt will be formed.

Figure 4.10 shows the result of preliminary rheological measurements performed on the LCP material (B420) in order to locate its nematic region. The complex viscosity η^* as a function of temperature for two shear rates of 0.02 and 0.1 s^{-1} and a strain of 3% shows a significant decrease between 280°C and 300°C. Thus the nematic transition can be considered to be completed at a temperature around 300°C.

LCP specimens were compression-molded at the nematic temperature. The LCP was first heated to a melt temperature of 300°C, then maintained for 5 min at this temperature, and finally rapidly cooled in a water bath to preserve the nematic morphology. FT-IR spectra were measured as previously described. However in this case a Spectra Tech IR-Plan Advantage microscope was also used in order to take into account the effect of different measurement areas. For a large measurement area (100 μm x 100 μm), the spectra measured in two mutually perpendicular directions (not shown here) were found to be exactly the same. However, when the measurement area was decreased to 20 μm x 20 μm, the two polarization directions gave different spectra as shown in Figure 4.11. The carbonyl band at 1725 cm^{-1} shows perpendicular dichroism because its transition moment is more-or-less perpendicular to the chain axis. Parallel dichroism, on the other hand, is observed for most of the other bands, including the ones at 1509 and 1470 cm^{-1}, which are known to be parallel bands associated with skeletal vibrations of the benzene and naphthalene rings in the polymer [31]. These results clearly indicate that in the nematic state, thermotropic liquid-crystalline polymers have a polydomain texture [32, 33], each domain having a significant molecular

orientation along a mean direction called the director [34, 35]. This molecular orientation apparently changes from one domain to another and is not homogeneous at a macroscopic level, since spectra measured over a larger area are exactly the same in two mutually perpendicular directions. It is therefore concluded that at the nematic temperature, polymer molecules in LCPs are clustered in domains with different directions of orientation, resulting in a polydomain texture characterized by a local order and a long-range random orientation. When this polymer is processed under elongational or shear flow, such as in the injection molding process, these polydomains should align in the flow direction, resulting in a high degree of molecular orientation and better mechanical properties in that direction. Figure 4.12 shows the spectra obtained at the surface of the injected LCP in directions parallel (0°) and perpendicular (90°) to the flow direction. These spectra were measured with the regular accessory over an area greater than 5 mm in diameter. The absorption bands at 1725, 1631, 1509 and 1470 cm^{-1} all show significant dichroism, indicating that polymer molecules at the skin layer of this molding are oriented in the flow direction. Similar results have been obtained by other authors [36, 37]. Such molecular orientation at the skin layer is due to the elongational flow at the advancing melt front, which seems to stretch the liquid crystalline domains in the flow direction and orient their polymer molecules along that direction [38]. Moreover, it is well known that at the subskin layer of the molding it is the shear flow that orients the molecules in the flow direction. The rotational nature of the shear flow can cause the liquid crystalline domains to tumble rather than orient in the flow direction. This results in a lower degree of molecular orientation at the subskin layer of the LCP moldings [38].

4.5.2 Variation of orientation of PET in the thickness direction

The molecular orientation at different layers across the thickness of the injected PET was characterized using the milling and polishing technique described in a separate paper [21]. At each layer, spectra were measured parallel and perpendicular to the flow direction and were used to calculate the molecular orientation functions for the absorption bands at 1725, 1340, and 729 cm^{-1}. These bands correspond respectively to carbonyl bond stretching, CH_2 wagging of *trans* conformers of the ethylene glycol unit, and an out-of-plane benzene ring C–H deformation. In addition, the spectra were used to calculate the "structure factor" in order to evaluate the crystallinity (based on the *trans* peak area) of the sample at each layer across the part's thickness. Figures 4.13 to 4.16 show the effect of the mold temperature on the crystallinity and the molecular orientation function of PET at different depths in the thickness direction and at different distances from the gate. Near the gate, the gapwise crystallinity structure was found to be greatly affected by the mold temperature. For samples injected at mold temperatures T_M lower than the glass transition temperature of the PET (T_M = 20°C and 60°C), a three layer amorphous-crystalline-amorphous-type structure was obtained in the thickness direction. The subskin layer at a depth of around 400 μm shows significant crystallinity as well as orientation. On increasing the mold temperature to values higher than the glass transition temperature of the PET (T_M = 120°C and 140°C), the morphology of the polymer becomes more crystalline overall and the maximum of crystallinity is shifted to the external surface of the molding. Similar results have been

obtained by Hsiung and Cakmak for injection-molded poly(aryletherketone) [8]. According to these authors, the development of the multilayer amorphous-crystalline-amorphous structure gradient in the thickness direction of specimens molded at low mold temperatures is a result of a complex interaction between the thermal and stress history experienced by the polymer during the whole injection process. It was suggested that the "stress-induced crystallization" phenomenon is the key factor responsable for the formation of this kind of crystalline structure in the thickness direction of injection-molded slow-crystallizing polymers.

The stress-or-strain-induced crystallization process is a well known phenomenon in polymers [39, 40]. It can manifest itself at high shear rates and at temperatures a few degrees above the crystalline melting point of the polymer [41]. When the molten polymer is highly stressed in one specific direction, its molecules will be highly oriented in that direction and this results in a strong tendency for them to crystallize at high temperatures. Row nucleation has also been a characteristic of crystallization of polymer melts under a stress field [42] and microscopic observations have revealed that the application of shear stress to a polymer melt leads to a large increase in the number of crystalline structures formed, which will in turn enhance the crystallization rate dramatically [43].

Recently, Chien and Weiss [44] studied the effect of the temperature, stress, and stressing time on the crystallization behavior of slow-crystallizing polymers such as PEEK

by means of parallel-plate rheometry. They characterized the crystallization kinetics by using the induction time, which is defined as the time elapsed from the beginning of the shearing to the onset of the crystallization. These authors have noted that an increase in the rate of shearing reduces the induction time significantly, and stress-induced crystallization is much less temperature-dependent than quiescent crystallization. Moreover, it was found that shearing is the predominant cause for the initiation of nucleation at high temperatures because it lowers the energy barrier for the initiation of nucleation. By increasing the shearing time, a longer shearing history will be introduced into the polymer, which in turn increases its crystallinity. In the subskin layer of the injected part, all three factors affecting the crystallinity of slow-crystallizing polymers (namely temperature, stress, and shearing time) are present. Therefore, this layer should have the highest degree of crystallinity, as indicated in Figure 4.13. In the core of the molding, the polymer molecules are less sheared (oriented), therefore less crystallinity is expected in this area. An increase in the mold temperature shifts the "shear-induced crystallization" process from the subskin to the skin layer of the molding. This is due, as shown by Wimberger-Friedl [4], to the decrease of the thickness of the skin layer on increasing the mold temperature, and the "shear-induced crystallization" process will basically take place near the mold wall during the filling stage. Far from the gate, the degree of crystallinity of PET was found to be almost constant across the part thickness. In this zone, the shear field is expected to be very small and the shearing time is very short; therefore the shearing is unable to heavily orient the polymer molecules and cause the "shear-induced crystallization" process (Figure 4.13). The crystallinity remains

low except when a high mold temperature results in slower cooling and therefore increased thermal crystallization.

Such crystallinity distributions in the flow and thickness directions of specimens molded at low mold temperatures agree well with the crystallization model recently proposed by Hsiung et al. [10]. This model provides an easy and comprehensive understanding of the step-by-step mechanism for the build-up of the crystallinity during the injection molding of slow-crystallizing polymers. The basic features of this model are: (i) for low mold temperatures, the maximum of crystallinity is located in the subskin layer at about 0.4 mm from the external surface of the molding, and this crystallinity decreases as the distance from the gate increases; (ii) an increase of the mold temperature increases the degree of crystallinity of the polymer and gives a more flat crystallinity profile across the part thickness. The only difference is noted at the surface of specimens injected with high mold temperatures (120°C and 140°C). In this case, a shift of the maximum of crystallinity was noted from the subskin to the skin layer of the molding on increasing the mold temperature. This is due, as mentioned above, to the decrease of the thickness of the skin layer on increasing the mold temperature, which shifts the "shear-induced crystallization" process toward the mold wall during the filling stage.

Figures 4.14 to 4.16 show the orientation functions for different absorption bands along the flow and the thickness directions at different mold temperatures. At low mold

temperatures the molecular orientation functions have much the same distributions as the crystallinity distribution of the polymer. At high mold temperatures the orientation is low but the crystallinity is high, as a result of thermal crystallization. The out-of-plane benzene ring C–H band at 729 cm^{-1} shows somewhat anomalous behaviour at the surface for high mold temperatures. This may be due to a tendency for the benzene rings in the crystalline phase to align parallel to the surface plane under certain circumstances [45]. Overall, these results confirm our previous speculation and clearly show that the presence of "shear-induced crystallization" during the filling process improves the molecular orientation in the flow direction since it helps to retain to a certain extent such an orientation and reduces the relaxation process of polymer molecules considerably. Moreover, the *trans* conformers of the ethylene glycol unit were found to have the highest degree of orientation. This is to be expected since the stretching of polymer molecules by shearing during the filling stage increases the number of these *trans* conformers and their orientation will be in the flow direction.

4.6 CONCLUSIONS

The results of this study can be summarized as follows:

- Molecular orientation at the skin layer of the molding depends on many factors such as flow stresses, the relaxation time of polymer molecules, the polymer chain rigidity,

and the crystallization kinetics of the polymer used. Basically, a long relaxation time combined with a high crystallization rate will produce a higher molecular orientation in the flow direction at the skin layer of the molding. An increase of the molecular chain rigidity as in liquid crystalline polymer can lead to a polydomain texture at high melt temperatures, which is characterized by a local order but a long-range random orientation. During the injection process, as a result of elongational flow at the melt front, these polydomains will align in the flow direction, resulting in a high degree of molecular orientation at the skin layer of the molding.

- For slow-crystallizing polymers such as PET, the crystallinity gradient in the thickness direction depends on the mold temperature. In fact, for mold temperatures lower than the glass transition temperature of the PET, near the gate, the maximum crystallinity was observed at the subskin layer (at about 0.4 mm from the external surface of the molding) as a result of the "shear-induced crystallization" generated during the filling stage. The skin and the core layers of the molding were found to be essentially amorphous at these mold temperatures. Far from the gate, the crystallinity in the thickness direction becomes almost constant, because in this zone the shear field is expected to be small and last only a short time; therefore it is unable to orient the polymer molecules in the flow direction and cause the "shear-induced crystallization". When the mold temperature was higher than the glass transition temperature of the PET, the maximum of crystallinity was found to shift from the

subskin layer to the skin layer of the molding. This is due to the decrease of the thickness of the skin layer with the increase of the mold temperature.

- For PET at low mold temperatures, the molecular orientation in the thickness direction was found to have much the same distribution as the crystallinity of the polymer. It appears therefore that the presence of crystallinity during the filling stage ("shear-induced crystallization") improves the degree of molecular orientation in the flow direction since it helps to preserve the orientation generated in that stage and reduces the relaxation process of the polymer molecules.

ACKNOWLEDGEMENTS

The authors would like to express their appreciation of the contributions from Mr. Y. Simard in the injection molding work, Mr. M. Carmel in the rheological and DMTA measurements, and Mr. E. Pellerin in the infrared measurements.

4.7 REFERENCES

1. Z. Tadmor, *J. Appl. Polym. Sci.*, **18**, 1753 (1974).

2. G. Menges and G. Wübken, *SPE ANTEC Techn. Papers*, 519 (1973).

3. M. R. Kamal and V. Tan, *Polym. Eng. Sci.*, **19**, 558 (1979).

4. R. Wimberger-Friedl, *Int. Polym. Process.*, **11**, 373 (1996).

5. R. L. Ballman and H. L. Toor, *Modern Plastics*, **38**, 113 (1960).

6. L. Mandelkern, *Crystallization of Polymers*, McGraw-Hill, New York (1964).

7. B. Wunderlich, *Macromolecular Physics*, Vols. 1-2, Academic Press, New York, (1973).

8. C. M. Hsiung and M. Cakmak, *J. Appl. Polym. Sci.*, **47**, 125 (1993).

9. C. M. Hsiung, M. Cakmak, and J. L. White, *Polym. Eng. Sci.*, **30**, 967 (1990).

10. C. M. Hsiung, M. Cakmak, and Y. Ulcer, *Polymer*, **37**, 4555 (1996).

11. Y. Ulcer, M. Cakmak, J. Miao, and C. M. Hsiung, *J. Appl. Polym. Sci.*, **60**, 669 (1996).

12. S. S. Katti and J. M. Schultz, *Polym. Eng. Sci.*, **22**, 1001 (1982).

13. V. Tan and M. R. Kamal, *J. Appl. Polym. Sci.*, **22**, 2341 (1978).

14. H. Ito, K. Minagawa, J. Takimoto, K. Tada, and K. Koyama, *Int. Polym. Process.*, **11**, 363 (1996).

15. F. H. Moy and M. R. Kamal, *Polym. Eng. Sci.*, **20**, 957 (1980).

16. Y. Sjönell, B. Terselius, and J.-F. Jansson, *Polym. Eng. Sci.*, **35**, 950 (1995).

17. J. Trotignon and J. Verdu, *J. Appl. Polym. Sci.*, **34**, 1 (1987).

18. K. C. Cole, J. Guèvremont, A. Ajji, and M. M. Dumoulin, *Appl. Spectrosc.*, **48**, 1513 (1994).

19. A. Cunningham, G. R. Davies, and I. M. Ward, *Polymer*, **15**, 743 (1974).

20. J. E. Bertie, S. L. Zhang, and C. D. Keefe, *J. Mol. Struct.*, **324**, 157 (1994).

21. H. Ben Daly, K. C. Cole, B. Sanschagrin, and K. T. Nguyen, submitted to *Polym. Eng. Sci.*

22. D. J. Walls, *Appl. Spectrosc.*, **45**, 1193 (1991).

23. M. Demiray and A. I. Isayev, *SPE ANTEC Techn. Papers*, 1576 (1996).

24. V. Tan and C. G. Gogos, *Polym. Eng. Sci.*, **16**, 512 (1976).

25. E. S. Hsiue, R. E. Robertson, and G. S. Y. Yen, *Polym. Eng. Sci.*, **23**, 74 (1983).

26. S. Kim and S. C. Kim, *Polym. Eng. Sci.*, **33**, 83 (1993).

27. K. A. Narh, E. Roa, M. D. Saindon, C. Cohen, and K. K. Wang, *SPE ANTEC Techn. Papers*, 2932 (1995).

28. K. C. Cole, A. Ajji, and C. Bimbeau, *Proc. Composites '96 and Oriented Polymers Symp.*, 119 (1996).

29. P. Painter and J. L. Koenig, *J. Polym. Sci., Polym. Phys. Ed.*, **15**, 1885 (1977).

30. R. Pearce, K. C. Cole, A. Ajji, and M. M. Dumoulin, *Proc. Composites '96 and Oriented Polymers Symp.*, 133 (1996).

31. I. Ouchi, M. Hosoi, and S. Shimotsuma, *J. Appl. Polym. Sci.*, **21**, 3445 (1977).

32. S. Onogi and T. Asada, p. 127 in *Rheology and Rheo-optics of Polymer Liquid Crystals*, Vol. 1, G. Astariata and G. Marrucci (Eds.), Plenum Press, New York, 1980 (papers presented at Eighth International Congress on Rheology, Naples, 1980).

33. B. A. Wood and E. L. Thomas, *Nature (London)*, **324**, 655 (1986).

34. G. Marucci, *Pure Appl. Chem.*, **57**, 1545 (1985).

35. K. F. Wissbrun, p. 1 in *Orienting Polymers*, A. Dold and B. Eckman (Eds.), Lecture Notes in Mathematics 1063, Springer-Verlag, New York, 1984.

36. Z. Ophir and Y. Ide, *Polym. Eng. Sci.*, **23**, 792 (1983).

37. Y. Ide and Z. Ophir, *Polym. Eng. Sci.*, **23**, 261 (1983).

38. G. G. Vida, D. G. Baird, and G. L. Wilkes, *Polym. Eng. Sci.*, **25**, 888 (1985).

39. A. Keller and M. Machin, *J. Macromol. Sci. - Phys.*, **B1**, 41 (1967).

40. R. Stein, M. Hashiyama, and M. Parpart, p. 331 in *Optical Studies of Stress-Induced Crystallization of Polymer Melts in Flow Induced Crystallization*, Gordon and Breach Science Publishers, Great Britain (1979).

41. A. K. Van Der Vegt and A. Smit, p. 313 in *Crystallization Phenomena in Flowing Polymers*, SCI Monograph No. 26, Society of the Chemical Industry, London, 1967.

42. B. Maxwell, *J. Polym. Sci.*, **C9**, 43 (1965).

43. T. W. Haas and B. Maxwell, *Polym. Eng. Sci.*, **9**, 225 (1969).

44. M. C. Chien and R. A. Weiss, *Polym. Eng. Sci.*, **28**, 6 (1988).

45. P. Lapersonne, D. I. Bower, and I. M. Ward, *Polymer*, **33**, 1266 (1992).

Table 4.1 - Molding conditions for the different polymers used.

	Melt Temperature (°C)	Injection Rate (cm/s)	Holding Pressure (MPa)	Cooling Time (s)	Mold Temperature (°C)
PET-9921	314	15	30	10	20, 60, 120, 140
PS-232	285	10	18.5	20	20
HDPE-6706	240	6.25	37	45	20
LCP-B420	290	5	44.5	10	20

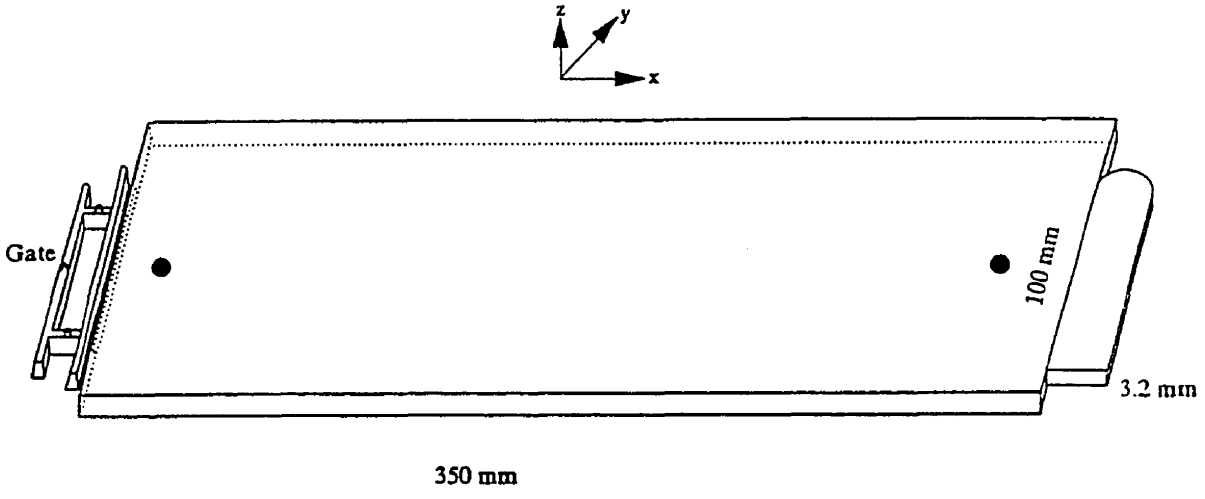

Figure 4.1 - Schematic representation of the injection-molded part and locations where molecular orientation was measured

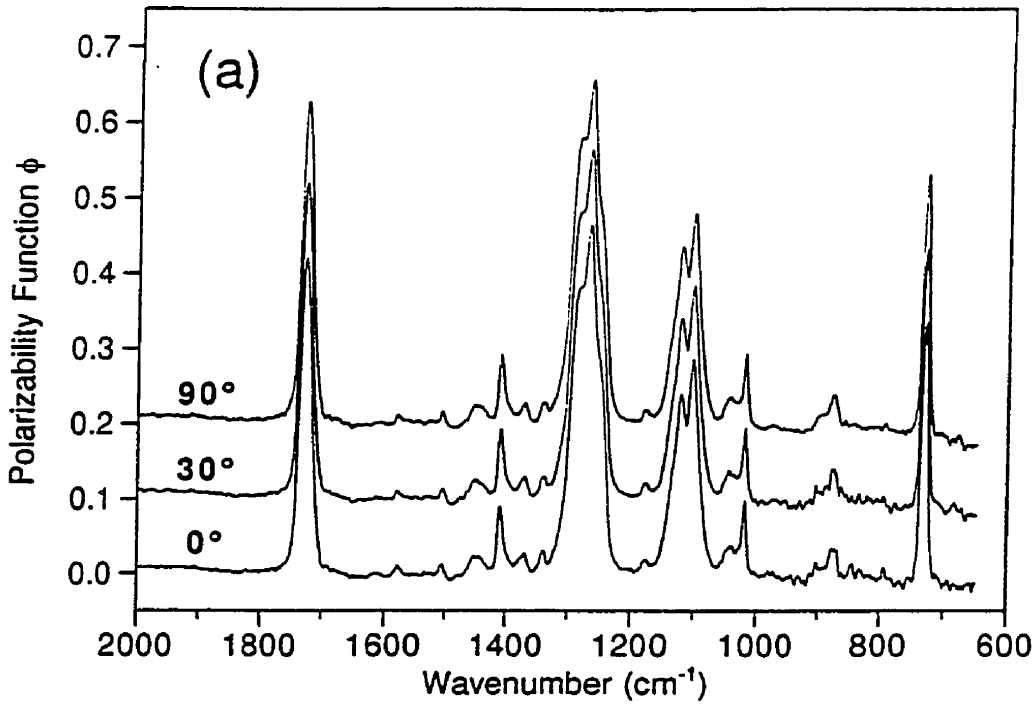

Figure 4.2a - Surface IR spectra of injection-molded PET measured near the gate for a sample molded with a wide gate and a mold temperature $T_M = 20°C$. Angles indicate direction of IR polarization with respect to flow direction.

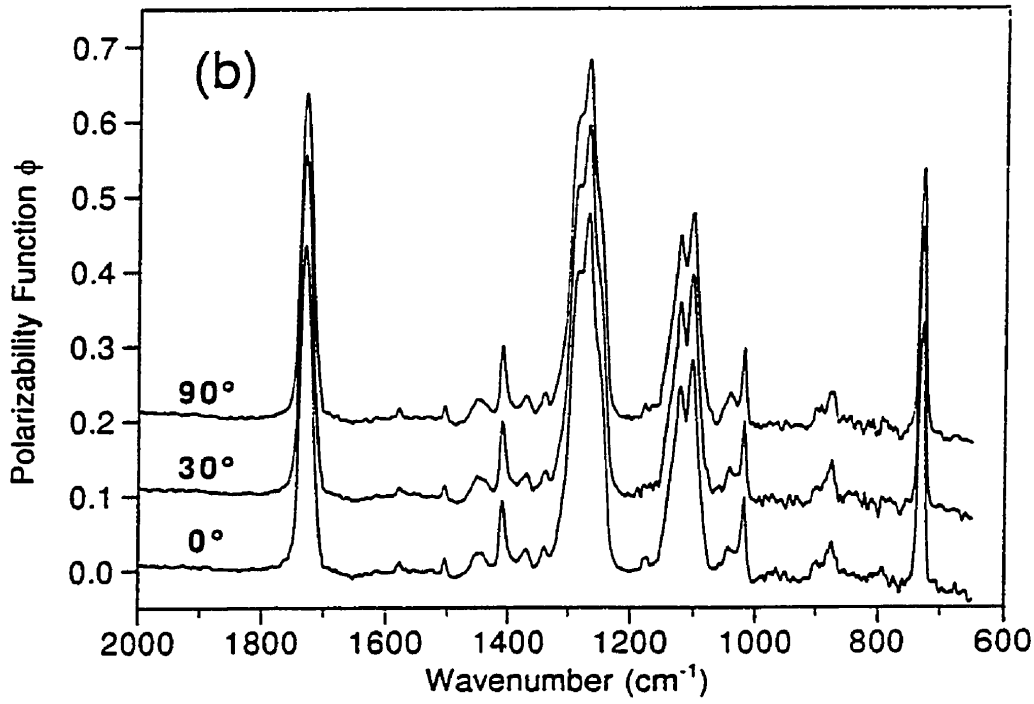

Figure 4.2b - Surface IR spectra of injection-molded PET measured far from the gate for a sample molded with a wide gate and a mold temperature T_M = 20°C. Angles indicate direction of IR polarization with respect to flow direction.

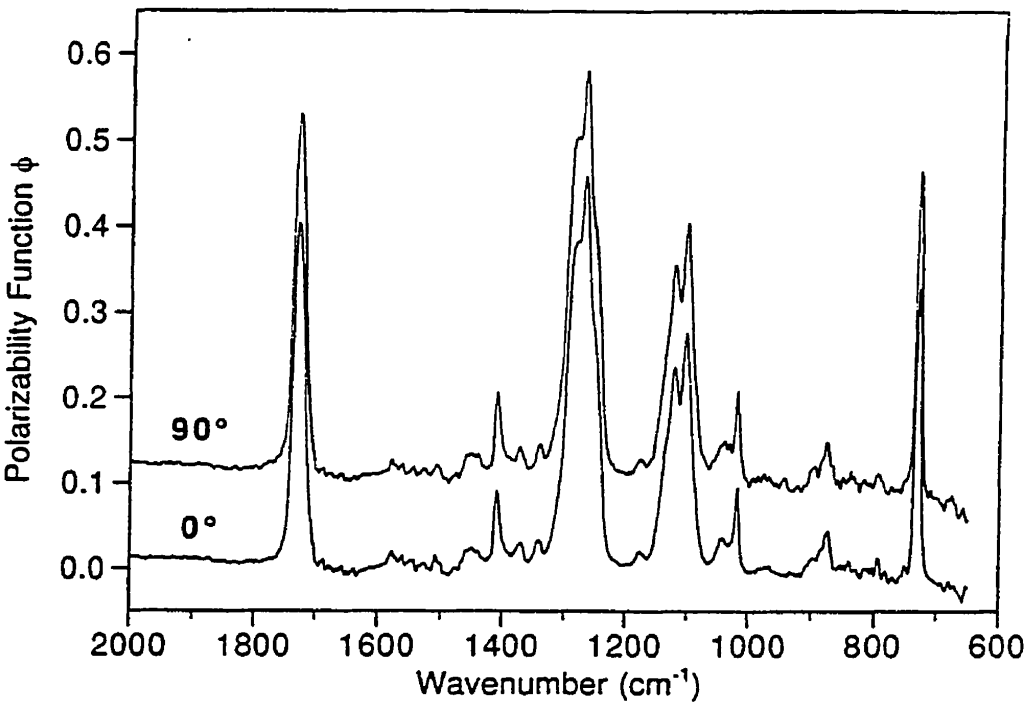

Figure 4.3 - Surface IR spectra of injection-molded PET measured near the gate for a sample molded with a pinpoint gate and a mold temperature T_M = 20°C. Angles indicate direction of IR polarization with respect to flow direction.

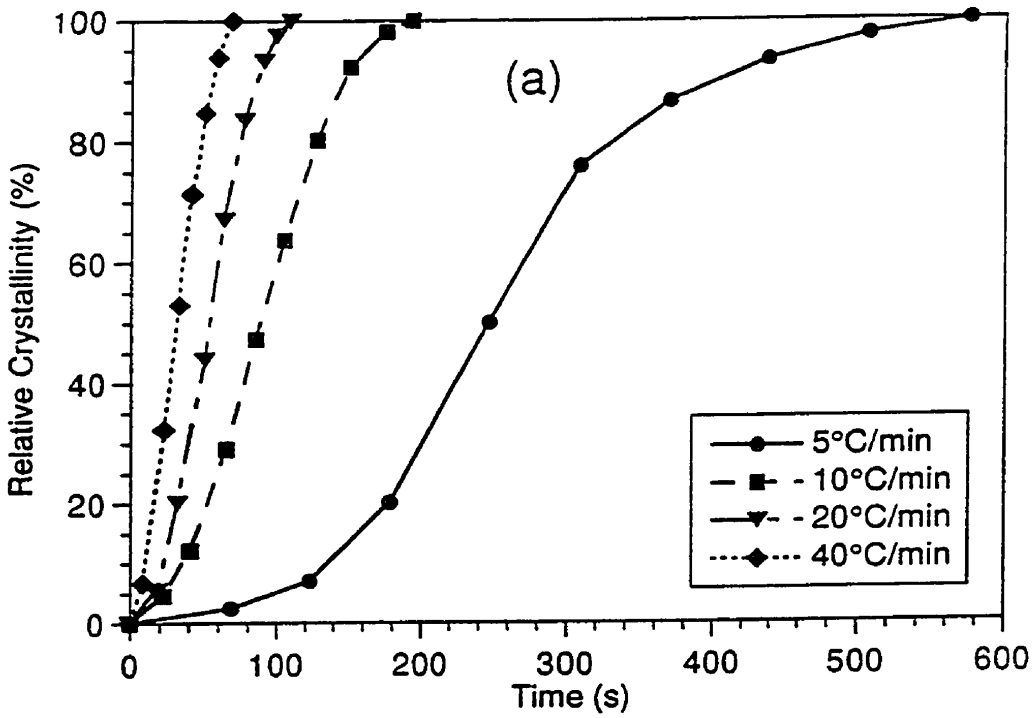

Figure 4.4a - Relative crystallinity at different cooling rates for PET

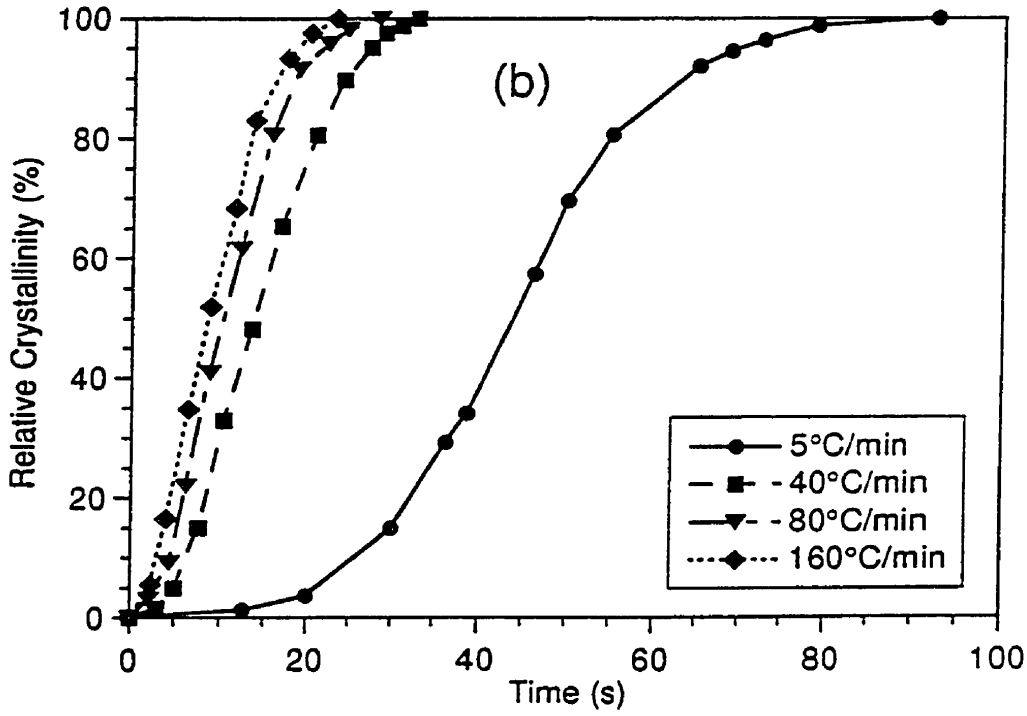

Figure 4.4b - Relative crystallinity at different cooling rates for HDPE

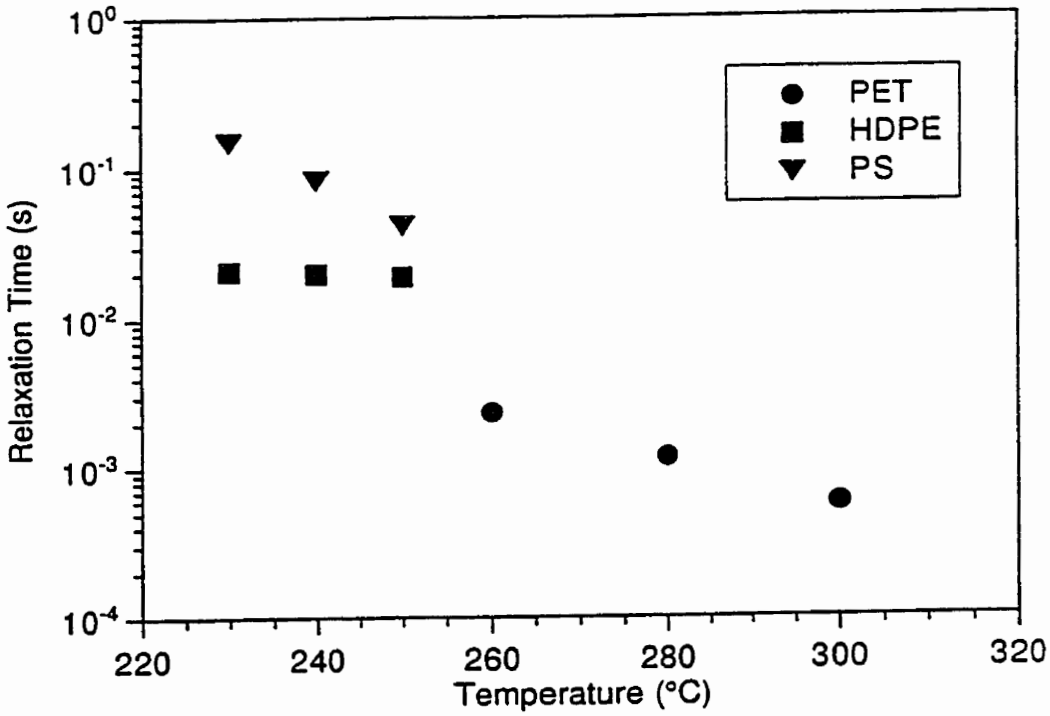

Figure 4.5 - Relaxation time of different polymeric materials as a function of temperature

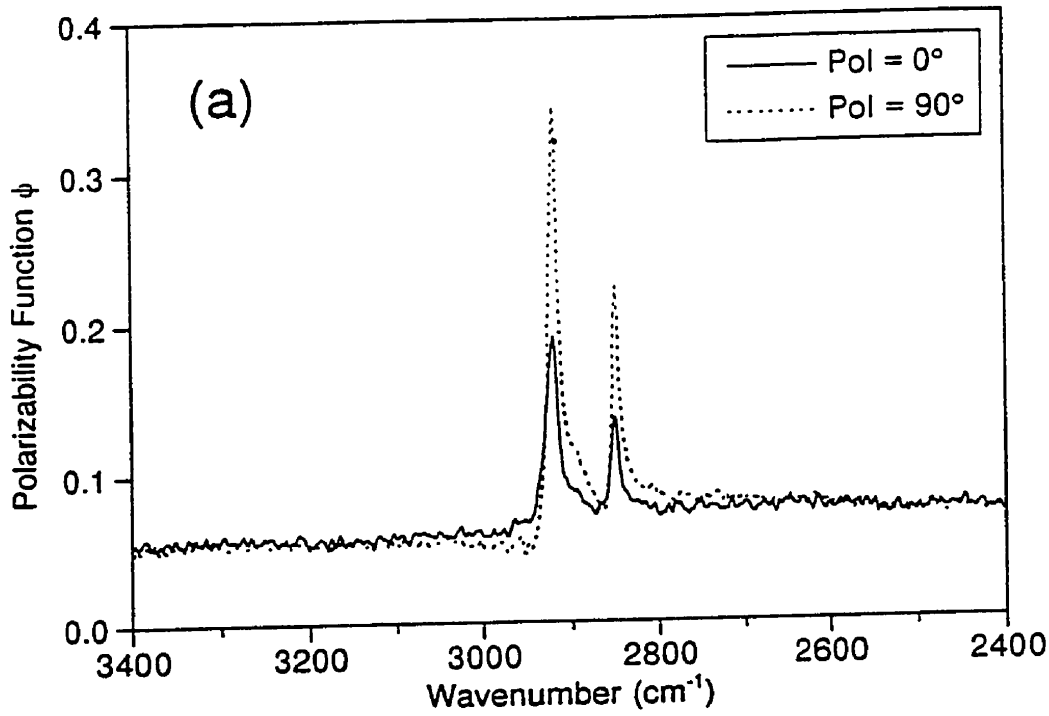

Figure 4.6a - Surface IR spectra of injection-molded HDPE. Angles indicate direction of IR polarization with respect to flow direction

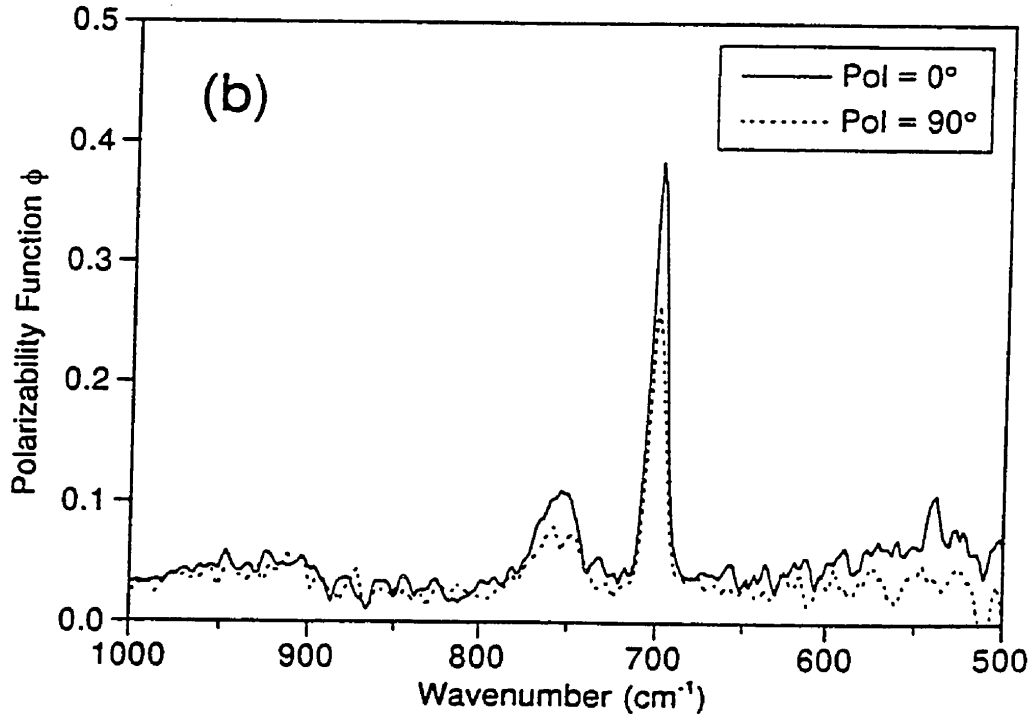

Figure 4.6b - Surface IR spectra of injection-molded PS. Angles indicate direction of IR polarization with respect to flow direction

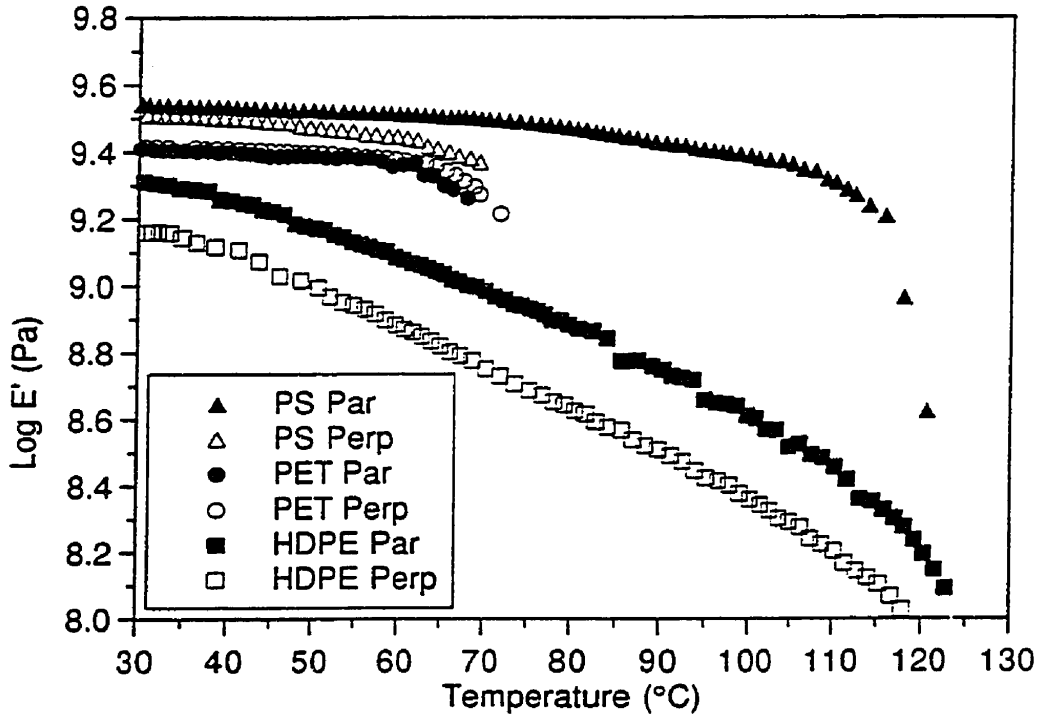

Figure 4.7 - DMTA traces for specimens taken from the surface of injected PET, HDPE, and PS

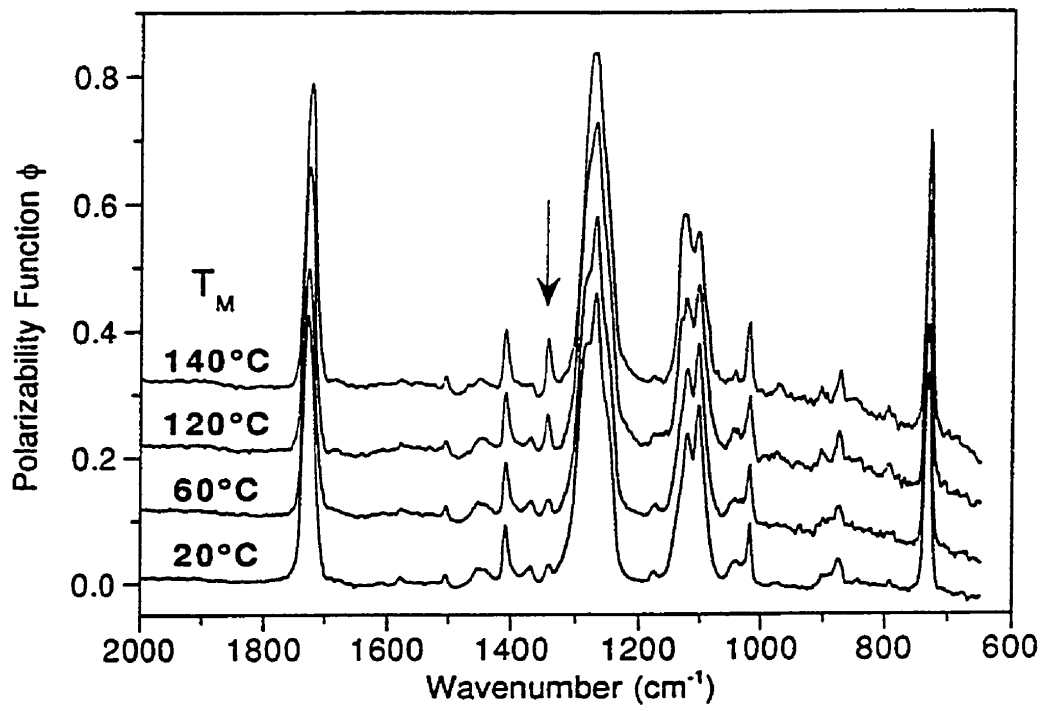

Figure 4.8 - "Structure factor" spectra measured at the surface of injected PET for different mold temperatures

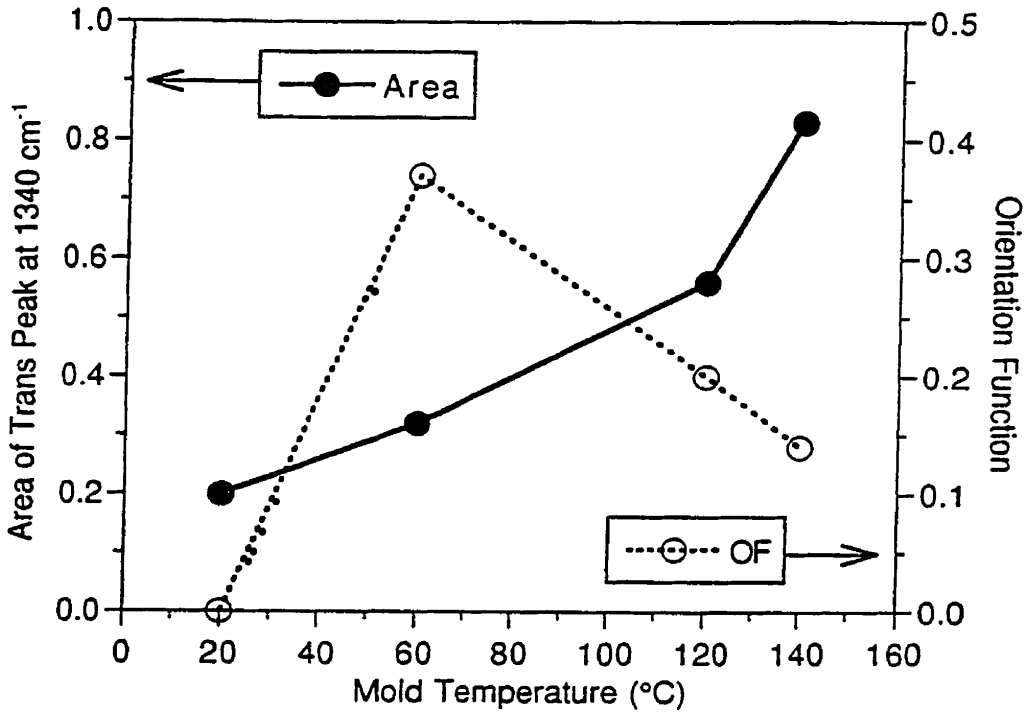

Figure 4.9 - Effect of the mold temperature on the content of glycol *trans* conformers (related to crystallinity) and on their orientation at the surface of injected PET near the gate

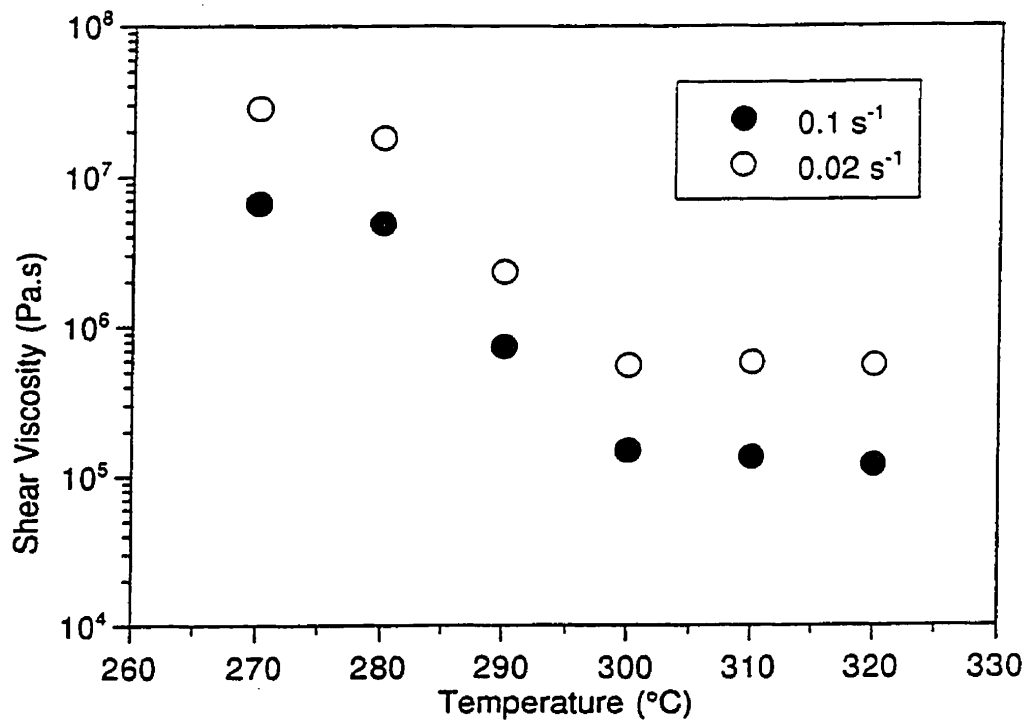

Figure 4.10 - Viscosity of Vectra B420 as a function of temperature at different shear rates

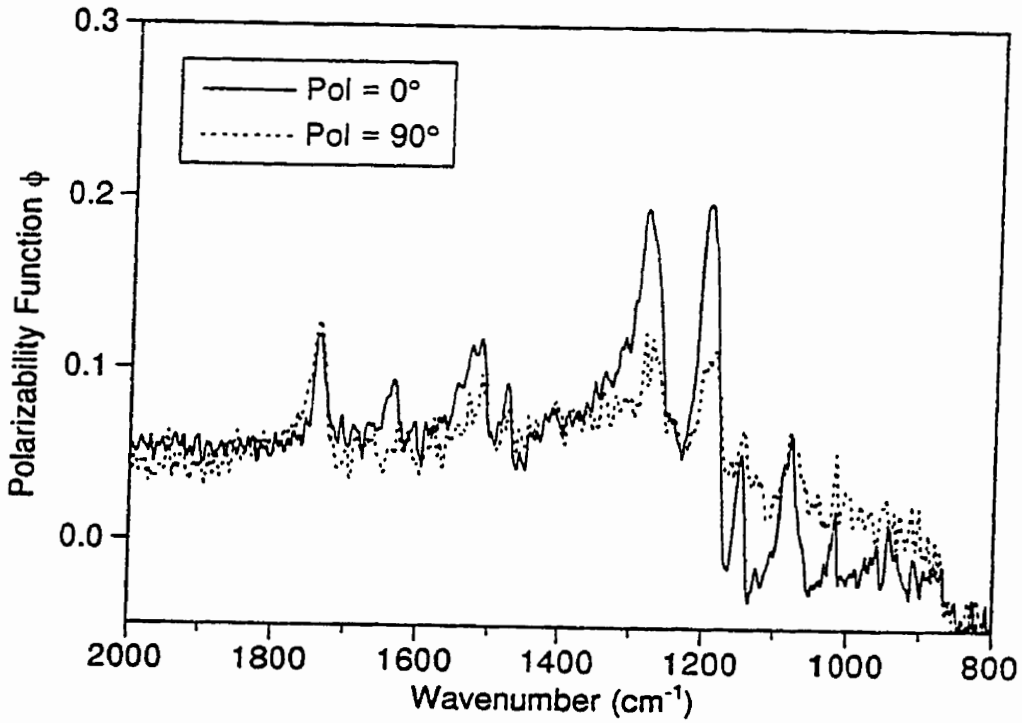

Figure 4.11 - Surface IR spectra of compression-molded LCP (20 μm x 20 μm area)

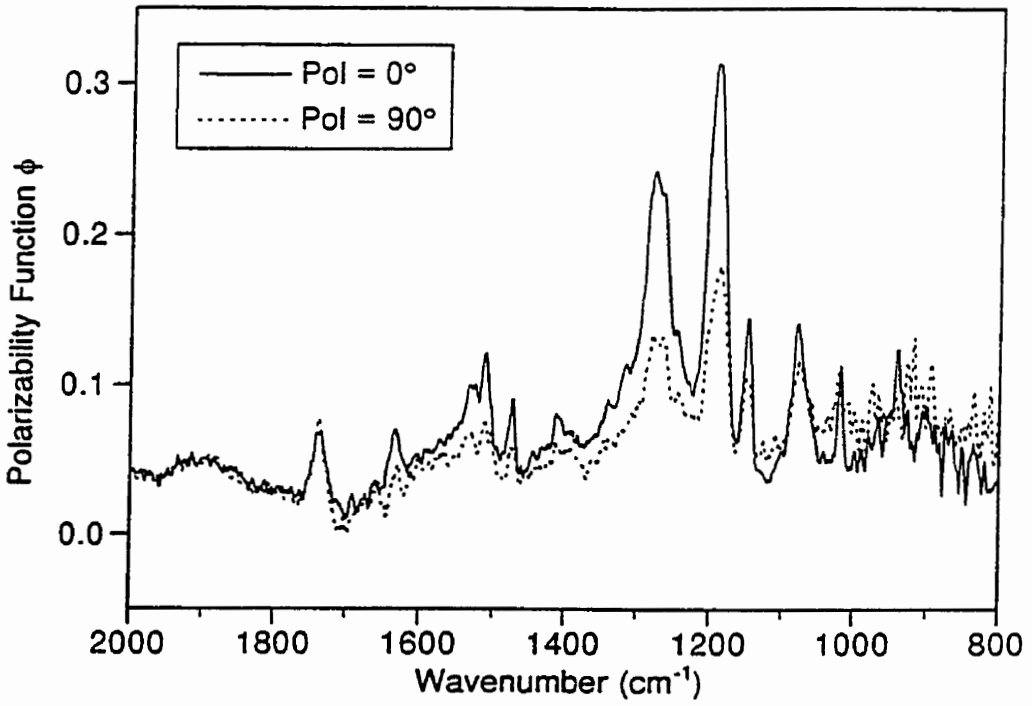

Figure 4.12 - Surface IR spectra of injection-molded LCP

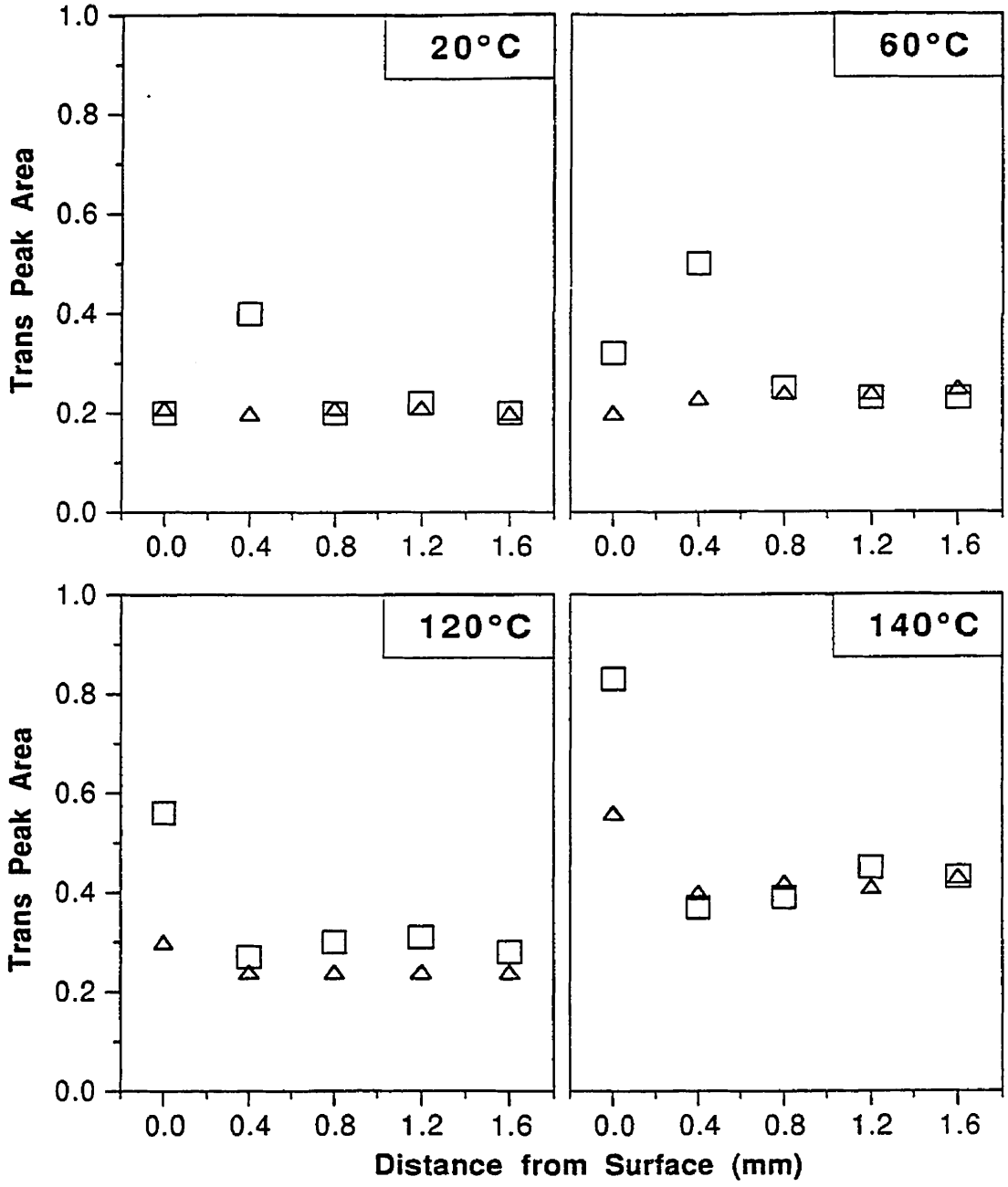

Figure 4.13. Variation of the glycol trans peak area in the thickness direction for different mold temperatures, near the gate (□) and far from the gate (Δ).

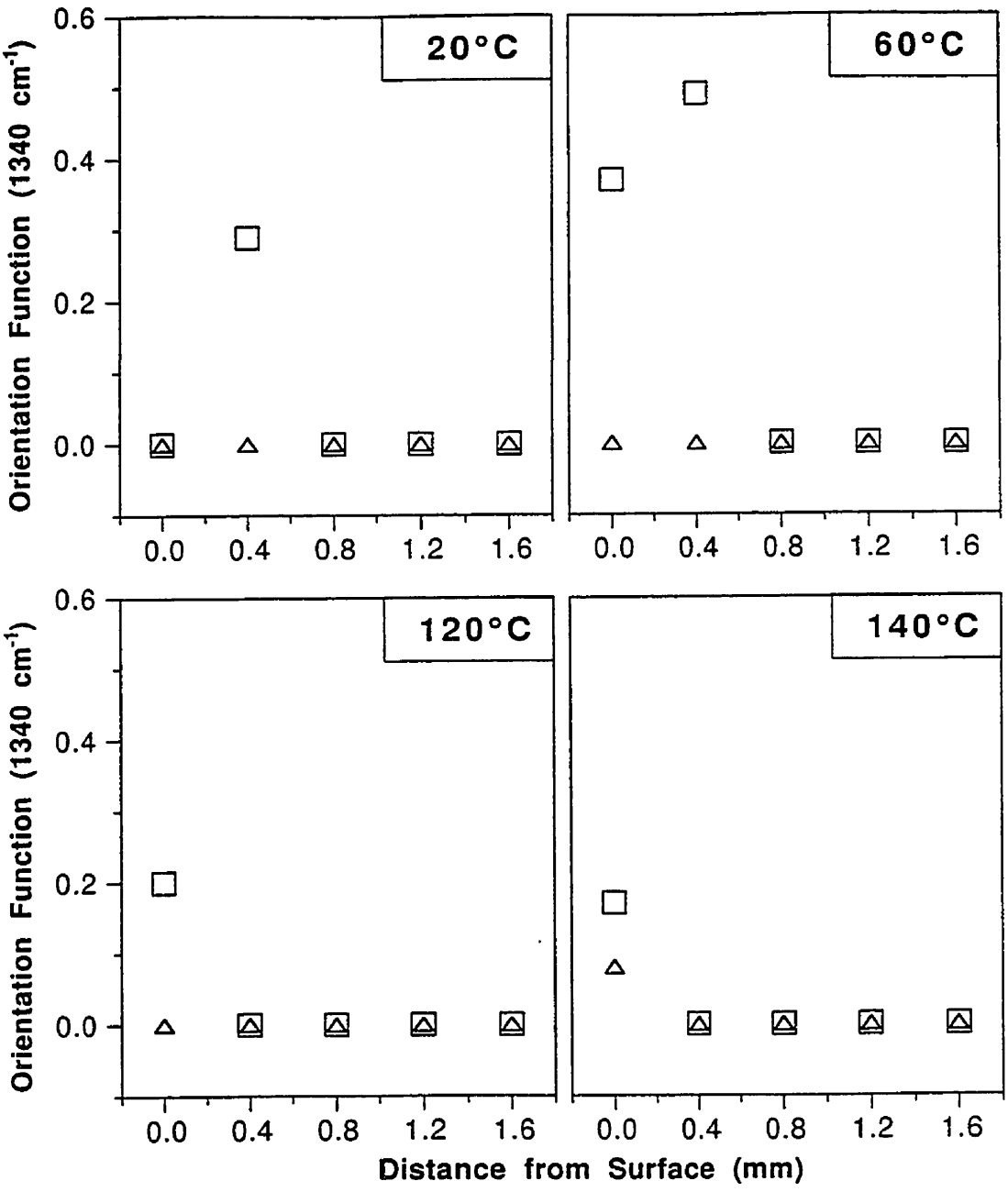

Figure 4.14. Variation of the molecular orientation function in the thickness direction for different mold temperatures, near the gate (□) and far from the gate (Δ), based on the dichroism of the peak at 1340 cm^{-1}.

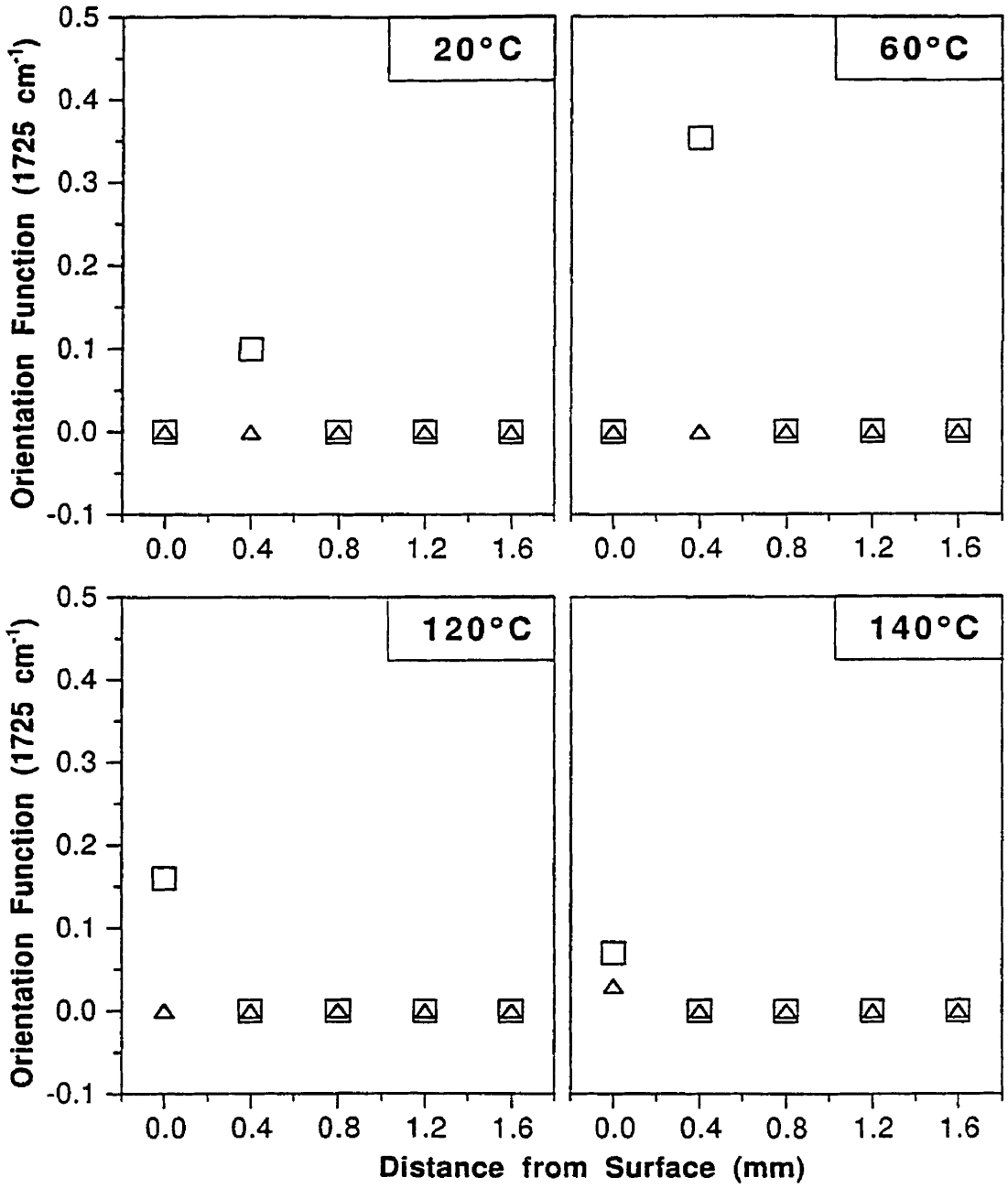

Figure 4.15. Variation of the molecular orientation function in the thickness direction for different mold temperatures, near the gate (□) and far from the gate (Δ), based on the dichroism of the peak at 1725 cm^{-1}.

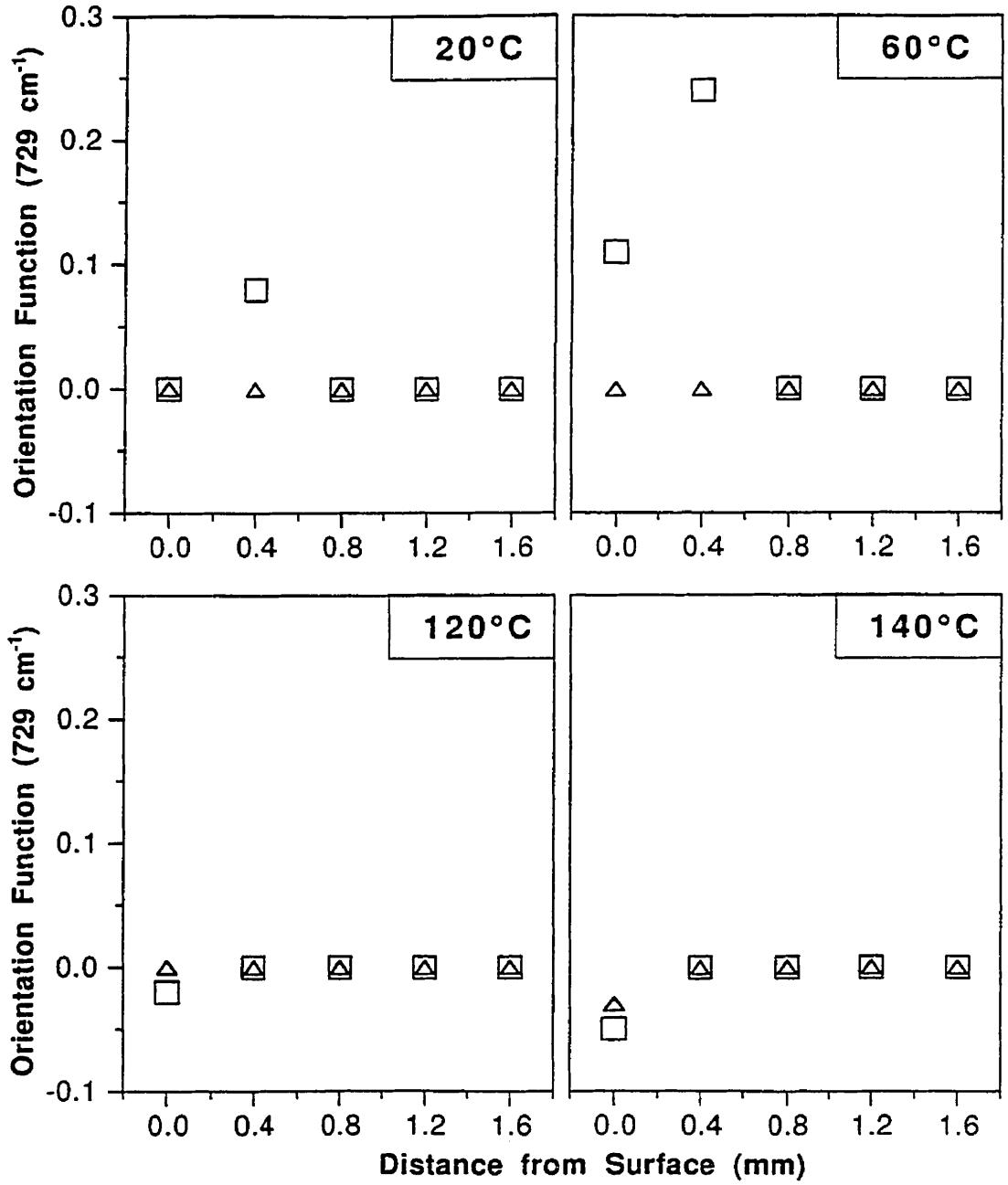

Figure 4.16. Variation of the molecular orientation function in the thickness direction for different mold temperatures, near the gate (□) and far from the gate (Δ), based on the dichroism of the peak at 729 cm^{-1}.

CHAPITRE V

A NEW APPROACH TO THE CHARACTERIZATION OF MOLECULAR ORIENTATION IN UNIAXIALLY AND BIAXIALLY ORIENTED SAMPLES OF POLY (ETHYLENE TEREPHTHALATE)

K.C. COLE[1*], H. BEN DALY[2], B. SANSCHAGRIN[2], and K.T. NGUYEN[1]

[1] *Industrial Materials Institute*

National Research Council Canada

75, boul. De Mortagne, Boucherville, Québec, Canada J4B 6Y4

[2] *Center for Applied Research on Polymers (CRASP)*

École Polytechnique

C.P. 6079, succursale Centre-ville, Montréal, Québec, Canada H3C 3A7

This chapter has been submitted for publication in the journal of Polymer.

5.1 RÉSUMÉ

La fonction d'orientation de Hermans (f), largement utilisée dans la littérature, a été proposée pour caractériser le degré d'orientation des chaînes moléculaires dans des échantillons uniaxialement orientés. Dans ce cas et en utilisant la spectroscopie infrarouge, elle est égale à (equation 4.2):

$$f = \frac{D - 1}{D + 2} \frac{2}{3\cos^2\alpha - 1}$$

où $D = A_{//} / A_{\perp}$ est le rapport dichroic d'un groupement moléculaire spécifique et $A_{//}$ et $A_{\perp}$ représentent respectivement l'absorption de ce groupement dans des spectres mesurés parallèlement et perpendiculairement à direction d'orientation. α étant l'angle entre la direction du moment de transition du groupement moléculaire considéré et l'axe de la chaîne. Pour le cas des échantillons biaxialement orientés, cette équation n'est plus valable. En effet, dans le cas d'une orientation équibiaxiale, $A_{//}$ et $A_{\perp}$ sont égales et la fonction d'orientation calculée selon l'équation précédente est donc nulle, indiquant qu'il n'y a pas d'orientation dans cet échantillon.

Dans ce chapitre, on propose une nouvelle approche permettant de déterminer le degré d'orientation des chaînes moléculaires dans des échantillons en PET uniaxialement et biaxialement orientés. L'approche utilisée consiste à comparer les spectres mesurés sur un

échantillon orienté à ceux mesurés sur un échantillon non orienté. Dans une direction spécifique de polarisation, la différence entre ces spectres permet de caractériser le degré d'orientation des chaînes moléculaires dans l'échantillon orienté.

Contrairement à la fonction d'orientation de Hermans discutée ci-haut, dans notre étude, nous avons défini un autre rapport dichroic. Ce rapport, noté R, est égal au rapport des hauteurs des pics d'absorption à 1265 et 1725 cm^{-1} (représentant les vibrations de certains groupements moléculaires orientés parallèlement et perpendiculairement à l'axe de la chaîne). Ces pics ont été choisis car le rapport de leur hauteur est très sensible à l'orientation.

Pour différents échantillons en PET orientés uniaxialement à des taux d'étirement différents, nous avons tracé la variation de leur fonction d'orientation (f) en fonction de la quantité ($R-R_o$), où R_o est égal à R dans le cas d'un échantillon non-orienté ($R_o = 1.12$). La variation de (f) en fonction de ($R-R_o$) est donnée par (equation 5.10):

$$f = \frac{R - R_o}{0.657 + 0.528\ R}$$

Cette équation a été testée sur des échantillons en PET unaxialement et biaxialement orientés. Les résultats obtenus indiquent clairement son efficacité. Il a été noté que dans le cas des échantillons uniaxialement orientés, l'équation de Hermans ainsi que notre approche donnent exactement les mêmes résultats. Dans le cas des échantillons biaxialement orientés,

les résultats de notre approche coïncident avec ceux obtenus par la technique de biréfringence, largement utilisée pour caractériser l'orientation moléculaire dans des échantillons uniaxialement et biaxialement orientés.

5.2 ABSTRACT

The usual approach that is used to characterize the molecular orientation in biaxially oriented samples by infrared spectroscopy is to measure spectra with polarization in all three directions—machine, transverse, and normal (or thickness). However, the latter measurement is rather difficult to make experimentally. In the present work we propose a new approach to characterizing the molecular orientation in both uniaxially and biaxially oriented samples of PET. It makes use of the ratio of the absorption bands at 1330-1240 and 1729 cm^{-1}, the first of which shows parallel dichroism and the second perpendicular dichroism. An equation is developed that relates this ratio to the molecular orientation with respect to the direction of measurement. Thus it is possible to determine individually the orientation functions with respect to the machine and transverse directions. The validity of functions determined in this way is confirmed by comparison with birefringence results.

5.3 INTRODUCTION

Many processing methods for producing polymeric articles can introduce molecular orientation into the final products. Some of them, like fibre spinning, introduce uniaxial orientation, while others, like extrusion blow molding, can introduce some degree of biaxial orientation. It has been found that the final degree of orientation in the molded products can affect both their optical and their mechanical properties. Therefore, its exact determination is of great importance since it can provide a better characterization of the end properties of the products. Various techniques have been used to measure both uniaxial and biaxial molecular orientation in amorphous and semi-crystalline polymers. These include heat shrinkage, birefringence, infrared spectroscopy, X-ray diffraction, differential scanning calorimetry, and nuclear magnetic resonance. Of these, the birefringence technique has been widely employed because of its simplicity.

The characterization of molecular orientation by means of optical methods has been described in detail by Ward and coworkers [1,2] and by Zbinden [3]. To completely describe the orientation, it is necessary to determine the detailed probability distribution function for the orientation of a coordinate axis system fixed in the molecular frame with respect to one fixed in the sample. Because many industrial samples possess at least orthorhombic symmetry, it is usually easy to define the sample axis system in terms of machine (M), transverse (T), and normal (N) or thickness directions. The molecular axis system (a, b, c)

is usually chosen so that one axis (generally c) coincides with the chain axis of the polymer molecule. The choice of the other two axes is important when the polymer possesses a well-defined crystalline structure, in which case the orientation of the a and b axes may be quite different. However, in many cases, including amorphous polymers, the polymer structural units may be considered as having rotational symmetry around the chain axis and the distinction between the a and b axes can be neglected. Under these circumstances, it is sufficient to define the orientation of the chain axis c, which can be described in terms of three Hermans-type orientation functions:

$$f_{cM} = \frac{1}{2} (3 \langle \cos^2\theta_{cM} \rangle - 1) \qquad \textbf{(5.1a)}$$

$$f_{cT} = \frac{1}{2} (3 \langle \cos^2\theta_{cT} \rangle - 1) \qquad \textbf{(5.1b)}$$

$$f_{cN} = \frac{1}{2} (3 \langle \cos^2\theta_{cN} \rangle - 1) \qquad \textbf{(5.1c)}$$

where the three θ variables represent the angles made by the chain axis c with respect to the M, T, and N directions, and the angle brackets indicate an average over all chain orientations. The three angles are not independent. The sum of the three squared cosines is equal to unity, and the sum of the three orientation functions is equal to zero:

$$f_{cM} + f_{cT} + f_{cN} = 0 \qquad \textbf{(5.2)}$$

Thus any two f values are sufficient to define the orientation, and the third can be determined by difference. The value of f ranges from –0.5, if the chain axes are perfectly perpendicular to the reference axis, to +1 if they are perfectly parallel. This representation of the orientation amounts to approximating the exact distribution function by an ellipsoid [3], but in most cases this is sufficient and in fact many techniques, including birefringence and infrared spectroscopy, cannot provide a more detailed representation.

White and Spruiell [4,5] have proposed somewhat different but related orientation factors that are useful for describing biaxial orientation. The following equations give their definition, as well as their relationship to the above orientation functions and to the refractive indices measured by birefringence:

$$\begin{aligned} f_{cM}^{B} &= \langle \cos^2\theta_{cM} \rangle - \langle \cos^2\theta_{cN} \rangle \text{ or } 2\langle \cos^2\theta_{cM} \rangle + \langle \cos^2\theta_{cT} \rangle - 1 \\ &= \frac{2}{3}(f_{cM} - f_{cN}) \text{ or } \frac{2}{3}(2f_{cM} + f_{cT}) \\ &= \frac{\Delta n_{MN}}{\Delta^0} \end{aligned} \tag{5.3a}$$

$$\begin{aligned} f_{cT}^{B} &= \langle \cos^2\theta_{cT} \rangle - \langle \cos^2\theta_{cN} \rangle \text{ or } 2\langle \cos^2\theta_{cT} \rangle + \langle \cos^2\theta_{cM} \rangle - 1 \\ &= \frac{2}{3}(f_{cT} - f_{cN}) \text{ or } \frac{2}{3}(2f_{cT} + f_{cM}) \\ &= \frac{\Delta n_{TN}}{\Delta^0} \end{aligned} \tag{5.3b}$$

In these equations, $\Delta n_{MN} = n_M - n_N$ and $\Delta n_{TN} = n_T - n_N$, where n is the index of refraction in the particular direction indicated and Δ^0 is the maximum or intrinsic birefringence. A number of methods may be used to evaluate the orientation factors of equation 5.3. White and Spruiell use the birefringence and wide angle X-ray methods, and one advantage of the factors defined in equation 5.3 is their simple relationship to the birefringence results.

In a sample that is uniaxially oriented in the machine direction M, the T and N directions are equivalent, in which case $n_T = n_N$, $f_{cT} = f_{cN} = -1/2\, f_{cM}$, and $f^B_{cT} = 0$. Only one parameter ($f_{cM} = f^B_{cM}$) is required to define the orientation. For biaxially oriented samples, two parameters are required (for example, f_{cM} and f_{cT}, or f^B_{cM} and f^B_{cT}). This means that the refractive index must be determined in all three directions M, T, and N, rather than in just the M and T directions.

Infrared (i.r.) spectroscopy is another valuable technique for characterizing orientation [3], and has the advantage of being able to provide specific information on the different phases (amorphous and crystalline) and molecular conformations present in the polymer. Dichroic i.r. spectroscopy measures the absorption intensity of different molecular vibrational modes with an i.r. beam whose electric field vector is polarized in a specific direction with respect to the sample. Each vibrational mode possesses a transition moment that can usually be considered to make a fixed angle α with respect to the chain axis. For the case of rotational symmetry about the chain axis, when a sample is analyzed with radiation

polarized in any particular direction J, it can be shown that the absorption intensity of a particular band is given by:

$$A_J = A_0[1 + \frac{1}{2}(3\langle\cos^2\theta_{cJ}\rangle - 1)(3\cos^2\alpha - 1)] = A_0[1 + f_{cJ}(3\cos^2\alpha - 1)] \quad (5.4)$$

where A_0 represents the absorption intensity that would be observed for an equivalent unoriented sample, θ_{cJ} is the angle between the chain axis and the direction of polarization J, and f_{cJ} is the orientation function with respect to that direction. Thus if measurements are made in the three directions M, T, and N, the following quantities are obtained:

$$A_M = A_0 [\, 1 + f_{cM} (3 \cos^2\alpha - 1) \,] \quad \textbf{(5.5a)}$$

$$A_T = A_0 [\, 1 + f_{cT} (3 \cos^2\alpha - 1) \,] \quad (5.5b)$$

$$A_N = A_0 [\, 1 + f_{cN} (3 \cos^2\alpha - 1) \,] \quad (5.5c)$$

and A_0 can be calculated from:

$$A_0 = \frac{1}{3} (A_M + A_T + A_N) \quad \textbf{(5.6)}$$

For the case of uniaxial orientation, the polymer chains are oriented towards the machine direction and there is no difference between the T and N directions. Hence $f_{cT} = f_{cN}$

$= -1/2\, f_{cM}$, and one needs to make measurements in only the M and T directions, then calculate the dichroic ratio D to eliminate the unknown quantity A_0:

$$D = \frac{A_M}{A_T} = \frac{1 + f_{cM}\,(3\cos^2\alpha - 1)}{1 + f_{cT}\,(3\cos^2\alpha - 1)} \tag{5.7}$$

Because $f_{cT} = -1/2\, f_{cM}$, equation 5.7 can be inverted to give the well known equation 4.2:

$$f_{cM} = \frac{D - 1}{D + 2} \cdot \frac{2}{3\cos^2\alpha - 1}$$

The single quantity f_{cM}, equivalent to the well known Hermans orientation function, is sufficient to describe the uniaxial orientation.

For general biaxial orientation, the M, T, and N directions are all different. In principle, it is possible to calculate f_{cM} and f_{cT} by means of equations 5.5a and 5.5b, but this requires the knowledge of A_0. Usually this quantity is unknown, because it depends on the properties of the particular specimen being analyzed (for example, the thickness in the case of a transmission spectrum, or the surface quality in the case of a reflection spectrum). Thus for biaxially oriented samples, the usual approach is to measure the absorption intensities A_M, A_T, and A_N in all three directions, calculate A_0 from equation 5.6, then determine f_{cM}, f_{cT}, and f_{cN} according to equation 5.5. However, the measurement of the spectrum in the normal direction is more difficult than that for the other two. For thin films in transmission it can be

obtained by making measurements on tilted films, and for attenuated total reflection (a.t.r.) it can be obtained by making measurements with different positions of the sample with respect to the plane of incidence. However, in both cases the analysis is considerably more tedious than that required for uniaxial samples. An alternative approach is to overcome the dependence of A_0 on specimen properties by using the ratio of two different bands in the same spectrum. This approach has been applied by Mirabella [6-8] to ATR spectra of oriented polypropylene.

In recent papers, one of the authors and his coworkers [9-11] as well as other groups [12-15] have demonstrated the possibilities of using front-surface infrared reflection for characterizing the surface orientation of thick uniaxially drawn samples. Furthermore, the present authors have shown that for polymers with glass transition temperatures above room temperature, careful milling and polishing of the specimen results in spectra of high quality without affecting the polymer structure [16]. One way to apply this technique to biaxially oriented samples (i.e. to determine A_N) is to section the sample and make measurements in the N direction with an infrared microscope. Because of the special equipment and considerable work required for this, we have developed an alternative approach. In the present paper we expand upon the peak ratio approach used by Mirabella and show how it can be successfully applied to front-surface reflection spectra of poly(ethylene terephthalate), or PET.

5.4 EXPERIMENTAL

The proposed method for characterizing orientation was developed with the use of data from samples that were prepared by uniaxially drawing thick PET sheet (extrusion grade, DuPont Selar PT 7086) at 80°C to different values of the draw ratio λ. Details on sample preparation and the measurement of *FT* i.r. (Fourier transform infrared) spectra are given in earlier publications [9-11]. Although these samples were not polished, they gave spectra of good quality. With the aid of the software Spectra-Calc™ from Galactic Industries Corporation, the measured reflectance spectra were subjected to Kramers-Kronig transformation in order to obtain the refractive index (n) and absorption index (k) spectra. The software was slightly modified in-house to allow calculation from the n and k spectra of the imaginary molecular polarizability function spectrum ϕ. The latter provides the closest correlation to the molecular properties, especially for the more intense absorption bands [17]. From the ϕ spectra, conventional dichroic ratios and orientation functions were calculated according to the usual procedures [9]. To correct for variations in the overall intensity of the spectra, arising from effects like surface quality and sample positioning, the spectra were normalized with respect to the area of the peak at 1410 cm^{-1}, which is known to be insensitive to both orientation and conformation [18].

The validity of the method was checked on two PET samples made from Eastman Chemicals PET 9921. A uniaxially oriented sample was prepared by stretching amorphous

sheet (obtained by molding in a laboratory press at 285 °C followed by quenching in water) at 80 °C and 2 cm/min to a draw ratio of 2.8 in an Instron tensile tester equipped with an environmental chamber. For this sample M, T, and N denote the drawing, width, and thickness directions respectively. A biaxially oriented sample was obtained from injection blowmolded bottles. These had a length of 248 mm and a rounded rectangular cross-section of 84 mm x 40 mm. The sample used in this study was cut from the surface that was highly stretched in the hoop direction. For this sample, M denotes the length direction of the bottle, T the hoop direction, and N the thickness direction.

The molecular orientation of these samples was characterized using front-surface specular reflection i.r. spectroscopy. Spectra were measured on a Nicolet 170SX *FT* i.r. spectrometer equipped with a Model 134 specular reflectance accessory and zinc selenide wire grid polarizer from Spectra-Tech Inc. Each spectrum was the result of an accumulation of 128 scans at a resolution of 4 cm^{-1}. The angle of incidence was 11 ° and a front-surface gold mirror was used as reference. For both samples used in the validation, spectra were first measured on the surface with polarization in both the M and T directions. The uniaxial sample was then cut parallel and perpendicular to the stretching direction and reflection spectra were measured on the cross-sectional MN and TN planes. This was done with the use of a Spectra-Tech IR Advantage microscope. The measurement area was equal to 50 μm x 50 μm. To ensure a high quality for these spectra, the cut specimens were mounted in epoxy resin and the MN and TN planes were carefully polished to a finish of 0.05 μm [16]. In the

case of the biaxially oriented sample, spectra were measured in the MT plane only, but at different depths across the thickness direction. This was done by removing layers of material by means of the polishing technique developed by the authors [16]. The average molecular orientation functions across the thickness were compared to those obtained by means of the birefringence technique. Details on the measurement of the degree of biaxial molecular orientation using the birefringence technique are given elsewhere [19]. It is to be noted that these birefringence measurements were performed before the mounting and polishing of the sample for infrared characterization.

5.5 RESULTS AND DISCUSSION

Some typical spectra of polished specimens of PET are shown for illustrative purposes. Figure 5.1 shows spectra of an amorphous undrawn sample measured with polarization in two mutually perpendicular directions that are designated M and T (although in this case the choice of M is arbitrary). As expected for an unoriented sample, the two polarizations give effectively identical spectra. The peaks in the reflectance spectra (Figure 5.1a) show a dispersion-like shape because of the contribution of the refractive index. The polarizability function (ϕ) spectra obtained by Kramers-Kronig transformation (Figure 5.1b) show peak shapes that more closely resemble those of conventional infrared absorption spectra. Figure 5.2 shows spectra of the same material after uniaxial drawing to $\lambda = 3.8$; in this case M designates the draw direction. The very obvious difference between the M and

T spectra is due to the dichroism resulting from molecular orientation. Some peaks, like the carbonyl band at 1729 cm^{-1} and the out-of-plane benzene ring C-H bands at 875 and 730 cm^{-1} are more intense in the T direction because their transition moments make a large angle α with respect to the polymer chain axis (i.e. they tend towards perpendicular). Other peaks are stronger in the M spectrum, because their transition moments tend to be more parallel to the chain axis (small angle α). These include the glycol CH_2 wagging peak at 1340 cm^{-1}, the in-plane benzene ring C-H peak at 1018 cm^{-1}, and the intense complex bands around 1330-1240 and 1160-1080 cm^{-1} that arise mainly from ester group vibrations.

The isotropic or "structural factor" spectrum, corresponding to A_0, can be calculated from the A_M and A_T spectra by means of equation 5.6, which reduces to $A_0 = 1/3\ A_M + 2/3\ A_T$ for a uniaxial sample because $A_N = A_T$. Structural factor spectra for the undrawn and drawn samples are shown in Figure 5.3. In this case the difference between the two is not due to dichroism but to changes in the molecular conformation produced by drawing, in particular the transformation of *gauche* glycol conformers into *trans* conformers.

For the set of samples drawn uniaxially to different values of λ, it was possible to calculate the overall orientation function f from the ϕ spectra by means of equation 4.2, based on certain peaks for which the value of the angle α is known or can be reasonably assumed. These include the benzene ring C–H in-plane bending peak at 1018 cm^{-1}, for which α has been reported [20] to be 20°; the C–H out-of-plane bending peak at 875 cm^{-1}, for

which α has been reported [21] to be 85°; and the C–H out-of-plane bending peak at 730 cm^{-1}, for which α should be close to 90°. The evolution of f with draw ratio is shown in Figure 5.4. The three peaks show the same trend, with some scatter, so they were combined to give an average result, also shown in the figure.

Of the remaining peaks in the PET spectrum, the most intense are the carbonyl peak at 1729 cm^{-1} and the complex ester peak at 1330-1240 cm^{-1}, which involves at least three components. The value of α is not known for these bands. Dichroic ratios were calculated from integrated band areas and the quantity (D-1)/(D+2) was plotted against the overall orientation function f (Figure 5.5). Reasonably good proportionality is observed, as expected from equation 4.2, and from the slopes of the regression lines the values of α were estimated to be 65° for the carbonyl band and 45° for the complex ester band. Because these bands are so intense, they have seldom been studied in transmission spectra. However, Dulmage and Geddes [22] have reported data for a set of very thin (2-6 μm) films drawn up to 500% extension. They were able to calculate dichroic ratios for the peaks at 1724, 1018, 875, and 728 cm^{-1}. The ratios shown graphically in their paper were analyzed by us in the same manner used for our reflection spectra and the two sets of data were found to be quite consistent. Their data give a value of 66° for α for the carbonyl peak. However, they did not report data for the ester peak.

Because the two peaks at 1330-1240 and 1729 cm^{-1} are quite intense in the reflection spectrum (and therefore can be quantified with good precision), and because they show opposite dichroic behavior, their ratio should be a good indicator of orientation. As mentioned previously, taking the ratio of two bands in the same spectrum can eliminate the problem of the dependence of the overall spectral intensity on the specific specimen and on the polarization direction. From equation 5.4, this ratio is given by (introducing subscripts 1 and 2 to designate the two different bands):

$$R_J = \frac{A_{1J}}{A_{2J}} = \frac{A_{10}}{A_{20}} \cdot \frac{1 + f_{cJ}(3\cos^2\alpha_1 - 1)}{1 + f_{cJ}(3\cos^2\alpha_2 - 1)} = R_0 \cdot \frac{1 + f_{cJ}(3\cos^2\alpha_1 - 1)}{1 + f_{cJ}(3\cos^2\alpha_2 - 1)} \quad (5.8)$$

where $R_0 = A_{10}/A_{20}$ is the band ratio corresponding to an unoriented sample. This equation can be inverted to give the variation of the orientation function f_{cJ} as a function of R_J:

$$f_{cJ} = \frac{R_J - R_0}{R_0 (3 \cos^2\alpha_1 - 1) - R_J (3 \cos^2\alpha_2 - 1)} \quad (5.9)$$

With equation (5.9), the orientation function with respect to any direction can be determined by making a measurement with the polarization in that direction. Thus for biaxially oriented samples, measurements in the M and T directions allow determination of f_{cM} and f_{cT}, from which f_{cN} can be calculated (equation 5.2). However, in order for this approach to succeed, certain conditions must be met. First of all, the two bands used must have significantly different values of α. Second, they should both measure the same orientation function,

generally the average orientation. For example, if one band is sensitive to the orientation of the amorphous phase and the other to that of the crystalline phase, the f_{cJ} values in the numerator and denominator of equation 5.8 will be different. Third, the ratio R_0 should be constant. This may not be the case if the bands are related to specific molecular conformations whose concentrations change upon drawing. In the present case, although the shape of the complex ester band in the structure factor spectrum changes somewhat upon drawing (Figure 5.3), its area remains constant, as does that of the carbonyl band (Figure 5.6). Thus the ratio R_0 is constant and equation 5.9 should be valid.

It remains to test the validity and determine the values of the different parameters. For the set of uniaxially drawn samples, the values of f_{cM} have already been determined as described above. From these the values of f_{cT} were calculated as $f_{cT} = -1/2\, f_{cM}$. The values of f_{cM} and f_{cT} were then correlated with the corresponding values of the ratio R of the areas of the bands at 1330-1240 and 1729 cm^{-1} in the individual ϕ spectra, recorded in both the M and T directions. The relationship is shown in Figure 5.7, and the solid line represents the fit obtained by nonlinear regression with equation 5.9. The best fit parameters are $R_0 = 2.086$, α (ester peak) = 44.5°, and α (carbonyl peak) = 66.4°. The fit is reasonably good and the α values are in excellent agreement with those determined by the more conventional approach. Hence equation 5.9 appears to be valid.

It would be simpler if, instead of having to perform the Kramers-Kronig transformation and calculate the ϕ spectra, the original reflectance spectra could be used. Because of the dispersion-type shape of the peaks (Figures 5.1a, 5.2a), it is difficult to calculate peak areas. However it is reasonable to consider the use of the maximum reflectance of each peak as a measure of its intensity. The general theoretical relationship between the reflectance R and the imaginary molecular polarizability ϕ depends on the Fresnel equations and is quite complex. However, at least for the present case, the relationship is empirically quite simple. Figure 5.8 shows a plot of the ratio calculated from the peak maxima in the reflectance spectra versus the ratio calculated from the band areas in the ϕ spectra. The relationship can be well described by a simple proportionality with a factor of 0.54. Figure 5.9 shows a plot of the orientation function versus the ratio calculated from the heights of the peaks in the reflectance spectra. It can be seen that equation 5.9 applies just as well as in the previous case (Figure 5.7). In this case, the relevant equation is:

$$f_{cJ} = \frac{R_J - 1.12}{0.657 + 0.528\ R_J} \qquad (5.10)$$

where R_J is the ratio of the heights of the reflectance peaks at 1243 and 1717 cm^{-1} in a spectrum measured with polarization in the direction J. It should be noted that the peak maxima in the reflection spectrum occur at somewhat different frequencies from those of the polarizability spectrum. It should also be noted that the good results obtained with the reflectance peak heights may be fortuitous and only obtainable in certain cases, like the present one, whereas the method based on peak areas in the ϕ spectra has a more sound

theoretical basis and should be more generally valid. The coefficients in equation 5.10 correspond to the following values of α: 43.3° for the ester band and 66.6° for the carbonyl band.

Equation 5.10 provides a very simple means for determining the orientation at the surface of PET. It was derived from the spectra recorded for a set of uniaxially drawn samples. To further test it, it was applied to a different uniaxially drawn sample ($\lambda = 2.8$) and to a biaxially oriented sample obtained from a blow-molded bottle. Details on the origin and the characterization of these specimens were given in the "Experimental" section.

Figure 5.10 shows the front-surface reflection spectra measured at the surface of the uniaxially drawn sample with polarization in the M and T directions. Figures 5.11 and 5.12 show the spectra obtained from the polished cross-sections of the same sample with the use of an infrared microscope. The M-direction and T-direction spectra measured in the MN and TN planes respectively are in excellent agreement with those measured on the surface (MT plane). Likewise, the two N-direction spectra are in good agreement and both closely resemble the T-direction spectrum. The similarity between the N and T spectra confirms the unixial orientation of the sample. It should be noted that while the two spectra measured in any given direction resemble each other in shape, their overall intensity is different. Taking the ratio of peak heights eliminates this problem.

Equation 5.10 was used to estimate the orientation function for each of the spectra shown in Figures 5.10 to 5.12, and the results obtained are summarized in Table 5.1. The quantitative results agree with the qualitative description. The orientation function f_{cM} was found to have a high and positive value (0.54), while the other functions f_{cT} and f_{cN} are negative and approximately equal, indicating that the polymer molecules in the specimen are uniaxially oriented in the M direction. Furthermore, good agreement is observed for the values of a given f as measured in the different planes. The small differences noted are an indication of the experimental error involved in the process. Thus the utility of equation 5.10 has been confirmed and it can be considered to give an adequate measurement of the degree of molecular orientation in the uniaxially oriented specimen of PET.

For the biaxially oriented (blowmolded) sample, spectra were initially measured in the MT plane for both the inside and outside surfaces. A significant difference was observed, suggesting the presence of an orientation gradient across the thickness direction. Because of this, spectra were not measured in the cross-sectional MN and TN planes. Instead, to further investigate this phenomenon, the orientation was measured at different distances across the thickness direction by mounting the sample in epoxy and polishing it to different depths. At each depth, reflection spectra were measured in the M and T directions and equation 5.10 was used to calculate the corresponding orientation functions. In order to more easily compare the results with those obtained from birefringence measurements, the biaxial orientation factors defined by White and Spruiell were calculated according to equation 5.3.

The variation of these factors as a function of the distance across the thickness is shown in Figure 5.13, which confirms that there is a significant gradient of molecular orientation in the thickness direction. The inside surface was found to be much more strongly oriented in the hoop direction T than in the axial or length direction M, whereas on the outside surface the axial orientation is higher and the orientation is closer to equibiaxial. The intermediate surfaces situated at 125 μm and 250 μm from the outside surface were found to have intermediate orientations. Results showing a similar gradient have been reported by Cakmak *et al.*[23]. They found that polymer molecules at the inside and outside surfaces of stretched blowmolded bottles of PET are biaxially oriented with a preferential orientation in the hoop direction. Moreover, it was noted that the inside surface of the bottle is much more oriented then the outside one. These results are somewhat different from those obtained in the present study, probably because of the difference in the shape of the bottles used in the two cases, but they clearly show the presence of a significant gradient of molecular orientation in the thickness direction of the blowmolded bottles of PET.

The orientation factors shown in Figure 5.13 were used to calculate average values across the thickness direction. In Table 5.2, these are compared with the values obtained from birefringence measurements [19]. Basically, both techniques indicate that the specimen under investigation is biaxially oriented with a preferred orientation in the hoop direction. Moreover, both techniques give almost the same average degree of orientation in the M and T directions. The small differences observed are undoubtedly due to the experimental error

involved in the measurements. Overall, the equation proposed in this study (equation 5.10) can be considered to provide adequate characterization of molecular orientation in biaxially oriented specimens of PET. Its main advantage is that the biaxial orientation can be characterized by making measurements in only the MT plane.

5.6 CONCLUSION

It has been demonstrated that it is possible to characterize the orientation in both uniaxially and biaxially oriented PET samples by measuring front-surface reflection infrared spectra with polarization in two mutually perpendicular directions, normally the machine (M) and transverse (T) directions. The ratio of the intensity of the complex ester band at 1330-1240 cm^{-1} with respect to that of the carbonyl band at 1729 cm^{-1} can be used to determine the orientation function with respect to the measurement direction, and an equation has been derived for this purpose. The validity of the equation has been confirmed by tests on uniaxially and biaxially oriented samples and by comparison with birefringence results. For PET the method can be applied with the use of either the peak heights in the measured reflectance spectra, or the peak areas in the imaginary molecular polarizability spectra obtained by Kramers-Kronig transformation. However the latter approach is more theoretically sound and should be valid for general application to other polymers that possess suitable infrared absorption bands.

Acknowledgements

The authors would like to thank Messrs. Éric Pellerin and Christian deGrandpré for their valuable assistance with the infrared measurements and the blow molding respectively.

5.7 REFERENCES

1 Ward, I. M. *Adv. Polym. Sci.* 1985, **66**, 81

2 Jarvis, D. A., Hutchison, I. J., Bower, D. I. and Ward, I. M. *Polymer* 1980, **21**, 41

3 Zbinden, R. 'Infrared Spectroscopy of High Polymers', Academic Press, New York, 1964

4 White, J. L. and Spruiell, J. E. *Polym. Eng. Sci.* 1981, **21**, 859

5 White, J. L. and Spruiell, J. E. *Polym. Eng. Sci.* 1983, **23**, 247

6 Mirabella, Jr., F. M. *J. Polym. Sci.: Polym. Phys. Ed.* 1984, **22**, 1283

7 Mirabella, Jr., F. M. *J. Polym. Sci.: Polym. Phys. Ed.*, 1984, **22**, 1293

8 Mirabella, Jr., F. M. *Appl. Spectrosc.* 1988, **42**, 1258

9 Cole, K. C., Guèvremont, J., Ajji, A. and Dumoulin, M. M. *Appl. Spectrosc.* 1994, **48**, 1513

10 Guèvremont, J., Ajji, A., Cole, K. C. and Dumoulin, M. M. *Polymer* 1995, **36**, 3385

11 Ajji, A., Guèvremont, J., Cole, K. C. and Dumoulin, M. M. *Polymer* 1996, **37**, 3707

12 Kaito, A. and Nakayama, K. *Macromolecules* 1992, **25**, 4882

13 Bensaad, S., Jasse, B. and Noël, C. *Polymer* 1993, **34**, 1602

14 Jansen, J. A. J., Paridaans, F. N. and Heynderickx, I. E. J. *Polymer* 1994, **35**, 2970

15 Everall, N. J., Chalmers, J. M., Local, A. and Allen, S. *Vibrational Spectrosc.* 1996, **10**, 253

16 Ben Daly, H., Cole, K. C., Sanschagrin, B. and Nguyen, K. T. *Polym. Eng. Sci.* (submitted for publication)

17 Bertie, J. E., Zhang, S. L. and Keefe, C. D. *J. Mol. Struct.* 1994, **324**, 157

18 Walls, D. J. *Appl. Spectrosc.* 1991, **45**, 1193

19 Ajji, A., Guèvremont, J., Matthews, R. G. and Dumoulin, M. M. *Proc. ANTEC '98* 1998 (submitted for publication)

20 Hutchinson, I. J., Ward, I. M., Willis, H. A. and Zichy, V. *Polymer* 1980, **21**, 55

21 Cunningham, A., Ward, I. M., Willis, H. A. and Zichy, V. *Polymer* 1974, **15**, 749

22 Dulmage, W. J. and Geddes, A. L. *J. Polym. Sci.* 1958, **31**, 499

23 Cakmak, M., Spruiell, J. E. and White, J. L. *Polym. Eng. Sci.* 1984, **24**, 1390

Table 5.1 - Orientation functions for the uniaxial PET specimen calculated from the spectra of Figures 5.10 to 5.12 by means of equation 5.10; values in parentheses were calculated by difference based on equation 5.2

Surface	f_{cM}	f_{cT}	f_{cN}
MT plane	0.54	–0.30	(–0.24)
MN plane	0.54	(–0.30)	–0.24
TN plane	(0.62)	–0.32	–0.30

Table 5.2 - Average biaxial orientation factors for the biaxially oriented specimen

Method	f_{cM}^{B}	f_{cT}^{B}
Infrared Reflection	0.10	0.47
Birefringence	0.14	0.43

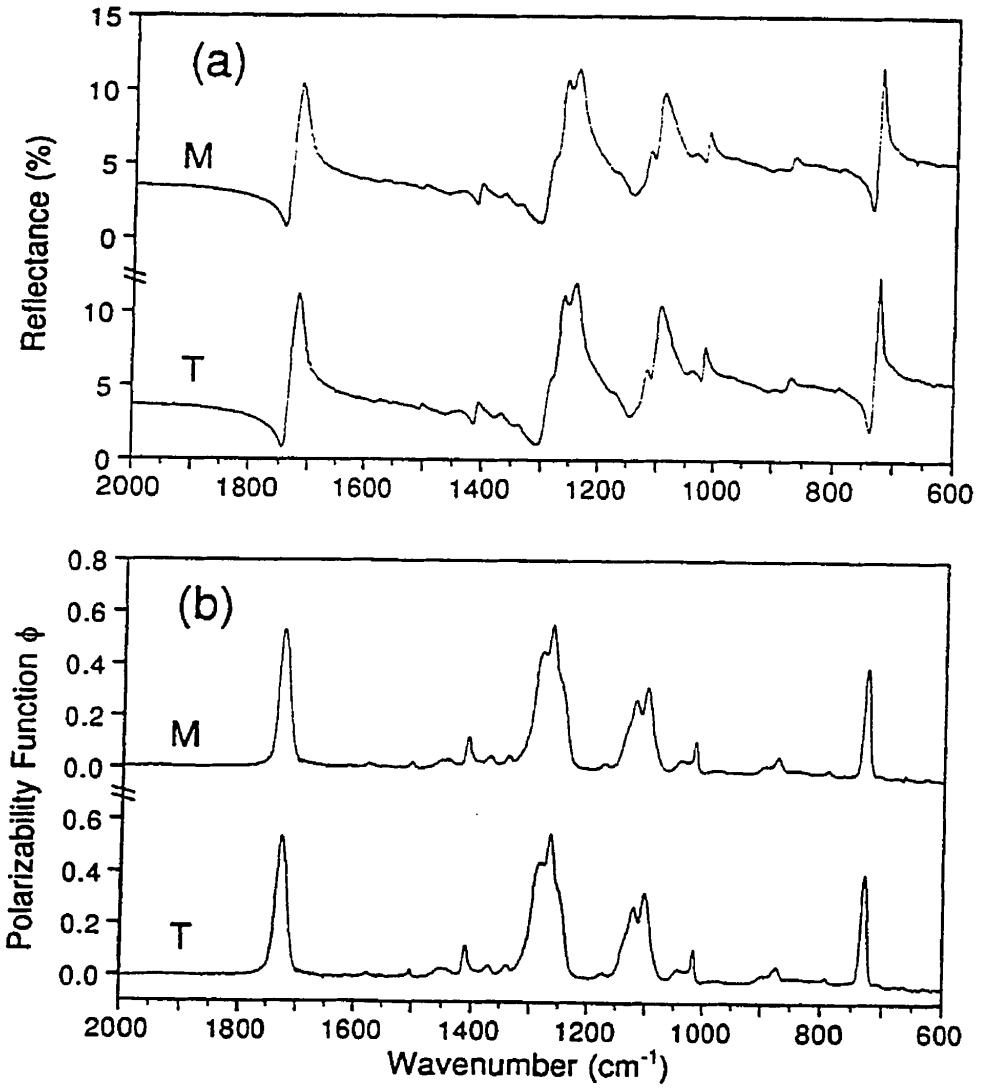

Figure 5.1 - Front-surface reflection i.r. spectra measured with polarization in two mutually perpendicular directions (arbitrarily designated M and T) at the surface of a Polished unoriented amorphous PET sample: (a) reflectance spectra as measured (%R); (b) imaginary molecular polarizability spectra (ϕ) obtained by Kramers-Kronig transformation of reflectance spectra

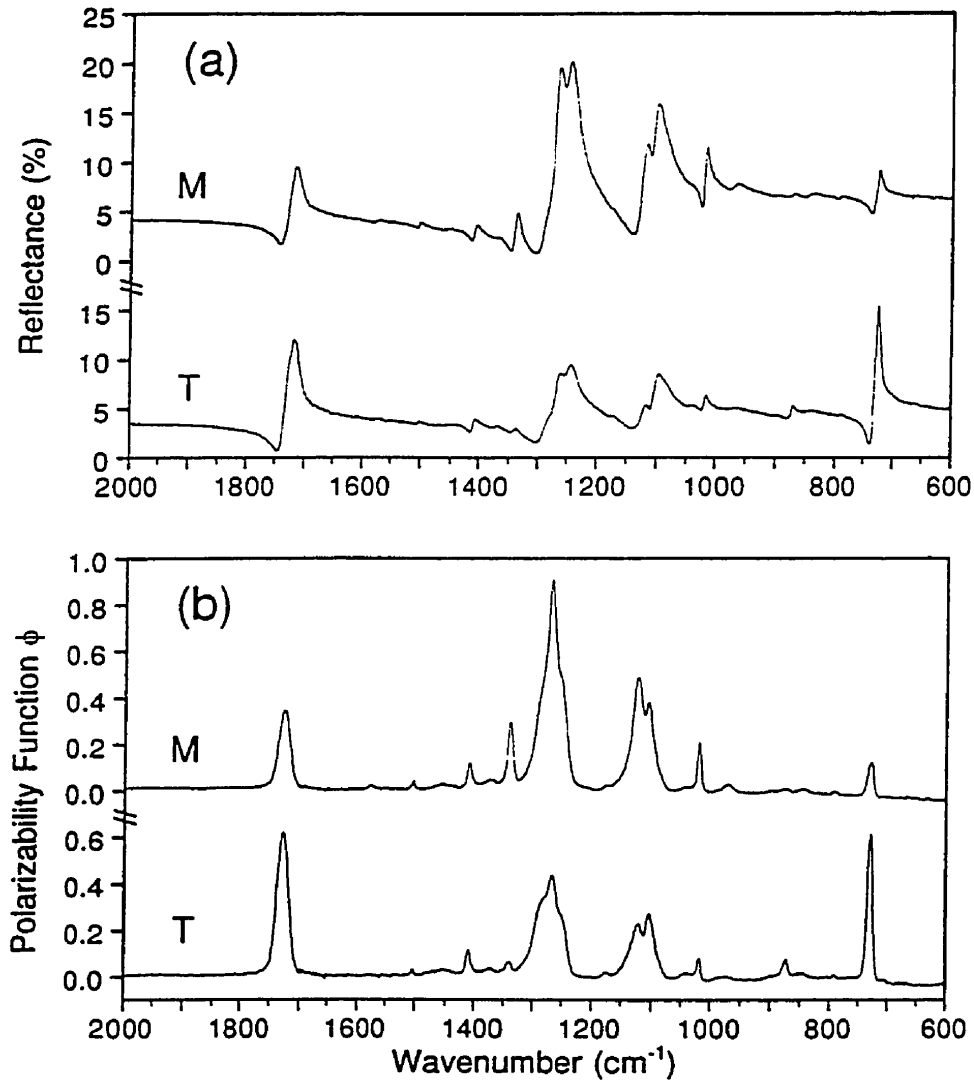

Figure 5.2 - Front-surface reflection i.r. spectra measured with polarization in machine (M) and transverse (T) directions at the surface of a polished PET sample uniaxially drawn to a draw ratio of 3.8: (a) reflectance spectra as measured (%R); (b) imaginary molecular polarizability spectra (ϕ) obtained by Kramers-Kronig transformation of reflectance spectra

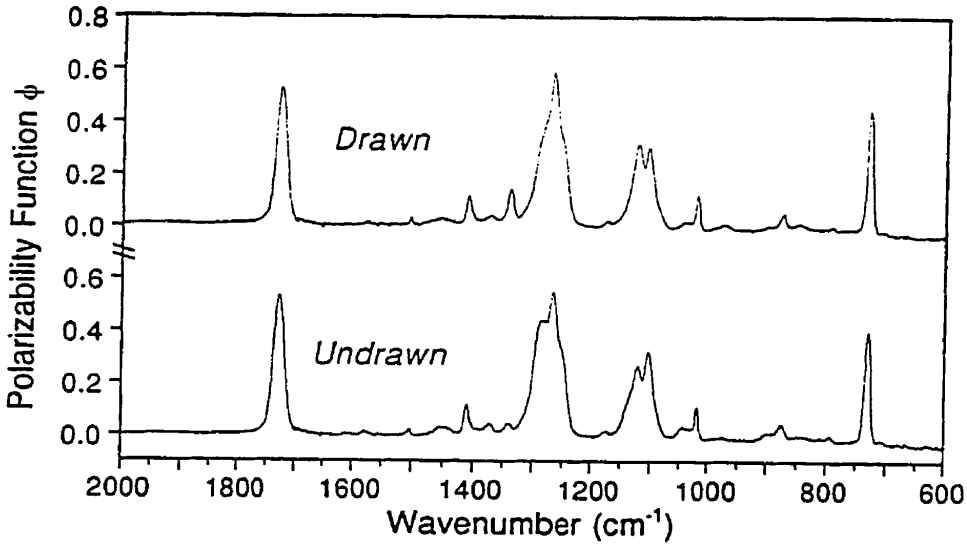

Figure 5.3 - Calculated structural factor spectra for the undrawn and drawn PET samples corresponding to Figures 5.1 and 5.2

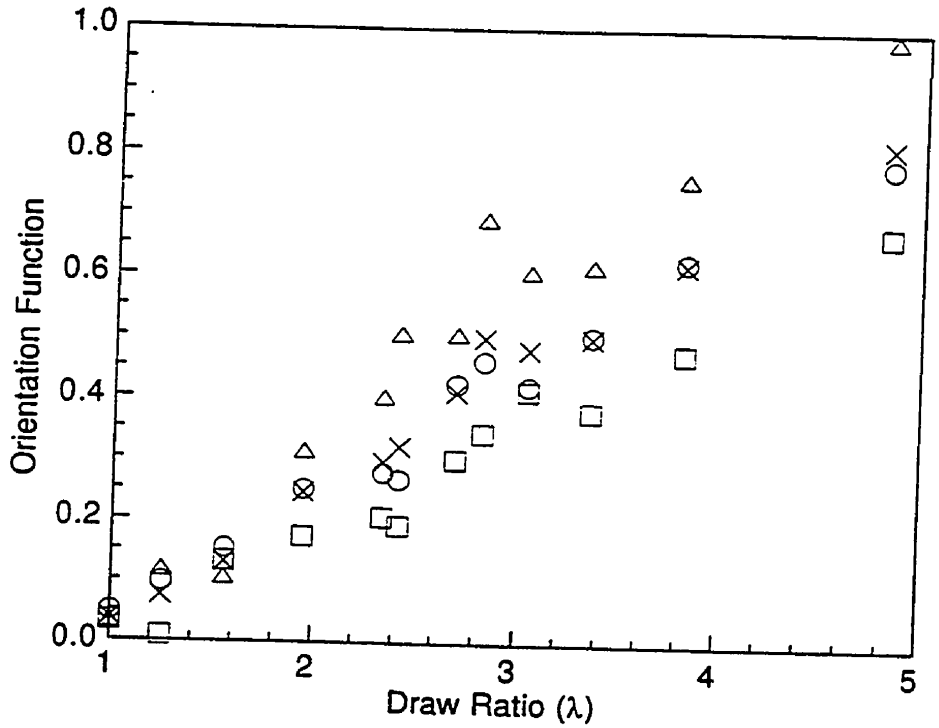

Figure 5.4 - Orientation function as a function of draw ratio for the set of uniaxially drawn PET samples, based on the dichroism of different peaks in the i.r. spectrum: 730 cm^{-1} (○); 875 cm^{-1} (Δ); 1018 cm^{-1} (□); average of all three (×)

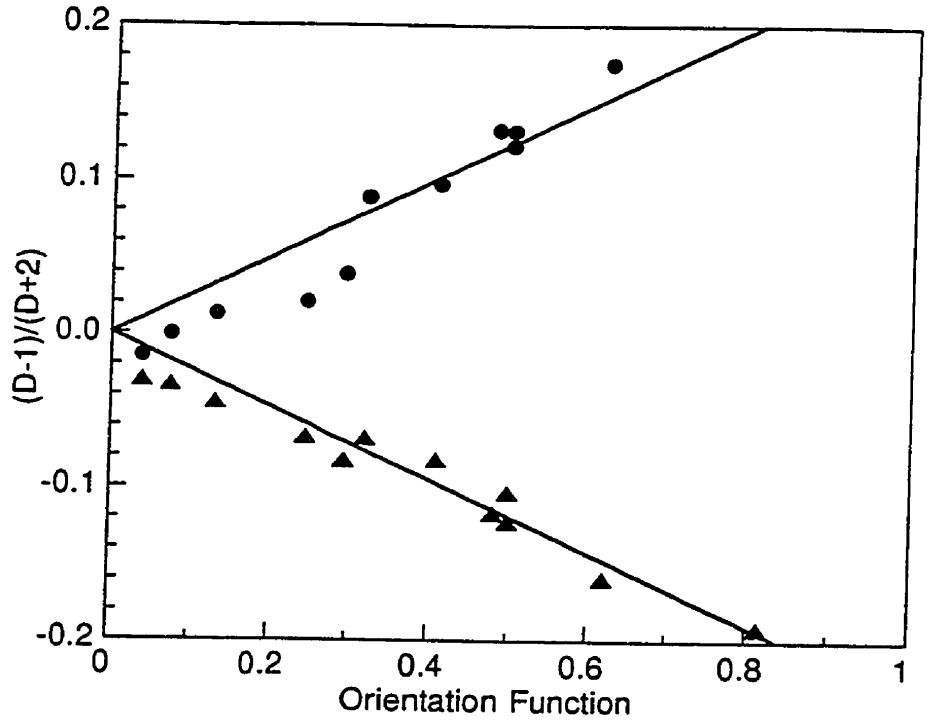

Figure 5.5 - Relationship between (D-1)/(D+2) and the orientation function for the complex ester peak at 1330-1240 cm^{-1} (●) and the carbonyl peak at 1729 cm^{-1} (▲)

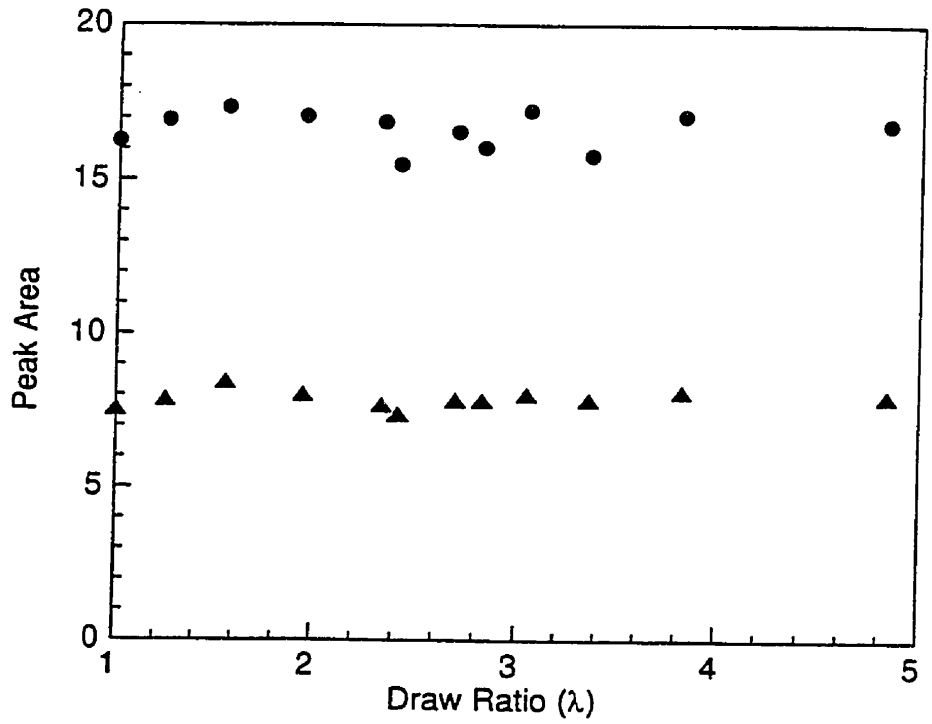

Figure 5.6 - Variation of peak area in the structural factor spectrum as a function of draw ratio, for the complex ester peak at 1330-1240 cm^{-1} (●) and the carbonyl peak at 1729 cm^{-1} (▲)

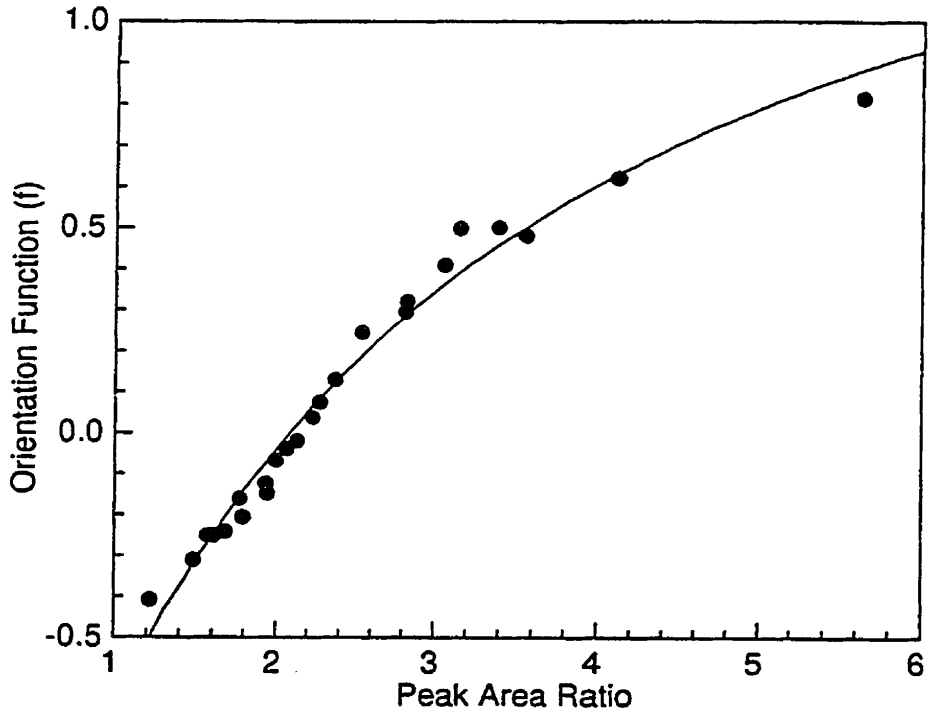

Figure 5.7 - Relationship between the orientation function and the ratio of the areas of the ester and carbonyl peaks in the molecular polarizability spectrum

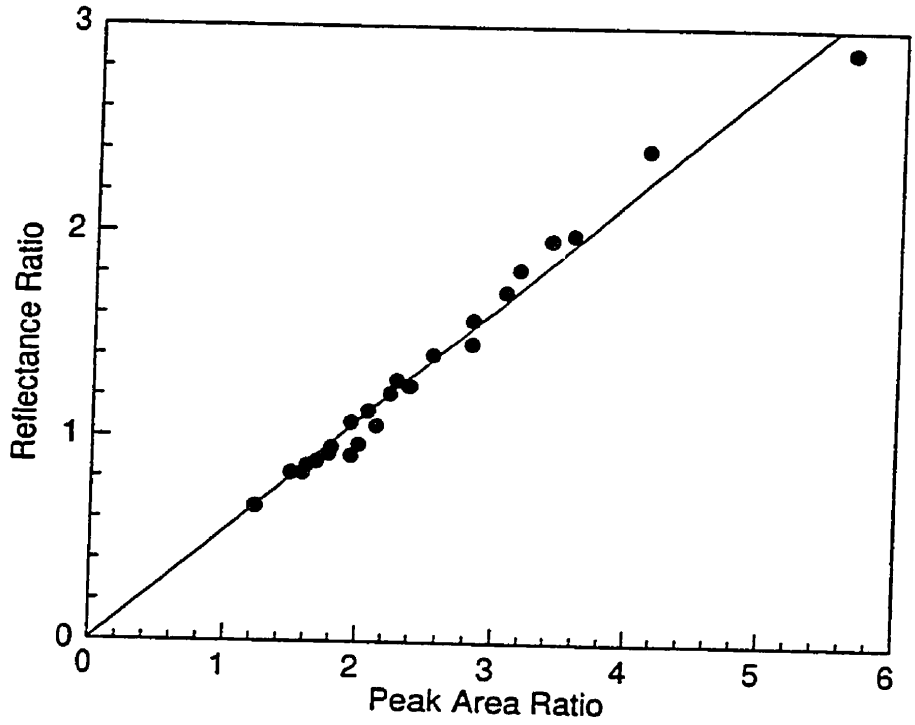

Figure 5.8 - Relationship between the ratio of the areas of the ester and carbonyl peaks in the molecular polarizability spectrum and the ratio of peak heights in the reflectance spectrum

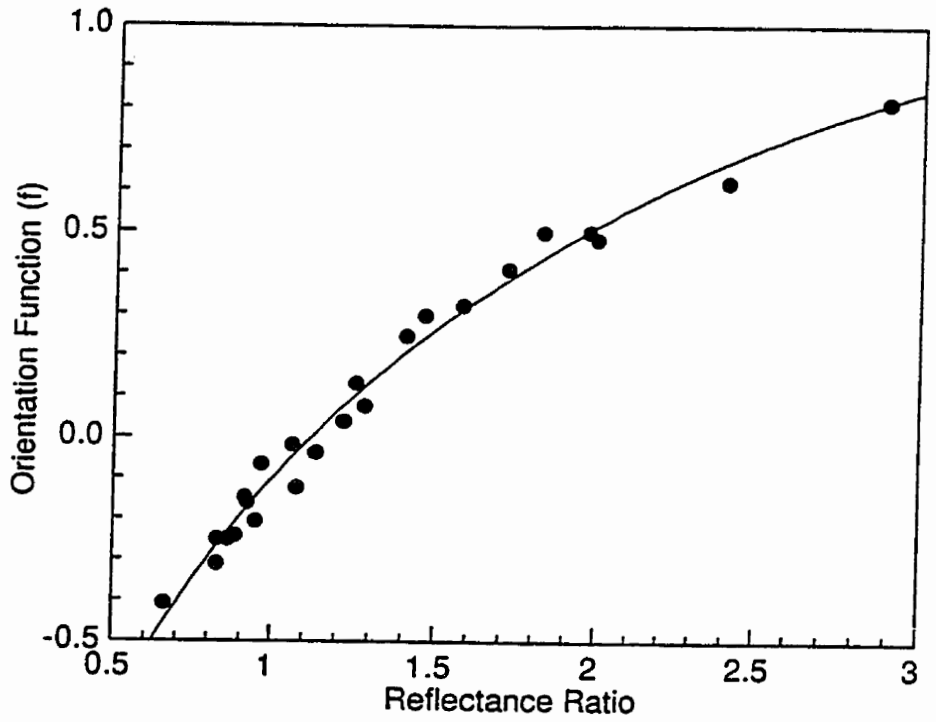

Figure 5.9 - Relationship between the orientation function and the ratio of the heights of the ester and carbonyl peaks in the reflectance spectrum

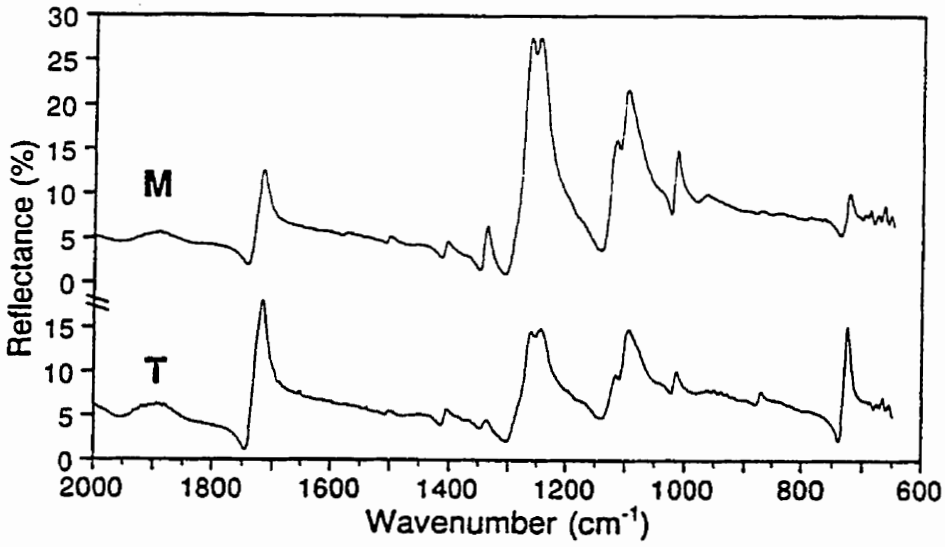

Figure 5.10 - Front-surface reflection spectra measured at the surface of the uniaxially oriented PET sample ($\lambda = 2.8$) with polarization in the M and T directions

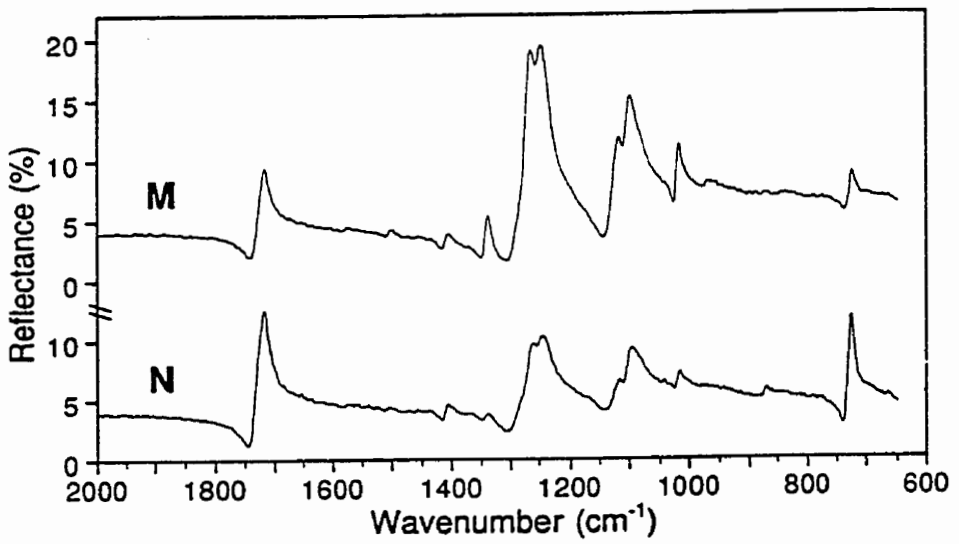

Figure 5.11 - Front-surface reflection spectra measured by i.r. microscopy for a cross-section in the MN plane of the uniaxially oriented PET sample, with polarization in the M and N directions

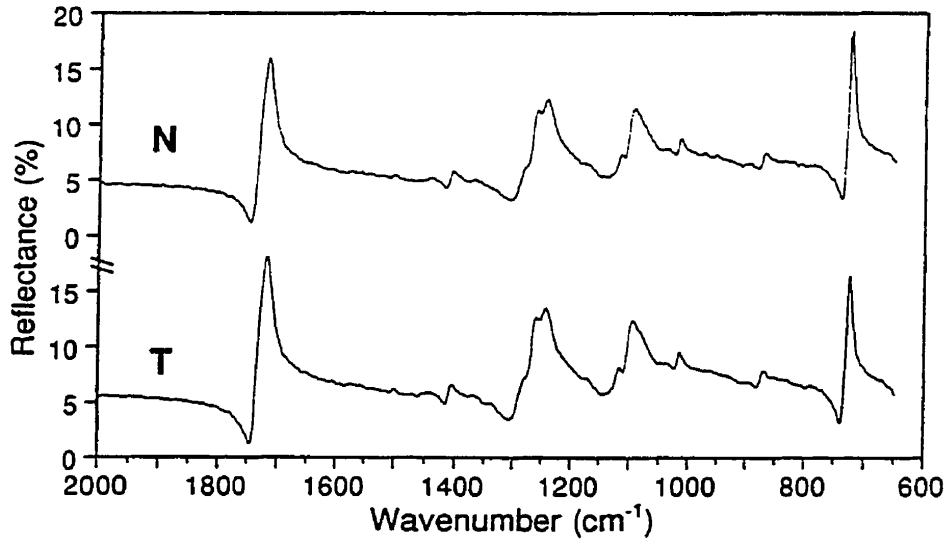

Figure 5.12 - Front-surface reflection spectra measured by i.r. microscopy for a cross-section in the TN plane of the uniaxially oriented PET sample, with polarization in the T and N directions

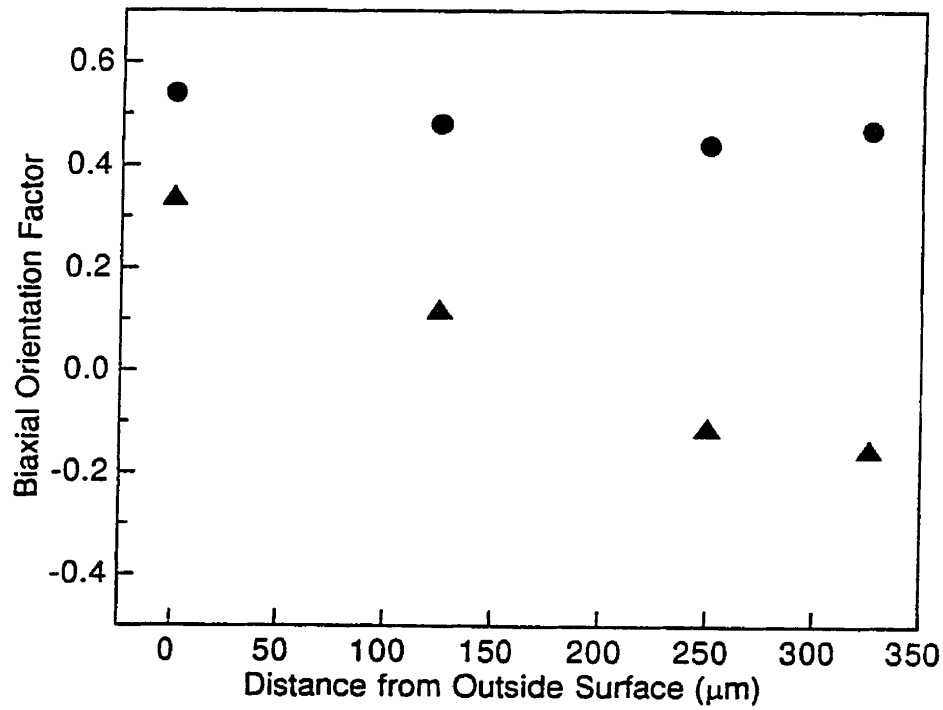

Figure 5.13 - Variation of the biaxial orientation factors of the blowmolded sample as a function of distance from the outside surface, as measured in the transverse, or hoop, direction T (●) and the machine, or axial, direction M (▲)

CONCLUSION GÉNÉRALE

Dans cette étude, nous avons discuté la morphologie des pièces en polyéthylène téréphtalate, PET, obtenues par injection et injection soufflage. En particulier, nous avons discuté la relation entre la cristallinité et l'orientation moléculaire dans ce type de pièce.

L'étude bibliographique présentée dans le chapitre 2 nous a permis de constater que la technique de microtomie, utilisée pour découper des échantillons le long des épaisseurs des pièces plastiques, peut affecter l'orientation moléculaire dans ces échantillons. Généralement, il a été noté que les caractéristiques du couteau utilisé, la vitesse de coupe ainsi que les dimensions de l'échantillon à obtenir affectent considérablement l'orientation moléculaire. Afin de mieux caractériser l'effet de la cristallinité sur l'orientation moléculaire dans nos pièces, nous avons proposé une autre technique de préparation des échantillons beaucoup plus fiable. La caractérisation de l'orientation moléculaire à travers l'épaisseur des pièces plastiques fut alors le premier point traité dans cette thèse.

La technique proposée et adoptée consiste à usiner l'échantillon par fraisage jusqu'au niveau où l'on veut mesurer l'orientation moléculaire et à polir la surface fraisée. Cette technique a été testée sur plusieurs polymères, uniaxialement orientés, ayant des propriétés thermiques (température de transition vitreuse) et mécaniques très différentes. Ces polymères

ont été étirés mécaniquement, dans une machine de traction, pour obtenir une orientation moléculaire constante à travers l'épaisseur. Le degré d'orientation des chaînes dans les échantillons obtenus, avant et après le fraisage et le polissage, a été mesuré en utilisant la technique d'infrarouge en mode de réflexion. Contrairement à d'autres techniques, cette technique permet de retracer l'orientation de chaque groupement moléculaire constituant la chaîne séparément. Le degré d'orientation de la chaîne par rapport à la direction d'orientation (d'étirement) est donné par la fonction de Hermans 4.2.

Les résultats de cette étude ont montré que la technique de fraisage et de polissage n'affecte pas l'orientation moléculaire dans les polymères ayant une température de transition vitreuse assez élevée, tels que le PET et le PEEK. En outre, il a été noté que les spectres infrarouges mesurés sur les surfaces polies ont une meilleure qualité que ceux mesurés sur les surfaces non-polies. En particulier, nous avons noté que le polissage augmente l'intensité des spectres mesurés et donne une meilleure planéité de leur ligne de base, ce qui permet une meilleure caractérisation du degré d'orientation des chaînes moléculaires dans ce type de polymères. Pour des échantillons en HDPE, un polymère à faible température de transition vitreuse (T_g = - 120°C), la technique de fraisage et de polissage a aussi permis d'obtenir une très bonne qualité des spectres infrarouges, cependant, elle change le degré d'orientation dans ces échantillons . Cela est du au phénomène de relaxation des chaînes moléculaires lors de la phase de polissage. Ce phénomène peut être minimisé en utilisant de l'azote liquide à la place de l'eau durant cette phase. De plus, la technique de fraisage et de polissage a été testée

sur des échantillons en LCP injectés. Ce type de polymère est caractérisé par une importante rigidité de ses chaînes moléculaires. Les résultats obtenus dans une couche située à une distance égale à 0.2 mm de la surface externe de ces échantillons concordent bien avec ceux récemment publiés dans la littérature. Cela montre, encore une autre fois, que la technique de fraisage et de polissage peut remplacer avantageusement la technique de microtomie et qu'elle peut être utilisée pour mieux caractériser l'orientation moléculaire dans le coeur des pièces plastiques ayant une température de transition vitreuse et une rigidité des chaînes élevées.

Cette technique, ainsi que la technique d'infrarouge, ont été utilisées pour déterminer le degré d'orientation des chaînes moléculaires et la cristallinité du polymère dans chaque couche à travers l'épaisseur des pièces en PET injectées. Dans chacune de ces couches, deux spectres ont été mesurés. Le premier spectre, noté $\phi_{//}$, a été mesuré parallèlement à direction d'écoulement de la matière dans le moule et le deuxième spectre, noté $\phi_{\perp}$, a été mesuré perpendiculairement à cette direction. À partir de ces spectres, nous avons calculé la fonction d'orientation de Hermans (f) à travers l'épaisseur du PET injecté. La cristallinité du PET dans chacune des couches condidérées a été caractérisée en utilisant un autre spectre appelé `` Structure factor spectrum `` ϕ_0 définie à l'équation 4.4. Dans ce spectre, l'aire sous le pic d'absorption à 1340 cm^{-1} est proportionnelle à la cristallinité du PET. Plus l'aire sous ce pic augmente, plus la cristallinité du PET est importante.

Les résultats obtenus dans cette étude montrent que la cristallinité du PET dépend considérablement de la température du moule d'injection utilisée. Pour de faibles températures de ce moule, inférieures à la température de transition vitreuse du PET, la cristallinité est minimale dans la couche peau, passe par un maximum dans les couches intermédiaires (situées juste derrière la couche peau) puis devient minimale dans le coeur des pièces injectées. En augmentant la température du moule à des valeurs supérieures à la température de transition vitreuse du PET, la cristallinité de ce matériau à travers l'épaisseur des pièces injectées augmente et le maximum de cristallinité passe des couches intermédiaires à la couche peau. Ce déplacement est du à la diminution de l'épaisseur de la couche peau par l'augmentation de la température du moule d'injection. Le maximum de cristallinité observé dans les couches intermédiaires à de faibles températures du moule d'injection est dû au phénomène de cristallisation sous contrainte (shear-induced crystallization). En effet, dans ces couches, les chaînes de polymère sont très fortement orientées lors du remplissage du moule, donc paralléles les unes aux autres. Cela va leur permettre de se cristalliser très rapidement même à de hautes températures de la matière. Les cristaux obtenus n'auront pas une forme sphérulitique, mais seront plutôt formés par des segments de chaînes fortement orientés dans la direction d'écoulement. La faible cristallinité observée dans la couche peau est due au phénomène de trempe du polymère lorsqu'il touche aux parois du moule froid. Dans le coeur des pièces injectées, et dues aux faibles contraintes de cisaillement générées dans cette zone lors du remplissage du moule, les chaînes de polymère n'auront pas un important degré d'orientation. Cela ne va pas favoriser la présence

du phénomène de la cristallisation sous contrainte (shear-induced crystallization) dans cette zone, ce qui explique par conséquent sa nature amorphe.

Cette distribution de cristallinité peut affecter le degré d'orientation des chaînes moléculaires à travers l'épaisseur des pièces injectées. Dans la littérature, la relation entre la cristallinité et le degré d'orientation des chaînes, pour le cas des polymères à faible vitesse de cristallisation injectés, n'a jamais été traitée. Dans notre étude, nous avons trouvé que le degré d'orientation des chaînes à travers l'épaisseur a la même distribution que celui de la cristallinité du polymère. Ce résultat montre que la présence de la cristallinité lors du remplissage du moule, (shear-induced crystallization) diminue la relaxation des chaînes moléculaires durant la phase de refroidissement et conserve, en partie, l'orientation généré durant la phase de remplissage.

La fonction de Hermans (f) utilisée ci-haut a été développée pour mesurer le degré d'orientation des chaînes moléculaires dans des échantillons uniaxialement orientés. Pour ce faire, il suffit de mesurer deux spectres infrarouges dans deux directions de polarisation mutuellement perpendiculaires, de déterminer le rapport dichroic D pour un groupement moléculaire spécifique et de calculer la fonction d'orientation (f). Pour le cas des échantillons biaxialement orientés, cette démarche n'est plus valable. En effet, dans le cas d'une orientation équibiaxiale par exemple, le rapport dichroic D de tous les groupements moléculaires est égale à 1 et la fonction d'orientation (f) est nulle, indiquant qu'il n'y a pas

d'orientation dans l'échantillon utilisé. Pour étudier l'orientation moléculaire dans des bouteilles obtenues par injection-soufflage (voir annexe A), il faudra donc proposer une autre fonction d'orientation beaucoup plus générale. Dans la deuxième partie de notre thèse, nous avons proposé une nouvelle approche pour caractériser l'orientation moléculaire dans des échantillons en PET uniaxialement et biaxialement orientés.

Cette approche consiste à comparer des spectres infrarouges mesurés sur la surface d'échantillons orientés à ceux mesurés sur la surface d'un échantillon non-orienté. Dans une direction de polarisation spécifique, la différence entre ces spectres permet de caractériser le degré d'orientation des chaînes moléculaires dans les échantillons orientés.

Contrairement à la fonction d'orientation de Hermans (f), dans cette approche, nous avons défini un autre rapport dichroic. Ce rapport, noté R, est égal au rapport des hauteurs des pics d'absorption à 1265 et 1725 cm^{-1}, mesurés dans le même spectre. Ces pics correspondent respectivement aux vibrations de certains groupements moléculaires orientés parallèlement et perpendiculairement à l'axe de la chaîne. Ces pics ont été choisis car le rapport de leur hauteur est très sensible à l'orientation. Pour des échantillons différents en PET orientés à des taux différents d'étirement, nous avons tracé la variation de leur fonction d'orientation (f) en fonction de la quantité ($R - R_0$, où R_0 est égal à R dans le cas d'un échantillon non-orienté ($R_0 = 1.12$ pour le PET). La variation de (f) en fonction de ($R - R_0$) est donnée par (équation 5.10) :

$$f = \frac{R - R_0}{0.657 + 0.528\ R}$$

Cette nouvelle fonction d'orientation a pour avantage de déterminer le degré d'orientation des chaînes moléculaires à partir d'un seul spectre infrarouge et non deux spectres tel que suggéré précédemment. Elle a été testée sur des échantillons uniaxialement et biaxialement orientés et les résultats obtenus ont montré son efficacité. Dans le cas des échantillons uniaxialement orientés, l'équation de Hermans ainsi que notre approche donnent exactement les mêmes résultats. Dans le cas des échantillons biaxialement orientés, les résultats de notre approche coïncident avec ceux obtenus par la technique de biréfringence, largement utilisée dans la littérature pour caractériser l'orientation moléculaire dans des échantillons uniaxialement et biaxialement orientés.

Cette équation, ainsi qu'une autre équation semblable à celle-ci développée pour caractériser l'orientation moléculaire dans des échantillons en HDPE, ont été utilisées pour mesurer l'orientation moléculaire à la surface de bouteilles en PET et HDPE obtenues par injection-soufflage. Les résultats de cette étude sont regroupés dans l'annexe A et seront bientôt soumis pour une nouvelle publication.

BIBLIOGRAPHIE

ABDALLAH, M.G. (1994). Residual Stresses in Composite Ring: Comparison of Four Measurement Techniques. Proceedings of the Fourth International Conference on residual stresses, Baltimore, Maryland, p. 81-89.

ABDALLAH, M.G. (1992). Residual Stresses in Thick-Walled Composite Rings. Proceedings of the Seventh International Congress on Experimental Mechanics, Las Vegas, Nevada, p. 1063-1070.

AJJI, A., DUMOULIN, M.M. et COLE, K.C. (1995). Solid State Roll-Drawing of Engineering Polymers: Orientation and Properties. SPE ANTEC Technical Papers, 1900-1904.

AJJI, A., GUÈVREMONT, J. COLE, K.C. et DUMOULIN, M.M. (1996). Orientation and Structure of Drawn Poly (ethylene terephthalate). Polymer, 37, p.3707-3714.

AJJI, A., GUÈVREMONT, J., MATTHEWS, R.G. et DUMOULIN, M.M. (1998). Measurements of Absolute Birefringence of Biaxially Oriented Films and Sheets On-Line or Of-Line. SPE ANTEC Technical Papers.

AKAY, M. et OZDEN, S. (1994). Measurement of Residual Stresses in Injection Moulded Thermoplastics. Polymer Testing, 13, p. 323-354.

BAAIJENS, F.P.T. et DOUVEN, L.F.A. (1991). Calculation of Flow-Induced Residual Stresses in Injection Moulded Products. Applied Scientific Research, 48, p. 141-157.

BAAIJENS, F.P.T. (1991). Calculation of Residual Stresses in Injection Molded Products. Rheologica Acta, 30, p. 284-299.

BAIN, M. F., JANICKI, S.L., ULMER, A.S. et THOMAS, L.S. (1992). Mold Shrinkage: Not a Single Data Point. SPE ANTEC Technical Paper, p. 977-980.

BALLMAN, R.L. et TOOR, H.L. (1960). Orientation in Injection Molding. Modern Plastics, 38, p. 113-207.

BARNES, H.A., HUTTON, J.F. et WALTERS, K. (1989). An Introduction to Rheology, Elsevier.

BARRES, O., FRIEDRICH, C., JASSE, B. et NOËL, C. (1991). FT-IR Photoacoustic and Xray Diffraction Study of Orientation of an Injection-Molded Liquid-Crystalline Poly (Ester-Amide). Makromol. Chem., Macromol. Symp., 52, 161-174.

BEN DALY, H., COLE, K.C., SANSCHAGRIN, B. et NGUYEN, K.T. (1997). An Experimental Technique for the Characterization of Molecular Orientation through the Thickness of Plastic Products. SPE ANTEC Techical Paper, p. 2201-2205.

BEN DALY, H., COLE, K.C., SANSCHAGRIN, B. et NGUYEN, K. T. (1997). Determination of Molecular Orientation in Molded Samples of PEEK, HDPE and LCP. SPE ANTEC Techical Paper, p. 2196-2200.

BEN DALY, H., COLE, K.C., SANSCHAGRIN, B. et NGUYEN, K.T. (1998). An Experimental Technique for the Characterization of Molecular Orientation Through the Thickness of Plastic Parts. submitted to Polymer Engineering and Science.

***BEN DALY, H., NGUYEN, K.T., COLE, K.C. et SANSCHAGRIN, B. To be published.

BENSAAD, S., JASSE, B. et NOËL, C. (1993). Orientation Developement in Injection Molded Plaque of Liquid Crystal Copolyesteramide Using Normal Incidence Specular Reflection. Polymer, 34, 1602-1605.

BERNIER, G.A. et KAMBOUR, R.P. (1968). The Role of Organic Agents in the Stress Crazing and Cracking of Poly (2,6-Dimethyl-1,4-Phenylene Oxide). Macromolecules, 1, 393-400.

BERTIE, J.E., ZHANG, S.L. et KEEFE, C.D. (1994). Infrared Intensities of Liquids XVI. Accurate Determination of Molecular Band Intensities From Infrared Refractive Index and Dielectric Constant Spectra. Journal of Molecular Structure, 324, 157-176.

CAKMAK, M., SPRUIELL, J.E. et WHITE, J.L. (1984). A Basic Study of Orientation in Poly (ethylene Terephthalate) Stretch-Blow Molded Bottles. Polymer Engineering and Science, 24, p.1390-1395.

CHANG, R.Y. et TSAUR, B.D. (1995). Experimental and Theoretical Studies of Shrinkage, Warpage, and Sink Marks of Crystalline Polymer Injection Molded Parts. Polymer Engineering and Science, 35, p. 1222-1230.

CHIEN, M.C. et WEISS, R.A. (1988). Strain-Induced Crystallization Behavior of Poly (Ether Ether Ketone) (PEEK). Polymer Engineering and Science, 28, p. 6-12.

CLAYDEN, N.J., EAVES, J.G. et CROOT, L. (1997). Orientation in Uniaxially Drawn Poly (ethylene terephthalate) (PET) Film by Two-Dimensional ^{13}C n.m.r. and F T i.r. Spectroscopy. Polymer, 38, 159-163.

COLE, K.C., AJJI, A. et BIMBEAU, C. (1996). Chracterization of Orientation and Structure in Roll-Drawn Polymers Using Birefringence and FTIR Spectroscopy. Proceedings Composites '96 and Oriented Polymers Symposium (National Research Council Canada, Boucherville, QC), Oct. 9-11, p. 119-132.

COLE, K.C., GUÈVREMONT, J., AJJI, A. et DUMOULIN, M.M. (1994). Characterization of Surface Orientation in Poly (ethylene terephthalate) by Front-Surface Reflection Infrared Spectroscopy. Applied Spectroscopy, 48, p. 1513-1521.

COLE, K.C., GUÉVREMENT, J., AJJI, A. et DUMOULIN, M.M. (1994). Characterization of Surface Orientation in Poly (ethylene terephthalate) by Front-Surface Reflection Infrared Spectroscopy. Applied Spectroscopy, 48, p. 1513-1521.

CORNÉLIS, H. et KANDER, R.G. (1996). A New Method to Evaluate Solvent Stress Cracking. Polymer Engineering and Science, 36, p. 869-878.

CUNNINGHAM, A., DAVIES, G.R. et WARD, I.M. (1974). Determination of Molecular Orientation by Polarized Infra-red Radiation in an Oriented Polymer of High Polarizability. Polymer, 15, 743-748.

CUNNINGHAM, A, WARD, I.M., WILLIS, H.A. et ZICHY, V. (1974). An Infra-red Spectroscopic Study of Molecular Orientation and Conformational Changes in Poly (ethylene terephthalate). Polymer, 15, p. 749-756.

DELBARRE, P., PABIOT, J., DAURELLE, J.F., LAMBLIN, V., et RIETSCH, F. (1991). Experimental Study of Processing Conditions on Shrinkage and on Warpage of Injected Parts. SPE ANTEC Techical Paper, p. 301-304.

DEMIRAY, M. et ISAYEV, A.I. (1996). Effect of Processing Conditions on Crystallinity and Microstructure of Injection Moldings of Polypropylenes of Various Molecular Weights. SPE ANTEC Technical Papers, p. 1576-1580.

DIETZ, W. et WHITE, J.L. (1978). A Simple Model for Calculating the Pressure Loss During the Mold Filling Stage and the Frozen-in Orientation in the Injection Molding of Amorphous Plastics. Rheological Acta, 17, 676-692.

DULMAGE, W.J. et GEDDES, A.L. (1958). Structure of Drawn Polyethylene Terephthalate. Journal of Polymer Science, 21, p. 499-512.

EVERALL, N.J., CHALMERS, J.M., LOCAL, A. et ALLEN, S. (1996). Measurement o Surface Orientation in Uniaxial Poly (ethylene teraphthalate) Films using Polarised Specular Reflectance Fourier Transform Infrared Microscopy. Vibrational Spectroscopy, 10, 253-259.

FERRARA, J.A. et GONCHARKO, M. (1996). Direct Measurement of Stress-Induced Crystallization using Differential Thermal Rheometry (DTR). SPE ANTEC Technical Paper, p. 2440-2443.

FLAMAN, A.A.M. (1993). Buildup and Relaxation of Molecular Orientation in Injection Molding. Part I: Formulation. Polymer Engineering and Science, 33, p. 193-201.

FLAMAN, A.A.M. (1993). Buildup and Relaxation of Molecular Orientation in Injection Molding. Part II: Experimental Verification. Polymer Engineering and Science, 33, p. 202-210.

GEIGER, K. (1993). Processing and Properties of Liquid Crystalline Polymers and LCP-Based Blends, D. Acierno and F. P. La Mantia (Eds.), ChemTec Publishing, Toronto, p.19-41.

GUÈVREMONT, J., AJJI, A., COLE, K.C. et DUMOULIN, M.M. (1995). Orientation and Conformation in Poly (ethylene terephtahalate) with Low Draw Ratios as Characterized by Specular Infra-Red Spectroscopy. Polymer, 36, 3385-3392.

GUÈVREMONT, J., AJJI, A., COLE, K.C. et DUMOULIN, M.M. (1995). Orientation and Conformation in Poly (ethylene terephthalate) With Low Draw Ratios As Characterized by Specular Reflection Infra-red Spectroscopy. Polymer, 36, p. 3385-3392.

HAAS, T.W. et MAXWEL, B. (1969). Effects of Shear Stress on the Crystallization of Linear Polyethylene and Polybutene-1. Polymer Engineering and Science, 9, p.225-241.

HARLAND, W.H., KANTAS, P. et HABIPIS, T. (1980). Orientation in Injection Moulding. Plastics and Rubber: Processing, 20, p. 65-67.

HAWORTH, B., HINDLE, C.S., SANDILANDS, G.J. et WHITE, J.R. (1982). Assessment of Internal Stresses in Injection-Moulded Thermoplastics. Plastics and Rubber Processing and Applications, 2, p. 59-71.

HEMSLEY, D.A. et ROBINSON, A.M. (1992). A Simple Method for the Assessment of Molecular Orientation in Transparent Plastics Mouldings. Polymer Testing, 11, p. 373-385.

HERMANS, P.H. et PLATZEK, P. (1939). Contributions to Knowledge of the Deformation Mechanism and Fine Structure of Hydrated Cellulose. Kolloid Zeitschrift, 88, 68-72.

HERMANS, J.J., HERMANS, P.H., VERMAAS, D. et WEIDINGER, A. (1946). Quantitative Evaluation of Orientation in Cellulose Fibers from the X-Ray Fiber Diagram. Recueil des Traveaux Chimiques de Pays-Bas, 65, 427-447.

HERMANS, P.H., HERMANS, J.J., VERMAAS, D. et WEIDINGER, A. (1948). Deformation Mechanism of Cellulose Gels. IV. General Relationship Between Orientation of the Crystalline and that of the Amorphous Portion. Journal of Polymer Science, 3, 1-9.

HINDLE, C.S., WHITE, J.R., DAWSON, D., GREENWOOD, W.J. et THOMAS, K. (1981). Characterization of Injection Moldings: Residual stresses, Orientation and Distortion. SPE ANTEC Techical Paper, p. 783-785.

HOARE, L. et HULL, D. (1977). The Effect of Orientation on the Mechanical Properties of Injection Molded Polystyrene. Polymer Engineering and Science, 17, p. 204-212.

HOUSKA, M. et BRUMMELL M. (1987). Characterization of Molecular Orientation in Injection-Molded Thermoplastics by Transmission and Reflection Infrared Spectroscopy. Polymer Engineering and Science, 27, 917-924.

HSIUE, E.S., ROBERTSON, R.E. et YEN, G.S.Y. (1983). Effects of Shearing Conditions on Crystalline Orientation and Relaxation in Polyethylene. Polymer Engineering and Science, 23, p. 74-78.

HSIUNG, C.M. et CAKMAK, M. (1993). Effect of Processing Conditions on the Structural Gradients Developed in Injection-Molded Poly (aryl ether ketone) (PAEK) Parts. I. Characterization by Microbeam X-ray Diffraction Technique. Journal of Applied Polymer Science, 47, p. 125-147.

HSIUNG, C.M., CAKMAK, M. et ULCER, Y. (1996). A Structure Oriented Model to Simulate the Shear Induced Crystallization in Injection Moulded Polymers: A Lagrangian Approach. Polymer, 37, p. 4555-4571.

HSIUNG, C.M., CAKMAK, M. et WHITE, J.L. (1990). Crystallization Phenomema in the Injection Molding of Poly Ether Ether Ketone and Its Influence on Mechanical Properties. Polymer Engineering and Science, 30, p. 967-980.

HU, C.P. (1983). Residual Stress Measurement by Photoelastic Coating Technique. Proceedings of the 4th Pan Pacific Conference on Nondestructive Testing, Sec.M2, Sidney, Australia.

HUTCHINSON, I.J., WARD, I.M., WILLIS, H.A. et ZICHY, V. (1980). Infra-red Measurements on One-Way Drawn Poly (ethylene terephthalalate) Films Subjected to Constant Strain. Polymer, 21, p. 55-65.

IDE, Y. et OPHIR, Z. (1983). Orientation Developement in Thermotropic Liquid Crystal Polymers. Polymer Engineering and Science, 23, p. 261-265.

ISAYEV, A.I. (1983). Orientation Development in the Injection Molding of Amorphous Polymers. Polymer Enginnering and Science, 23, p. 271-284.

ISAYEV, A.I. et HIEBER, C.A. (1980). Toward a Viscoelastic Modelling of the Injection Molding of Polymers. Rheological Acta, 19, p. 168-182.

ITO, H., MINAGAWA, K., TAKIMOTO, J., TADA, K. et KOYAMA, K. (1996). Effect of Pressure and Shear Stress on Crystallization Behaviors in Injection Molding. International Polymer Processing, 11, p. 363-368.

JANSEN, J.A.J., PARIDAANS, F.N. et HEYNDERICKX, I.E.J. (1994). Molecular Orientation in Flat Plates of Liquid-Crystalline Polymer using Low-Cost Reflectance Fourier-Transform Infra-Red Microscopy. Polymer, 35, 2970-2976.

JANSEN, J.A.J., personal communication.

JARVIS, D.A., HUTCHINSON, I.J., BOWER, D.I. et WARD, I.M. (1980). Characterization of Biaxial Orientation in Poly (ethylene terephthalate) by Means of Refractive Index Measurements and Raman and Infra-red Spectroscopies. Polymer, 21, 41-54.

KABANEMI, K.K., AÏT-KADI, A. et TANGUY, P.A. (1995). Prediction of Residual Flow and Thermoviscoelastic Stresses in Injection Molding. Rheologica Acta, 34, p. 97-108.

KAITO, A. et NAKAYAMA, K. (1992). Surface Orientation in the Sheet of a Liquid Crystalline Poly (ester amide) Characterized by Reflection Infrared Spectroscopy. Macromolecules, 25, 4882-4887.

KAITO, A. et NAKAYAMA, K. (1992). Surface Orientation in the Sheet of a Liquid Crystalline Poly (ester amide) Characterized by Reflection Infrared Spectroscopy. Mocromolecules, 25, p. 4882-4887.

KAMAL, M.R. et TAN, V. (1979). Orientation in Injection Molded Polystyrene. Polymer Engineering and Science, 19, p. 558-563.

KAMBOUR, R.P. (1973). A Review of Crazing and Fracture in Thermoplastics. Journal of Polymer Science: Macromolecular Reviews, 7, p. 1-154.

KAMBOUR, R.P., ROMAGOSA, E.E. et GRUNER, C.L. (1972). Swelling, Crazing and Cracking of an Aromatic Copolyether-Sulfone in Organic Media. Macromolecules, 5, 335-340.

KAMBOUR, R.P., GRUNER, C.L. et ROMAGOSA, E.E. (1973). Solvent Crazing of "Dry" Polystyrene and "Dry" Crazing of Plasticized Polystyrene. Journal of Polymer Science: Polymer Physics Edition, 11, 1879-1890.

KANTZ, M.R. (1974). The Effects of Melt Processing Variables on the Morphology and Properties of Injection Molded Polypropylene. International Journal of Polymeric Material, 3, p. 245-258.

KANTZ, M.R., NEWMAN JR, H.D. et STIGALE, F.H. (1972). The Skin-Core Morphology and Structure-Property Relationships in Injection-Molded Polypropylene. Journal of Applied Polymer Science, 16, p. 1249-1260.

KATTI, S.S. et SCHULTZ, J.M. (1982). The Microstructure of Injection-Molded Semicrystalline Polymers: A Review. Polymer Engineering and Science, 22, p. 1001-1017.

KELLER, A. et MACHIN, M. J. (1967). Oriented Crystallization in Polymers. Journal of Macromolar Science - Phys., B1, 1, p. 41-91.

KELSEY, R.A. (1956). Measuring Non-Uniform Residual Stresses by the Hole Drilling Method. Proceedings of the Society for Experimental Stress Analysis, 14, p. 181-194.

KIM, S.P. et KIM, S.C. (1993). Crystallization Kinetics of Poly (ethylene terephthalate): Memory Effect of Shear History. Polymer Engineering and Science, 33, p. 83-91.

LAPERSONNE, P., BOWER D.I. et WARD I.M. (1992). Molecular Orientation and Conformational Changes Due to Uniaxial-Planar Deformation of Poly (ethylene Terephtalate) Films. Polymer, 33, 1277-1283.

LUNDBERG, L., SJÖNELL, Y., STENBERG, B., TERSELIUS, B. et JANSSON, J.F. (1994). Influence of Microtomy on Measurements of Orientation. Polymer Testing, 13, p. 441-459.

MANDELKERN, L. (1964). Crystallization of Polymers, McGraw Hill: New York.

MARUCCI, G. (1985). Rheology of Liquid Crystalline Polymers. Pure and Applied Chemistry, 57, 1545-1552.

MAVRIDIS, H., HRYMAK, A.N. et VLACHOPOULOS, J. (1988). The Effect of Fountain Flow on Molecular Orientation in Injection Molding. Journal of Rheology, 32, p. 639-663.

MAXWELL, B. et RAHM, L.F. (1949). Rheological Properties of Polystyrene Below 80°C. Industrial and Engineering Chemistry, 41, 1988-1993.

MAXWELL, B. (1965). Morphological Fondations of Plastics Processing. Journal of Polymer Science, C9, p. 43-60.

MCDONACH, A., MCKELVIE, J., MACKENZIE, P. et WALKER, C.A. (1983). Improved Moire Interferometry and Applications in Fracture Mechanics, Residual Stress and Damaged Composites. Experimental Technics, 7, p. 20-24.

MCKELVEY, J.M. (1962). Polymer Processing, John Wiley & Sons, Inc.

MENGES, G., DIERKES, A., SCHMIDT, L. et WINKEL, E. (1980). Residual Stresses in Plastics Due To Cooling. SPE ANTEC Techical Paper, p. 300-306.

MENGES, G. et WÜBKEN, G. (1973). Influence of Processing Conditions on Molecular Orientation in Injection Moldings. SPE ANTEC Techical Paper, p. 519-522.

METHAR, J. (1934). Determination of Initial Stresses by Measuring the Deformation around Drilled Holes, Transaction ASME, 56, p. 249-254.

MIRABELLA, JR, F.M. (1984). Surface Orientation of Polypropylene. I. Theoretical Considerations for the Application of Internal Reflection Spectroscopy. Journal of Polymer Science: Polymer Physics Edition, 22, p. 1283-1291.

MIRABELLA, JR, F.M. (1984). Surface Orientation of Polypropylene. II. Determination for Uniaxially and Biaxially Oriented Films Using Internal Reflection Spectroscopy. Journal of Polymer Science: Polymer Physics Edition, 22, p. 1293-1304.

MIRABELLA, JR, F.M. (1988). A Critical Evaluation of Internal Reflection Spectroscopic Methods for Determining Macromolecular Orientation in Polymer Surfaces. Applied Spectroscopy, 42, p. 1258-1264.

MOY, F.H. et KAMAL, M.R. (1980). Crystalline and Amorphous Orientations in Injection Molded Polyethylene. Polymer Engineering and Science, 20, p. 957-964.

NARH, K.A., ROA, E., SAINDON, M.D, COHEN, C. et WANG, K.K. (1995). Rheo-Kinetic Measurements for the Determination of Stress-Induced Crystallinity in Polyethylene Terephthalate. SPE ANTEC Technical Papers, p. 2932-2936.

NELSON, D.V. et MCCRICKERD, J.T. (1986). Residual-Stress Determination Though Combined Use of Holographic Interferometry and Blind-hole Drilling. Experimental Mechanics, 26, p. 371-378.

NIKU-LARI, A., LU, J. et FLAVENOT, J.F. (1985). Measurement of Residual-Stress Distribution by the Incremental Hole-Drilling Method. Experimental Mechanics, 25, 175-185.

O'DONNELL, B. et WHITE, J.R. (1993). Young's Modulus Variation within Polystyrene Injection Moldings. Journal of Applied Polymer Science, 47, p. 189-198.

ONOGI, S. et ASADA, T. (1980). Rheology and Rheo-optics of Polymer Liquid Crystals, ASTARIATA, G. Marrucci, G., (Eds.), Plenum: New York, 1, p. 127 (papers presented at Eighth International Congress on Rheology, Naples, 1980).

OPHIR, Z. et IDE, Y. (1983). Injection Molding of Thermotropic Liquid Crystal Polymers. Polymer Engineering and Science, 23, p. 792-796.

OUCHI, I., HOSOI, M. et SHIMOTSUMA, S. (1977). Infrared Spectra of Poly (ethylene 2,6-Naphthalate) and Some Related Polyesters. Journal of Applied Polymer Science, 21, p. 3445-3456.

PAINTER, P.C. et KOENIG J.L. (1977). A Normal Vibrational Analysis of Isotactic Polystyrene. Journal of Polymer Science: Polymer Physics Edition, 15, p. 1885-1903.

PEARCE, R., COLE, K.C., AJJI, A. et DUMOULIN, M.M. (1996). Studies of Relaxation Phenomena in Poly (Ethylene Terephthalate) by Infrared Spectroscopy. Proceedings on Composites '96 and Oriented Polymers Symposium, p. 133-142.

PIGEON, M., PRUD'HOMME, R.E. et PÉZOLET, M. (1991). Characterization of Molecular Orientation in Polyethylene by Raman Spectroscopy. Macromolecules, 24, p. 5687-5694.

REID, N. et BEESLEY J.E. (1991), Sectioning and Cryosectioning for Electron Microscopy, Elsevier.

RÖBER, S. et ZACHMANN, H.G. (1992). Determination of Molecular Orientation in Poly (ethylene terephthalate) by means of ^{2}H Nuclear Magnetic Resonance. Polymer, 33, p. 2061-2075.

ROGERS, M.G. (1991). Characterization of Molecular Orientation by Differential Scanning Calorimetry. Journal of Materials Science, 26, p. 4285-4287.

SACK, R.A. (1961). Indirect Evaluation of Orientation in Polycrystalline Materials. Journal of Polymer Science, 54, 543-560.

SANDILANDS, G.J. (1983). Internal Stresses and Fatigue Fracture in a Methyl Pentene Polymer. Ph.D Thesis, University of Newcastle upon Tyne.

SCHAJER, G.S. (1988). Measurement of Non-Uniform Residual Stresses using the Hole-Drilling Method. Part I-Stress Calculation Procedures. Journal of Engineering Materials and Technology, 110, p. 338-343.

SCHAJER, G.S. (1988). Measurement of Non-Uniform Residual Stresses Using the Hole-Drilling Method. Part II-Practical Application of the Integral Method. Journal of Engineering Materials and Technology, 110, p. 344-349.

SCHMIDT, L.R. (1974). A Special Mold and Tracer Technique for Studying Shear and Extensional Flows in a Mold Cavity during Injection Molding. Polymer Engineering and Science, 14, p. 797-800.

SIEGMANN, A., KENIG, S. et BUCHMAN, A. (1987). Residual Stresses in Injection-Molded Amorphous Polymers. Polymer Engineering and Science, 27, p. 1069-1078.

SIEGMANN, A., BUCHMAN, A. et KENIG, S. (1981). Residual Stresses in Polymers. II. Their Effect on Mechanical Behavior. Polymer Engineering and Science, 21, p. 997-1002.

SJÖNELL, Y., TERSELIUS, B. et JANSSON, J.F. (1995). Injection Molding of Polypropylene Discs. I: Effect of Holding Pressure on Orientation Distribution. Polymer Engineering and Science, 35, p. 950-956.

STEIN, R.S. (1958). The X-Ray Diffraction, Birefringence, and Infrared Dichroism of Stretched Polyethylene. II. Generalized Uniaxial Crystal Orientation. Journal of Polymer Science, 31, 327-334.

STEIN, R., HASHIYAMA, M. et PARPART, M. (1979). Optical Studies of Stress-Induced Crystallization of Polymer Melts in Flow Induced Crystallization, Gordon and Breach Science Publishers, Great Britain, p.331.

STRUIK, L.C.E. (1978). Orientation Effects and Cooling Stresses in Amorphous Polymers. Polymer Engineering and Science, 18, p. 799-811.

TADMOR, Z. (1974). Molecular Orientation in Injection Molding. Journal of Applied Polymer Science, 18, p. 1753-1772.

TAN, V. et KAMAL, M.R. (1978). Morphological Zones and Orientation in Injection-Molded Polyethylene. Journal of Applied Polymer Science, 22, p. 2341-2355.

TAN, V. et GOGOS, C.G. (1976). Flow-Induced Crystallization of Linear Polyetylene Above Its Normal Melting Point. Polymer Engineering and Science, 16, p. 512-525.

THOMPSON, M. et WHITE, J.R. (1984). The Effect of a Temperature Gradient on Residual Stresses and Distortion in Injection Moldings. Polymer Engineering and Science, 24, p. 227-241.

TITOMANLIO, G., DRUCATO, V. et KAMAL, M.R. (1987). Mechanism of Cooling Sress Build-Up in Injection Molding of Thermoplastic Polymers. International Polymer Processing, 1, p. 55-59.

TREUTING, R.G. et READ JR, W.T. (1951). A Mechanical Determination of Biaxial Residual Stress in Sheet Materials. Journal of Applied Physics, 22, p. 130-134.

TROTIGNON, J.P. et VERDU, J. (1987). Skin-Core Structure-Fatigue Behavior Relatioships for Injection-Molded Parts of Polypropylene. I. Influence of Molecular Weight and Injection Conditions on the Morphology. Journal of Applied Polymer Science, 34, p. 1-18.

ULCER, Y., CAKMAK, M., MIAO, J. et HSIUNG, C.M. (1996). Structural Gradients Developed in Injection-Molded Syndiotactic Polystyrene (sPS). Journal of Applied Polymer Science, 60, p. 669-691.

VAN DER VEGT, A.K. et SMIT, P.P.A. (1966). Crystallization Phenomena in Flowing Polymers, SCI Monographs No. 26, Society of the Chemical Industry, London, p.313-326.

VINOGRADOV, V.M. (1975). Residual Stresses in Plastics Articles. International Polymer Science and Technology, 2, p. T/91-T/99.

VIOLA, G.G., BAIRD, D.G. et WILKES, G.L. (1985). The Developement of Molecular Orientation and Morphological Texture in Thermotropic Copolyesters. Polymer Engineering and Science, 25, p. 888-895.

VOICE, A.M., BOWER, D.I. et WARD, I.M. (1993). Molecular Orientation in Uniaxially Drawn poly (Aryl Ether Ether Ketone): 2. Infra-Red Spectroscopic Study. Polymer, 34, 1164-1173.

WALLS, D.J. (1991). Application of ATR-IR to the Analysis of Surface Structure and Orientation in Uniaxially Drawn Poly (ethyleneterephthalate). Applied Spectroscopy, 45, 1193-1198.

WALLS, D.J. (1991). Application of ATR-IR to the Analysis of Surface Stucture and Orientation in Uniaxially Drawn Poly (ethyleneterephthalate). Applied Spectroscopy, 45, p. 1193-1198.

WARD, I.M. (1985). Determination of Molecular Orientation by Spectroscopic Techniques. Advances in Polymer Science, 66, 81-115.

WENIG, W. et HERZOG, F. (1993). Injection Molding of Polypropylene: Xray Investigation of the Skin-Core Morphology. Journal of Applied Polymer Science, 50, p. 2163-2171.

WHITE, J.L et Dee, H.B. (1974). Flow Visualization for Injection Molding of Polyethylene and Polystyrene Melts. Polymer Engineering Science, 14, p. 212-222.

WHITE, J.L. et SPRUIELL, J.E. (1981). Specification of Biaxial Orientation in Amorphous and Crystalline Polymers. Polymer Engineering and Science, 21, p. 859-868.

WHITE, J.L. et SPRUIELL, J.E. (1983). The specification of Orientation and Its Development in Polymer Processing. Polymer Engineering and Science, 23, p. 247-256.

WILCHINSKY, Z.W. (1959). On Crystal Orientation in Polycrystalline Materials. Journal of Applied Physics, 30, 792-793.

WIMBERGER-FRIEDL, R. et HENDRIKS, R.D.H.M. (1989). The Measurement and Calculation of Birefringence in Quenched Polycarbonate Specimens. Polymer, 30, p. 1143-1149.

WIMBERGER-FRIEDL, R. (1996). Molecular Orientation in Polycarbonate induced by Cooling Stresses. International Polymer Processing, 11, p. 373-382.

WISSBRUN, K.F. (1984). Orienting Polymers, A. Dold and B. Eckman (Eds.), Lecture Notes in Mathematics 1063, Springer-Verlag, New York, p.1.

WOOD, B.A. et THOMAS, E.L. (1986). Are Domains in Liquid Crystalline Polymers Arrays of Disclinations. Nature (London), 324, p. 655-657.

WUNDERLICH, B. (1973). Macromolecular Physics, Academic: New York; Vols. 1 and 2.

ZBINDEN, R. (1964). Infrared Spectroscopy of High Polymers, Academic Press.

ZOETELIEF, W.F., DOUVEN, L.F.A. et HOUSZ, A.J.I. (1996). Residual Thermal Stresses in Injection Molded Products. Polymer Engineering and Science, 36, p. 1886-1896.

ANNEXE A

ORIENTATION MOLÉCULAIRE SUR LA SURFACE DES BOUTEILLES EN PET ET HDPE OBTENUES PAR INJECTION-SOUFFLAGE

Dans le chapitre 5 de cette thèse, nous avons développé une équation qui permet de mesurer l'orientation moléculaire unaxiale et biaxiale dans des échantillons en polyéthylène téréphtalate, PET. L'approche utilisée pour développer cette équation consiste à comparer des spectres infrarouges mesurés sur des échantillons orientés à ceux mesurés sur des échantillons non-orientés. Dans une direction de polarisation spécifique, la différence entre ces spectres détermine le degré d'orientation des chaînes moléculaires dans les échantillons orientés, dans cette direction de polarisation.

Une approche similaire peut être utilisée pour déterminer le degré d'orientation moléculaire dans des échantillons en polyéthylène HDPE. Pour ce faire, nous avons considéré des échantillons uniaxialement étirés à des taux d'étirement égales à 1, 2, 3, 4 et 4.8. Ces échantillons ont été étirés sur une machine de traction (MTS) à une température égale à 100°C et avec une vitesse d'étirement égale à 2 cm/min. Une fois la longueur finale est obtenue, l'échantillon étiré est refroidi sous tension à l'air libre puis trempé dans l'eau froide. L'orientation moléculaire dans les échantillons obtenus a été mesurée par spectroscopie infrarouge en mode de réflexion et de transmission. En mode de transmission, le pic d'absorption utilisé pour calculer la fonction d'orientation de Hermans (f) est celui à

2015 cm^{-1}. En mode de réflexion, le pic considéré se trouve à une fréquence d'absorption égale à 2915 cm^{-1}. Ces pics correspondent aux vibrations des groupements moléculaires C-H orientés perpendiculairement à l'axe de la chaîne ($\alpha = 90°$). Pour les spectres mesurés en mode de réflexion, nous avons défini un autre rapport dichroic Q. Ce rapport est différent de celui suggéré pour le PET. Pour ce matériau, nous avons défini un rapport dichroic (R) égale au rapport des hauteurs des pics d'absorption à 1265 et 1725 cm^{-1}. Ces pics ont été choisis car ils sont orientés respectivement parallèlement et perpendiculairement à l'axe de la chaîne et leur rapport est, par conséquent, très affecté par le degré d'orientation. Pour le cas du HDPE, les spectres obtenus en mode de réflexion ne présentent pas plusieurs pics d'absorption. Dans ces spectres, les seuls pics utilisables sont ceux à 2814 et 2915 cm^{-1}. Ces deux pics correspondent aux vibrations des groupements moléculaires C-H orientés perpendiculairement à l'axe de chaîne. Le rapport de ces deux pics n'est pas très sensible à l'orientation. Donc, pour ce matériau, nous avons proposé un autre rapport dichroic Q égal à :

$$Q = \frac{H_{2915}}{H_{ref}} - 1 \qquad \text{(A.1)}$$

où H_{2915} est la hauteur du pic d'absorption à 2915 cm^{-1} mesurée dans un spectre obtenu en mode de réflexion et H_{ref} est la hauteur moyenne de la ligne de base de ce spectre dans cette gamme de fréquences.

La variation de la fonction d'orientation de Hermans (f) (mesurée en mode de transmission) en fonction de Q est montrée dans la Figure A.1. Cette fonction varie linéairement avec Q. Lorsque Q est nul (c.a.d H_{2915} est égal à H_{ref}), alors l'absorption du pic à 2915 cm^{-1} est minimale, indiquant que ce pic est orienté perpendiculairement à la direction de polarisation considérée. Puisque ce pic est orienté perpendiculairement à l'axe de la chaîne, alors il devient facile de conclure que la direction de polarisation considérée est parallèle à l'axe de la chaîne, ce qui donne une fonction d'orientation maximale (égale à 1), voir Figure A.1. Dans le cas contraire, dans une autre direction de polarisation perpendiculaire à la première, Q à une valeur maximale et la fonction d'orientation est égale à - 1/2. Cela indique que la chaîne est orientée perpendiculairement à cette direction de polarisation.

D'après la Figure A.1, la variation de (f) en fonction de Q est :

$$f = 1 - \frac{Q}{1.054} \qquad \text{(A.2)}$$

Cette équation, ainsi que l'équation (5.10) développée dans le chapitre 5, ont été utilisées pour caractériser l'orientation moléculaire à la surface des bouteilles en PET et en HDPE obtenues par injection-soufflage. Notre but était d'étudier l'effet de la cristallinité initiale générée dans les préformes injectées ainsi que l'effet de la forme du moule de soufflage sur le degré d'orientation des chaînes moléculaires dans ces bouteilles. La Figure

A.2 montre la forme ainsi que les dimensions des préformes et des bouteilles utilisées. Les conditions de soufflage de ces préformes sont résumées dans la Figure A.3.

Les polymères thermoplastiques ont des comportements très différents durant la phase de soufflage. La présence de la cristallinité avant et pendant cette phase peut considérablement affecter le taux d'étirement du polymère. En pratique, on distingue trois types de comportement en soufflage [1] :

a/ *Première catégorie*: Il s'agit des polymères amorphes. Ces polymères présentent une bonne transparence à l'état non orienté, mais bénéficient d'une amélioration limitée de leurs propriétés lors de l'étirage. La biorientation pour ce type de polymères s'effectue à 10-30°C au-dessus de la température de transition vitreuse.

b/ *Deuxième catégorie*: Il s'agit des polymères semi-cristallins ayant une vitesse de cristallisation très rapide (HDPE), ne pouvant pas être obtenus à l'état amorphe par trempe. La structure cristalline de ces polymères est constituée par des sphérulites disposées de façon aléatoire et induisant, de ce fait, une opalescence marquée selon l'épaisseur du produit, et la taille des sphérulites.

La forme sphérulitique des zones cristallines a pour conséquence, au cours du biétirage, une forte tendance à la striction qui se traduit par une hétérogénéité très marquée d'étirage, rendant l'obtention des produits finis d'épaisseur uniforme particulièrement

difficile. La biorientation de ce type de polymère a pour objectif d'améliorer les propriétés optiques des produits et leur résistance aux chocs, sans modification notable de leur rigidité. Elle s'effectue entre 5 et 30°C en dessous du point de fusion du polymère.

c/ *Troisième catégorie*: Il s'agit des polymères semi-cristallins, pour lesquels, la préforme peut être moulée tout en conservant le polymère à l'état amorphe (PET). Pour ce type de polymère, lors de l'étirage, il se produit une cristallisation sous contrainte qui, de ce fait, ne présente pas les caractéristiques de la forme sphérulitique ordinaire. Cette cristallisation régularise spontanément l'étirage du matériau et augmente considérablement le niveau d'orientation induit par la partie amorphe. De ce fait, se trouvent simultanément assurées les qualités de transparence, de brillance, de résistance aux chocs et de rigidité des produits finis. La biorientation, comme dans le cas des polymères amorphes, s'effectue de 10 à 30°C au dessus de la température de transition vitreuse du polymère.

Le degré d'orientation des chaînes moléculaires dans les produits finis dépend aussi de la forme du moule de soufflage utilisé, des dimensions des préformes injectées et des paramètres de mise en oeuvre. La forme du moule de soufflage dicte le taux d'étirement du polymère dans chaque direction. Généralement, pour les produits soufflés, on définit deux taux d'étirement H et A [2]. H étant le taux d'étirement dans la direction circonférentielle de ces produits et A est le taux d'étirement dans la direction axiale. Ils sont définis comme suit (équations 2.1 et 2.2) :

$$H = \frac{D_1}{D_2}$$

$$A = \frac{L_1}{L_2}$$

où D_1, L_1 , D_2 et L_2 représentent respectivement le diamètre du produit fini, la longueur de ce produit, le diamètre de la préforme injectée et sa longueur. À partir de ces deux taux d'étirement, on définit un autre taux, appelé le taux de déformation total BUR (Blowup ratio) égal à (équation 2.3) :

$$BUR = H \cdot A = \frac{D_1}{D_2} \cdot \frac{L_1}{L_2}$$

Le BUR est largement utilisé dans la littérature. Pour générer une orientation biaxiale dans des bouteilles en PET par exemple, certains auteurs ont trouvé que H doit être compris entre 4 et 7 et que le BUR doit être supérieur ou égal à 10.

Les Figures A.4 et A.5 montrent les variations des fonctions d'orientation f_x, f_y et f_z mesurées sur la surface des bouteilles en PET et HDPE , type I, en fonction de la température du moule d'injection. Pour des faibles températures du moule et pour les deux matériaux utilisés, on a noté que les chaînes moléculaires sur la surface de ces bouteilles sont orientées dans le plan (xz), avec une orientation préférentielle dans la direction axiale (x). En

augmentant la température du moule d'injection à des valeurs beaucoup plus importantes, on a remarqué une augmentation de l'orientation moléculaire dans la direction circonférentielle (y) et une diminution du degré d'orientation dans la direction de l'épaisseur (z). Ces résultats sont différents de ceux publiés dans la littérature. Selon Cakmak *et al* [3], l'orientation des chaînes moléculaires à la surface des bouteilles soufflées est biaxiale, avec une orientation préférentielle dans la direction circonférentelle. La différence entre ces résultats et les nôtre est probablement due à la différence entre les dimensions des moules de soufflage utilisés dans les deux études. En effet, durant les phases de soufflage et d'étirage de la préforme, le polymère peut se déformer dans toutes les directions et le degré d'orientation des chaînes moléculaires dans chacune de ces directions dépend du taux d'étirement subi par le polymère. Plus le taux d'étirement dans une direction spécifique est élevé, plus le degré d'orientation dans cette direction est important. Telle que suggérée précédemment, l'orientation biaxiale du PET se produit à des valeurs de (A) comprises entre 1.4 et 2.6 et à des valeurs de (H) variant entre 4 et 7. Dans notre cas, (A) est égale à 2.25 et (H) est égale à 2.1. Une comparaison entre ces valeurs indique que les chaînes moléculaires à la surface de nos bouteilles doivent être orientées totalement dans la direction axiale, tel qu' indiqué sur les Figures A.4 et A.5.

Pour de faibles températures de moule d'injection, nous avons détecté, Figures A.4 et A.5, la présence d'une orientation moléculaire à travers l'épaisseur des bouteilles et que cette orientation diminue en augmentant la température de ce moule. Ce résultat indique

qu'une augmentation considérable de la température du moule d'injection peut orienter les chaînes moléculaires dans le plan (xy), i.e. permettra l'obtention d'une orientation biaxiale. La présence d'une orientation moléculaire significative à travers l'épaisseur est probablement due au phénomène de trempe du polymère lorsque la préforme soufflée touche aux parois du moule froid [4]. En effet, durant cette phase de trempe, il y aura un flux important de chaleur à travers l'épaisseur de la bouteille (de la surface interne vers la surface externe) et cela orientera les chaînes de polymère dans cette direction. Lorsque la température du moule d'injection devient relativement importante, cette orientation générée par le phénomène de trempe peut relaxer, ce qui diminue par conséquent le degré d'orientation à travers l'épaisseur des bouteilles.

Après le moulage par injection, les préformes en PET étaient transparentes, donc très peu cristallines, alors que celles en HDPE étaient blanches et opaques indiquant la présence d'une forte cristallinité dans ces préformes. La présence de la cristallinité dans les préformes en HDPE avant la phase de soufflage peut affecter le degré d'orientation des chaînes moléculaires dans les produits finis. Une comparaison entre les Figures A.4 et A.5 indique que l'orientation des chaînes de polymère à la surface des bouteilles en HDPE dans la direction axiale est beaucoup plus importante que celle obtenue à la surface des bouteilles en PET. Il apparait alors évident que la cristallinité initiale de HDPE diminue la relaxation des chaînes moléculaires lors d'un éventuel refroidissement et permet de conserver le degré d'orientation générée durant la phase de soufflage. Pour le cas du PET, le taux d'étirement

dans la direction axiale est égale à 2.25, juste à la limite pour commencer à générer de la cristallinité sous contrainte [5]. Les bouteilles en PET auront donc une faible cristallinité, ce qui permet la relaxation d'une partie de l'orientation générée durant la phase de soufflage.

Les Figures A.6-A.8 montrent la variation des fonctions d'orientation f_x, f_y et f_z mesurées sur la surface des bouteilles en PET, type II, aux points A, B et C en fonction de la température du moule d'injection. Les résultats obtenus montrent qu'en ces points, les chaînes moléculaires sont plutôt orientées dans la direction circonférentielle de la bouteille, avec la présence d'une faible orientation à travers l'épaisseur.

Les bouteilles utilisées dans ce cas, Figure A.2b, ont une forme géométrique beaucoup plus complexe que celles utilisées précédemment, Figure A.2a. À la surface de ces bouteilles, le polymère, dans les directions axiale et circonférentielle, subi des taux de déformation différents. Ces déformations peuvent être simultanées ou séquentielles. Chacun de ces deux modes de déformation génère une orientation moléculaire spécifique à la surface de ces bouteilles. Dans la littérature, pour assimiler et analyser le phénomène d'orientation généré durant l'étirage et le soufflage des préformes, plusieurs auteurs ont utilisé des films de polymères et les ont orientés biaxialement. Ces films ont été orientés mécaniquement en utilisant les deux modes d'étirement; soit le mode simultané, soit le mode séquentiel. Récemment, Chandran et Jabrin [5] ont présenté une comparaison entre la morphologie des films en PET obtenue en mode simultané d'étirement et celle obtenue après un mode

séquentiel d'étirement. Les résultats de cette comparaison sont les suivants : (i) lors d'une orientation uniaxiale, le phénomène de cristallisation sous contrainte (shear-induced cristallization) se produit à des taux d'étirement supérieurs ou égaux à 2.5, (ii) pour des échantillons équibiaxialement orientés, le mode simultané d'étirement génère le même degré d'orientation des chaînes moléculaires dans les deux directions d'étirement. Dans le cas du mode séquentiel d'étirement, les chaînes s'orientent dans la deuxième direction d'étirement et leur degré d'orientation augmente avec le taux de déformation total BUR, (iii) pour des échantillons ayant subi des taux d'étirement différents dans les deux directions, le mode séquentiel d'étirement oriente d'abord les chaînes dans la première direction d'étirement. Plus le taux d'étirement dans cette direction augmente, plus le degré d'orientation des chaînes augmente. Durant la deuxième phase d'étirement, les chaînes commencent à s'orienter dans la deuxième direction. Ce changement d'orientation de la première à la deuxième direction se produit à un BUR supérieur ou égal à 7.

Les points A, B et C ont subi, durant les phases d'étirage et de soufflage des préformes, des taux d'étirement axial et circonférentielle A et H égales à 1.94 et 2.8 respectivement. Ces taux d'étirement ont été calculés en utilisant les équations (2.1) et (2.2). D'après la figure A.9, ces points se déforment premièrement dans la direction axiale (due à l'avancement rapide de la tige d'étirage) avec un faible taux d'étirement dans cette direction, puis dans la direction circonférentielle due à l'effet de la pression. Par conséquent, ces points subissent un mode séquentiel d'étirement. Pendant la première phase de déformation, le

polymère, dans la direction axiale, ne subit pas de phénomène de cristallisation sous contrainte (A = 1.94) et ses chaînes moléculaires seront par conséquent faiblement orientées. Durant la deuxième phase de déformation, phase de soufflage, les chaînes de polymère seront étirées dans la direction circonférentielle avec un taux d'étirement égale à 2.8. Ce taux d'étirement est supérieur à celui suggéré par Chandran et Jabran [5] pour générer de la cristallisation sous contrainte (shear-induced crystallization). La présence de ce type de cristallinité dans la direction circonférentielle permettra de bloquer l'orientation moléculaire générée durant la phase de soufflage dans cette direction. Ainsi, à la fin des phases d'étirage et de soufflage, après le refroidissement de la matière, les points A, B et C auront une orientation moléculaire dans la direction circonférentielle de la bouteille.

Les Figures A.10-A.12 montrent la variation des fonctions d'orientation f_x, f_y et f_z mesurées aux points D, E et F en fonction de la température du moule d'injection. Ces points sont situés sur la deuxième surface des bouteilles de type II. Pour des faibles températures de ce moule, les chaînes moléculaires au point D sont orientés dans la direction axiale. Au milieu de la bouteille, au point E, l'orientation moléculaire devient faible mais biaxiale. Au point F, les chaînes changent d'orientation et ces dernières deviennent orientées dans la direction circonférentielle de la bouteille. Cette distribution d'orientation le long de cette surface est difficile à interpréter mais nous croyons qu'elle est assez logique. En effet, sur cette surface, le mécanisme de déformation des chaînes de polymère change d'un point à un autre. Tel que suggéré précédemment, tous les points de la préforme subissent,

premièrement, une déformation axiale suivie d'une autre déformation circonférentielle. Ce pendant, dans la direction axiale, les points D, E et F ne subissent pas le même degré de déformation. D'après la Figure A.9, ce sont les points qui sont situés près de la tête de la préforme (zone avec filetage) qui commencent à s'étirer les premiers dans la direction axiale. Ce phénomène d'étirement peut se poursuivre durant tout le cycle de moulage, (l'épaisseur des bouteilles dans cette zone est le plus faible). Les chaînes moléculaires en ces points auront donc le temps nécessaire pour se déformer dans cette direction et leur orientation, à la fin de ce cycle, devrait être assez importante. Les points se trouvant en bas de cette zone (le milieu de la préforme) auront ainsi moins de temps pour s'étirer dans la direction axiale. Les chaînes en ces points seront par conséquent moins orientées dans cette direction. En bas de la préforme, l'orientation moléculaire axiale devrait alors atteindre son niveau le plus faible. De plus, tous ces points, durant la phase de soufflage, subissent le même taux d'étirement dans la direction circonférentielle de la bouteille. Ce taux est égal à 1.33, inférieur à la valeur suggérée par Chandran et Jabarin [5] pour générer le phénomène de la cristallisation sous contrainte. La déformation globale aux points D, E et F sera donc la résultante des deux déformations axiale et circonférentielle. Ainsi, au point D, les chaînes moléculaires devraient être orientées dans la direction axiale, mais dans la direction circonférentielle au point F. Le point E, situé à mi-chemin entre les points D et F, devrait par conséquent avoir une orientation moléculaire intermédiaire, donc biaxiale, tel que montré sur la figure A.11.

Les résultats des Figures A.10-A.12 montrent aussi une diminution des fonctions d'orientation f_x, f_y et f_z lorsque la température du moule d'injection augmente. Cette diminution du degré d'orientation est due au phénomène de relaxation des chaînes moléculaires par l'augmentation de la température de ce moule.

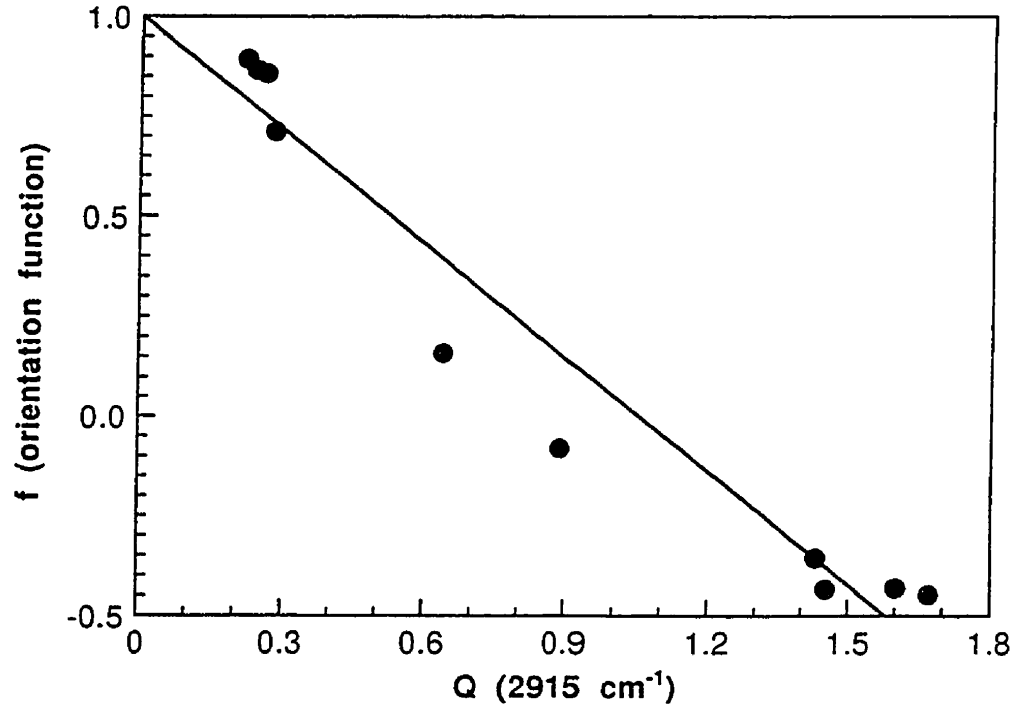

Figure A.1 - Variation de la fonction d'orientation du HDPE en fonction du rapport Q

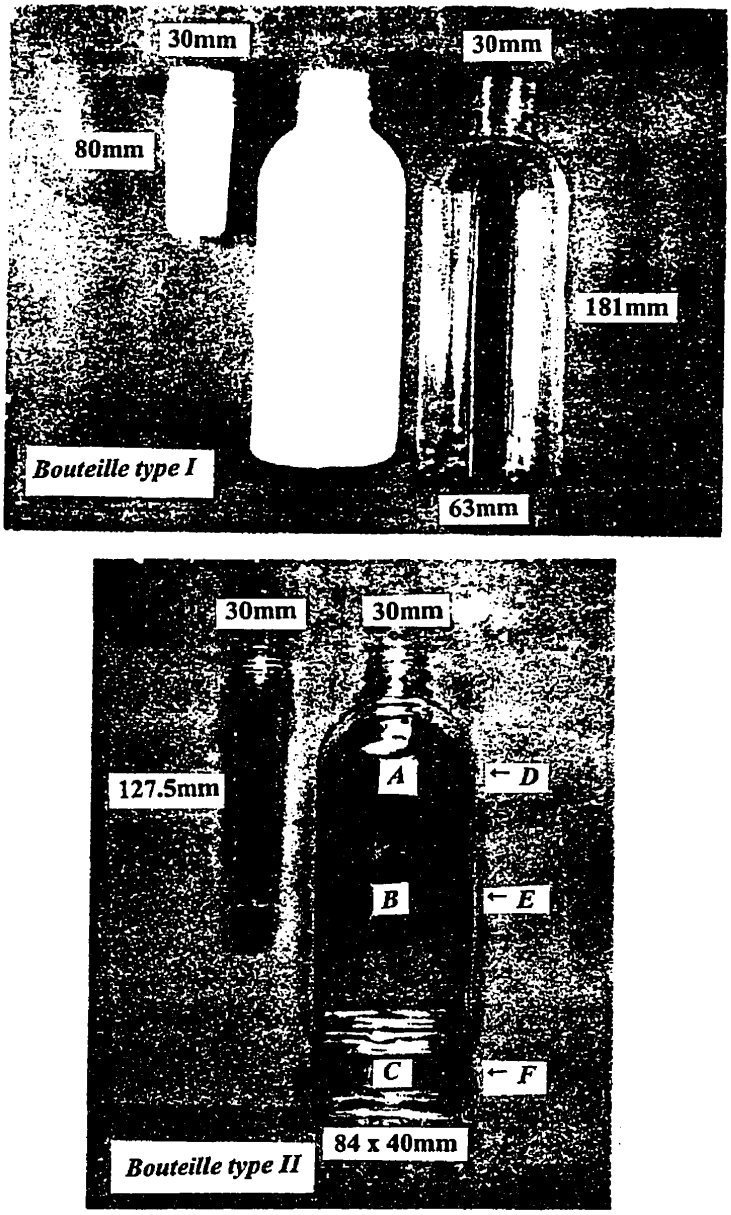

Figure A.2 - Dimensions des préformes et des bouteilles utilisées

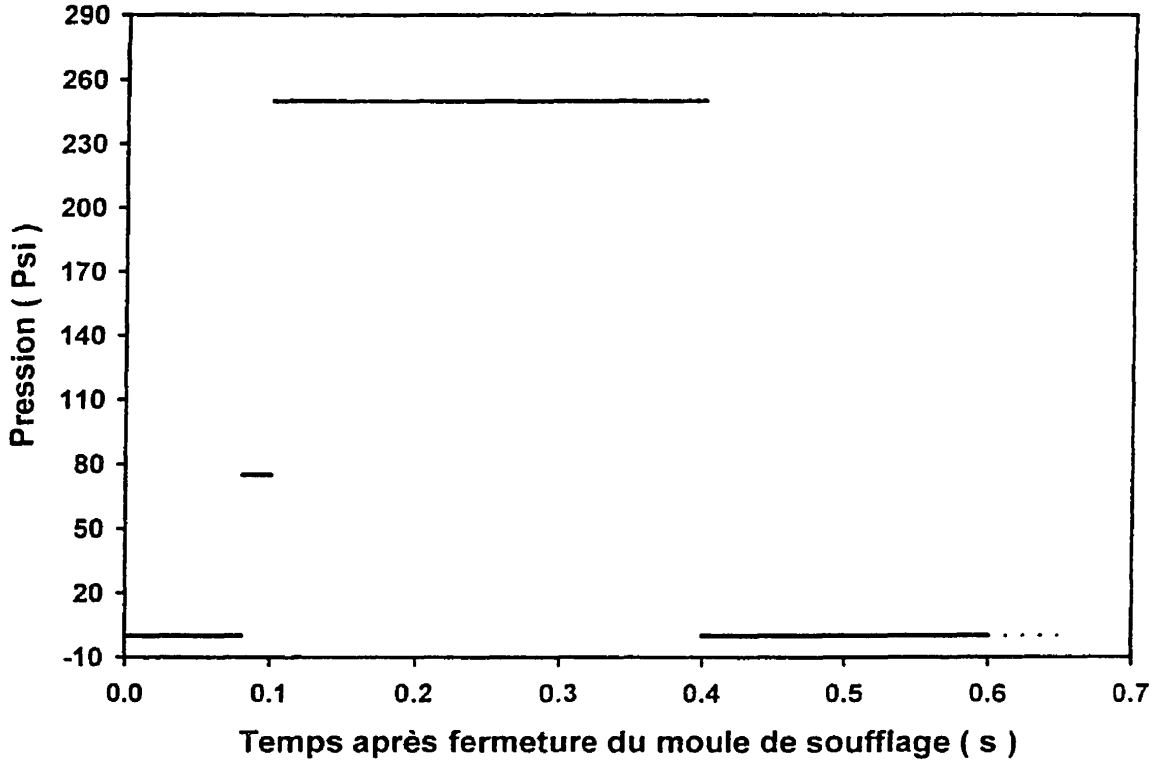

Figure A.3 - Conditions de soufflage des bouteilles en PET et en HDPE

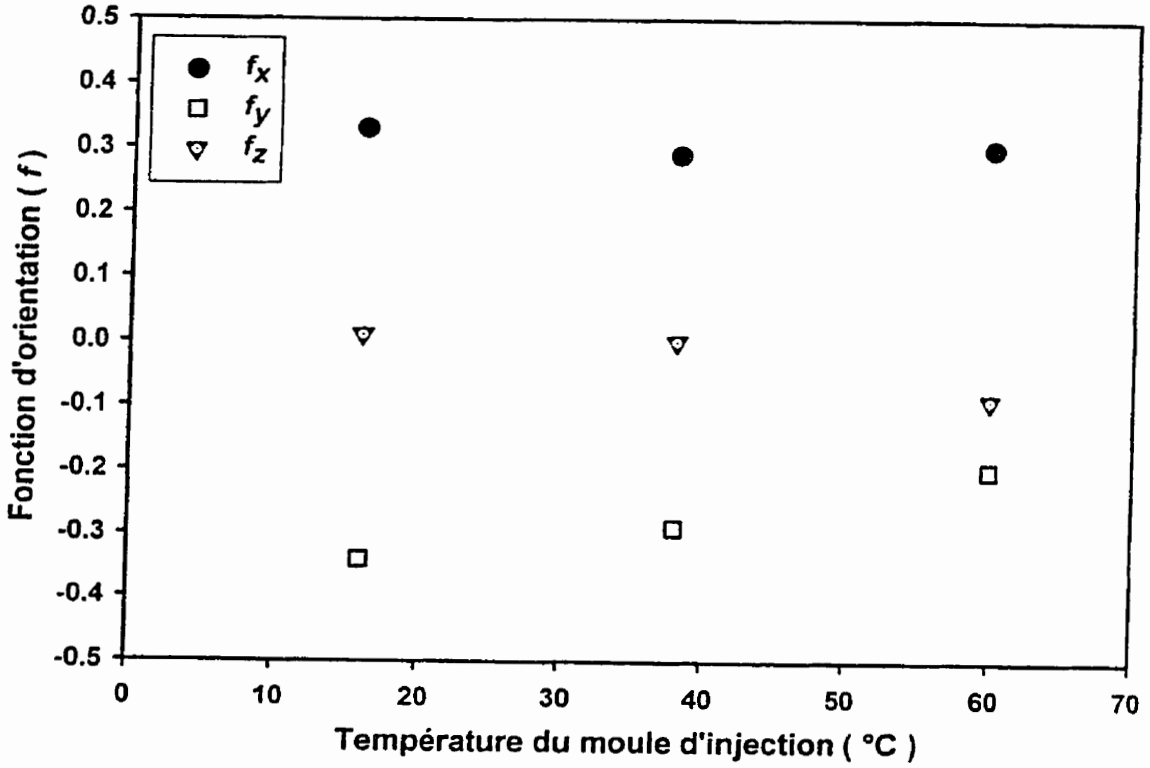

Figure A.4 - Variation des fonctions d'orientation f_x, f_y et f_z sur la surface des bouteilles en PET du type I en fonction de la température du moule d'injection

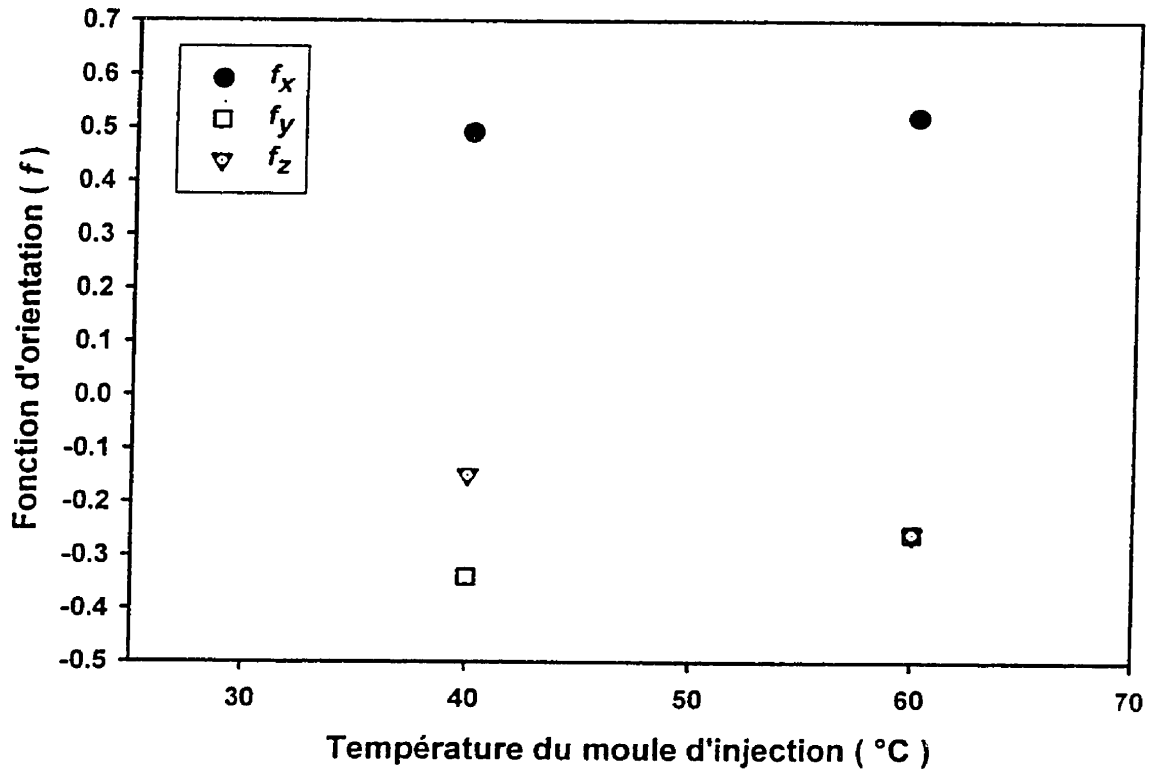

Figure A.5 - Variation des fonctions d'orientation f_x, f_y et f_z sur la surface des bouteilles en HDPE du type I en fonction de la température du moule d'injection

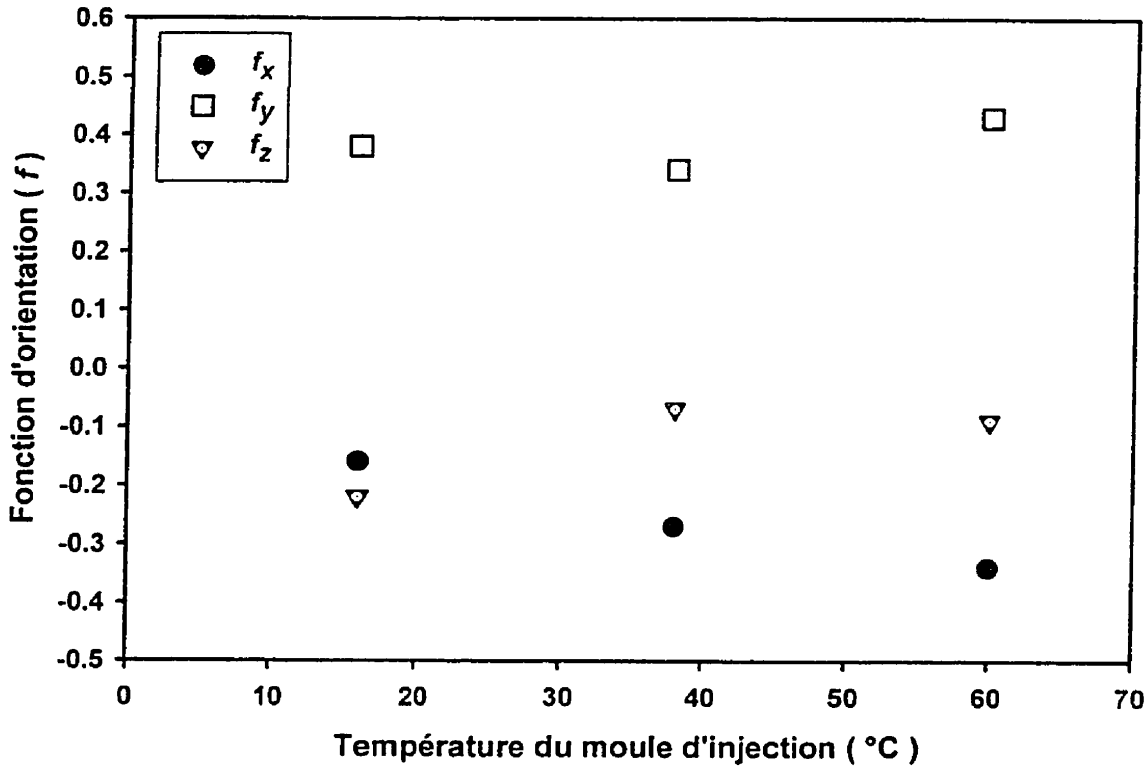

Figure A.6 - Variation des fonctions d'orientation f_x, f_y et f_z au point A (bouteille du type II) en fonction de la température du moule d'injection

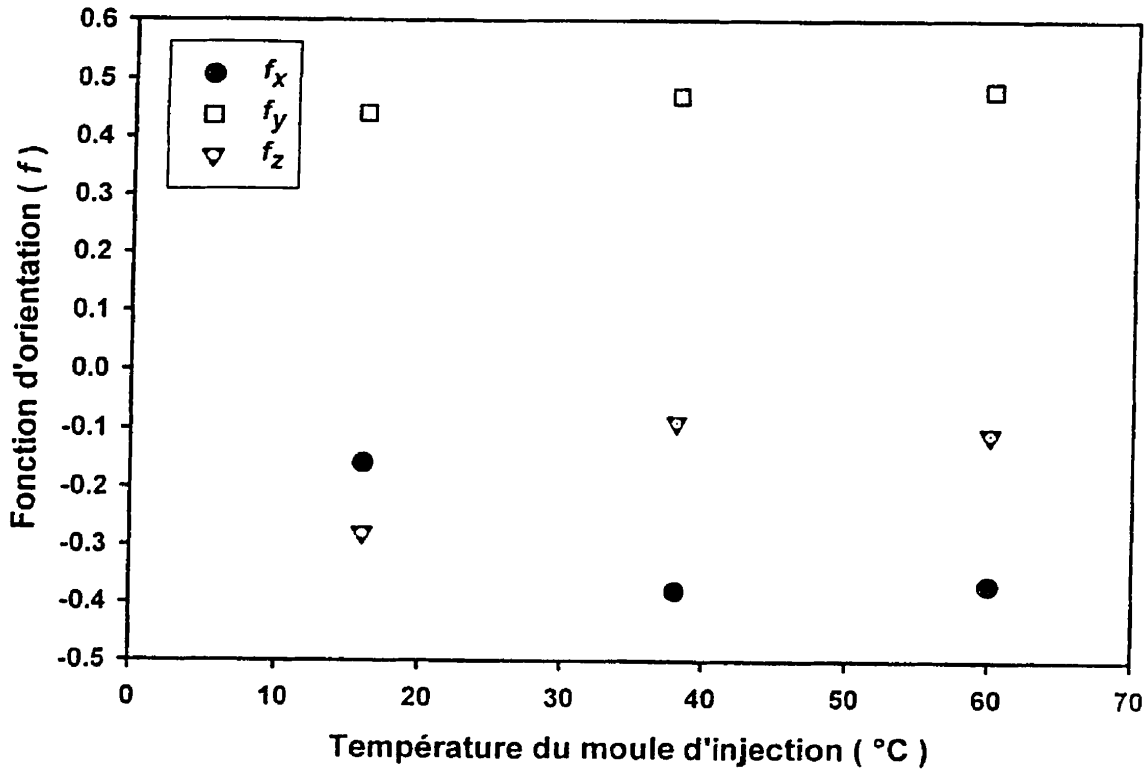

Figure A.7 - Variation des fonctions d'orientation f_x, f_y et f_z au point B (bouteille du type II) en fonction de la température du moule d'injection

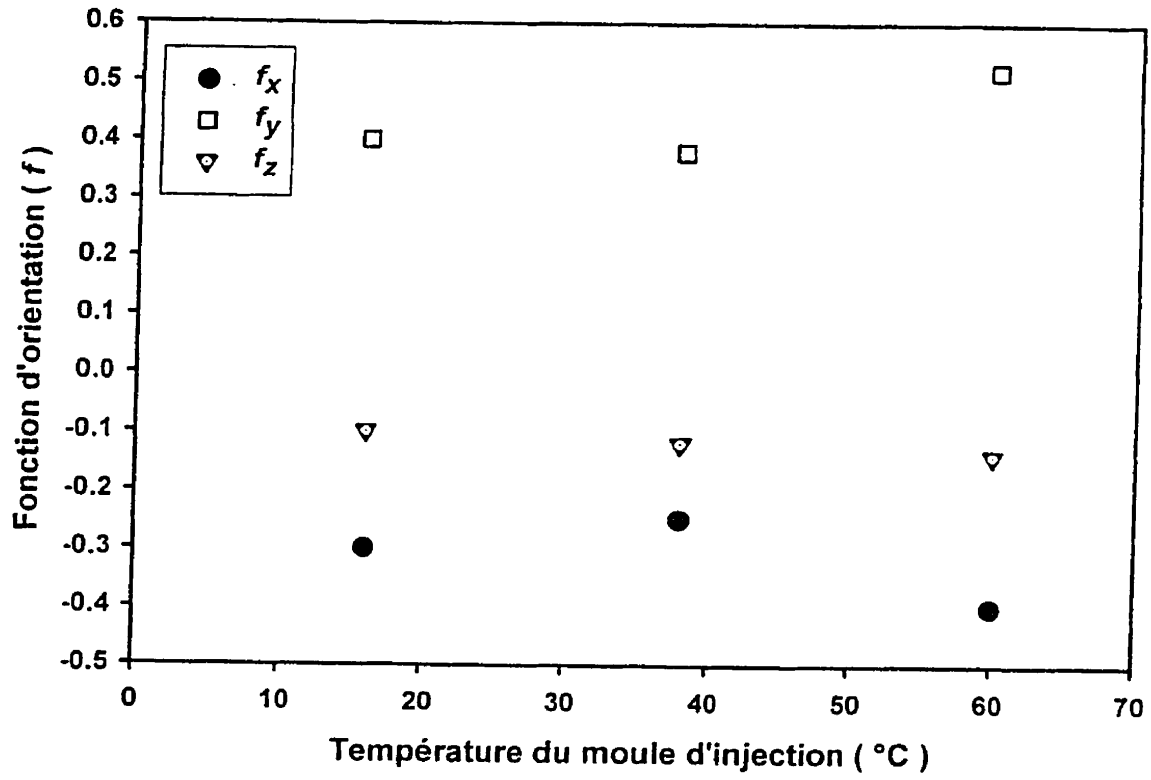

Figure A.8 - Variation des fonctions d'orientation f_x, f_y et f_z au point C (bouteille du type II) en fonction de la température du moule d'injection

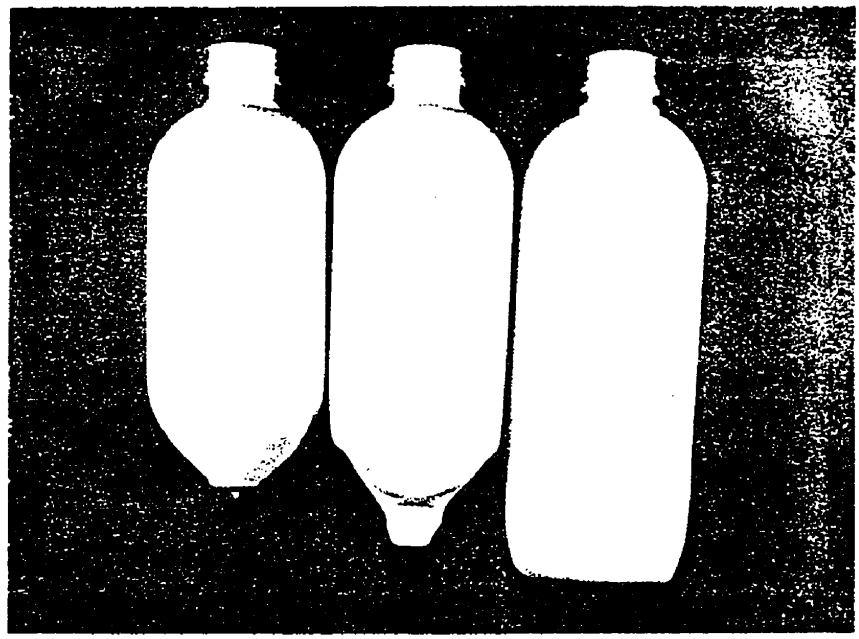

Figure A.9 - Évolution de l'étirage et soufflage des bouteilles de type II

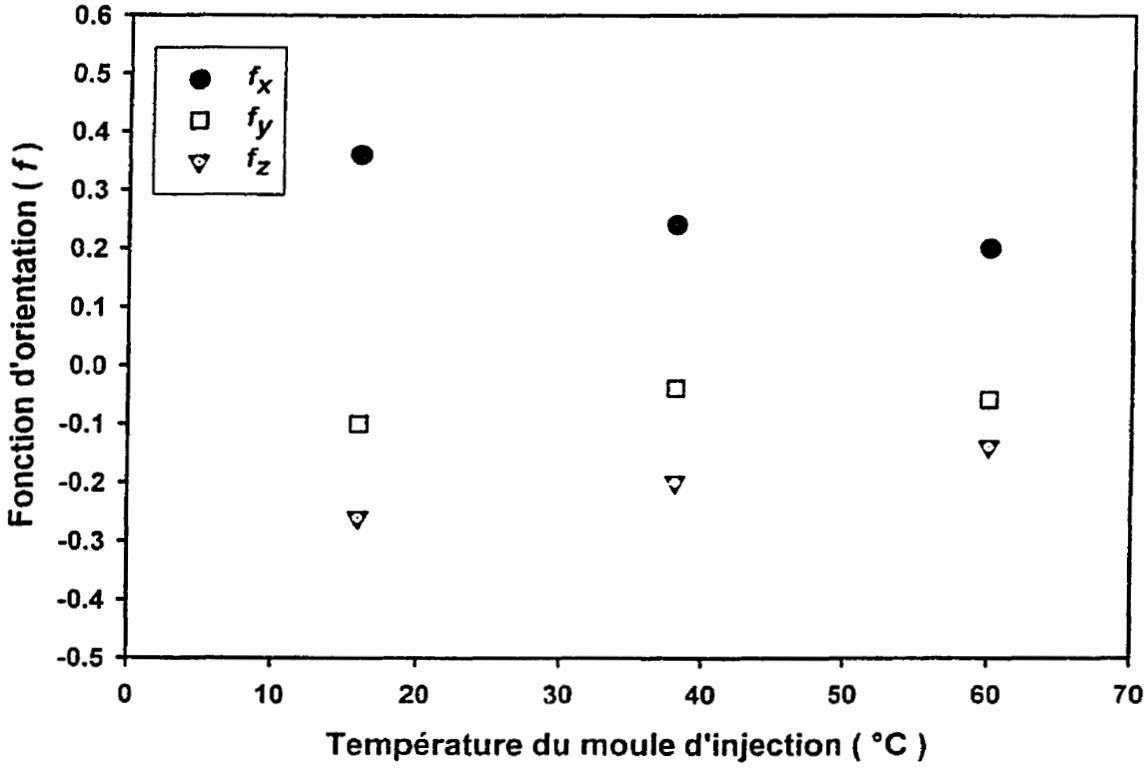

Figure A.10 - Variation des fonctions d'orientation f_x, f_y et f_z au point D (bouteille du type II) en fonction de la température du moule d'injection

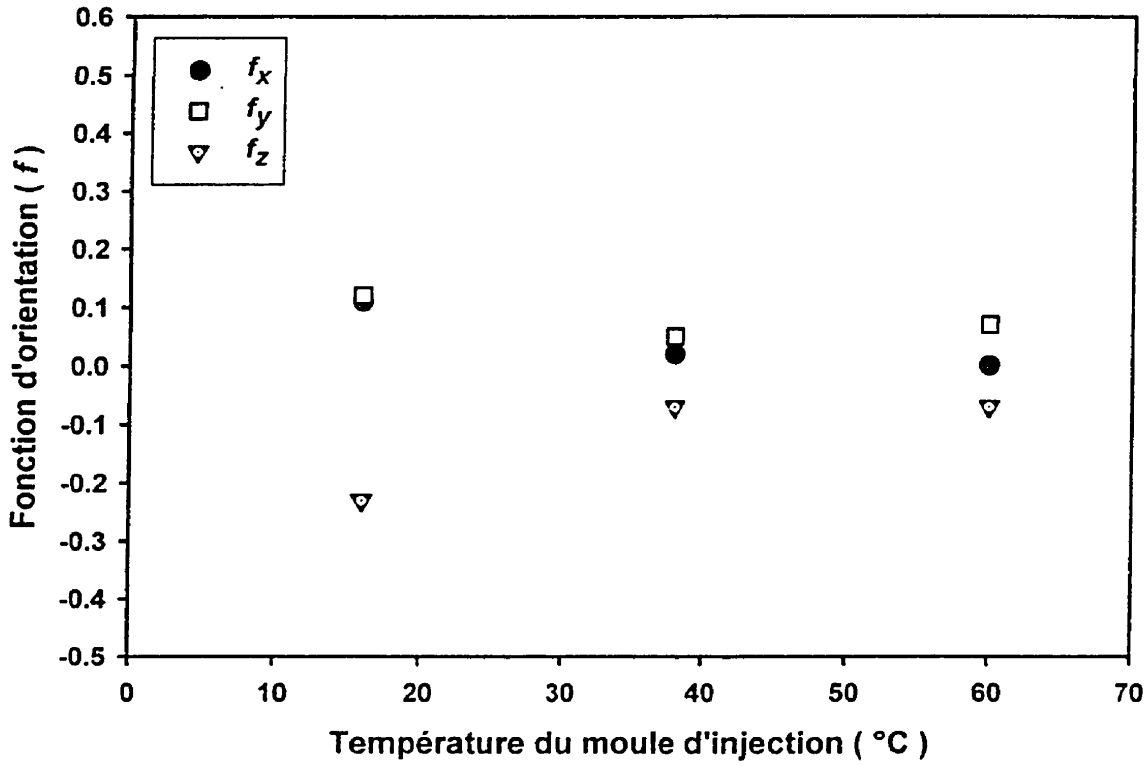

Figure A.11 - Variation des fonctions d'orientation f_x, f_y et f_z au point E (bouteille du type II) en fonction de la température du moule d'injection

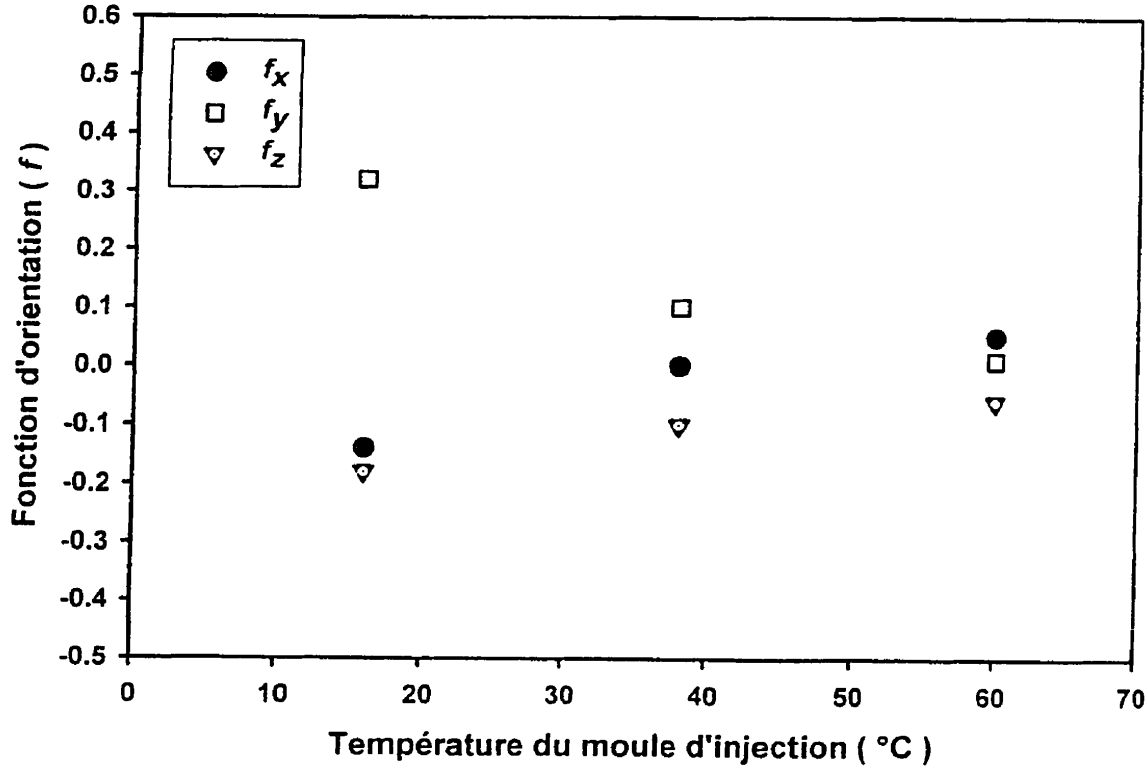

Figure A.12 - Variation des fonctions d'orientation f_x, f_y et f_z au point F (bouteille du type II) en fonction de la température du moule d'injection

Références

1. BOST, J. (1982). Matières plastiques, II, technologie plasturgie, Technique et documentation Lavoisier.

2. LEE, N. (1990). Plastic Blow Molding Handbook, Chapman and Hall.

3. CAKMAK, M., SPRUIELL, J.E. et WHITE, J.L. (1984). A Basic Study of Orientation in Poly (ethylene Terephthalate) Stretch-Blow Molded Bottles. Polymer Engineering and Science, 24, 1390-1395.

4. ISAYEV, A.I. (1983). Orientation Development in the Injection Molding of Amorphous Polymers. Polymer Engineering and Science, 23, 271-284.

5. CHANDRAN, P. et JABARIN, S. (1993). Biaxial Orientation of Poly (ethylene Terephthalate). Part III: Comparative Structure and Property Changes Resulting From Simultaneous and Sequential Orientation. Advances in Polymer Technology, 12, 153-165.

IMAGE EVALUATION TEST TARGET (QA-3)

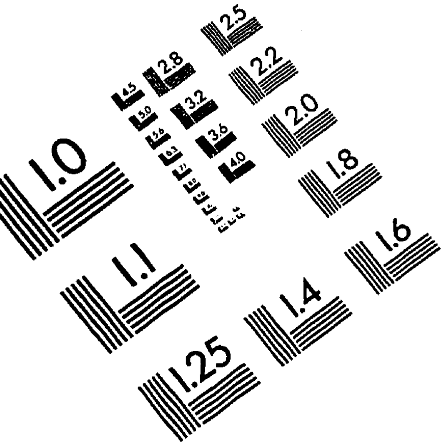

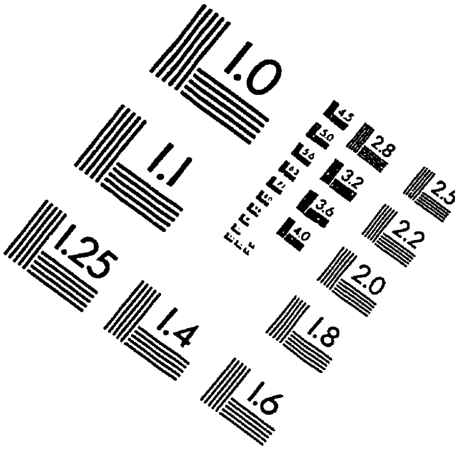

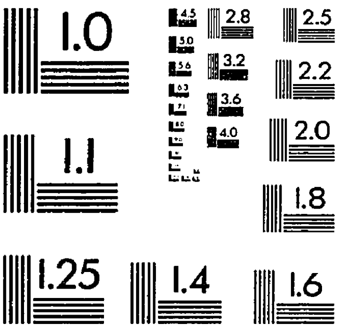

150mm

6″

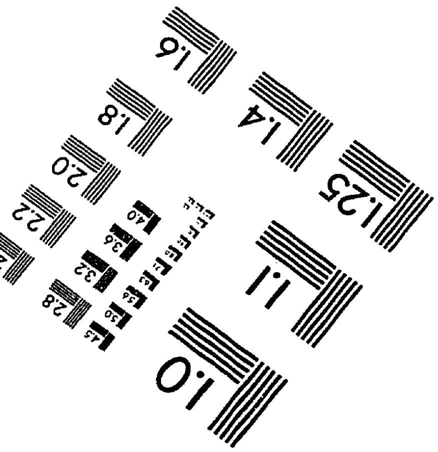

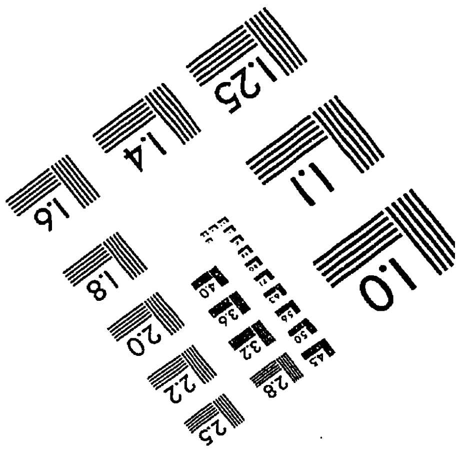

APPLIED IMAGE, Inc
1653 East Main Street
Rochester, NY 14609 USA
Phone: 716/482-0300
Fax: 716/288-5989